UAB
Universitat Autònoma de Barcelona

A new plant-based nanovesicle platform based on alkyl polyglucosides and β-sitosterol for topical delivery

Marta Alcaina Hernando

ADVERTIMENT. L'accés als continguts d'aquesta tesi doctoral i la seva utilització ha de respectar els drets de la persona autora. Pot ser utilitzada per a consulta o estudi personal, així com en activitats o materials d'investigació i docència en els termes establerts a l'art. 32 del Text Refós de la Llei de Propietat Intel·lectual (RDL 1/1996). Per altres utilitzacions es requereix l'autorització prèvia i expressa de la persona autora. En qualsevol cas, en la utilització dels seus continguts caldrà indicar de forma clara el nom i cognoms de la persona autora i el títol de la tesi doctoral. No s'autoritza la seva reproducció o altres formes d'explotació efectuades amb finalitats de lucre ni la seva comunicació pública des d'un lloc aliè al servei TDX. Tampoc s'autoritza la presentació del seu contingut en una finestra o marc aliè a TDX (framing). Aquesta reserva de drets afecta tant als continguts de la tesi com als seus resums i índexs.

ADVERTENCIA. El acceso a los contenidos de esta tesis doctoral y su utilización debe respetar los derechos de la persona autora. Puede ser utilizada para consulta o estudio personal, así como en actividades o materiales de investigación y docencia en los términos establecidos en el art. 32 del Texto Refundido de la Ley de Propiedad Intelectual (RDL 1/1996). Para otros usos se requiere la autorización previa y expresa de la persona autora. En cualquier caso, en la utilización de sus contenidos se deberá indicar de forma clara el nombre y apellidos de la persona autora y el título de la tesis doctoral. No se autoriza su reproducción u otras formas de explotación efectuadas con fines lucrativos ni su comunicación pública desde un sitio ajeno al servicio TDR. Tampoco se autoriza la presentación de su contenido en una ventana o marco ajeno a TDR (framing). Esta reserva de derechos afecta tanto al contenido de la tesis como a sus resúmenes e índices.

WARNING. The access to the contents of this doctoral thesis and its use must respect the rights of the author. It can be used for reference or private study, as well as research and learning activities or materials in the terms established by the 32nd article of the Spanish Consolidated Copyright Act (RDL 1/1996). Express and previous authorization of the author is required for any other uses. In any case, when using its content, full name of the author and title of the thesis must be clearly indicated. Reproduction or other forms of for profit use or public communication from outside TDX service is not allowed. Presentation of its content in a window or frame external to TDX (framing) is not authorized either. These rights affect both the content of the thesis and its abstracts and indexes.

Universitat Autònoma de Barcelona

A new plant-based nanovesicle platform based on alkyl polyglucosides and β-sitosterol for topical delivery

Marta Alcaina Hernando

Tesi Doctoral

Programa de Doctorat en Química

Directores

Dra. Alba Córdoba Insensé

Prof. Nora Ventosa Rull

Tutora

Prof. Nora Ventosa Rull

Departament de Química

Facultat de Ciències

2024

La present memòria es presenta per aspirar a Grau de Doctor per:

Marta Alcaina Hernando

Vist i plau:

Dr. Alba Córdoba Insensé

Prof. Nora Ventosa Rull

Bellaterra, juliol 2024

ALBA CÓRDOBA INSENSÉ, Technology Transfer & Business Development Director of Nanomol Technologies SL and **NORA VENTOSA RULL**, Research Professor of the Spanish National Research Council at the Institute of Materials Science of Barcelona (ICMAB-CSIC)

CERTIFY:

That **Marta Alcaina Hernando**, Master's Degree in Advanced Biotechnology and Bachelor's Degree in Biochemistry, has performed, under their management, the research work entitled "**A new plant-based nanovesicle platform based on alkyl polyglucosides and β-sitosterol for topical delivery**". This work has been performed under the frame of Chemistry Ph.D program of the Chemistry Department of the Autonomous University of Barcelona.

And in witness whereof this is signed by

Directors

Dr. Alba Córdoba Insensé

Prof. Nora Ventosa Rull

Bellaterra, July 2024

Nothing in life is to be feared, it is only to be understood. Now is the time to understand more, so that we may fear less.

– Marie Curie

Agraïments

Quan aquesta etapa ja està arribant a la seva fi, arriba el moment de mirar enrere i recordar per agrair a totes aquelles persones que han estat al meu costat acompanyant-me i m'han ajudat de moltes maneres diferents a que aquesta tesi hagi sigut possible.

Primer de tot, vull agrair de tot cor a les meves dues directores de tesi, la Prof. Nora Ventosa i la Dra. Alba Córdoba. Totes dues sou referents per creure'ns que el futur de la ciència cada cop pot ser més en femení. Nora, moltes gràcies per donar-me l'oportunitat de fer la tesi en un grup tan potent com Nanomol. Gràcies per la confiança que m'has mostrat sempre i pels teus consells perquè les coses acabin sortint rodones. Alba, moltes gràcies per aquests anys de feina, ha sigut molt enriquidor poder viure aquest projecte des dels inicis aprenent molt de la teva professionalitat, ajuda i consells en cada pas. És molt emocionant poder haver vist com es va començar i com estem ara.

A més, també vull donar les gràcies a en Santi Sala. Estic molt agraïda per l'experiència de fer un doctorat industrial en una empresa com Nanomol Technologies i totes les oportunitats professionals que hi han derivat. L'ambient que hi ha des que vaig arribar i que s'ha mantingut durant aquests anys amb tants canvis fa que aquest camí hagi sigut molt més fàcil i agradable. També vull donar les gràcies a la Lidia Ferrer, per la teva ajuda i disponibilitat sempre que ho he necessitat, per la teva rigorositat en tota la feina que hem fet i a la vegada la confiança que m'has donat sempre impulsant cap endavant. Finalmente, también quiero agradecer a Ivana Malvacio todo el tiempo que pudimos trabajar juntas. Siempre me acordaré de ese primer día de prácticas en el que entramos juntas y toda la ayuda y confianza que me mostraste durante los inicios de este doctorado. Sin esa primera etapa contigo mi doctorado no hubiera sido igual. Me hizo mucha ilusión podernos reencontrar, aunque fuera por muy poco tiempo, en tu nuevo hogar en Parma.

Quiero expresar también mi agradecimiento al Ministerio de Ciencia, Innovación y Universidades por el financiamiento recibido a través de las ayudas para contratos para la formación de doctores en empresas (Doctorados Industriales). Igualment, vull expressar el meu agraïment al finançament rebut de l'ajuda de Doctorat Industrial de l'Agaur, ambdues ajudes permetent-me realitzar aquest doctorat.

I want to acknowledge the opportunity to collaborate with the *Universita Degli Studi Di Parma* trough the European Union's Horizon 2020 research and innovation programme

"Micro4Nano" (Multifunctional nanocarriers for nonlinear microscopy: new tools for biology and medicine, agreement number 101007804). I would like specially to thank Prof. Silvia Pescina (ADDRes Lab, Department of Food and Drug) and Prof. Cristina Sissa (Department of Chemistry, Life Sciences and Environmental Sustainability), for accepting me in your laboratories, your kind welcome and all the scientific work we did, I learned a lot from you for the quick but intense period I stayed with you. I would also like to thank Ilaria for all the help and time we spent together in the microscope to obtain such great results, and Annalisa for all the work done with the epidermal models. I would like to expand my gratitude to all the people I shared lab with: Felipe, Adriana, Sara, Massimilliano and Andrea D. Finalment, també vull agrair al Guillem per acollir-me i cuidar-me durant la meva estada, va ser tota una sort coincidir amb tu allà.

I would also like to express my gratitude again to the European Union's Horizon 2020 research and innovation programme for the funding received to perform the SAXS analysis via the TamaTA INNOV call (no. 101004728) at the BL11-NCD-SWEET beamline from the ALBA synchrotron. I would like specially to thank Dr. Cristián Huck-Iriart from ALBA synchrotron for all the time spent performing and analyzing the samples, and Prof. Jan Skov Pedersen from Aarhus University (Denmark) for the help analyzing the results.

Vull agrair també a tots els professionals que m'han ajudat a fer les caracteritzacions de les mostres presentades en aquesta tesi. Començant pel Servei de Microscòpia i Difracció de Raigs X de la UAB, vull agrair totes les caracteritzacions de cryo-TEM que hem realitzat. En especial, vull donar les gràcies a en Martí de Cabo per totes les hores, les imatges que hem obtingut i la paciència quan les mostres no han sigut fàcils, sempre amb la teva energia característica. També vull agrair al Laboratori de Luminescència i Espectroscòpia de Biomolècules (LLEB) de la UAB, en concret a en Salvador Bartolomé, per l'ajuda en les mesures de fluorescència i per prestar-nos sempre que ho hem necessitat la làmpada d'UV per fer els assajos funcionals. Vull donar també les gràcies al Servei d'Anàlisi Tèrmica i Calorimetria de l'Institut de Química Avançada de Catalunya (IQAC-CSIC) per les mesures de microDSC, en especial a la Sonia Pérez. Finalment, també vull agrair al Marc Martínez del Bioservice de l'ICMAB-CSIC per la feina feta amb els estudis d'irritació en pell, la paciència i dedicació per implementar de zero aquests estudis en un temps rècord. Vull donar també les gràcies a tot el personal tècnic i d'admisnitració de l'ICMAB que m'han ajudat sempre que he anat perduda a la recerca d'una solució als meus problemes, en especial a la Carme Gimeno, l'Arnau Jaumandreu i la Soraya Hernandez.

També m'agradaria agrair tot el treball realitzat per diferents estudiants que han fet estades amb nosaltres i ens han ajudat en aquesta recerca perquè la seva participació ha sigut molt

valuosa. Vull donar les gràcies al Marc Orozco, a l'Alberto Carnicero, a la Pargol Esfahani, l'Albert Oms i la María Marín.

Vull donar també de forma especial les gràcies a totes aquelles persones que en el meu dia a dia m'han ajudat de diferents formes a fer tot aquest camí. Moltes gràcies a la Judit, la Lídia, i l'Estela, heu sigut fonamentals en aquests anys. Moltes gràcies per les estones compartides dins i fora de la feina, per escoltar-me i animar-me quan ho he necessitat per continuar endavant i amb energies renovades. Gràcies al Josep i al David Piña, per estar disponibles cada cop que hi ha hagut una fuga indetectable, s'ha trencat una vàlvula o el diafiltrador no funcionava. Mai hauria pensat que quan em diguessin "connexió en forma de T amb rosca femella de ¾ gyrolok" entendria que m'estàveu demanant, em sento ja amb esperit d'enginyera. Moltes gràcies a l'Arnau, per les mesures d'HPLC realitzades, però encara més per tot el suport que m'has donat durant aquests anys (sempre serem l'equip de les supernenes). També estic molt agraïda d'haver pogut compartir tot aquest camí amb tu Carla, està clar que aquest viatge no hagués estat igual sense la teva companyia en tots els moments, presentacions i conferències, has sigut una companya de viatge literal i metafòricament genial.

I evidentment també vull donar les gràcies a totes les companyes i companys amb els que he compartit en algun moment aquesta etapa tan intensa. A tota la familia de Nanomol Technologies, la Yolanda i la Sara, sempre amenitzant les estones fora i dins del laboratori amb les seves històries i liades (o yolandilles), la Teresa, l'Oscar, la Laura G, l'Arnau Guasch, el Xavi, la Sandra i la Marta V. Vull també donar les gràcies als companys de Nanomol grup, que, tot i que cada cop he anat passant menys temps a l'ICMAB, sempre m'han fet sentir benvinguda. Gràcies a la Nerea, Ángel, Guillem, Eli, Mariana, Aida, Sara G, Sara R, Xavi, Albert R, Albert G, Marc, Paula, Angelica, Alejandro, Laia, Júlia, Elba, Núria, Giovanni, Rubén, Ehsan, Nicolas, Edu. Moltes gràcies a tots per compartir part d'aquesta etapa amb mi!

Per acabar, vull acabar donant les gràcies a totes aquelles persones que m'han acompanyat fora del laboratori. Totes elles, potser algunes sense acabar d'entendre en què he estat treballant aquests anys tot i preguntar múltiples vegades, m'han ajudat a desconnectar i agafar forces per continuar treballant. A les meves amigues de tota la vida (quasi literalment), la Celia, la Júlia, la Laura i la Marta. A Raquel, fue una suerte llegar aquel primer día tarde a la clase y sentarme a tu lado por casualidad. Als amics de la uni, Jessica, Alex, Laura, Adri i Mireia; van ser uns anys bojos que ens han portat on estem.

També vull donar les gràcies a tota la meva família, àvies, tiets i cosins. En especial als meus pares i al meu germà, que m'han portat a ser la persona que soc ara, moltíssimes gràcies per tot el que m'heu donat i ensenyat, no hi ha paraules per agrair-vos-ho.

Per acabar, moltes gràcies Javi. Vas ser tu qui ja fa vuit anys em vas empènyer a agafar una assignatura que en aquell moment no em feia massa gràcia: nanotecnologia. Si no hagués pres aquella decisió, no estaria on estic ara. Moltes gràcies per estar-hi sempre, donar-me força, i viure amb mi tota aquesta etapa empenyent-me cap endavant i ajudant-me a superar-me a mi mateixa.

Moltes gràcies de tot cor a tots.

Abstract

Delivery systems have been widely used in the last decades to enhance the efficacy and safety of drugs and active molecules. Vesicles are one of the most popular drug delivery options in pharmaceutical and healthcare applications. To overcome the limitations of the first vesicular systems, such as conventional liposomes, the research has led to finding novel compositions which increase the stability and tolerability of the vesicular formulations. Nonetheless, this search is a challenging process that depends on different factors such as the components used, the interactions between them or the dispersant media.

This Industrial Thesis presents the development of new vesicular systems using plant-based, biocompatible and biodegradable components as building blocks, for topical delivery in healthcare and cosmetic applications. The new delivery systems have been prepared using the DELOS process, a single-step methodology based on compressed fluids which is robust, scalable and with a low environmental impact.

The vesicles were formed by the self-assembly of β-sitosterol (Sit) and alkyl polyglucoside surfactants, mainly lauryl glucoside (LGL) and lauryl glucose carboxylate (LGC). Different systems were developed and characterized by advanced techniques such as dynamic light scattering, cryo-electron microscopy and small-angle X-ray scattering.

With the objective to evaluate their role as delivery systems, several active ingredients of interest for dermocosmetic applications were formulated in the novel nanovesicles (NVs) of Sit, LGL and LGC. Small hydrophobic molecules like α-tocopherol (vitamin E), an antioxidant ingredient, and 7-dehydrocholesterol, a precursor of vitamin D, were efficiently loaded in the vesicles. Besides their physicochemical properties, the functionality of the payloads after formulation was also characterized proving that both maintained their activity once they were integrated in nanovesicles. Moreover, other types of active molecules were also tested as payloads, such as ascorbyl glucoside (vitamin C) and niacinamide (vitamin B_3), both small hydrophilic molecules, and proteins such as basic fibroblast growth factor, which is a larger biomolecule.

In view of their topical application, the most promising prototypes were assessed in terms of their biological performance. First, *in vitro* biocompatibility assays with reconstructed human epidermis showed positive results for all the systems tested, with non-irritant effects. Second, *ex vivo* skin retention studies using multiphoton microscopy and NVs

labelled with the fluorophore Nile red demonstrated improved skin permeability of the poorly water-soluble fluorophore in comparison with the free molecule.

Finally, exploration of further applications beyond personal care and cosmetics were also evaluated in this Thesis. As a proof of concept, the vesicular systems based on Sit and LGL were tuned with components accepted for pharmaceutical usage. In particular, two derivatives of cholesterol were self-assembled with Sit and LGL to form nanovesicles: a PEG polymer moiety (cholesterol-PEG_{600}) and an ionizable derivative with a tertiary amine (DC-cholesterol), which allowed to obtain stable non-ionic or cationic systems, respectively. To complete the proof of concept, the ability to integrate different drug molecules was evaluated for NVs with DC-cholesterol. Cannabidiol, methotrexate and human growth hormone, each payload with different chemical structure and characteristics, were integrated.

Overall, the results obtained in this Thesis point to the successful development of an attractive and versatile platform, based on stable and homogeneous nanovesicles composed of plant-derived ingredients, for topical delivery in dermocosmetic, healthcare and pharmaceutical industries.

Contents

Agraïments 9

Abstract 15

Contents 17

List of Abbreviations 23

1. Introduction 29

1.1. Delivery systems: searching new vehicles for active compounds 29

1.2. Vesicles as self-assembled structures for drug delivery 33

1.2.1. Types of vesicular systems 34

1.3. Methods for the preparation of nanovesicles 37

1.3.1. DELOS method for the preparation of nanovesicles 38

1.4. Topical delivery as administration route 40

1.5. The use of delivery systems in cosmetics 42

1.5.1. Regulation of nanotechnology in cosmetic industry 45

1.5.2. Prospects and challenges of delivery systems in the cosmetic industry 46

1.6. Bibliography 47

2. Objectives 55

3. New plant-based nanovesicles based on alkyl polyglucosides and β-sitosterol 59

3.1. The need of plant-based delivery systems 59

3.1.1. β-Sitosterol as building block in delivery systems 61

3.1.2. Alkyl polyglucoside surfactants as building block for novel nanovesicles 62

3.2. Synthesis of β-sitosterol and lauryl glucoside nanovesicles 64

3.2.1. Synthesis of nanovesicles using cosmetic-grade lauryl glucoside 64

3.2.2. Synthesis of nanovesicles using pure-grade lauryl glucoside 69

3.3. Stabilization of Sit:LGL nanovesicles with anionic additives 73

3.3.1. Stabilization by adding 3% of anionic surfactants 73
3.3.2. Screening and replacement of non-ionic surfactant LGL by the anionic surfactant LGC 77
3.4. Effect of surfactant alkyl chain length in the formation of vesicles 79
3.4.1. Impact of manufacturing methodology in the formation of NVs. Comparison of DELOS *vs.* thin film hydration techniques 81
3.5. Loading of α-tocopherol in the nanovesicles 85
3.6. Impact of membrane composition on the lamellarity of the nanovesicles 89
3.7. Biocompatibility and skin permeation analysis of the new nanoformulations 93
3.7.1. *In vitro* skin irritation assays 93
3.7.2. Retention of the nanovesicles in skin explants assessed by two-photon microscopy 95
3.8. Summary of the Chapter and future perspectives 102
3.9. Bibliography 104
4. Formulation of the vitamin D precursor 7-dehydrocholesterol in alkyl polyglucosides and β-sitosterol nanovesicles 111
4.1. Vitamin D supplementation: an increased necessity worldwide 111
4.1.1. The role of vitamin D in the skin 113
4.2. Preparation of the 7-DHC loaded nanovesicles 115
4.3. Impact of the Sit:7-DHC ratio on the lamellarity of the nanovesicles 119
4.4. 7-DHC is successfully converted to vitamin D when structured in nanovesicles 121
4.5. Biocompatibility analysis of the 7-DHC nanoformulations 124
4.6. Summary of the Chapter and future perspectives 126
4.7. Bibliography 129
5. Formulation of hydrophilic payloads in alkyl polyglucosides and β-sitosterol nanovesicles 133
5.1. Formulation of hydrophilic payloads with vesicles 133
5.2. Loading the basic fibroblast growth factor in Sit:LGC nanovesicles 136
5.2.1. Use of growth factors in healthcare and cosmetic products 136
5.2.2. Loading of bFGF in Sit:LGC nanovesicles by DELOS process 138

5.2.3. Summary of the Section and future perspectives on the nanoformulation of growth factors 144

5.3. Loading of vitamins C and B_3 in Sit:LGC nanovesicles 145

5.3.1. Use of hydrophilic vitamins in healthcare and cosmetic products 145

5.3.2. Loading of ascorbyl glucoside and niacinamide in Sit:LGC nanovesicles by DELOS process 148

5.3.3. Summary of the Section and future perspectives on the nanoformulation of hydrophilic small molecules 151

5.4. Bibliography 153

6. Tuning of alkyl polyglucosides and β-sitosterol nanovesicles for pharmaceutical applications 157

6.1. New horizons for alkyl polyglucosides and β-sitosterol nanovesicles: pharmaceutical applications 157

6.2. Synthesis of Sit/LGL nanovesicles stabilized with cholesterol-PEG_{600} 159

6.2.1. Cholesterol-PEG_{600} as building block 159

6.2.2. Synthesis and stabilization of Sit:LGL nanovesicles using chol-PEG_{600} 161

6.2.3. Summary of the Section and future perspectives 164

6.3. Synthesis of pH-sensitive Sit/LGL nanovesicles with DC-cholesterol 165

6.3.1. DC-Cholesterol as building block 165

6.3.2. Synthesis and stabilization of Sit:LGL nanovesicles by adding 3% of the cationic lipid DC-chol 166

6.3.3. Screening and replacement of the neutral lipid Sit by the ionizable lipid DC-chol 169

6.4. Loading of payloads in the cationic Sit:LGL:DC-chol nanovesicles by DELOS process 172

6.4.1. Loading of cannabidiol in the nanovesicles 173

6.4.2. Loading of methotrexate in the nanovesicles 176

6.4.3. Loading of human growth hormone in the nanovesicles 179

6.4.4. Summary of the Section 183

6.5. Future perspectives 183

6.6. Bibliography 185

7. General Conclusions 191

8. Experimental section 195

8.1. Materials 195

8.2. Preparation of nanovesicles 197

8.2.1. Preparation of nanovesicles by DELOS methodology 197

8.2.2. Preparation of nanovesicles by thin film hydration 202

8.3. Physicochemical characterization of nanovesicles 203

8.3.1. Dynamic light scattering and electrophoretic light scattering 203

8.3.2. Morphological characterization by cryogenic transmission electron microscopy 204

8.3.3. Optical microscopy 205

8.3.4. Study of the lamellarity by small-angle X-ray scattering 205

8.3.5. UV-vis spectroscopy 208

8.3.6. Fluorescence spectroscopy 216

8.3.7. Measurements of pH 218

8.4. Krafft temperature determination by differential scanning calorimetry 219

8.5. Functional assays of the integrated biomolecules 219

8.5.1. Evaluation of antioxidant capacity of α-tocopherol by DPPH assay 219

8.5.2. Study of 7-dehydrocholesterol conversion to cholecalciferol 220

8.6. *In vitro* assays 222

8.6.1. Skin irritation test using *in vitro* reconstructed human epidermis 222

8.6.2. Retention of the nanovesicles in skin explants assessed by two-photon microscopy 223

8.7. Statistical analysis 225

8.7.1. Statistical analysis for the DPPH assay 225

8.7.2. Statistical analysis for the skin irritation assay 225

8.8. Bibliography 226

Annex I – Scientific Contributions 229

List of Abbreviations

A	**Å**	Angstrom
	Abs	Absorbance
	AG	Ascorbyl 2-glucoside, ascorbyl glucoside
	APG	Alkyl polyglucoside
B	**bFGF**	Basic fibroblast growth factor
C	**CBD**	Cannabidiol
	CENTR	Centrifugated sample
	CF	Compressed fluid
	Chol-PEG$_{600}$	Cholesterol-PEG$_{600}$, cholesterol-(polyethylene glycol-600)
	cm	Centimeter
	CMC	Critical micellar concentration
	CO$_2$	Carbon dioxide
	Cryo-TEM	Cryogenic transmission electron microscopy
	CSIC	Consejo Superior de Investigaciones Científicas
	CTAB	Hexadecyltrimethylammonium bromide
D	**D**	Repeat distance between bilayers of multilamellar vesicles
	Da	Dalton
	DC-Chol	DC-Cholesterol, 3β-[N-(N′,N′-dimethylaminoethane)-carbamoyl] cholesterol
	DELOS	Depressurization of an expanded liquid organic solution
	DGL	Decyl glucoside
	DGL-m$_{Cn-(n+x)}$	Decyl glucoside containing a mixture of alkyl glucosides of different carbon chain length from C*n* to C*(n+x)*
	DIAF	Diafiltrated sample by TFF
	DLS	Dynamic light scattering
	DMSO	Dimethyl sulfoxide
	DNA	Deoxyribonucleic acid
	DPBS	Dulbecco's Phosphate Buffered Saline

	DPPH	2,2-Diphenyl-1-picrylhydrazyl
	DS	Delivery System
	DSC	Differential scanning calorimetry
E	**e.g.**	For example
	EE	Entrapment efficiency
	EGF	Epidermal growth factor
	ELS	Electrophoretic light scattering
	EMA	European Medicines Agency
	EtOH	Ethanol
F	**f_{mono}**	Fraction of monolayers
	FDA	U.S. Food and Drug Administration
	FGF	Fibroblast growth factor
	FI	Fluorescence emission intensity
	fs	Femtosecond
G	**g**	Gram
	GRAS	Generally recognized as safe
	GUV	Giant unilamellar vesicle
H	**HGH**	Human growth hormone
	HPLC	High-performance liquid chromatography
I	**I**	Intensity
	i.e.	That is
	ICMAB	Institut de Ciència de Materials de Barcelona
	INCI	International nomenclature of cosmetic ingredients
J	**J**	Joule
K	**kDa**	Kilodalton
	keV	Kiloelectronvolt
	KGF	Keratinocyte growth factor

L	**LGC**	Lauryl glucose carboxilate sodium salt
	LGL	Lauryl glucoside
	LGL-m$_{Cn-(n+x)}$	Lauryl glucoside containing a mixture of alkyl glucosides of different carbon chain length from C*n* to C*(n+x)*
	LUV	Large unilamellar vesicle
M	**mg**	Milligram
	MHz	Megahertz
	min	Minute
	mL	Milliliter
	MLV	Multilamellar vesicle
	mm	Millimeter
	MPa	Mega pascal
	MTT	3-(4,5-dimethylthiazol-2-yl)-2,5-diphenyltetrazolium bromide
	MTX	Methotrexate
	mV	Millivolt
	MVV	Multivesicular vesicle
N	**n**	Sample size, number of replicates
	N_2	Nitrogen
	N_{av}	Average number of bilayers per vesicle
	NaCl	Sodium chloride
	NCA	Niacinamide
	NIBS	Non-invasive backscatter technology
	NIR	Near-infrared light
	nm	Nanometer
	NP	Nanoparticle
	NR	Nile red
	NS	Non-significant differences
	NV	Nanovesicle
O	**OECD**	Organization for Economic Co-operation and Development
	OGL	Octyl glucoside
P	***p***	Statistical *p*-value

	P	Pressure
	PBS	Phosphate buffered saline
	P_c	Critical pressure
	PDI	Polydispersity index
	PEG	Polyethylene glycol
	PES	Polyethersulfone
	pI	Isoelectric point
	PVDF	Polyvinylidene fluoride
	P_W	Working pressure
Q	**q**	Modulus of scattering vector in SAXS
R	**R^2**	Coefficient of determination
	RHE	Reconstructed human epidermis
	rh	Recombinant human
	RNA	Ribonucleic acid
	rpm	Revolutions per minute
	RSD	Relative standard deviation
	RT	Room temperature
S	**SAXS**	Small-angle X-ray scattering
	SC	Stratum corneum
	SD	Standard deviation
	SDS	Sodium dodecyl sulfate
	S_{head}	Scale of the Gaussian for the head layers
	SHG	Second harmonic generation
	Sit	β-Sitosterol
	SL	Sodium laurate
	SLS	Sodium lauroyl sarcosinate
	SOD	Superoxide dismutase
	SUV	Small unilamellar vesicle
T	**T**	Temperature
	T_c	Critical temperature
	TCP	α-Tocopherol

	TFF	Tangential flow filtration
	THF	Thin film hydration
	T_K	Krafft temperature
	TPEF	Two-photon excited fluorescence
	T_W	Working temperature
U	**UV**	Ultraviolet
V	**Vis**	Visible
	VitD	Cholecalciferol, vitamin D_3
X	**X_{CO2}**	CO_2 molar fraction
Z	**ζ-Pot**	ζ-Potential
Others	**2PM**	Two-photon microscopy
	7-DHC	7-Dehydrocholesterol
	°C	Celsius
	Δ^9-THC	Delta-9-tetrahydrocannabionol
	λ	Wavelength
	µm	Micrometer
	µM	Micromolar
	σ_{head}	Sigma of the head layer Gaussian
	χ^2	Reduced weighted chi-square

1 Introduction

1.1. Delivery systems: searching new vehicles for active compounds

From their origins, humans have used active molecules for different therapeutic and healthcare purposes. Initially, these molecules were derived from medicinal plants but over the years, their sources have expanded to include synthetic drugs. Moreover, since beginning of the 1950s, a new line of research emerged focused on enhancing the efficacy and safety of drugs and active molecules: delivery systems (DSs)[1].

DSs are formulations or devices that transport and release active molecules in the body in a controlled manner regulating the kinetics, concentration and location[2,3]. They can be used with different objectives: to extend the molecule's lifetime in the body, to target the specific organ for drug action and/or to minimize the side effects that some drugs can cause[3]. They can be also involved in several steps of the process for the drug delivery to the specific target: administration of the active molecule, release of the drug from the DS to the target and the transport of the active molecule across the biological barriers and membranes to the site of action[2].

The design of a DSs must consider multiple factors (**Figure 1.1**). The strategy for developing a delivery system depends first on the type of payload involved (i.e., small hydrophilic or lipophilic molecules, peptides and proteins or RNA and DNA) and the target site (i.e., specific organs or cellular types, a tumor or for example wounds or sites of infection). Considering these two factors, payload and target, it is necessary to define the optimal approach to deliver the payload. First, depending on the target it is necessary to decide the more appropriate delivery route (i.e., oral, nasal, ocular, subcutaneous, topical or parenteral). Second, the size of the DS is also important depending on the type of technology used: from macroscopic devices such as dermal patches, implants or inserts that release the active molecule, to micro and nanoscopic matrices and particles formulations that integrate or encapsulate the payloads to deliver. Then, the material of which these matrices and particles are formed is also important. The choice of material is based on the nature of the payload to ensure an efficient integration but also the compatibility with the delivery route. Furthermore, the materials and excipients approved by the regulatory agencies can differ depending on the administration route. Finally, the release mechanism of the molecules from the delivery system must be carefully considered, as it should be chosen according to the biological barriers that the payloads have to overcome to reach their target. All in all, developing an efficient DS requires simultaneous consideration of all these factors [1,4].

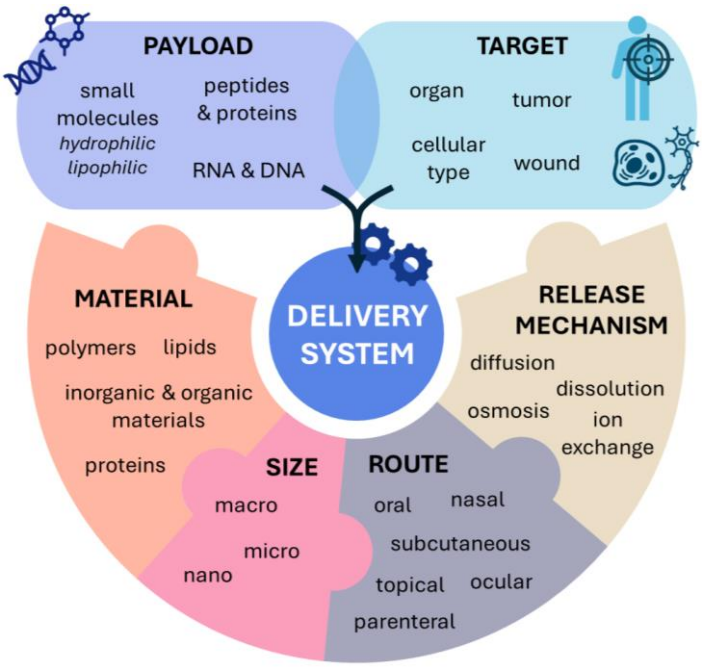


Figure 1.1. Scheme of the general factors to consider when designing a delivery system.

The design and technology of DSs have evolved over the years. The first DSs were developed at the beginning of the decade of 1950. They were devices like dermal patches, subcutaneous implants, or inserts for ophthalmic or intrauterine applications, that allowed a zero-order release based on mechanisms such as dissolution, diffusion, osmosis or ion exchange[1,5]. These first devices were mainly for dermal, transdermal and oral delivery[6,7].

From 1960, in parallel with those first DSs, a new era started for sustained release[1,5]. For example, smart polymers and hydrogels matrices were developed. They were sensitive to the environment and were reactive to different stimuli like pH, temperature or to levels of specific molecules like glucose[8–10]. Another example were the first biodegradable microparticles basically made of polymers that were used to deliver from small molecules to proteins and peptides[11,12].

Finally, during the 1980s decade, a new scale appeared in the DSs field: nanotechnology. Advances in particles but also technology enable the use of nanoparticles (NPs) as delivery systems made of different types of materials. Together with the *nano* era two new concepts arise: controlled release and targeted delivery.

Working at the nanoscale offer some advantages in relation to previous DSs. Nanocarriers, due to their size, present a large specific surface area which allow higher dosing per unit of volume. They also demonstrate improved circulation time and bioavailability of drug where it is needed. Nanoparticles can permeate better through biological and physiological barriers because of their reduced size. Additionally, they help to reduce the dose needed decreasing at the same time the side effects of the loaded drugs. The surface of nanoparticles can be easily chemically modified with different functional groups that allow to modulate the pharmacokinetic and/or pharmacodynamic properties in addition to target specific cell types. For example, the use of polyethyleneglycol (PEG) is well known to modify the surface properties stabilizing nanoparticle formulations, or the use of peptides as targeting moieties. Finally, their diversity in terms of size, shape and composition allow a high variety of delivery strategies[3,13].

It is important to highlight that over the past few decades, different types of nanoparticles have been developed as DSs. These can be classified based on different criteria such as surface functionality, size and shape or nanoparticles nature. However, one of the most common way to classify them is by their composition (**Figure 1.2A**): inorganic nanoparticles (e.g., metallic, magnetic and silica nanoparticles, quantum dots or carbon-based nanomaterials) and organic nanoparticles including lipid-based nanoparticles (e.g., vesicles such as liposomes and non-liposomal vesicles, micelles and solid-lipid nanoparticles),

polymeric-based nanoparticles (e.g., polymeric nanoparticles, polymeric micelles, dendrimers or nanogels) and protein-based nanoparticles (e.g., protein-complexes or virus-like particles)[14–16].

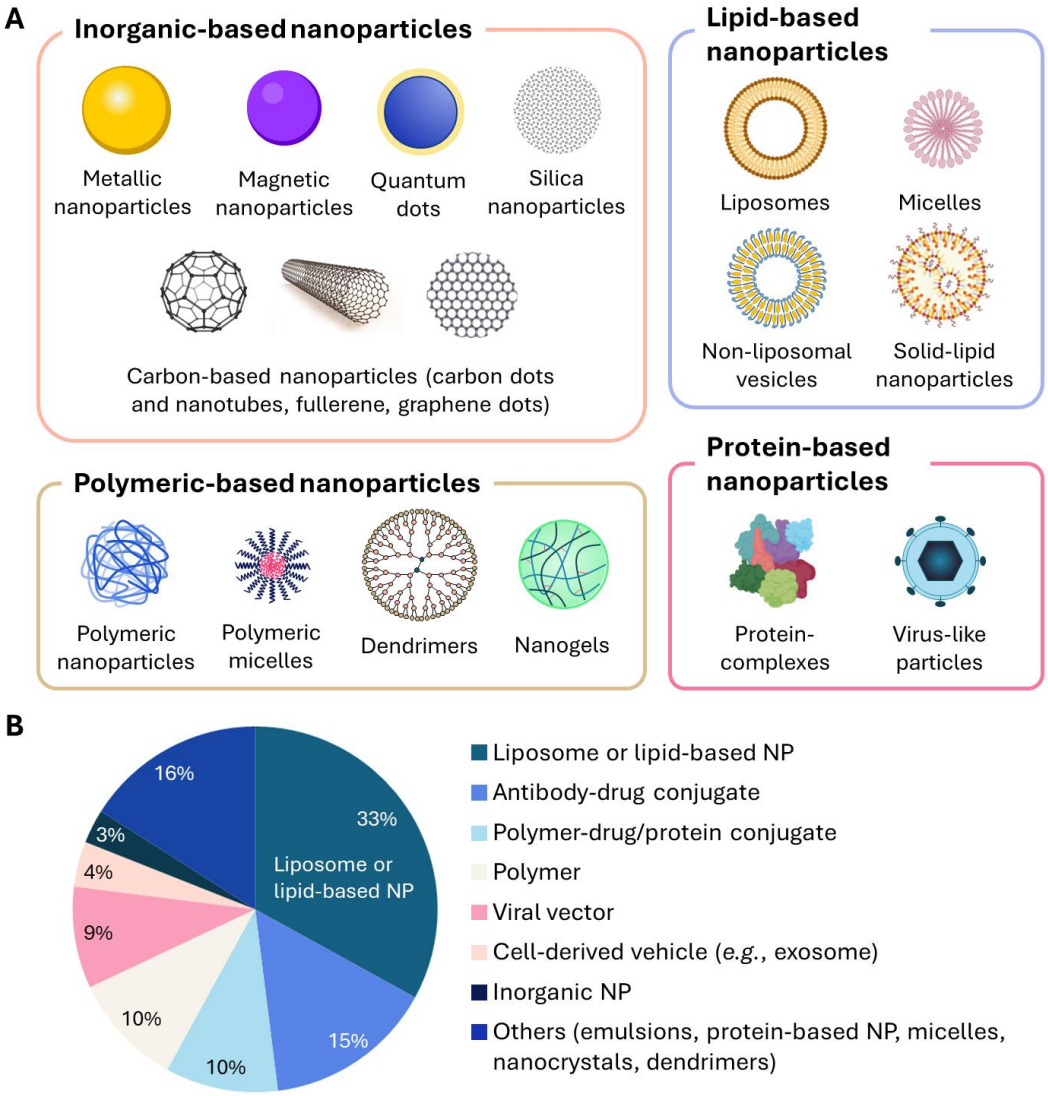


Figure 1.2. **(A)** Scheme representing the different commonly used nanoparticle for drug delivery, classified depending on their composition. **(B)** Overview of nanomedicines accessible in the market or in clinical translation classed on type of nanoparticle. Adapted from Shan *et al.*[17].

Among all the different kind of NPs developed, as illustrated in **Figure 1.2B**, lipid-based NP are the most commonly used as drug delivery systems in nanomedicine due to their success in reaching to clinical phases and the market[17]. Beyond nanomedicine, lipid-based nanoparticles are also widely used in healthcare and cosmetic industries, which were among the earliest to recognize their benefits. Moreover, they are also employed in the food

industry and nutrition to deliver functional components such as proteins, enzymes, vitamins and flavors, or even to a lesser extent, in agricultural applications[18].

1.2. Vesicles as self-assembled structures for drug delivery

Vesicles are one of the most studied classes of lipid-based nanoparticles, and they can be described as self-assembled colloidal systems[19].

Molecular self-assembly is the spontaneous and reversible association of molecular species to form larger, more complex and ordered supramolecular entities. The success of self-assembly depends on different characteristics of the system: the components used, the interactions between them, the reversibility of the complex and the environment[20].

Normally, self-assembled colloids are formed by amphiphilic molecules, which possess a hydrophilic moiety (water-soluble) and a lipophilic moiety (organic-soluble)[21]. When they are in aqueous environments, their dual character promotes their association through weak, non-covalent interactions to form ordered assemblies thanks to the called *hydrophobic effect*: the hydrophobic part of the molecule minimize the contact with the aqueous environment being the hydrophilic moiety at the interface between them[22]. Different kind of aggregate shape can be observed, from spherical and rod-like micelles to planar bilayers and vesicles[21,22]. The form of the colloidal aggregate depends mainly on the amphiphile geometry, but the external environment, concentration of the monomers and the preparation method can also dictate the formation of the self-assembled structures.

Vesicles are formed by amphiphiles self-assembled in spherical membrane bilayers that enclose an aqueous compartment (**Figure 1.3**). They can be composed by different kind of molecules, including lipids, polymers and organic and inorganic small molecules. In the bilayer, the hydrophobic moieties (i.e., non-polar tails) form the core of the bilayer while the hydrophilic moieties (i.e., polar head groups) are exposed to the aqueous solution[21,23].

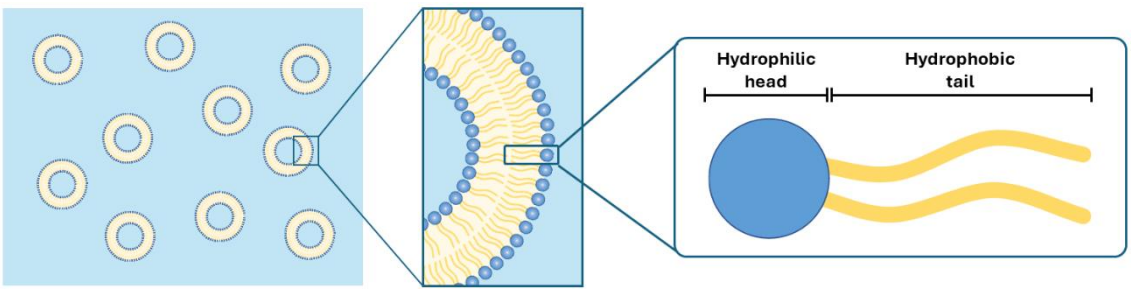


Figure 1.3. Scheme of the vesicles composed by the self-assembly of amphiphilic molecules in aqueous environments.

These colloids have been extensively used for drug delivery since they can entrap both hydrophobic compounds within the bilayers (lipidic compartment) and hydrophilic compounds in the aqueous lumen. Furthermore, they can efficiently transport and protect the payloads within the body and deliver them to the target site.

Depending on the size and quantity of bilayers, vesicles can be classified in different categories: small unilamellar vesicles (SUVs, single bilayer and size diameter < 200 nm), large unilamellar vesicles (LUVs, single bilayer and size diameter 200–1000 nm), giant unilamellar vesicles (GUVs, single bilayer and size diameter > 1000 nm), multilamellar vesicles (MLVs, composed by more than one bilayer) and multivesicular vesicles (MVVs, containing small vesicles inside a larger one)[21,24].

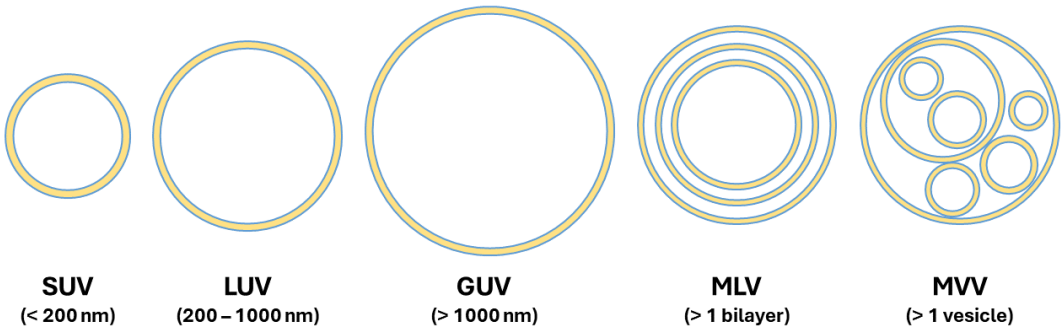


Figure 1.4. Schematic illustration of vesicles classified regarding their size and lamellarity: SUV, small unilamellar vesicles; LUV, large unilamellar vesicles; GUV, giant unilamellar vesicles; MLV, multilamellar vesicles; and MVV, multivesicular vesicles. Adapted from Grimaldi *et al*.[23].

1.2.1. Types of vesicular systems

Vesicles can be also grouped based on their membrane composition[23,25–27]. Some of the most studied vesicular systems are described in **Table 1.1**.

Among all the vesicular systems described previously, liposomes, basically formed by phospholipids, were the first to be discovered and are the most widely studied due to their biocompatibility and biodegradability. They allow the protection of sensitive molecules and a controlled permeation of the active ingredients in the target site, providing greater efficiency than the payloads alone[28,29]. Nevertheless, liposomes present some drawbacks regarding the physicochemical properties and stability, which affect their reproducibility and limit their applications[30–32].

Table 1.1. List of different developed vesicular systems. Adapted from Zafar *et al.*[25].

Vesicular system	Composition	Description	Limitations
Liposomes	Phospholipids (Cholesterol)	Closed lipid bilayer membrane with an aqueous core	Chemical and physical instability Drug leakage Early clearance
Niosomes	Cholesterol Non-ionic surfactants	Vesicles composed by surfactants, cheaper and more stable than phospholipids	Physical instability Fusion and aggregation Drug leakage
Quatsomes	Cholesterol Cationic surfactants	Composed by quaternary ammonium surfactants and thermodynamically stable	Limited use of quaternary ammonium surfactants for some applications
Exosomes	Lipids Proteins	Extracellular vesicles	Low storage stability Low purity
Polymersomes	Amphipathic co-polymers	Composed by diblock or triblock co-polymers	Slow degradation times Higher toxicity in relation to liposomes
Transferosomes	Phospholipids Surfactants	Similar to liposomes but highly deformable and elastic	Chemical instability Low purity
Ethosomes	Phospholipids Alcohols	Vesicle containing phospholipids and high amounts of ethanol	Expensive Excipients can cause skin irritation

Another kind of delivery system are niosomes[33], vesicles composed of non-ionic surfactants and cholesterol. They are considered as liposome analogues with improved physicochemical properties and lower material cost, although short stability due to aggregation, fusion swelling and drug leakage problems have been reported[34,35].

On the other hand, *quatsomes*, a particular type of nanovesicles (NVs) formed by self-assembly of cholesterol molecules and quaternary ammonium surfactants, are potential delivery systems for pharmaceutical ingredients because of their outstanding physicochemical properties and long-term stability due to their thermodynamically stable nature[36]. They present high homogeneity in size and unilamellarity, they are stable up to three years, and their morphology is maintained upon temperature or dilution. Both components can self-assemble in a bimolecular synthon that acts as a single entity to form the nanovesicular membrane (**Figure 1.5**).

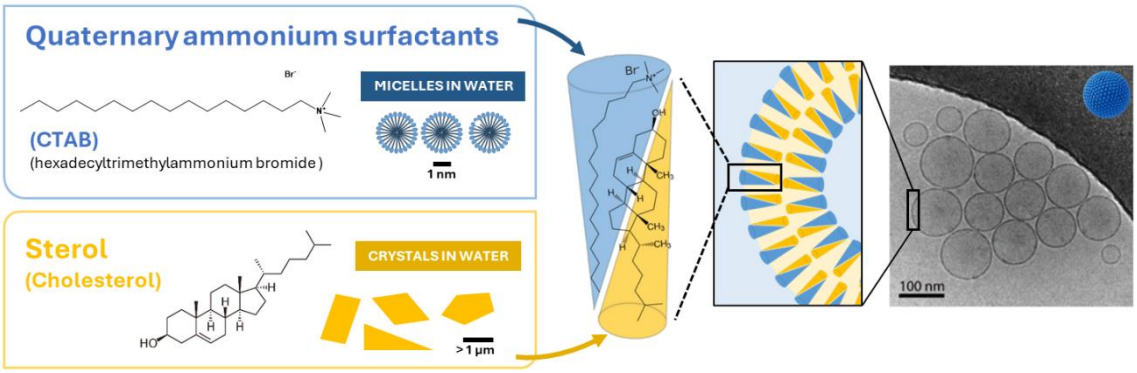


Figure 1.5. Schematic representation of *quatsomes* composed by cholesterol and CTAB. From left to right: molecular structures of both components with a scheme of each component in water. Schematic of the organization of the CTAB-cholesterol synthon and its organization forming a membrane. Adapted from Ferrer-Tasies *et al*.[37].

They were first developed by Nanomol group (Institut de Ciència de Materials de Barcelona, ICMAB-CSIC) and during the last years they have been extensively used either by Nanomol group and Nanomol Technologies S.L. for pharmaceutical and bioimaging applications[38–40]. So far, different payloads have been successfully integrated: hydrophobic fluorescent dyes (e.g., carbocyanine, diketopyrrolopyrroles, fluorenyl and squaraine dyes)[41–44], hydrophilic molecules (e.g., fluorescein) and large biomolecules such as recombinant human-epidermal growth factor (rh-EGF)[45] and oligonucleotides[46].

Nevertheless, although the use of quaternary ammonium surfactants in pharmaceutical industry is accepted for topical applications by the regulatory agencies, their use in skin delivery for other markets such as healthcare and cosmetic applications is limited[47].

Moreover, other types of NVs have been developed during the last decades[23,25,26]. Some examples are listed in **Table 1.1**, like exosomes, naturally occurring NVs which lately have been a trending topic in pharma applications[48], or transferosomes[49] and ethosomes[50], liposomes-derived NVs designed to enhance skin permeation. All of them have their advantages and limitations, but the research has not stopped to open multiple possibilities looking for the most suitable option depending on the payload and delivery route.

Nevertheless, the search for new components to form novel formulations of vesicles is not neither simple nor obvious. As explained at the beginning of **Section 1.2**, the success of self-assembly to form vesicles depends on several characteristics of the systems: the components used, the interactions between them, the reversibility of the complex and the environment. All of them must be aligned to finally obtain self-assembled stable vesicles, which is more complex than just mixing different amphiphilic molecules together.

1.3. Methods for the preparation of nanovesicles

The optimal performance of a nanovesicular formulation is closely related to their structural characteristics, i.e., shape, size, surface properties, lamellarity and homogeneity. At the same time, all these parameters are highly influenced by the preparation method (**Table 1.2**).

Table 1.2. List of manufacturing technologies for vesicle preparation.

Manufacturing procedure	Scalability	Environmental impact[a)]
Thin film hydration	Difficult (complex design)	
Reverse phase evaporation	Difficult (complex design)	
Extrusion	Difficult (complex design)	
Microfluidics	Moderate (complex design, blocking, scale-out)	
DELOS	Easy (simple design, easy control)	

[a)] ***Environmental impact:*** *red = high impact due to toxic solvents, high temperature; yellow = moderate impact, use of not so toxic solvents; green = low impact, minimal energy required, no pollution or toxics generated.*

There are a series of conventional methods that are widely used at bench-scale and even some of them at industrial scale for the preparation of vesicles. Some examples are thin film hydration, solvent injection or reverse-phase evaporation[51,52]. However, the use of conventional methods to prepare nanovesicles is normally associated with poor homogeneity of the nanoformulations leading to post-processing steps that are time-consuming and difficult to scale up[52,53]. Additionally, these methods usually require large quantities of organic solvents, which are associated to toxic residues that are challenging to remove[54].

For these reasons, the development of new methodologies for the preparation of nanovesicular systems became necessary. They need to be easy scalable processes, provide a better control over the characteristics of the systems obtained, and be environmentally friendly.

Up to now, microfluidics and compressed fluid-based technologies are two of the main alternatives to conventional methods. In the case of microfluidics, the final vesicular formulations do not require post-processing steps and can be manufactured at large scale in continuous mode. Still, scalability capacity is limited due to the dependency of geometry

and flow with the physicochemical properties of the vesicles produced. To solve this problem, nowadays the solution has been the scale-out approach, i.e., increasing the equipment units to increase the production capacity[51]. On the contrary, the use of technologies based on compressed fluids (CF) are one of the most promising alternatives due to its easy scalability among other benefits.

1.3.1. DELOS method for the preparation of nanovesicles

CF-based technologies are efficient and environmental respectful methods for the preparation of micro- and nanoparticulate materials on an industrial scale[55]. They make use of the properties of CF to replace the conventional organic solvents[56].

In fact, these technologies benefit from supercritical fluids properties (highly-compressed fluids), which is a state of the matter reached above its critical pressure and temperature (P_C and T_C) and where the matter exhibits intermediate properties between those of the gases and the liquids[57]. As gases, supercritical fluids present low viscosity and high diffusivity, whereas as liquids, they show high density and solvating power. There is no phase boundary between the gas and the liquid phases, so with small pressure and temperature variations their properties can be adjusted from one state to the other[58].

Carbon dioxide (CO_2) is the most commonly used supercritical fluid for pharmaceutical applications since it is classified by the FDA as a safe solvent and non-toxic, it is inexpensive, non-flammable, recyclable and environmentally friendly. Furthermore, it has low T_C (31.1 °C) and P_C (7.38 MPa) (**Figure 1.6**)[57,58].

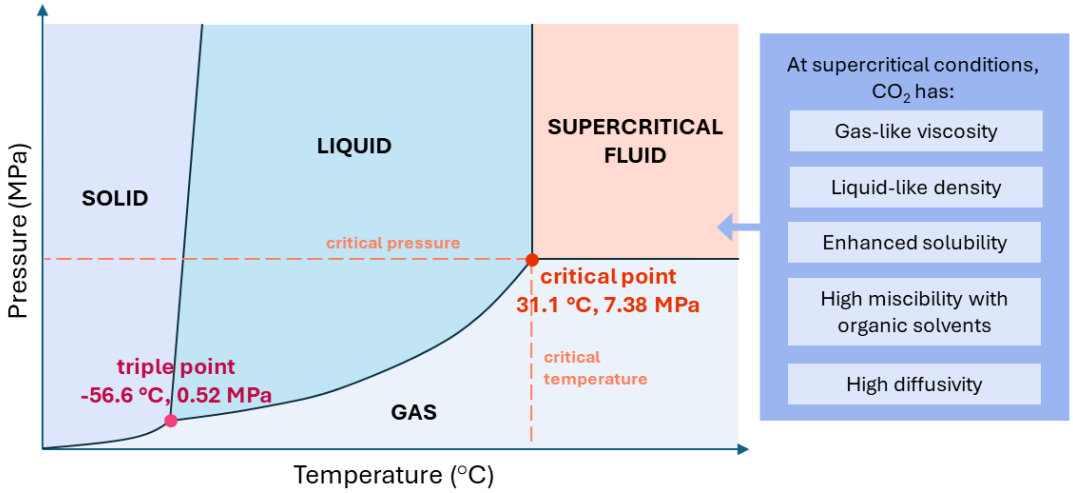


Figure 1.6. Phase diagram of carbon dioxide (not scaled) and its properties at supercritical conditions. Adapted from Soh *et al.*[55].

Different CO_2-based methodologies have been implemented for the manufacturing of DSs which present improved homogeneity in terms of physicochemical properties, reduced number of process steps and reduction of organic solvent used. One of these novel methods based on compressed CO_2 is called Depressurization of an Expanded Organic Solution (DELOS), and it was developed by Nanomol group (ICMAB-CSIC) and it is currently owned, scaled-up and commercialized by Nanomol Technologies S.L.[59].

This process was first used to produce micro- and submicron-sized crystalline particles with high polymorphic purity[60,61]. Through this process, the solute to be crystallized is completely solubilized in a mixture of organic solvent and CO_2, which acts as a co-solvent since they are completely miscible at a given pressure and temperature[62,63].

Later, the DELOS method was improved for the manufacturing of colloidal suspensions. The process enables the preparation by just one step of multifunctional cholesterol-rich nanovesicles such as liposomes or other types of vesicles, as well as nanovesicle-(bio)active hybdrids[64–66]. DELOS process involves milder conditions of pressure and temperature (< 10 MPa and 35 °C) than other CFs-based methods, allowing the work with heat-labile compounds at the same time of reducing investment costs for the scale-up production.

Briefly, the DELOS procedure for the obtention of colloidal suspensions includes (**Figure 1.7**):

A. Loading of the solution containing the hydrophobic membrane components (lipids and surfactants) and the desired hydrophobic payloads in an organic solvent (e.g., ethanol) into a high-pressure vessel previously driven to the working temperature ($T_W \approx 35$ °C) and atmospheric pressure (**Figure 1.7A**).
B. Formation of a CO_2-expanded solution by the addition of liquid compressed CO_2 with the membrane components dissolved at $T_W \approx 35$ °C and working pressure $P_W \approx 10$ MPa (**Figure 1.7B**).
C. Lastly, depressurization of the CO_2-expanded solution over an aqueous phase containing the hydrophilic membrane components and hydrophilic payloads (**Figure 1.7C**). A flow of N_2 at $P_W \approx 11$ MPa is used to plunge the CO_2-expanded solution, maintaining a constant pressure inside the vessel during the depressurization. During this step, the expanded solution experiences a large, abrupt, and extremely homogenous cooling caused by CO_2 evaporation from the expanded solution. This phenomena could be a possible reason why this method produces more vesicle-to-vesicle homogeneity and supramolecular organization, in comparison to conventional procedures[65,66].

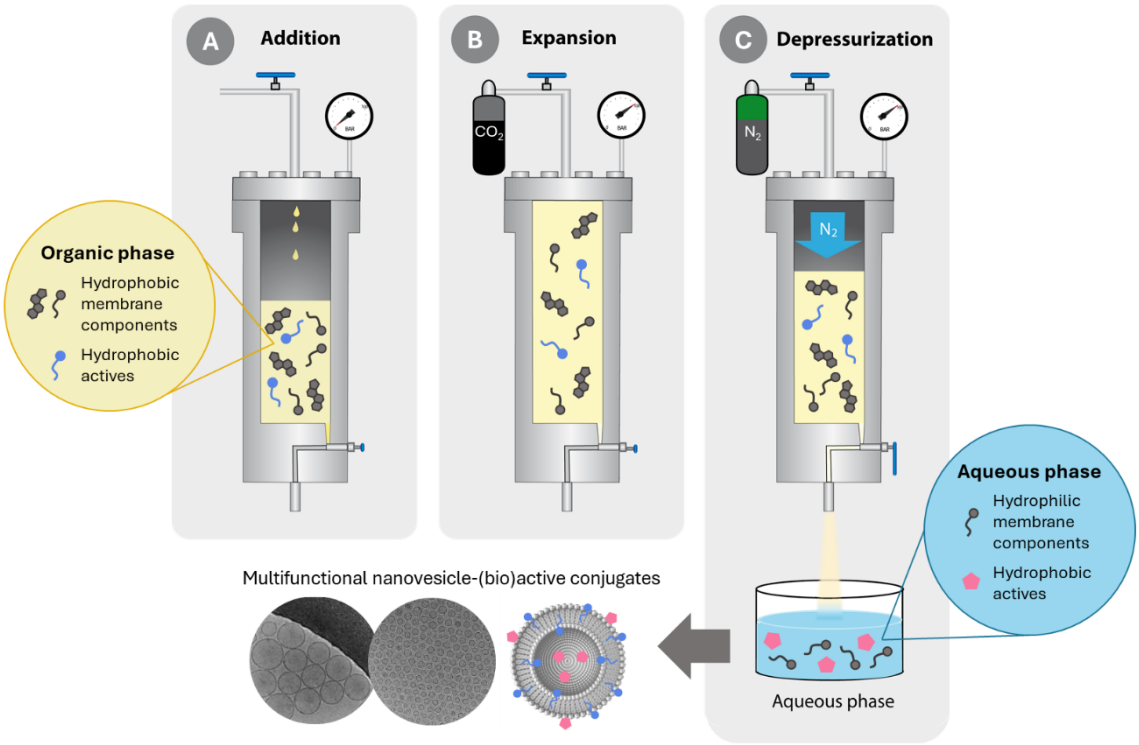


Figure 1.7. Schematic representation of DELOS method for the preparation of multifunctional nanovesicle-(bio)active hybrids incorporation different payloads (drugs, molecules for imaging, targeting agents, etc.). The three steps of the process are described in the text.

DELOS technology presents several advantages over conventional methods. First, it is a simple, robust and a scalable one-step process, essential attributes for scale-up translation. Additionally, conventional methods, considering that are multi-step processes, normally involve a specific stage to eliminate the organic solvent, which make difficult to obtain aqueous vesicular formulations rich in sterols content. In contrast, DELOS as it is a single-step process do not present this free-solvent state, thus allowing the incorporation of high amounts of sterols in vesicles and enabling the stabilization of highly lipophilic molecules[66,67].

1.4. Topical delivery as administration route

Topical delivery is defined as the application of an active molecule contained in a formulation to the skin[68]. With respect to other administration routes, topical delivery is convenient and easy to apply, bringing better user compliance and self-application. Furthermore, it is possible to deliver the payloads selectively to specific areas (e.g., in pharmaceutical applications wounds, skin diseases or infections, in healthcare and cosmetics specific sites such as face skin, body skin, lips or hair)[68,69].

The skin is the largest accessible organ of the human body. It is a membranous and flexible cover with protective function that is formed by three main layers: epidermis, dermis and hypodermis (**Figure 1.8**).

Epidermis is the external layer, composed mainly by keratinocytes cells, and it is not vascularized. It is divided in different sublayers, and the outermost is called stratum corneum (SC), formed by bands of dead keratinocytes called corneocytes, and an extracellular lipid-rich environment with a 40% of lipids, 40% of protein, and just a 20% of water[69,70]. The SC is a dynamic barrier in continuous renewal with a main function: protection against external environment such as infection, dehydration, chemical and mechanical stress[71,72]. Below the SC, there are more strata of viable keratinocytes. Underneath epidermis, there is the second layer of the skin called dermis. It is a vascularized tissue containing fibroblast among other types of cells with a network of blood and lymphatic vessels, hair follicles and sweat glands. The main components of the extracellular matrix of dermis are collagen, elastin and proteoglycans[73]. The last layer of the skin is the hypodermis, basically composed of adipocyte-subcutaneous fatty tissue[70].

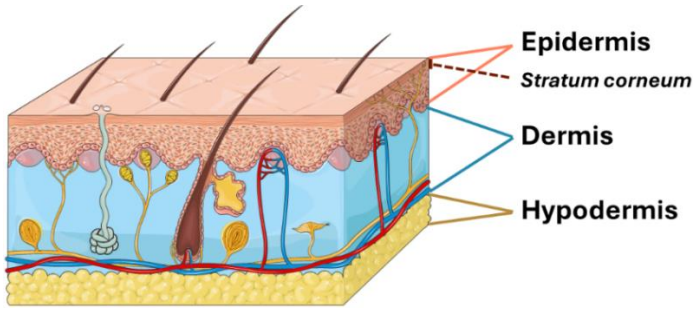


Figure 1.8. Illustration of human skin layers: epidermis, dermis and hypodermis. Adapted from *Servier Medical Art*[74].

Although topical application as administration route can be user friendly, due to the main function of the skin, acting as a physical barrier, sometimes the permeation of certain payloads can be challenging. Due to the composition and structure of SC, lipophilicity and molecular weight of the molecules are important parameters that can determine if a molecule is able or not to cross the SC. It has been seen that large (> 500 Da) or polar molecules have difficulties to permeate through the skin[69,71,72].

Due to these limitations, delivery systems have arisen as a potential solution to overcome the permeation problems of some payloads, enhancing efficacy and tolerability of topical formulations[68]. Vesicular systems can be suitable for topical delivery since they are soft and

flexible materials[75]. Different types of vesicles such as liposomes, niosomes or ethosomes, listed in **Section 1.2.1**, have been successfully used to enhance skin permeation of several molecules[75–77]. Physicochemical properties of the vesicles are important parameters to consider to enhance skin permeation: surface charge, particle size, in addition to the type of lipid, surfactant and concentration play an important role on the efficiency of the permeation[70,72]. For example, particles over 600 nm are not able to delivery molecules into the deeper layers of the skin, while particles below 300 nm are capable[70,78].

The transport across the SC can be generally distinguished between two pathways (**Figure 1.9**): transepidermal, i.e., between interspace of epidermis cells (intercellular) or by the epidermis cells (transcellular), which are the main pathways; and transappendageal, i.e., through hair follicles or sweat conducts[79,80]. In the case of delivery systems like vesicles, the mechanisms of transport through the skin are the same, but it has to be also considered the effect of the membrane components to the skin since they can act as permeation enhancers for example increasing the fluidity of the SC and thus, the skin permeability[75,76].

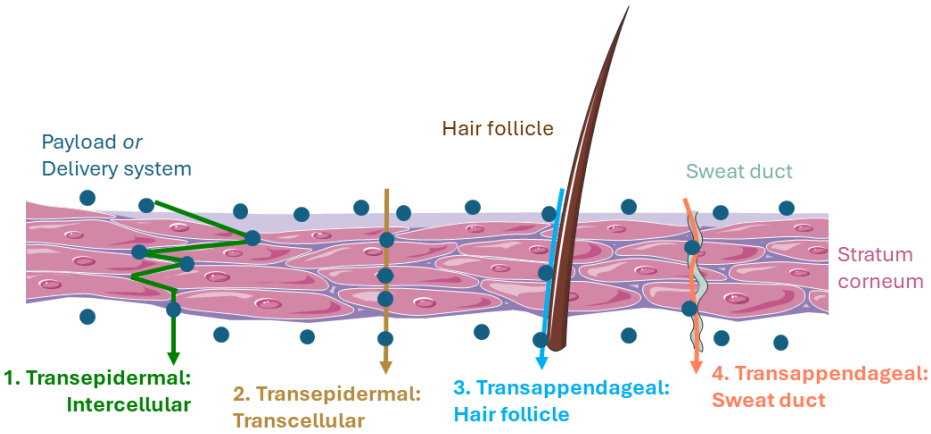


Figure 1.9. Scheme of transdermal delivery mechanisms of payloads and delivery systems through the stratum corneum. Adapted from *Servier Medical Art*[74].

1.5. The use of delivery systems in cosmetics

One of the main applications of delivery systems is their pharmaceutical use either for therapeutic or diagnostic applications. Still, besides medical applications delivery systems are also used in other markets, and in the last decades they have boomed in the healthcare and cosmetic sector.

Cosmetic industry was, indeed, pioneer in the use of delivery systems, in particular of liposomal formulations, which offered at that time enhanced stability and efficacy of

formulations at the same time that increased permeation of the ingredients into the skin[73]. The first cosmetic product containing liposomes was introduced by Dior in 1986 and was named Capture, which contained thymus extract, collagen and elastin peptides with hyaluronic acid in soya lecithin liposomes[18]. From that moment, different delivery systems have been used to topically deliver different kind of molecules: vitamins, amino acids, minerals, plant extracts or proteins.

The use of delivery systems for cosmetic applications commonly aims to enhance efficacy of the product, reduce the quantities of active ingredients to either decrease the product cost or avoid risks associated with skin toxicity or irritancy, increase the permeation of the active substance or purely for marketing strategies looking for more innovative products[81]. They are incorporated in a wide type of forms, from antiwrinkle, moisturizing or skin whitening creams to hair repairing shampoos or hair serums[82].

With regard to the type of delivery systems used in the cosmetic industry, several kinds of carriers are used. For example, solid lipid NPs, which are composed of a lipidic core surrounded by a single layer of a surfactant and can stabilize lipophilic substances in aqueous formulations[81]. Marketed formulations of solid lipid NPs are, for instance, Allure Body Cream of Chanel which is a body moisturizer or Cutanova Cream NanoVital Q10 of Dr. Rimpler for antiaging and skin repair[18,82]. Another type of carrier used in cosmetics are nanoemulsions. They are dispersions of an oil phase and a water phase stabilized with surfactants which provide a rapid permeation across the skin. They are applied in a diverse range of products and some examples are Bepanthol-Protect Facial Cream Ultra of Bayer HealthCare for moisturizing, antiaging and antipollution or Coco Mademoiselle Fresh Moisture Mist of Chanel to prolong fragrance effect[82]. Polymeric carriers are also used for cosmetic applications. Natural polymers such as cellulose, chitosan or protein-derived polymers are widely used for their low toxicity. Nanocapsules are one type of polymeric particles and some marketed product containing this type of carrier are the sunscreen of Lancome, Soleil Instant Cooling Sun Spritz SPF 15, or the antiaging Eye Contour Nanolif from Euoko[80,81].

Among all these types of delivery systems used for dermocosmetics, vesicular systems are also among the most exploited carriers. Liposomes, niosomes and ethosomes are examples of marketed products, and some examples are listed in **Table 1.3**. In cosmetics, liposomes are also the most common systems. They are usually composed of phospholipids of vegetal origin and they are loaded with vitamins, fragrances or botanical extracts to formulate in different forms, e.g., body sprays, deodorants, creams or sunscreens[82]. But although they are

biocompatible, biodegradable and can increase the efficacy of the products, they have a high production cost and low physical and chemical stability. Hence, other vesicular systems have been also imposed. Ethosomes are a type of liposomes with high concentration of ethanol, which increase the elasticity of the vesicle membrane and also can disturb the SC, both enhancing the permeation of the vesicles[18,73]. Niosomes are another type of vesicles without phospholipids, composed of cholesterol and non-ionic surfactants. They were developed and patented by L'Oréal to find an alternative to liposomes at 1970 and nowadays they are present in several cosmetic products[82].

Table 1.3. Marketed vesicular systems in cosmetic formulations. Adapted from Kaul *et al*. [82] and Tenchov *et al*.[18].

Vesicular system	Product name	Manufacturer	Activity claims
Liposomes	Capture Totale	Dior	Antiaging and skin repair
	Advanced Night Repair Protective Recovery Complex	Estée Lauder	Skin repair
	Future Perfect Skin Gel	Estée Lauder	Anti-wrinkle
	Dermosome	Microfluidics	Skin moisturizer
	Russel Oganics Liposome Concentrate	Russell Organics	Skin moisturizer
	Kerstin Florian Rehydrating Liposome Day Crème	Kerstin Florian	Skin moisturizer
	Decorte Moisture Liposome Face Creaam	Decorte	Skin moisturizer
	Decorte Moisture Liposome Eye Creaam	Decorte	Skin moisturizer, conditioner
	C-Vit Liposomal Serum	Sesderma	Skin moisturizer, conditioner
	Natural Progesterone Liposomal Skin Cream	NOW Solutions	Skin conditioner
	Clinicians Complex Liposome Face & Neck Lotion	Clinicians Complex	Skin conditioner
	Fillderma Lips Lip Voluminzer	Sesderma	Lip volumizer
Ethosomes	Decorin Cream	Genome Cosmetics	Antiaging and skin repair
	Nanominox	Sinere	Hair growth stimulant
	Cellulite EF	Hampden Health	Anti-cellulite
	Skin Genuity	Physonics	Anti-cellulite
	Lipoduction	Osmotics	Anti-cellulite

Vesicular system (Cont.)	Product name	Manufacturer	Activity claims
Niosomes	Niosome+ Perfected Age Treatment	Lancôme	Anti-wrinkle
	Niosome+	Lancôme	Anti-wrinkle
	Anti-Age Response Cream	Simply Man Match	Anti-wrinkle
	Mayu Niosome Base Cream	Laon Cosmetics	Skin moisturizer
	Identik Masque Floral Repair	Identik	Hair repair
	Identik Shampooing Floral Repair	Identik	Hair repair
	Eusu Niosome Makam Pom Whitening Facial Cream	Eusu	Skin whitener

1.5.1. Regulation of nanotechnology in cosmetic industry

Over the last decades nanotechnology has caused a progress in many aspects of our daily life, including the healthcare and cosmetic routines. As it has been reported in the above sections, it has also impacted in the field of topical delivery trough nanocarriers and delivery systems, enhancing absorption, solubility and shelf life of products. Nonetheless, nanotechnology has also generate some concern in the society due to the toxic effect of some nanomaterials either to health or environment[83]. In consequence, all the countries worldwide have regulated the introduction of nanomaterials in cosmetic products, considering also that the security requirements for their approval by the authorities and commercialization are more lax than for pharmaceutical applications[82].

Focusing on the European Union, its regulation defines a nanomaterial in cosmetic products as *"an insoluble or biopersistent and intentionally manufactured material"* and also adds that *"a nanomaterial has one or more external dimensions, or an internal structure, on the scale from 1 to 100 nm"*[84]. Based on the European regulation, cosmetic products containing nanomaterials other than colourants, preservatives and UV-filters are subject to additional procedures and if the safety of a nanomaterial is not ensured, a scientific committee has to perform a risk assessment to finally approve or not the product. Furthermore, nanomaterials must be specially labelled with the word "nano" in brackets after the name of the substance[84].

It seems to be a consensus in regulation that nanomaterials are on the scale from 1 to 100 nm. It is important to take into account that delivery systems can be above this range

between the 100 – 1000 nm, and thus not being considered as nanomaterials. In any case, a proper characterization of the delivery systems must be carried out to determine the physicochemical properties of novel carriers and evaluate in which frame of the regulation they fit in, although it is also interesting to do in any case a complementary toxicological assessment.

1.5.2. Prospects and challenges of delivery systems in the cosmetic industry

The cosmetics industry is an extremely dynamic market. Manufacturers are always looking for innovation and focusing on the obtention of high value-added products[81]. Furthermore, consumers have become extremely aware of the products that they use in terms of quality, efficiency and safety[85]. For these reasons, over the last years several products containing different types of delivery systems have been developed, but new strategies and carriers must be implemented continuously to innovate. These days, marketing trends are turning towards natural and green cosmetics, i.e., cosmetics based on plant and fruit extracts and concentrates. Additionally, consumers also look for environmental protection and sustainable products. Globally, the newest trends in cosmetic development are based on the search of natural ingredients, which also includes the composition of delivery systems if they want to be used[85].

Thus, there is a challenge to find new delivery systems composed of plant-based ingredients, while at the same time obtaining robust carriers that can overcome the limitations of the actual systems found in the market such as the physical and chemical instability or the expensive raw materials. Additionally, this search of new components that meet the necessities of the market must be paired with a sustainable manufacturing process able to be scaled up.

Therefore, in the present Thesis, the formulation of new vesicular delivery systems based on sterols and surfactants, both from vegetal origin, has been evaluated using DELOS methodology. The development of this new platform of nanovesicles and the evaluation of its versatility as a novel delivery systems platform is deeply described in the following chapters.

1.6. Bibliography

1. K. Park. Controlled drug delivery systems: Past forward and future back. *J. Control. Release* **2014**, 190, 3–8.
2. K.K. Jain. An Overview of Drug Delivery Systems. In *Drug Delivery Systems*; Methods in Molecular Biology, **2020**; Vol. 2059, pp 1–54.
3. S. Adepu, S. Ramakrishna. Controlled drug delivery systems: Current status and future directions. *Molecules* **2021**, 26, 5905.
4. W. Poon, B.R. Kingston, B. Ouyang, W. Ngo, W.C.W. Chan. A framework for designing delivery systems. *Nat. Nanotechnol.* **2020**, 15, 819–829.
5. A.S. Hoffman. The origins and evolution of "controlled" drug delivery systems. *J. Control. Release* **2008**, 132, 153–163.
6. A. Zaffaroni. Bandage for administering drugs. US3598122A, 1969.
7. F. Theeuwes, T. Higuchi. Osmatic dispersing device for releasing beneficial agent. US3845770A, 1972.
8. A.S. Huffman, A. Afrassiabi, L.C. Dong. Thermally reversible hydrogels: II. Delivery and selective removal of substances from aqueous solutions. *J. Control. Release* **1986**, 4, 213–222.
9. L. Dong, A.S. Hoffman. A novel approach for preparation of pH-sensitive hydrogels for enteric drug delivery. *J. Control. Release* **1991**, 15, 141–152.
10. R.A. Siegel, M. Falamarzian, B.A. Firestone, B.C. Moxley. pH-Controlled release from hydrophobic/polyelectrolyte copolymer hydrogels. *J. Control. Release* **1988**, 8, 179–182.
11. J.S. Kent, D.H. Lewis, L.M. Sanders, T.R. Tice. Microencapsulation of water soluble active polypeptides. US4675189A, 1987.
12. L.R. Beck, D.R. Cowsar, D.H. Lewis, et al. A new long-acting injectable microcapsule system for the administration of progesterone. *Fertil. Steril.* **1979**, 31, 545–551.
13. W. Jiang, B.Y.S. Kim, J.T. Rutka, W.C.W. Chan. Advances and challenges of nanotechnology-based drug delivery systems. *Expert Opin. Drug Deliv.* **2007**, 4, 621–633.

14. G. Chen, I. Roy, C. Yang, P.N. Prasad. Nanochemistry and Nanomedicine for Nanoparticle-based Diagnostics and Therapy. *Chem. Rev.* **2016**, 116, 2826–2885.

15. B.H. Alshammari, M.M.A. Lashin, M.A. Mahmood, et al. Organic and inorganic nanomaterials: fabrication, properties and applications. *RSC Adv.* **2023**, 13, 13735–13785.

16. Z. Gu, A. Biswas, M. Zhao, Y. Tang. Tailoring nanocarriers for intracellular protein delivery. *Chem. Soc. Rev.* **2011**, 40, 3638–3655.

17. X. Shan, X. Gong, J. Li, et al. Current approaches of nanomedicines in the market and various stage of clinical translation. *Acta Pharm. Sin. B* **2022**, 12, 3028–3048.

18. R. Tenchov, R. Bird, A.E. Curtze, Q. Zhou. Lipid Nanoparticles from Liposomes to mRNA Vaccine Delivery, a Landscape of Research Diversity and Advancement. *ACS Nano* **2021**, 15, 16982–17015.

19. A.C. Apolinário, L. Hauschke, J.R. Nunes, L.B. Lopes. Lipid nanovesicles for biomedical applications: 'What is in a name'? *Prog. Lipid Res.* **2021**, 82, 101096.

20. G.M. Whitesides, M. Boncheva. Beyond molecules: Self-assembly of mesoscopic and macroscopic components. *Proc. Natl. Acad. Sci. U. S. A.* **2002**, 99, 4769–4774.

21. E. Elizondo, E. Moreno, I. Cabrera, et al. Liposomes and other vesicular systems: Structural characteristics, methods of preparation, and use in nanomedicine. *Prog. Mol. Biol. Transl. Sci.* **2011**, 104, 1–52.

22. R.S. Tu, M. Tirrell. Bottom-up design of biomimetic assemblies. *Adv. Drug Deliv. Rev.* **2004**, 56, 1537–1563.

23. N. Grimaldi, F. Andrade, N. Segovia, et al. Lipid-based nanovesicles for nanomedicine. *Chem. Soc. Rev.* **2016**, 45, 6520–6545.

24. A. Akbarzadeh, R. Rezaei-Sadabady, S. Davaran, et al. Liposome: Classification, preparation, and applications. *Nanoscale Res. Lett.* **2013**, 8, 102.

25. A. Zafar, Asim-ur-Rehman, N. Ahmed. Nanovesicles for target specific drug delivery. In *Applications of Nanovesicular Drug Delivery*; **2022**; pp 149–165.

26. Y. Ren, L. Nie, S. Zhu, X. Zhang. Nanovesicles-Mediated Drug Delivery for Oral Bioavailability Enhancement. *Int. J. Nanomedicine* **2022**, 17, 4861–4877.

27. A.K. Sharma, P. Prasher, A.A. Aljabali, et al. Emerging era of "somes": polymersomes

as versatile drug delivery carrier for cancer diagnostics and therapy. *Drug Deliv. Transl. Res.* **2020**, 10, 1171–1190.

28. L. Sercombe, T. Veerati, F. Moheimani, et al. Advances and challenges of liposome assisted drug delivery. *Front. Pharmacol.* **2015**, 6, 286.

29. C. Zylberberg, S. Matosevic. Pharmaceutical liposomal drug delivery: a review of new delivery systems and a look at the regulatory landscape. *Drug Deliv.* **2016**, 23, 3319–3329.

30. M. Grit, D.J.A. Crommelin. Chemical stability of liposomes: implications for their physical stability. *Chem. Phys. Lipids* **1993**, 64, 3–18.

31. A. V. Yadav, M.S. Murthy, A.S. Shete, S. Sakhare. Stability aspects of liposomes. *Indian J. Pharm. Educ. Res.* **2011**, 45, 402–413.

32. V.G.S. Sainaga Jyothi, R. Bulusu, B. Venkata, et al. Stability characterization for pharmaceutical liposome product development with focus on regulatory considerations: An update. *Int. J. Pharm.* **2022**, 624, 122022.

33. R. Muzzalupo, E. Mazzotta. Do niosomes have a place in the field of drug delivery? *Expert Opin. Drug Deliv.* **2019**, 16, 1145–1147.

34. S. Taymouri, J. Varshosaz. Effect of different types of surfactants on the physical properties and stability of carvedilol nano-niosomes. *Adv. Biomed. Res.* **2016**, 5, 1–16.

35. Z. Ertekin, Z. Bayindir, N. Yuksel. Stability Studies on Piroxicam Encapsulated Niosomes. *Curr. Drug Deliv.* **2015**, 12, 192–199.

36. M. Köber, S. Illa-Tuset, L. Ferrer-Tasies, et al. Stable nanovesicles formed by intrinsically planar bilayers. *J. Colloid Interface Sci.* **2023**, 631, 202–211.

37. L. Ferrer-Tasies, E. Moreno-Calvo, M. Cano-Sarabia, et al. Quatsomes: Vesicles formed by self-assembly of sterols and quaternary ammonium surfactants. *Langmuir* **2013**, 29, 6519–6528.

38. G. Vargas-Nadal, M. Muñoz-Ubeda, P. Alamo, et al. MKC-Quatsomes: a stable nanovesicle platform for bio-imaging and drug-delivery applications. *Nanomedicine Nanotechnology, Biol. Med.* **2020**, 24, 102136.

39. G. Vargas Nadal. Novel Quatsome nanovesicles, prepared using CO2, for the

development of advanced nanomedicines, Universitat de Barcelona, **2020**.

40. L. Ballell i Hosa. Translation of DELOS nanovesicle formulations into new pharmaceutical candidates, Universitat Autònoma de Barcelona, **2022**.

41. A. Ardizzone. New fluorescent nanovesicles, by self-assembly of organic fluorophores, sterols and surfactants, as probes for bioimaging, Universitat Autònoma de Barcelona, **2017**.

42. J. Morla-Folch, G. Vargas-Nadal, T. Zhao, et al. Dye-Loaded Quatsomes Exhibiting FRET as Nanoprobes for Bioimaging. *ACS Appl. Mater. Interfaces* **2020**, 12, 20253–20262.

43. X. Liu, A. Ardizzone, B. Sui, et al. Fluorenyl-Loaded Quatsome Nanostructured Fluorescent Probes. *ACS Omega* **2017**, 2, 4112–4122.

44. N. Bordignon, M. Köber, G. Chinigò, et al. Quatsomes Loaded with Squaraine Dye as an Effective Photosensitizer for Photodynamic Therapy. *Pharmaceutics* **2023**, 15, 902.

45. L. Ferrer-Tasies, H. Santana, I. Cabrera-Puig, et al. Recombinant Human Epidermal Growth Factor/Quatsome Nanoconjugates: A Robust Topical Delivery System for Complex Wound Healing. *Adv. Ther.* **2021**, 4, 1–14.

46. A. Boloix, N. Feiner-Gracia, M. Köber, et al. Engineering pH-Sensitive Stable Nanovesicles for Delivery of MicroRNA Therapeutics. *Small* **2021**, 18, 2101959.

47. Y. Jiao, L. na Niu, S. Ma, et al. Quaternary ammonium-based biomedical materials: State-of-the-art, toxicological aspects and antimicrobial resistance. *Prog. Polym. Sci.* **2017**, 71, 53–90.

48. R. Kalluri, V.S. LeBleu. The biology, function, and biomedical applications of exosomes. *Science (80-.).* **2020**, 367, 6478.

49. N. Matharoo, H. Mohd, B. Michniak-Kohn. Transferosomes as a transdermal drug delivery system: Dermal kinetics and recent developments. *WIREs Nanomed Nanobiotechnol* **2024**, 16, e1918.

50. A. Jafari, S. Daneshamouz, P. Ghasemiyeh, S. Mohammadi-Samani. Ethosomes as dermal/transdermal drug delivery systems: applications, preparation and characterization. *J. Liposome Res.* **2023**, 33, 34–52.

51. J. Tomsen-melero, J. Merlo-mas, A. Carreño, et al. Liposomal formulations for treating lysosomal storage disorders. *Adv. Drug Deliv. Rev.* **2022**, 190, 114531.

52. S. Shah, V. Dhawan, R. Holm, M.S. Nagarsenker, Y. Perrie. Liposomes: Advancements and innovation in the manufacturing process. *Adv. Drug Deliv. Rev.* **2020**, 154–155, 102–122.

53. P. Liu, G. Chen, J. Zhang. A Review of Liposomes as a Drug Delivery System: Current Status of Approved Products, Regulatory Environments, and Future Perspectives. *Molecules* **2022**, 27, 1372.

54. L.A. Meure, N.R. Foster, F. Dehghani. Conventional and Dense Gas Techniques for the Production of Liposomes: A Review. *AAPS PharmSciTech* **2008**, 9, 798–809.

55. S.H. Soh, L.Y. Lee. Microencapsulation and Nanoencapsulation Using Supercritical Fluid (SCF) Techniques. *Pharmaceutics* **2019**, 11, 21.

56. P. Trucillo, R. Campardelli, E. Reverchon. Liposomes: From bangham to supercritical fluids. *Processes* **2020**, 8, 1022.

57. B. William, P. Noémie, E. Brigitte, P. Géraldine. Supercritical fluid methods: An alternative to conventional methods to prepare liposomes. *Chem. Eng. J.* **2020**, 383, 123106.

58. I. Pasquali, R. Bettini. Are pharmaceutics really going supercritical? *Int. J. Pharm.* **2008**, 364, 176–187.

59. N. Ventosa, J. Veciana, S. Sala, M. Cano. Method for obtaining micro- and nano-disperse systems. WO2006/079889, 2006.

60. S. Sala, A. Córdoba, E. Moreno-Calvo, et al. Crystallization of Microparticulate Pure Polymorphs of Active Pharmaceutical Ingredients Using CO2-Expanded Solvents. *Cryst. Growth Des.* **2012**, 12, 1717–1726.

61. S. Sala, E. Elizondo, E. Moreno, et al. Kinetically driven crystallization of a pure polymorphic phase of stearic acid from CO2-expanded solutions. *Cryst. Growth Des.* **2010**, 10, 1226–1232.

62. N. Ventosa, S. Sala, J. Veciana, J. Torres, J. Llibre. Depressurization of an Expanded Liquid Organic Solution (DELOS): A New Procedure for Obtaining Submicron- Or Micron-Sized Crystalline Particles. *Cryst. Growth Des.* **2001**, 1, 299–303.

63. N. Ventosa, S. Sala, J. Veciana. DELOS process: A crystallization technique using compressed fluids - 1. Comparison to the GAS crystallization method. *J. Supercrit. Fluids* **2003**, 26, 33–45.

64. M. Cano-Sarabia, N. Ventosa, S. Sala, et al. Preparation of uniform rich cholesterol unilamellar nanovesicles using CO2-expanded solvents. *Langmuir* **2008**, 24, 2433–2437.

65. E. Elizondo, J. Veciana, N. Ventosa. Nanostructuring molecular materials as particles and vesicles for drug delivery, using compressed and supercritical fluids. *Nanomedicine* **2012**, 7, 1391–1408.

66. I. Cabrera, E. Elizondo, O. Esteban, et al. Multifunctional nanovesicle-bioactive conjugates prepared by a one-step scalable method using CO2-expanded solvents. *Nano Lett.* **2013**, 13, 3766–3774.

67. E. Elizondo, J. Larsen, N.S. Hatzakis, et al. Influence of the preparation route on the supramolecular organization of lipids in a vesicular system. *J. Am. Chem. Soc.* **2012**, 134, 1918–1921.

68. I.K. Tadwee, S. Gore, P. Giradkar. Advances in Topical Drug Delivery System: A Review. *Int. J. Pharm. Res. Allied Sci.* **2011**, 1, 14–23.

69. M. Sharadha, D. V. Gowda, N. Vishal Gupta, A.R. Akhila. An overview on topical drug delivery system – updated review. *Int. J. Res. Pharm. Sci.* **2020**, 11, 368–385.

70. N.G. Kotla, B. Chandrasekar, P. Rooney, et al. Biomimetic Lipid-Based Nanosystems for Enhanced Dermal Delivery of Drugs and Bioactive Agents. *ACS Biomater. Sci. Eng.* **2017**, 3, 1262–1272.

71. M.S. Roberts, H.S. Cheruvu, S.E. Mangion, et al. Topical drug delivery: History, percutaneous absorption, and product development. *Adv. Drug Deliv. Rev.* **2021**, 177, 113929.

72. M. Cui, C. Wiraja, S.W.T. Chew, C. Xu. Nanodelivery Systems for Topical Management of Skin Disorders. *Mol. Pharm.* **2021**, 18, 491–505.

73. S. Saraf, C.D. Kaur, A. Gupta, N. Verma. Skin targeting approaches in cosmetics. *Indian J. Pharm. Educ. Res.* **2019**, 53, 577–594.

74. SMART - Servier Medical ART https://smart.servier.com/ (accessed Apr 23, 2024).

75. B.A. Witika, L.L. Mweetwa, K.O. Tshiamo, et al. Vesicular drug delivery for the treatment of topical disorders: current and future perspectives. *J. Pharm. Pharmacol.* **2021**, 73, 1427–1441.

76. I.A. Chacko, V.M. Ghate, L. Dsouza, S.A. Lewis. Lipid vesicles: A versatile drug delivery platform for dermal and transdermal applications. *Colloids Surfaces B Biointerfaces* **2020**, 195, 111262.

77. J.J. Carreras, W.E. Tapia-Ramirez, A. Sala, et al. Ultraflexible lipid vesicles allow topical absorption of cyclosporin A. *Drug Deliv. Transl. Res.* **2020**, 10, 486–497.

78. D.D. Verma, S. Verma, G. Blume, A. Fahr. Particle size of liposomes influences dermal delivery of substances into skin. *Int. J. Pharm.* **2003**, 258, 141–151.

79. D. Ramadon, M.T.C. McCrudden, A.J. Courtenay, R.F. Donnelly. Enhancement strategies for transdermal drug delivery systems: current trends and applications. *Drug Deliv. Transl. Res.* **2022**, 12, 758–791.

80. H. Zhou, D. Luo, D. Chen, et al. Current advances of nanocarrier technology-based active cosmetic ingredients for beauty applications. *Clin. Cosmet. Investig. Dermatol.* **2021**, 14, 867–887.

81. A. Mihranyan, N. Ferraz, M. Strømme. Current status and future prospects of nanotechnology in cosmetics. *Prog. Mater. Sci.* **2012**, 57, 875–910.

82. S. Kaul, N. Gulati, D. Verma, S. Mukherjee, U. Nagaich. Role of Nanotechnology in Cosmeceuticals: A Review of Recent Advances. *J. Pharm.* **2018**, 2018, 1–19.

83. R. Yadwade, S. Gharpure, B. Ankamwar. Nano Express Nanotechnology in cosmetics pros and cons. *Nano Express* **2021**, 2, 22003.

84. European Commission. Nanomaterials - European Commission https://single-market-economy.ec.europa.eu/sectors/cosmetics/cosmetic-products-specific-topics/nanomaterials_en (accessed Apr 29, 2024).

85. N. Amberg, C. Fogarassy. Green consumer behaviour in cosmetic market. *Resources* **2019**, 8, 1–19.

2 Objectives

This Industrial Thesis is dedicated to the formulation of new vesicular systems for topical delivery in healthcare and cosmetic applications using plant-based, biocompatible and biodegradable components as buildings blocks, and using a robust, reproducible and sustainable manufacturing method.

Within this context, the following specific objectives have been addressed:

1. Design of new vesicular systems for dermocosmetic applications composed by the sterol β-sitosterol and alkyl polyglucosides surfactants as main building blocks. Characterization of their physicochemical properties and study of the impact of membrane composition on parameters such as particle size and homogeneity, surface charge, morphology or lamellarity.
2. Study of their role as versatile delivery systems integrating diverse payloads, from lipophilic and hydrophilic small molecules to large biomolecules like proteins.
3. Evaluation of their biological performance, in terms of biocompatibility with the skin using *in vitro* models and enhancement of skin permeation of a lipophilic fluorescent probe trough *ex vivo* evaluation.

4. Exploration of applications beyond healthcare and cosmetic industries, tuning the novel vesicular systems for pharmaceutical usage with the introduction of pegylated-cholesterol moieties and ionizable sterols to the vesicular formulations.

To accomplish the above listed objectives the methodological approach shown in **Figure 2.1** has been followed. The results obtained to achieve each specific objective are detailed in the corresponding following **Chapters**.

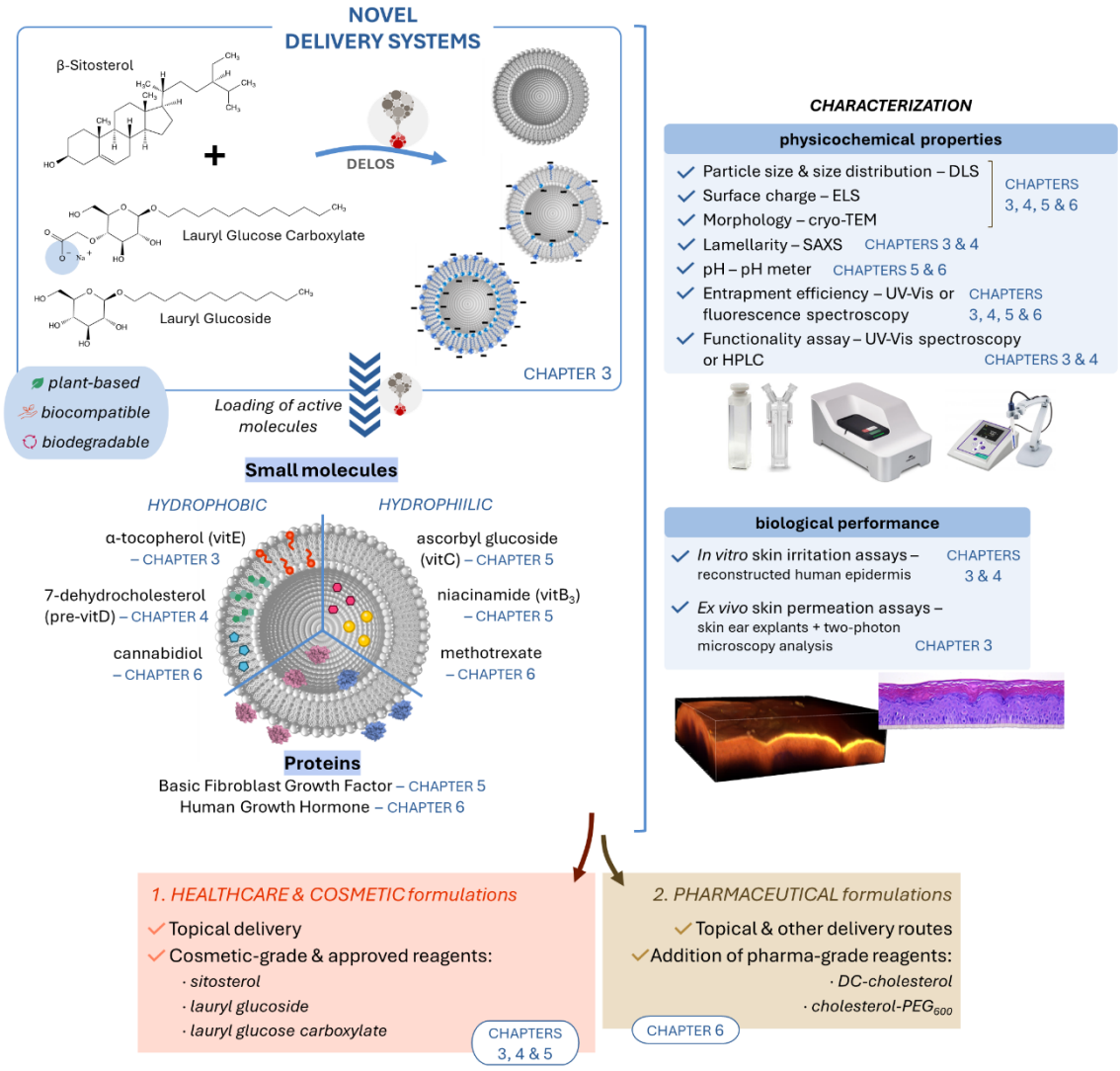


Figure 2.1. Methodological approach followed to completes the objectives of the present Doctoral Thesis.

Besides, in **Chapter 8** the reader can find the specific methodologies employed to fulfill this work, explained in depth.

New plant-based nanovesicles based on alkyl polyglucosides and β-sitosterol

3

3.1. The need of plant-based delivery systems

As explained in the introduction of this Thesis, different lipid-based delivery systems, and specially vesicles, have been extensively explored to be applied for pharmaceutical, healthcare and cosmetic use. Liposomes or niosomes are examples of vesicles present in pharmaceutical, cosmetic and nutraceutical marketed products, although they present some limitations regarding physical or chemical stability, drug leakage and reproducibility[1–5]. On the other hand, *quatsomes* are a type of vesicles composed of cholesterol and quaternary ammonium surfactants currently under advanced pharmaceutical development which have not arrived yet to the market. They present outstanding physicochemical properties and long-term stability due to their thermodynamically stable nature[6]. However, despite the use of quaternary ammonium surfactants is accepted for topical applications by the regulatory agencies in the pharmaceutical industry [7], their application in skin delivery for personal care and cosmetic usage is limited[8,9]. Additionally, the presence of cholesterol in personal care products, even if it is naturally occurring in all human tissues, has a negative perception by consumers, especially those aligned with current vegan trends[10,11].

To overcome these different problems, it is challenging to find alternative stable nanovesicle systems using non-animal derived membrane components that are also biocompatible and biodegradable.

*Thus, the work presented in this **Chapter** is focused on the development for the first time of novel stable vesicular systems based on plant-derived sterols and sugar-based surfactants, that not only are consumer-friendly, but also contribute to more sustainable manufacturing.* **Figure 3.1** *summarizes the approach followed to obtain these new vesicular systems.*

*In particular, β-sitosterol and alkyl polyglucosides were investigated in this Thesis as vesicle membrane components. Both compounds have been used independently in different delivery systems, but to our best knowledge, they have never been investigated in combination to achieve self-assembled vesicles. In this context, this **Chapter** is devoted to investigating the formation of small homogeneous vesicular systems by self-assembly of β-sitosterol and the alkyl polyglucosides surfactants lauryl glucoside and lauryl glucose carboxylate as the main building blocks. As described in the following sections, a new platform of nanovesicles using these plant-based compounds has been achieved and fully characterized in terms of size, stability, lamellarity and morphology. Furthermore, to prove their role as delivery systems, it has been evaluated the loading of a non-water-soluble active compound such as the antioxidant α-tocopherol, studying its functionality after loading. Finally, the biocompatibility of the most promising systems with the skin has been tested in vitro and ex vivo. First, in vitro irritancy assays with reconstructed human epidermis have been carried out. Then, the permeation of Nile red, a poorly water-soluble fluorophore, loaded in NVs through skin explants has been investigated using two-photon microscopy.*

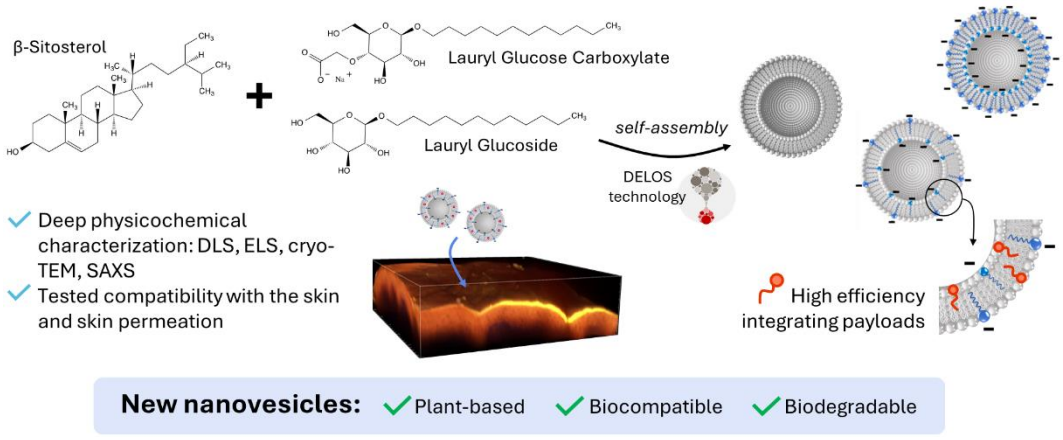


Figure 3.1. Graphical summary of the work described in **Chapter 3**.

3.1.1. β-Sitosterol as building block in delivery systems

Phytosterols are a subclass of plant-based steroids present in a wide range of organisms, including plants, animals, and fungi. β-Sitosterol (Sit), stigmasterol and campesterol, are the most abundant phytosterols in the human diet[12]. They all have structural similarity to cholesterol, with the same tetracyclic core structure, but different substitution at C24 and absence or presence of a double bond at C22[12,13]. Specifically, Sit has an ethyl group at C24 (**Figure 3.2**).

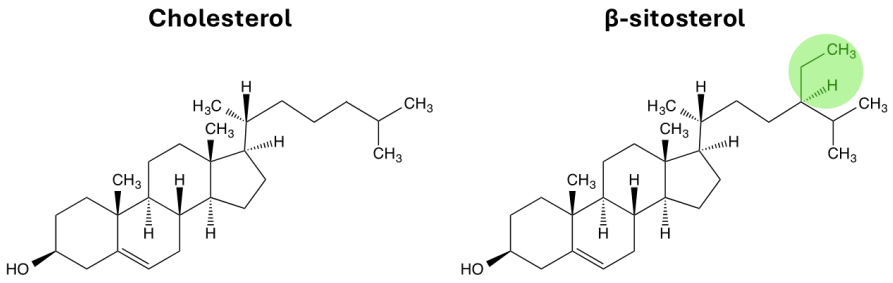


Figure 3.2. Comparison of the molecular structure of cholesterol and β-sitosterol.

It is reported in literature that phytosterols play essential roles in the physiology of eukaryotic organisms. They are critical to control cell membrane fluidity, they are also involved in the embryonic growth of plants and have an important role in the formation of liquid-ordered membrane states (lipid "rafts") which have a fundamental role in biological processes such as signal transduction[14].

It is also important to highlight that, with a long history of consumption in cosmetic, food and pharmaceutical products, phytosterols have been generally recognized as safe (GRAS)[15].

Sit is widely used and approved for cosmetic, food and pharmaceutical use. Focusing on personal care and cosmetic products, it is used in different functions such as emulsion stabilizer, fragrance, skin conditioning or light stabilizer[16], and it is employed in a different variety of preparations such as sunscreens, moisturizers, body wash and anti-aging formulations[17]. Furthermore, several *in vitro* and *in vivo* studies have also shown different interesting properties for topical application of Sit, such as antioxidant or anti-inflammatory activities[18,19].

It is also worth mentioning that Sit has been previously used to produce other delivery systems such as liposomes[20,21], micelles[22] or polymeric nanoparticles[23].

Overall, Sit presented promising characteristics as a candidate to replace cholesterol as a plant- based building block for novel nanovesicles.

3.1.2. Alkyl polyglucoside surfactants as building block for novel nanovesicles

Alkyl polyglucosides (APGs) are a new generation of green, biocompatible and biodegradable non-ionic surfactants consisting of a hydrophilic saccharide moiety and a hydrophobic fatty alkyl chain (**Figure 3.3**).

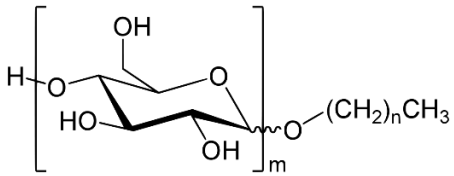


Figure 3.3. Generic molecular structure of alkyl polyglucoside surfactants (APGs).

APGs were first produced in the last decade of the 19th century, but it was not until the last decades of the 20th century that the process was translated to the industrial scale production[24]. They are synthesized from renewable raw materials such as vegetable oils and starch and have excellent ecotoxicological profiles and are readily biodegradable[24,25].

In the last decades they have drawn attention to different markets including the cosmetic and healthcare industry because, unlike other existing surfactants, they are mild to the skin and present high dermatological compatibility[24,26].

This new family of surfactants is approved for cosmetic use, and they are employed mainly for cleansing functions in body wash products, facial cleaning lotions, shampoos or oral care products[16,24].

Regarding their use in the development of new delivery systems, several examples can be found in literature, including their use in non-liposomal vesicles[27], lipid solid nanoparticles[28] or emulsions[29].

As stated above, APGs are a big family of surfactants. Several APGs have been evaluated in the present work as vesicle membrane components, also taking into account different quality, purity, and length of the alkyl chain, as summarized in **Table 3.1**. Whereas the APGs provided by cosmetic suppliers were mixtures of APGs with different alkyl chain lengths (LGL-m_{C12-16}, LGL-m_{C10-16}, DGL-m_{C8-C16} or DGL-m_{C8-C10}) and purities below 50%, the APGs of pure grade (>98%) contained only the APG with the corresponding alkyl chain (LGL, DGL or OGL).

Table 3.1. Overview of the APGs evaluated as vesicle membrane building blocks.

Code	Chemical description	Alkyl chain length	Trade name	INCI[a)]
LGL	C12 fatty alcohol glucoside	12	Dodecyl β-D-glucopyranoside	Lauryl Glucoside
LGL-m_{C12-16}	C12-16 fatty alcohol glucoside	12 – 16	Plantacare® 1200 UP	Lauryl Glucoside
LGL-m_{C10-16}	C10-16 fatty alcohol glucoside	10 – 16	BergaSoft LG 50	Lauryl Glucoside
LGC	Anionic alkyl glucoside carboxylate	10 – 16	Plantapon® LGC Sorb	Sodium Lauryl Glucose Carboxylate (and) Lauryl Glucoside
DGL	C10 fatty alcohol glucoside	10	Decyl β-D-glucopyranoside	Decyl Glucoside
DGL-m_{C8-C16}	C8-16 fatty alcohol glucoside	8 – 16	Plantacare® 2000 UP	Decyl Glucoside
DGL-m_{C8-C10}	C8-10 fatty alcohol glucoside	8 – 10	Plantacare® 810 UP	Caprylyl / Capryl Glucoside
OGL	C8 fatty alcohol glucoside	8	Octyl β -D-glucopyranoside	Caprylyl glucoside

[a)] *International Nomenclature of Cosmetic Ingredients (INCI): unique identifier name for cosmetic ingredients*

From all these APGs, the most used in this work were lauryl glucoside, composed by a glucose ring and an alkyl chain of C12, and sodium lauryl glucose carboxylate, an anionic derivative of lauryl glucoside with a carboxylic group in the glucose ring (**Figure 3.4**).

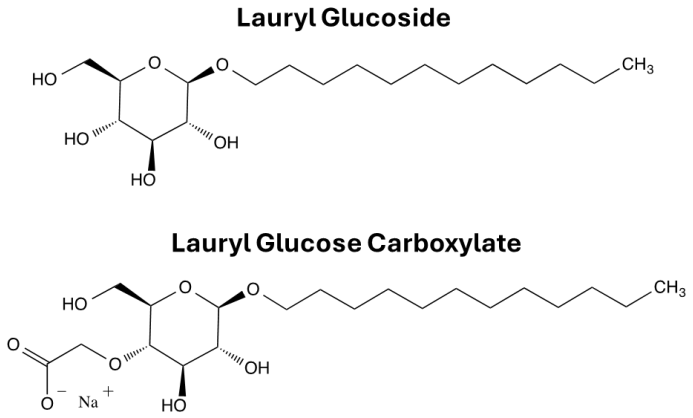


Figure 3.4. Molecular structure of lauryl glucoside (LGL) and lauryl glucose carboxylate (LGC) surfactants.

3.2. Synthesis of β-sitosterol and lauryl glucoside nanovesicles

The first objective of the present Thesis was the development of a new platform of nanovesicles for the cosmetic market, specifically using Sit and APGs as membrane components. To evaluate the possibility to form Sit/LGL vesicles by DELOS procedure, LGL surfactants of different quality and purity were used.

3.2.1. Synthesis of nanovesicles using cosmetic-grade lauryl glucoside

Considering this objective, for this first study the formation of NVs composed by Sit and lauryl glucoside (LGL) using reagents from cosmetic grade was investigated. Cosmetic grade reagents contained mixtures of surfactants with different alkyl chain lengths (LGL-$m_{Cn-(n+x)}$). Two different lauryl glucoside reagents were tested: LGL-m_{C12-16} and LGL-m_{C10-16} (**Table 3.1**).

All the sample prototypes described in this **Section 3.2.1** were produced by DELOS single-step procedure using the intermediate laboratory scale equipment, as described in **Chapter 8** - **Section 8.2.1**. In all cases, Sit was dissolved in the organic phase, while the surfactant was dissolved in the aqueous phase, as shown in **Figure 3.5**. Samples obtained by DELOS method were filtered with 0.45 μm pore size polyethersulfone (PES) membrane syringe filters in order to eliminate impurities coming from the starting materials.

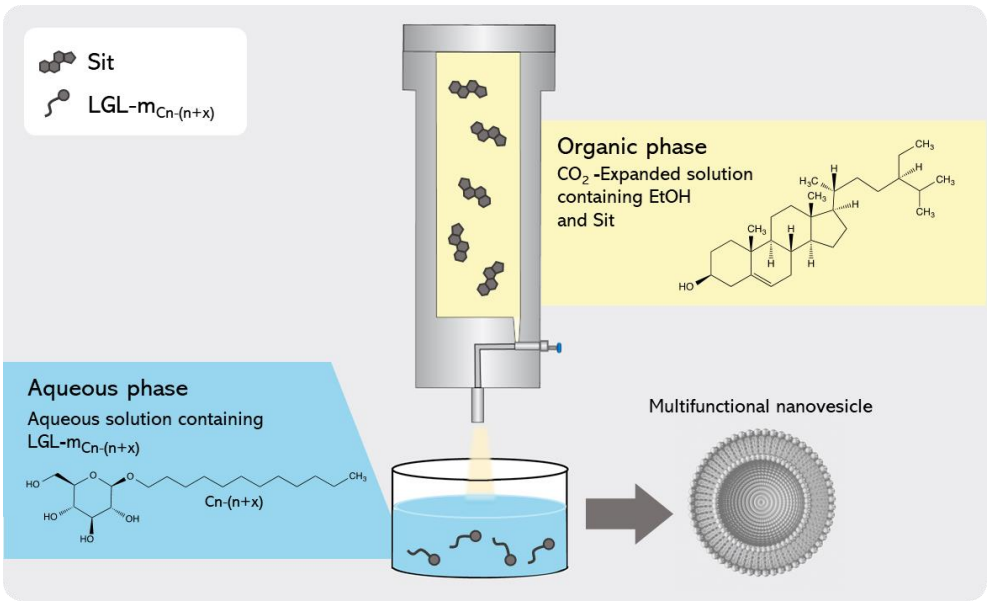


Figure 3.5. Schematic representation of DELOS methodology used for the preparation of nanovesicles composed of Sit and LGL-$m_{Cn-(n+x)}$ in **Section 3.2.1**.

Different formulation factors were tested to evaluate under which conditions was possible to obtain Sit/LGL nanovesicles. First, the type of lauryl glucoside used (LGL-m_{C12-16} or

LGL-m_{C10-16}). Second, Sit:LGL-$m_{Cn-(n+x)}$ molar ratio (1:0.75 to 1:2). Third, the membrane components concentration (4.67 to 7.11 mg/mL), which was calculated by keeping constant the final concentration of Sit (2.65 mg/mL) and changing the concentration of LGL-$m_{Cn-(n+x)}$ in relation to the molar ratio tested. The different samples produced are detailed below in **Table 3.2**.

The obtained nanoformulations were evaluated by dynamic light scattering (DLS) to study mean particle size and particle size distribution (or dispersity index (PDI)), electrophoretic light scattering (ELS) to evaluate the apparent ζ-potential (ζ-Pot), and cryogenic transmission electron microscopy (cryo-TEM) to obtain an individual inspection of the morphology of each sample. The methodology used is described in **Chapter 8** - **Sections 8.3.1** and **8.3.2**.

Table 3.2. Composition and physicochemical characterization of nanovesicle formulations prepared by DELOS technique with Sit/LGL using cosmetic grade surfactants of different carbon chain length (n = 1).

Surfactant	Sit:LGL-$m_{Cn-(n+x)}$		Hydrodynamic diameter mean [nm]	Size PDI	Apparent ζ-Pot [mV]	Stability [months]
	Molar ratio	Concentration [a] [mg/mL]				
LGL-m_{C12-16}	1:0.75	4.67	313 ± 1	0.24 ± 0.02	-42 ± 2	> 12
LGL-m_{C12-16}	1:1	5.30	368 ± 16	0.18 ± 0.03	-32.1 ± 0.3	> 12
LGL-m_{C10-16}	1:1	4.86	249 ± 3	0.25 ± 0.01	-32 ± 1	> 2
LGL-m_{C12-16}	1:1.25	5.99	438 ± 11*	0.06 ± 0.05*	-30 ± 0.1*	< 2
LGL-m_{C10-16}	1:1.5	5.99	437 ± 7*	0.41 ± 0.24*	-13 ± 0.1*	< 2
LGL-m_{C10-16}	1:2	7.11	463 ± 5*	0.06 ± 0.04*	-20 ± 0.3*	< 2

[a] *Theoretical concentration.*

** Results in red did not meet quality criteria of the technique, they were not reliable.*

Together, the presented findings suggested that NVs were formed in any of the tested conditions when using cosmetic-grade surfactants LGL-m_{C12-16} and LGL-m_{C10-16}, containing a mixture of alkyl glucosides of different carbon chain length.

However, according to DLS and ELS measurements (**Table 3.2**) and cryo-TEM images (**Figure 3.6**), not all the formulations presented similar physicochemical properties and colloidal stability. In terms of mean particle size, PDI and ζ-Pot (**Table 3.2**) only the samples produced at a molar ratio Sit:LGL-$m_{Cn-(n+x)}$ of 1:1 and 1:0.75 gave reliable results according to the quality parameters of the measurements (quality parameters compiled in **Chapter 8** -

Section 8.3.1.1). These samples (Sit:LGL-m_{C12-16} at 1:1 and 1:075, and Sit:LGL-m_{C10-16} at 1:1) presented mean particle sizes between 200 – 300 nm, and PDI values between 0.20 – 0.25, indicating that nanosized and homogeneous formulations were obtained. Regarding ζ-Pot results, all of them were around or under -30 mV, suggesting that they were stable colloidal suspensions.

It is important to mention that nanoparticle dispersions with high positive or negative ζ-Pot values, i.e., > +30 mV or < -30 mV, are considered in the literature as stable formulations. This is because highly charged particles tend to avoid particle aggregation due to electrical repulsion. In contrast, in nanoparticle dispersions with small ζ-Pot values between +30 mV and -30 mV, attraction overcomes repulsion, and the samples are expected to first aggregate and then evolve to sedimentation[30].

The DLS and ELS results were supported by cryo-TEM images (**Figure 3.6A**, **B** and **C**) where mainly homogeneous nanovesicles in terms of particle size were observed. When speaking of morphology, different types of nanovesicles were detected: unilamellar vesicles, multilamellar vesicles and multivesicular vesicles. The presence of these different types of vesicles could be explained by the fact that the surfactant used, lauryl glucoside, does not present any charge. In this way, there is not electrostatic repulsion between bilayers allowing the possibility to form multilamellar and multivesicular vesicles.

With regards to samples produced at molar ratios Sit:LGL-$m_{Cn-(n+x)}$ 1:1.25, 1:1.5 and 1:2, the measurements did not present reliable size, PDI or ζ-Pot data. The explanation to that fact was that formulations were too heterogeneous and presented large structures and precipitates, preventing the equipment to perform proper and reliable measurements. This was confirmed by cryo-TEM images (**Figure 3.6D**), which showed beside some heterogeneous vesicles, large and elongated aggregated membranous structures.

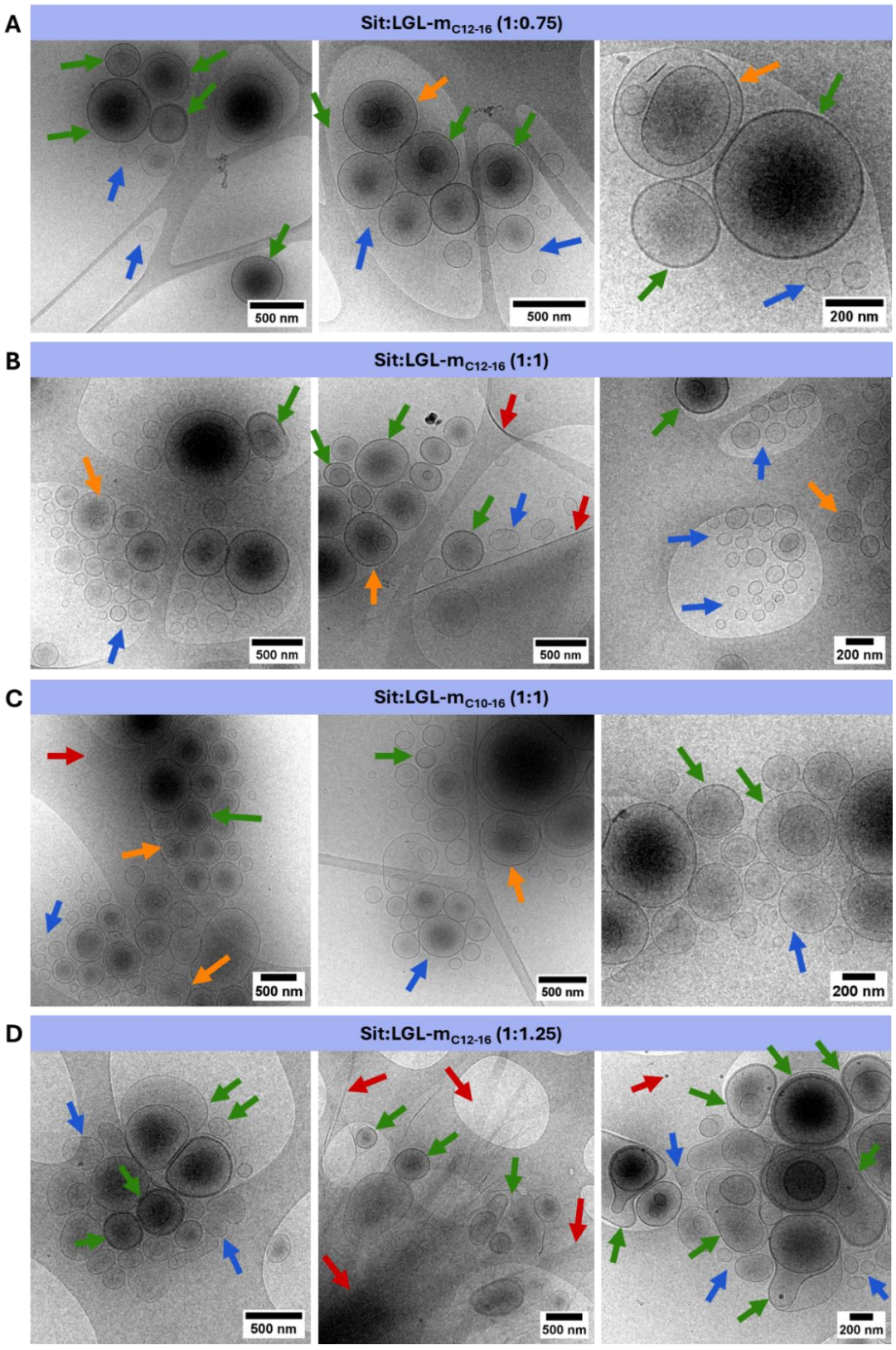
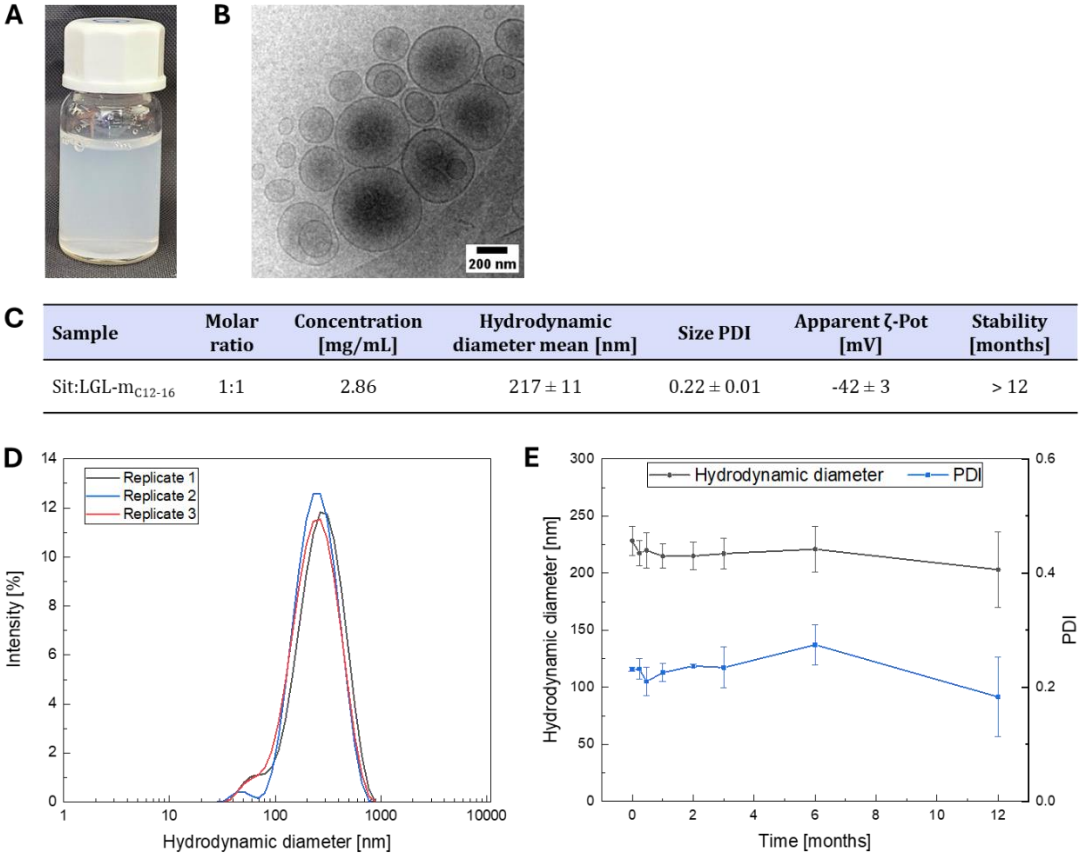


Figure 3.6. Representative cryo-TEM images of **(A)** Sit:LGL-$m_{C12\text{-}16}$ (1:0.75 molar ratio), **(B)** Sit:LGL-$m_{C12\text{-}16}$ (1:1 molar ratio), **(C)** Sit:LGL-$m_{C10\text{-}16}$ (1:1 molar ratio) and **(D)** Sit:LGL-$m_{C12\text{-}16}$ (1:1.25 molar ratio) nanoformulations. Unilamellar vesicles (blue arrows), multilamellar vesicles (green arrows), multivesicular vesicles (orange arrows) and big structures, aggregates or precipitates (red arrows) can be distinguished.

In summary, the results of this study conclude that for the obtention of stable and homogeneous Sit:LGL-$m_{Cn-(n+x)}$ NVs a molar ratio of 1:1 or 1:0.75 between membrane components is preferred.

Although three of the developed nanoformulations meet this criteria, it was decided to select the prototype Sit:LGL-m_{C12-16} at molar ratio 1:1 was selected for further studies. This prototype was selected as a starting point to develop the new platform because the LGL reagent itself had less variation of carbon chain lengths (C12-16 instead of C10-16). **Figure 3.7** reports the detailed physicochemical characterization of this NV prototype Sit:LGL-m_{C12-16} (1:1) with macroscopical appearance, nanovesicular morphology, physicochemical characterization and stability. The concentration of membrane components was adjusted from 5.3 to 2.86 mg/mL to obtain NVs with lower particle size and better homogeneity.



Sample	Molar ratio	Concentration [mg/mL]	Hydrodynamic diameter mean [nm]	Size PDI	Apparent ζ-Pot [mV]	Stability [months]
Sit:LGL-m_{C12-16}	1:1	2.86	217 ± 11	0.22 ± 0.01	-42 ± 3	> 12

Figure 3.7. Summary of Sit:LGL-m_{C12-16} (molar ratio 1:1) NVs physicochemical characterization. **(A)** Macroscopical appearance of the sample 1 year after production. **(B)** Representative cryo-TEM image after 10 days of production. **(C)** Characterization by DLS and ELS of three independent replicates of the same nanoformulation 7 days after production and mean hydrodynamic diameter, size PDI and ζ-Pot values. **(D)** Particle size distribution of each of the three independent replicates. **(E)** Stability over time up to 12 months in terms of particle size and size PDI (n = 3).

3.2.2. Synthesis of nanovesicles using pure-grade lauryl glucoside

In the first study of this Thesis, cosmetic-grade lauryl glucoside reagents were used to obtain formulations of Sit:LGL-$m_{Cn-(n+x)}$ NVs. These nanoformulations are already suitable for the cosmetic market, because the reagents used are compliant. Nevertheless, as already explained in **Section 3.1.2**, these reagents are mixtures of APGs with different alkyl chain lengths and purities around or below 50%. Due to these both factors it was difficult to deeply understand the molecular basis of the formation of Sit:LGL NVs. For this reason, we decided to evaluate the vesicles formation using a pure-grade (98% purity) LGL (**Table 3.1**) following the same methodology described in **Section 8.2.1** and the intermediate laboratory scale equipment.

Surprisingly, the pure version of the LGL surfactant did not form vesicles with Sit under the same DELOS procedure experimental conditions used for the cosmetic-grade reagents. The first experiment reproduced the same DELOS processing conditions that worked for the Sit:LGL-m_{C12-16} (molar ratio 1:1) NVs. However, the first difference was the solubility of the surfactant in water. Whereas LGL-$m_{Cn-(n+x)}$ surfactants were soluble in aqueous media, the pure LGL had limited water solubility at room temperature (RT) and it was better dissolved in ethanol. Nevertheless, despite dissolving the LGL in the organic phase with the Sit, and keeping constant the other conditions, NVs were not formed.

For this reason, several variables were studied trying to obtain Sit:LGL NVs with pure-grade LGL: varying the molar ratio Sit:LGL (1:0.5, 1:1, 1:1.5), membrane components concentration (0.4 – 5 mg/mL), CO_2 molar fraction (0.3 – 0.5), and the aqueous phase media (water, histidine buffer, carbonate buffer, urea buffer). Nonetheless, any of these conditions led to obtain Sit:LGL NVs.

Instead, Sit:LGL (1:1) vesicles were finally obtained only when the aqueous phase temperature was increased to 60 °C during the depressurization step (**Figure 3.8A**).

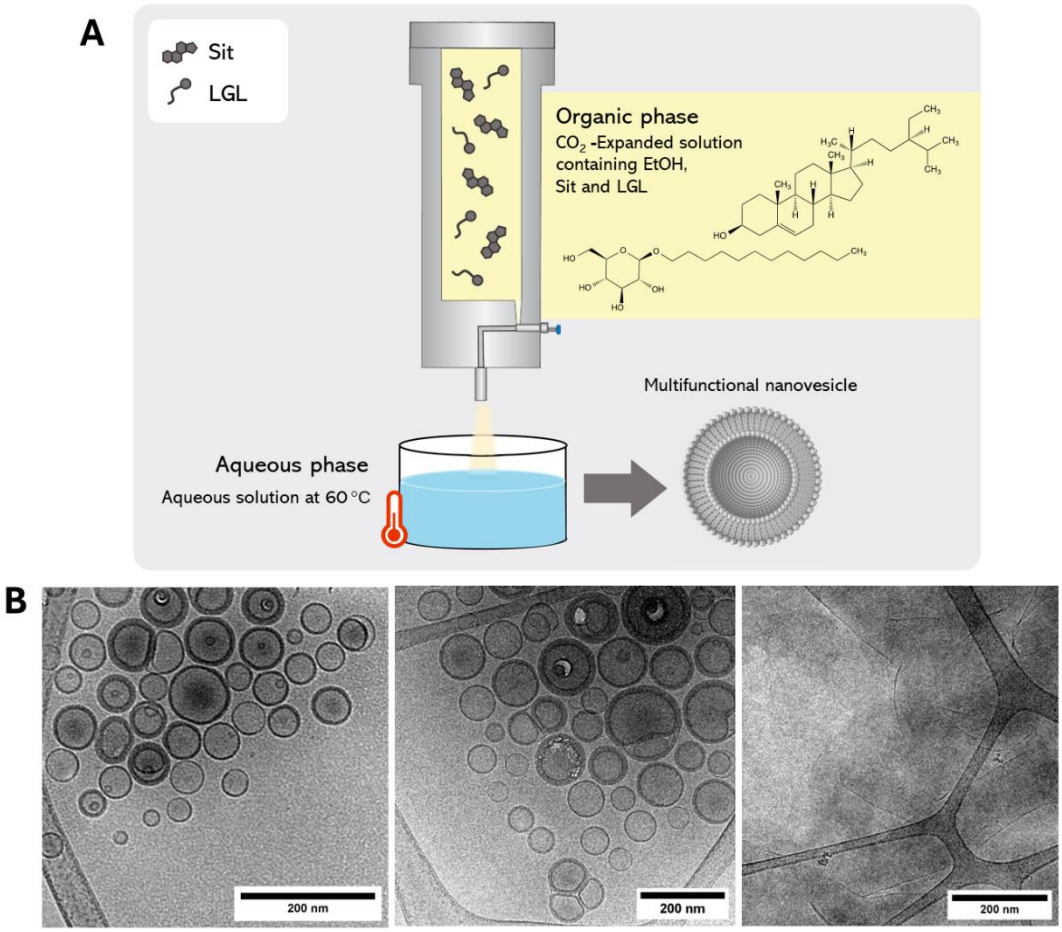


Figure 3.8. **(A)** Schematic representation of DELOS methodology used for the preparation of nanovesicles composed of Sit and pure LGL, heating the aqueous phase at 60ºC. **(B)** Representative cryo-TEM images of the Sit:LGL (molar ratio 1:1) formulation.

Table 3.3. Composition and characterization of the Sit/LGL nanovesicle formulation prepared with pure LGL surfactant by DELOS method (n = 2).

Surfactant	Sit:LGL Molar ratio	Sit:LGL Concentration[a] [mg/mL]	Hydrodynamic diameter mean [nm]	Size PDI	Apparent ζ-Pot [mV]	Stability [months]
LGL	1:1	2.76	529 ± 218	0.3 ± 0.2	-35 ± 2	< 1

[a] *Theoretical concentration.*

However, Sit:LGL vesicles were larger and exhibited greater heterogeneity than those produced with LGL-$m_{Cn-(n+x)}$ surfactants (**Table 3.3**). These results are in accordance with cryo-TEM analysis (**Figure 3.8B**), in which in addition to small nanovesicles, other planar membranous structures were also observed (third image). These larger structures could be interfering in the particle size measurements showing higher particle size values. Moreover,

vesicles prepared with the pure surfactant tended to aggregate, and the samples showed precipitation in less than one month after production.

3.2.2.1. Evaluation of thermal behavior of LGL and LGL-m$_{C12-16}$

The previous results obtained when using pure LGL as nanovesicle membrane component highlighted that the aqueous phase temperature was a critical parameter for vesicles formation when pure surfactants were used, since it was only possible to observe NVs when the aqueous phase was kept at 60 °C. On the contrary, cosmetic-grade surfactants did not show the same behavior, since the obtention of NVs was possible with the aqueous phase at RT.

In order to understand this difference in the thermal behavior of both types of surfactants, differential scanning calorimetry (DSC) was used to characterize them. This technique assess heat energy uptake of the analyzed samples, which allows to monitor the changes of phase transitions[31]. In this particular case, we aimed to determine the Krafft temperature (T_K) of the surfactants, which is the minimum temperature in which surfactants can form micelles, a process which has been reported in bibliography that may affect vesicle formation[32].

Solutions of pure LGL and LGL-m$_{C12-16}$ in water/EtOH 15% (v/v) were prepared and analyzed as described in **Section 8.4**. The dispersant media was the same as NVs produced by DELOS process. After their evaluation, T_K was determined as the onset point of the endothermic peak obtained for each surfactant[33,34].

The DSC results (**Figure 3.9**) showed a clear difference: the thermogram of LGL presented a peak that could correspond to a T_K of 30.8°C, above RT, whereas LGL-m$_{C12-16}$ showed this peak at 5.8 °C, significantly below RT.

These findings support the results obtained, showing that at RT LGL-m$_{C12-16}$ could be completely solubilized and form micelles, but for pure LGL the working temperature of the aqueous phase should be higher than 30.8 °C during the DELOS process. Therefore, it is necessary to heat the aqueous phase to be able to form NVs with Sit and LGL. These results obtained with LGL are also in accordance with the work of Muzzalupo *et al.*[35], where vesicles of LGL and cholesterol were prepared at 60 °C using thin film hydration procedure, above the T_K of LGL.

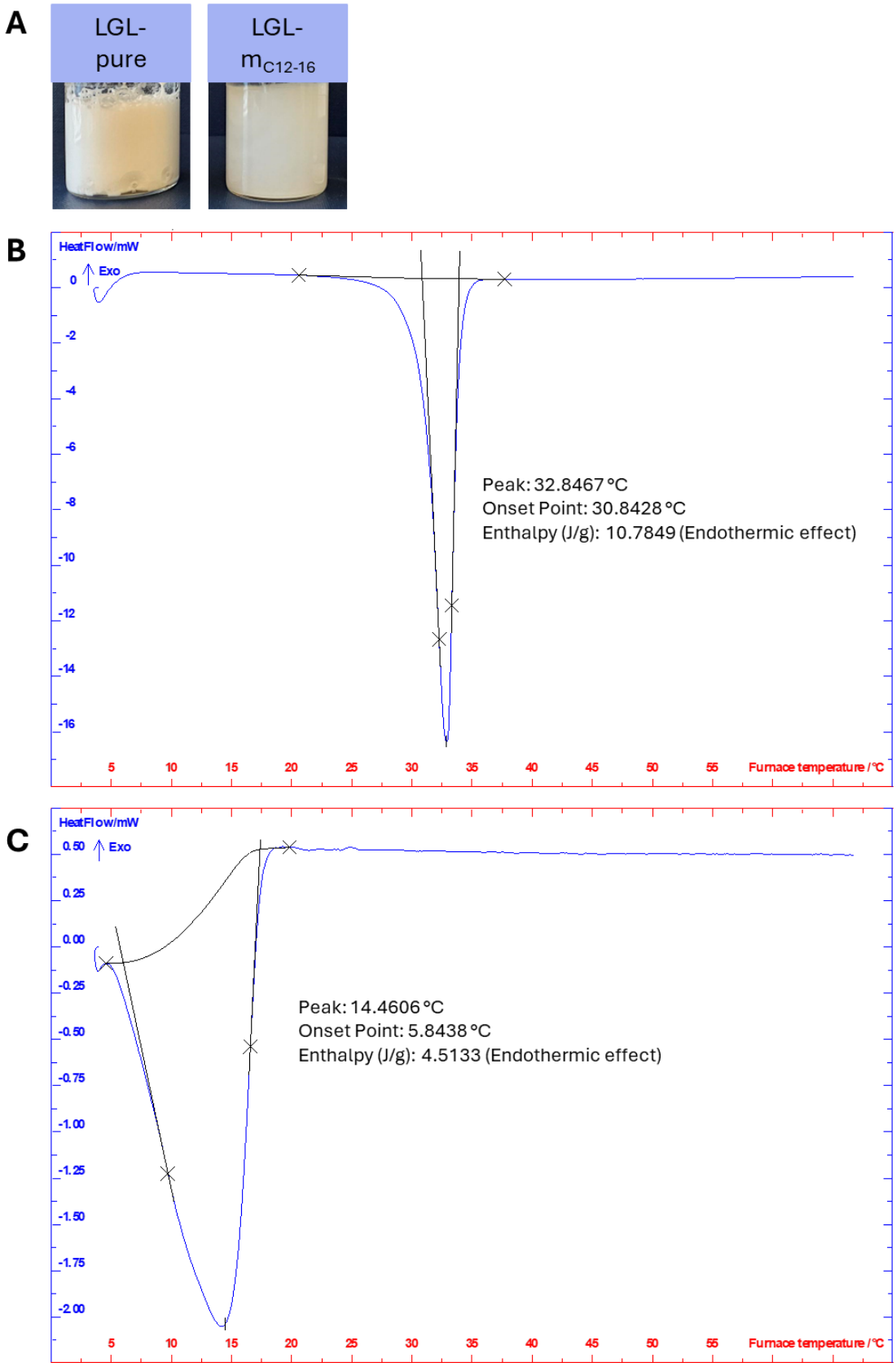


Figure 3.9. **(A)** Macroscopical appearance of solutions of pure LGL (left) and LGL-m_{C12-16} (right) in water/EtOH 10% after 7 days of stabilization at 5 ± 3 °C. DSC thermograms of **(B)** pure LGL and **(C)** LGL-m_{C12-16}.

In summary, β-sitosterol and lauryl glucoside could self-assemble to form nanovesicles. However, it has been proved that the type and purity of lauryl glucoside used had an impact on the process parameters during the manufacturing and the physicochemical properties of the colloids obtained.

Cosmetic-grade lauryl glucoside reagents (LGL-$m_{Cn-(n+x)}$) were used to obtain stable and homogeneous NVs in combination with Sit at different concentrations and molar ratios (Sit:LGL-$m_{Cn-(n+x)}$ 1:1 and 1:0.75). On the contrary, the use of pure-grade LGL required adjusting the process parameters obtaining more heterogeneous and less stable NVs in combination with Sit.

3.3. Stabilization of Sit:LGL nanovesicles with anionic additives

The formation of Sit:LGL nanovesicles with pure LGL showed to be more challenging than for those NVs composed by LGL-$m_{Cn-(n+x)}$ cosmetic grade surfactants. Although finally the NVs with pure LGL were obtained increasing the temperature of the aqueous phase up to 60 °C, the NVs obtained presented worse physicochemical properties and poorer colloidal stability than those composed by Sit and LGL-$m_{Cn-(n+x)}$. Furthermore, working at 60 °C can hinder the loading of biomolecules sensitive to high temperatures, such as some proteins. Still, it was of our interest to obtain stable NVs with pure-grade LGL to have the possibility to use them in other markets beside the cosmetic.

In this way, the aim was to increase the colloidal stability of Sit:LGL NVs and, if possible, avoid the use of temperature for the proper self-assembly of the membrane components. To do so, we added different amounts of negatively charged surfactants to increase the colloidal stability of the formulation. The use of charged molecules to increase the colloidal stability is well reported [36–38], because of the electrostatic repulsion generated between the particles in suspension, avoiding interaction and agglomeration between them.

3.3.1. Stabilization by adding 3% of anionic surfactants

The first strategy consisted of adding 3% (w/w) of a charged surfactant to the NVs membrane components to improve colloidal stability by charge repulsion.

Three anionic surfactants were selected (**Figure 3.10**): sodium lauryl glucose carboxylate (LGC), a derivative of lauryl glucoside with a carboxylic moiety in the glucose ring; sodium laurate (SL), which is the sodium salt of a fatty acid (lauric acid); and sodium lauroyl sarcosinate (SLS), an anionic surfactant derived from the amino acid sarcosine. All of them come from a lauryl alcohol of C12 chain length and approved for cosmetic use[16].

It was interesting to evaluate the use of anionic surfactants because not only the colloidal stability of the nanovesicular systems could improve, but they have been also reported as skin permeation enhancers[39,40].

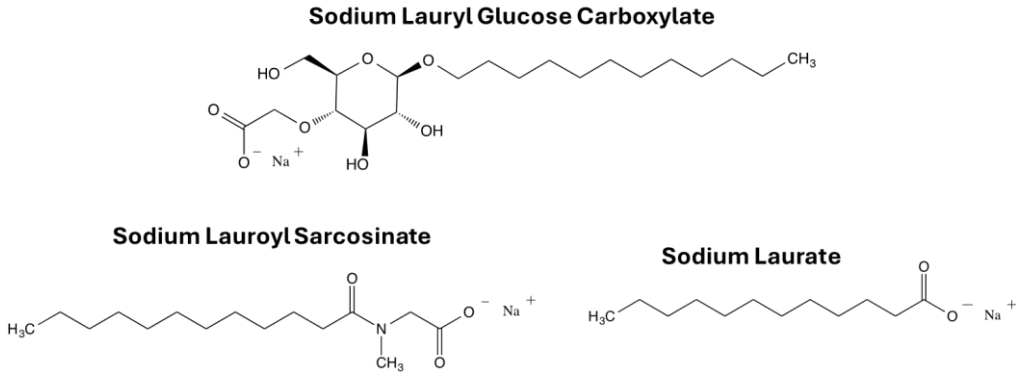


Figure 3.10. Molecular structure of sodium lauryl glucose carboxylate (LGC), sodium lauroyl sarcosinate (SLS) and sodium laurate (SL) surfactants, evaluated as stabilizers of Sit/LGL NVs systems.

Again, DELOS methodology was used to produce the different formulations with the intermediate laboratory scale equipment (see **Section 8.2.1**) and the samples were filtered after production. The composition of the nanovesicles is detailed in **Table 3.4**. In all the cases Sit and LGL were dissolved in the organic phase with ethanol, whereas the different anionic surfactants were dissolved in the organic or aqueous phase depending on their solubility (**Figure 3.11**).

Table 3.4. Composition and physicochemical characterization of nanovesicle formulations prepared in **Section 3.3.1** (n = 3) adding stabilizer additives.

Additive	Sit:LGL:additive		Hydrodynamic diameter mean [nm]	Size PDI	Apparent ζ-Pot [mV]	Stability [months]
	Molar ratio	Concentration [a] [mg/mL]				
LGC[b]	1:1:0.05	2.76	193 ± 4	0.24 ± 0.03	-51 ± 2	> 12
SLS	1:1:0.08	2.76	179 ± 8	0.21 ± 0.02	-54 ± 5	> 12
SL	1:1:0.1	2.76	166 ± 2	0.20 ± 0.04	-41 ± 7	> 12

[a] *Theoretical concentration.*

[b] *LGC reagent used was a mixture of APGs, intended as alkyl glucosides of C10-16 chain length, and the corresponding carboxylates; thus, the ratio 1:1:0.05 refers to the mixture and not the real content of LGC.*

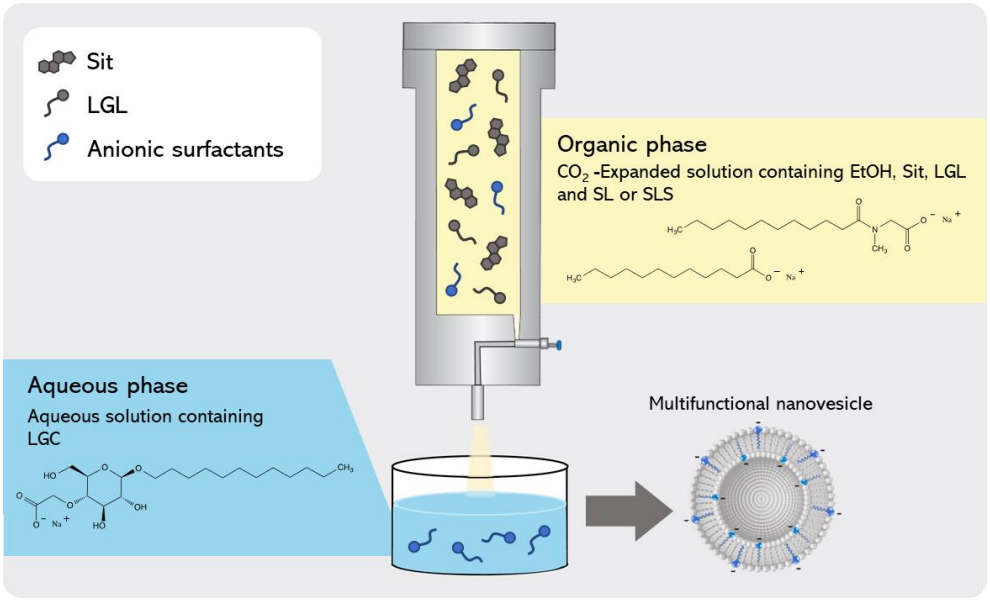


Figure 3.11. Schematic representation of DELOS methodology used for the preparation of nanovesicles composed of Sit, LGL and an anionic surfactant as additive (LGG, SL or SLS) described in **Section 3.3.1**.

The combination of Sit and LGL with any of the three tested anionic additives (LGC, SL or SLS) gave rise to NVs formation. As reported in **Table 3.4**, the formulations obtained presented suitable physicochemical properties in terms of particle size (between 150 – 200 nm) and PDI ~ 0.2 indicating the obtention of homogeneous colloidal suspensions. Regarding ζ-Pot, the values were below -40 mV, higher in absolute value than with plain Sit:LGL NVs, due to the presence of the low amount of anionic surfactant. This change in ζ-Pot value can be an indicator of the integration of these anionic surfactants to the

nanovesicular membranes and an indicator of higher colloidal stability in comparison with Sit:LGL NVs. This improvement in colloidal stability was confirmed by measurements of particle size and size PDI (**Figure 3.12A**), which remained stable for more than one year. This was an important step forward in relation to previous Sit:LGL NVs stability which was less than one month.

With regards to morphology of the NVs obtained (**Figure 3.12B**), in all cases the presence of nanovesicular structures was observed, mainly unilamellar NVs but also multilamellar ones.

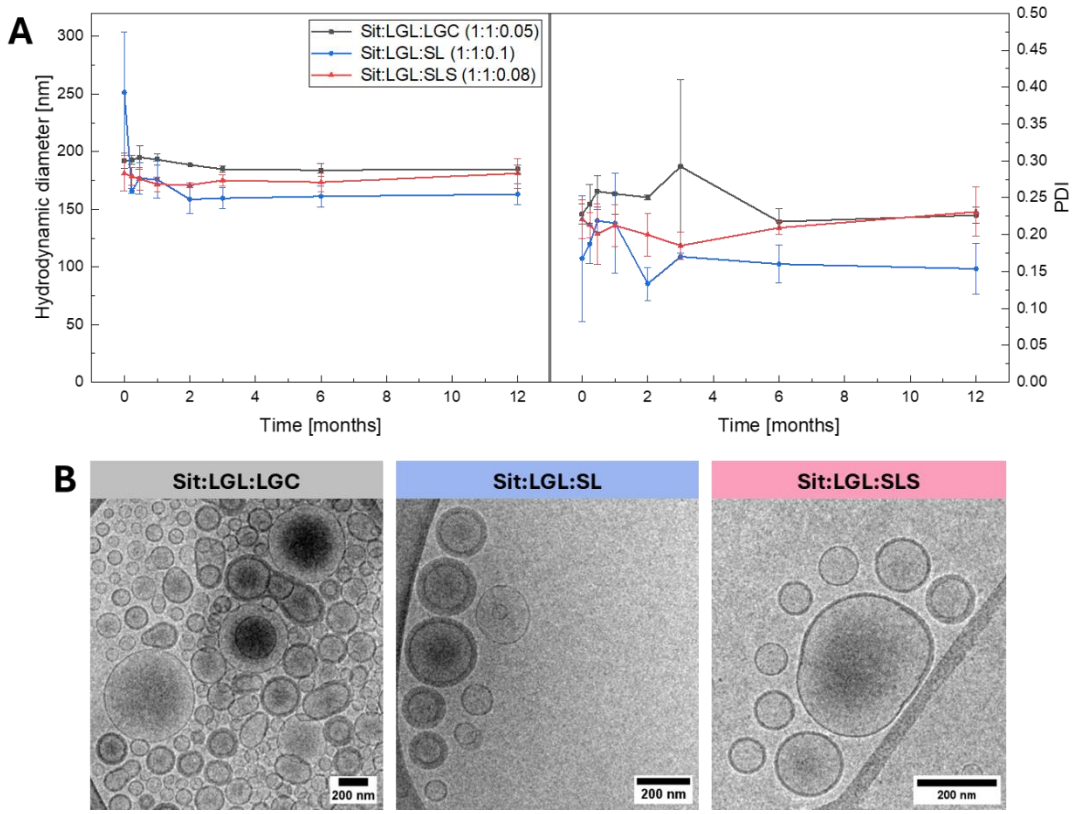


Figure 3.12. Physicochemical characterization of Sit:LGL:LGC NVs (in gray), Sit:LGL:SL NVs (in blue) and Sit:LGL:SLS NVs (in red). **(A)** Stability over time in terms of particle size and size PDI (n = 3). **(B)** Representative cryo-TEM images.

Finally, it is also important to remark that the incorporation of these anionic surfactants allowed us to produce the NVs without heating the aqueous phase to 60 °C. This process parameter was also important in order to produce in further steps, if necessary, formulations containing thermolabile biomolecules.

In conclusion, the strategy of adding an anionic surfactant to stabilize the Sit/LGL colloidal formulation was considered very promising, as it allowed to obtain more homogeneous and

stable nanovesicular prototypes with pure LGL, without the need of heating the aqueous phase above RT.

3.3.2. Screening and replacement of non-ionic surfactant LGL by the anionic surfactant LGC

Afterwards, considering the benefits provided by the anionic surfactant LGC to the nanovesicle formulation, the versatility of the new sugar-based delivery platform was explored by screening different molar ratios of LGL:LGC.

The nanovesicular formulations were produced as in the previous **Section 3.3.1** (**Figure 3.11**) by DELOS methodology, filtered and characterized.

Table 3.5. Composition and characterization of Sit:LGL:LGC nanovesicle formulations prepared in **Section 3.3.2** (n = 3) varying the surfactants molar ratio.

Sit:LGL:LGC[a)]		Hydrodynamic diameter mean [nm]	Size PDI	Apparent ζ-Pot [mV]	Stability [months]
Molar ratio	Concentration[b)] [mg/mL]				
1:0.8:0.2	3	182 ± 9	0.22 ± 0.01	-61±2	> 12
1:0.5:0.5	3	148 ± 4	0.20 ± 0.01	-52±5	> 12
1:0.2:0.8	3	153 ± 10	0.187 ± 0.002	-64±7	> 12
1:0:1	2.86	161 ± 8	0.18 ± 0.05	-70±5	> 12

[a)] LGC reagent used was a mixture of APGs, intended as alkyl glucosides of C10-16 chain length, and the corresponding carboxylates; thus, the different ratios refer to the mixture and not the real content of LGC.

[b)] Theoretical concentration.

As it can be seen in **Table 3.5** and **Figure 3.13**, a complete replacement of the LGL by LGC could be achieved, also testing different intermediate surfactant molar ratios, without compromising the formation of homogeneous and stable vesicles with a macroscopical appearance of opalescent whitish stable dispersions. The greatest change in particle size was observed between LGL:LGC molar ratios of (0.8:0.2) and (0.5:0.5) where a slight decrease in particle size was observed, while further increasing LGC concentration did not generate significant changes in the physicochemical properties of the NVs. Regarding the ζ-Pot values, no significant changes were observed between the NVs containing LGC; however, the ζ-Pot value was more negative compared to Sit:LGL NVs, as expected.

Furthermore, the use of LGC in any of the compositions tested significantly increased the stability of Sit/LGL NVs from less than 1 month to more than 12 (**Figure 3.13D**).

To conclude, promising results were achieved from this study, obtaining stable and homogeneous formulations when using different proportions of LGC. For this reason, two formulations were selected to be further characterized in depth: NVs Sit:LGL:LGC (1:0.8:0.2) and NVs Sit:LGC (1:1).

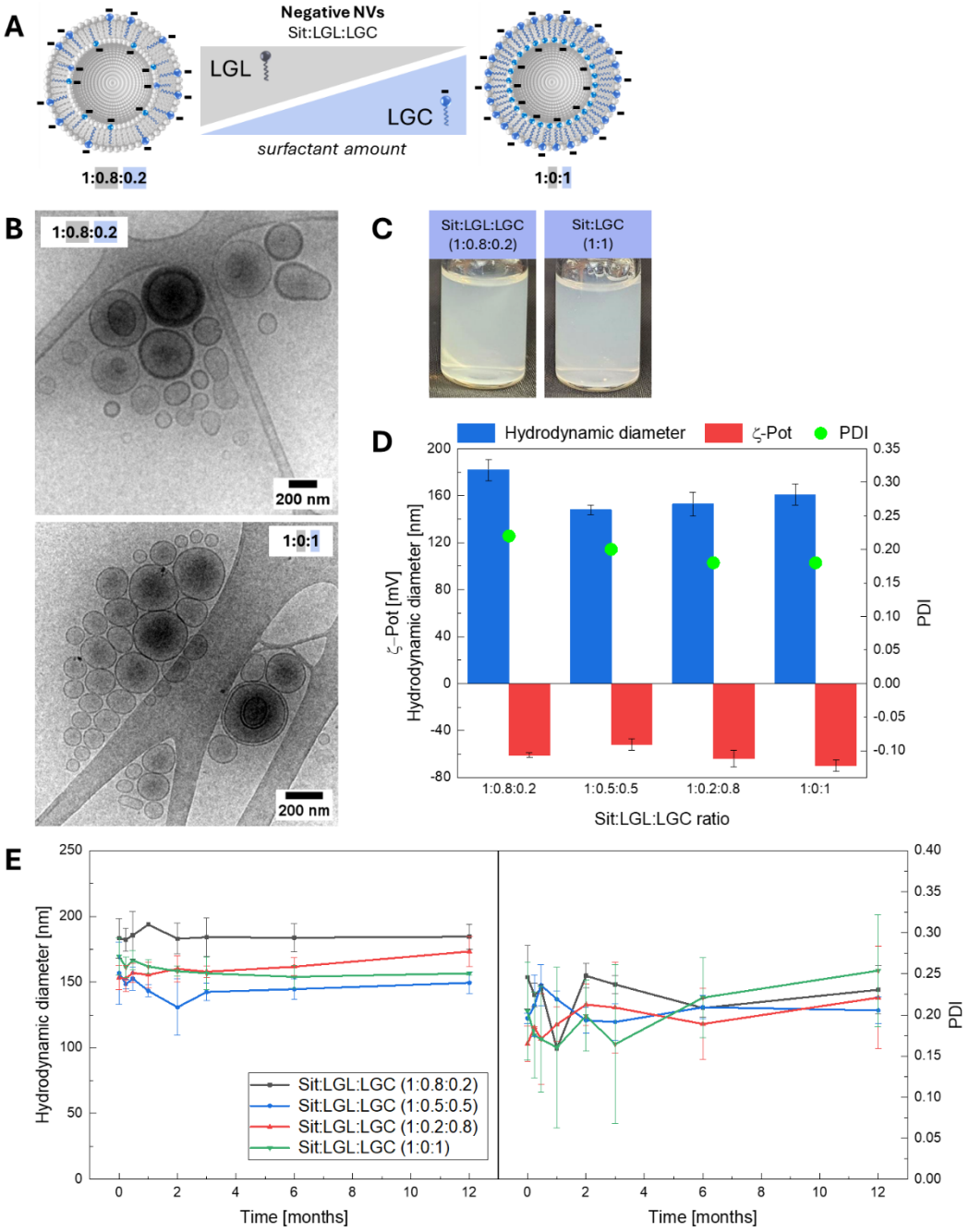


Figure 3.13. **(A)** Schematic representation of the screening performed, replacing LGL by LGC in Sit/LGL/LGC nanovesicles. **(B)** Representative cryo-TEM images of Sit:LGL:LGC NVs (molar ratios 1:0.8:0.2 and 1:0:1). **(C)** Macroscopical appearance of the NVs samples (Sit:LGL:LGC (1:0.8:0.2 and 1:0:1)) 1 year after production. **(D)** Physicochemical characterization of negatively charged Sit:LGL:LGC NVs in terms of hydrodynamic diameter, size PDI and apparent ζ-Pot of three independent replicates. **(E)** Stability over time in terms of particle size and size PDI (n = 3).

As a main conclusion of this **Section**, the use of different anionic surfactants as additives (LGC, SLS or SL) worked to stabilize the Sit:LGL NVs using pure-grade LGL. The addition to the membrane composition of any of the tested anionic surfactant gave rase to homogeneous and stable formulations of NVs without the need to heat the aqueous phase to 60 ºC during manufacturing process.

Additionally, we proved that LGL can be completely replaced by LGC to obtain stable and homogeneous anionic Sit:LGC NVs (molar ratio 1:1).

3.4. Effect of surfactant alkyl chain length in the formation of vesicles

Due to the promising results obtained with LGL, other APGs were tested to self-assemble in NVs with Sit. The effect of the carbon chain length of the APG surfactant in the formation of Sit-based NVs was studied by comparing the systems obtained with LGL with those formed with decyl glucoside (DGL) and octyl glucoside (OGL), i.e., alkyl polyglucosides surfactants with a carbon chain length of respectively C10 and C8 (**Table 3.1** and **Figure 3.14**).

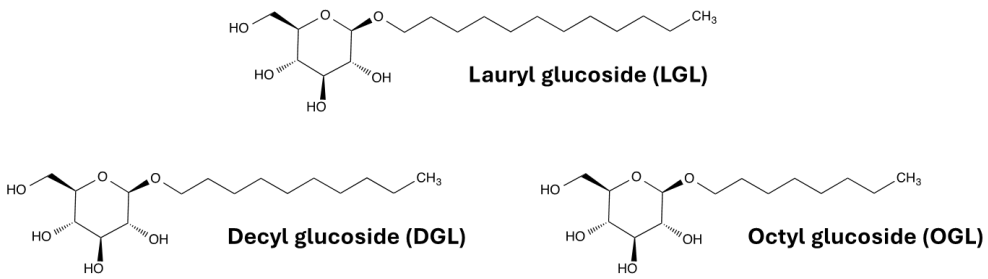


Figure 3.14. Molecular structure of lauryl glucoside, decyl glucoside and octyl glucoside.

To produce these new formulations using DGL and OGL, DELOS methodology was used with the intermediate scale equipment (see **Section 8.2.1**) and the same conditions than for pure LGL were applied, i.e., same membrane components concentration, molar ratio and heating the aqueous phase to 60 ºC during depressurization step.

Surprisingly, no vesicles were obtained when using DGL or OGL surfactants. When adding 3% of anionic additives LGC or SLS, vesicles were not formed either.

As discussed in **Section 3.2.2** using pure LGL, the use of pure-grade reagents was challenging. For this reason, cosmetic-grade APGs were also evaluated. In this sense, two different reagents were used: DGL-m_{C8-10}, containing a mixture of alkyl chains of C8-10; and DGL- m_{C8-16}, containing a mixture of alkyl chains of C8-16 (**Table 3.1**).

When using the DGL-m_{C8-10} surfactant, no NVs were observed, the same result as with pure-grade DGL surfactant. Instead, when the DGL-m_{C8-16} surfactant was employed, a formulation containing NVs was produced (**Table 3.6** and **Figure 3.15**).

Table 3.6. Composition and physicochemical characterization of nanovesicle formulation prepared by DELOS in **Section 3.4.**

Surfactant	Sit:DGL-m_{C8-16}		Hydrodynamic diameter mean [nm]	Size PDI	Apparent ζ-Pot [mV]	Stability [months]
	Molar ratio	Concentration[a] [mg/mL]				
DGL-m_{C8-16}	1:1	5.15	211.2 ± 0.4	0.16 ± 0.01	-34 ± 1	> 1

[a] *Theoretical concentration.*

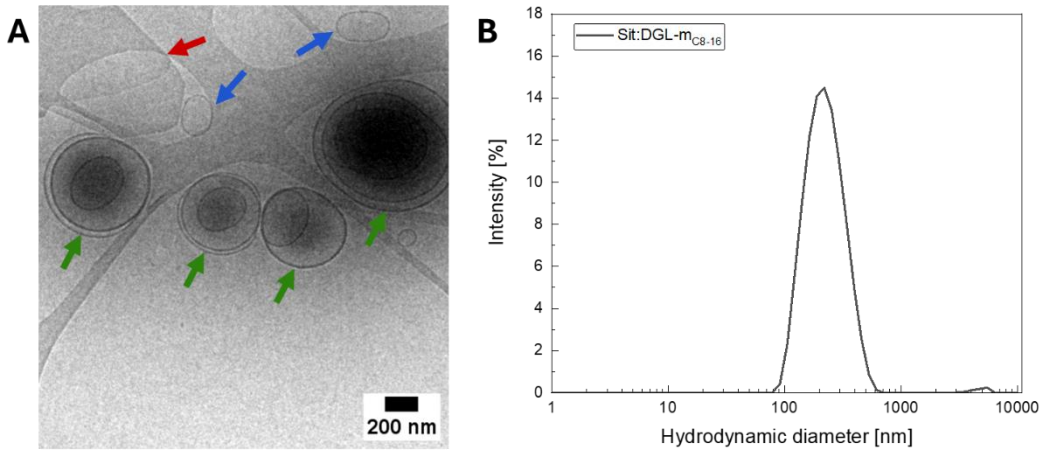


Figure 3.15. **(A)** Representative cryo-TEM image of Sit:DGL-m_{C18-16} NVs. Different kind of structures were observed: mainly unilamellar vesicles (blue arrows) and multilamellar vesicles (green arrows), but also some precipitates (red arrows). **(B)** Particle size distribution of the Sit:DGL-m_{C18-16} NVs.

The main conclusion obtained from all these experimental results was that Sit/APGs NVs seem to be formed only when the surfactant carbon chain length was ≥12C, as shown in **Table 3.7**. Therefore, the explanation of these results is related to the length of the alkyl chain of the APGs. On the one hand, for other types of vesicles formed by sterols and surfactants, it is known the importance of the bimolecular synthon, where the sterol, which is

hydrophobic, is mainly located inside the bilayer interacting with the alkyl chain of the surfactant and below their hydrophilic heads, which is the part in contact with the aqueous environment[6,37]. On the other hand, it has been also reported the impact that the alkyl chain length might have on the surfactant packing parameter in the process of the self-assembly of amphiphiles to form bilayers[41,42]. Thus, if the alkyl chain of OGL and DGL is too short to form the bimolecular synthon with Sit and self-assemble in bilayers, the Sit molecule is not stabilized in the aqueous media, leading to its precipitation due to the high hydrophobicity of sterols.

Table 3.7. Effect of alkyl chain length of the APG surfactant on the formation of Sit:APGs NVs.

APG surfactant	Carbon chain length	Additive component	Sit:APG:Additive (molar ratio)	Vesicles
OGL[a)]	C8	-	1:1:0	No
DGL [a)]	C10	-	1:1:0	No
DGL	C10	LGC [b)]	1:1:0.05	No
DGL	C10	SLS	1:1:0.08	No
DGL-m_{C8-C10}	C8-C10	-	1:1:0	No
DGL-m_{C8-C16}	C8-C16	-	1:1:0	Yes

[a)] During production with DELOS process, the aqueous phase was heated to 60 °C.

[b)] LGC reagent used was a mixture of LGL, intended as alkyl glucosides of C10-16 chain length, and the corresponding carboxylates; thus, the ratio 1:1:0.05 refers to the mixture and not the real content of LGC.

3.4.1. Impact of manufacturing methodology in the formation of NVs. Comparison of DELOS *vs.* thin film hydration techniques

Although all the evidence pointed to the importance of the alkyl chain length of the APGs used to self-assemble in NVs with Sit, the results obtained were unexpected. Previous literature reported the formation of NVs when using DGL or OGL and cholesterol[27,35], and due to the similarity in the chemical structure of cholesterol and β-sitosterol (**Figure 3.2**), we did not expect such different behavior.

Besides the sterol used, another difference between the previously published results and our formulations was the manufacturing methodology. In our work, DELOS methodology was employed, while in the previous results described in the literature, thin film hydration (TFH) method was used. With a view of evaluating if results were dependent on the NVs production method, we decided to perform a comparative study using the same procedure

reported by Muzzalupo *et al.*, which described the obtention of NVs using cholesterol and OGL, DGL and LGL by TFH[35]. This methodology is a conventional preparation method to obtain NVs that is widespread at laboratory scale to formulate nanovesicles.

Thus, three different surfactants, OGL, DGL and LGL, were used to evaluate the formation of NVs with β-sitosterol (**Figure 3.16** and **Table 3.8**). The detailed methodology to produce the samples is described in **Section 8.2.2**. In this case, the conditions to produce the samples were selected to mimic those from literature. Then, the formulations were characterized by optical microscopy (see **Section 8.3.3**), DLS, ELS and cryo-TEM.

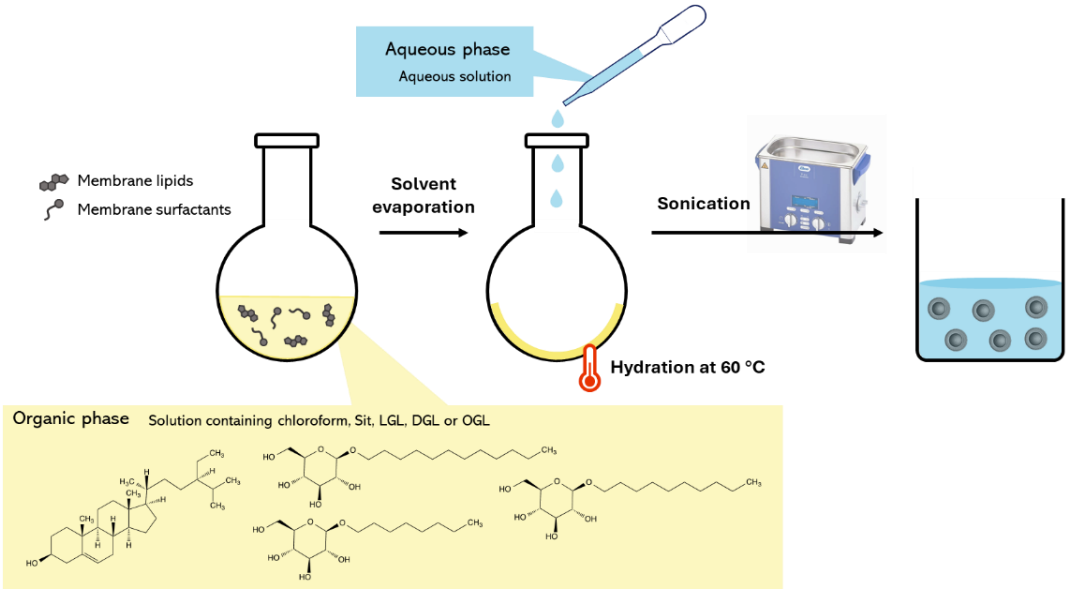


Figure 3.16. Schematic representation of nanovesicle preparation by thin film hydration method.

Table 3.8. Composition and physicochemical characterization of Sit/APG nanovesicle formulations prepared by THF method in **Section 3.4.1**.

Formulation	Molar ratio	Concentration[a)] [mg/mL]	Hydrodynamic diameter mean [nm]	Size PDI	Apparent ζ-Pot [mV]
Sit:OGL	1:1	3.68	4000 ± 1000*	1 ± 0*	18 ± 3*
Sit:DGL	1:1	3.79	7000 ± 3000*	0.6 ± 0.2*	25 ± 3*
Sit:LGL	1:1	4.07	250 ± 4	0.23 ± 0.05	-32.3 ± 0.3

a) Theoretical concentration.

** Results in red do not meet quality criteria of the technique, they are not reliable.*

First of all, just by analyzing the macroscopic appearance of the three samples prepared by THF (**Figure 3.17A**) it was considerably clear that the results obtained with OGL and DGL were different than with LGL. The Sit:LGL formulations obtained by THF presented an homogeneous aspect with whitish color. In contrast, Sit:OGL and Sit:DGL formulations appeared completely sedimented with a white precipitate at the bottom of the vial and showing a clear two- phase separation.

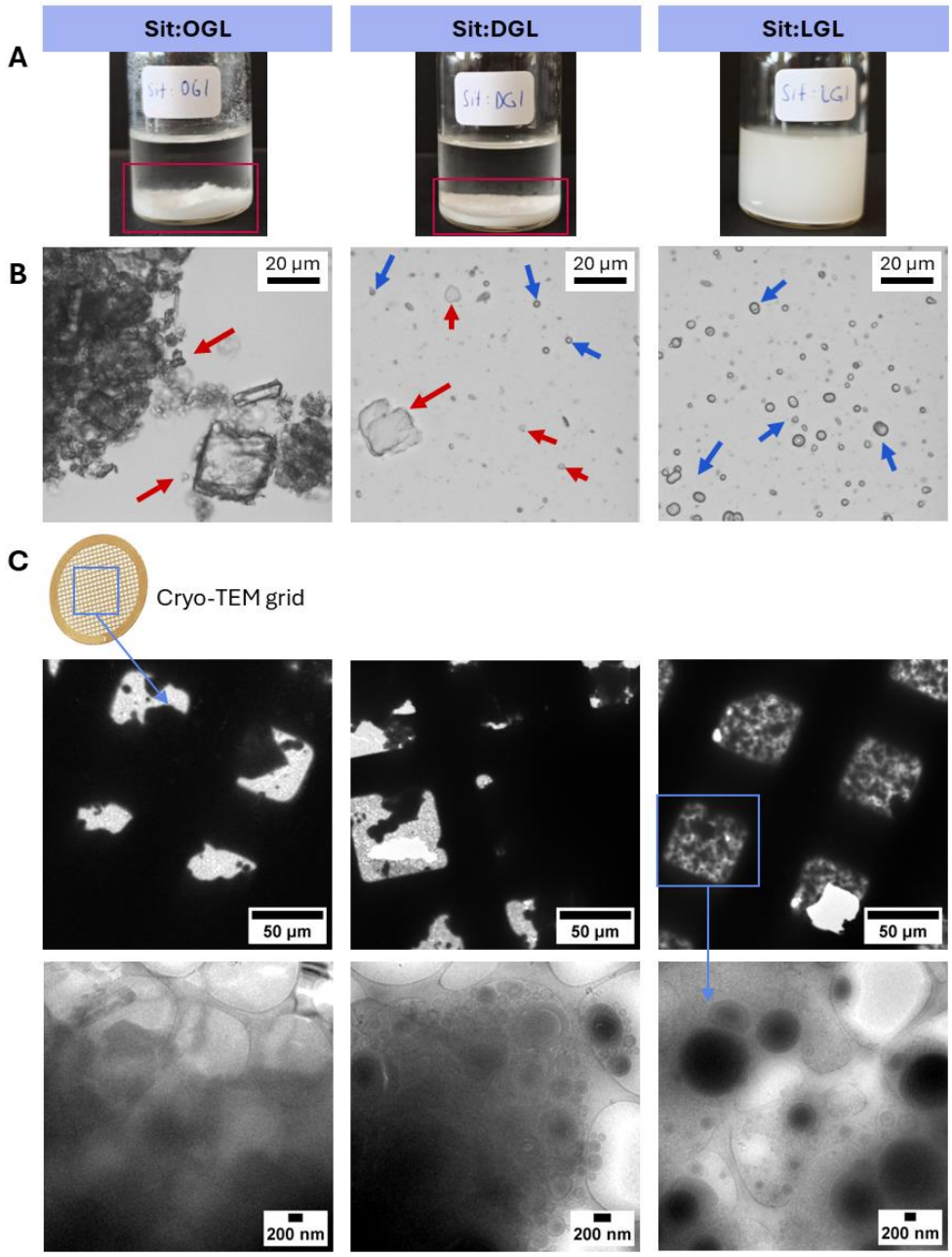


Figure 3.17. Analysis of Sit:OGL (first column), Sit:DGL (second column) and Sit:LGL (third column) formulations prepared by THF method. **(A)** Macroscopic appearance of each sample 1 week after production. **(B)** Optical microscopy images taken at 50x. Vesicular-like structures (blue arrows) and precipitates (red arrows). **(C)** Cryo-TEM images of general views of the grid (top images, 50x) and focused on nanostructures (bottom images, 3000x).

In order to better analyze the type of precipitate present in the different formulations, the samples were characterized by optical microscopy (**Figure 3.17B**). Two different kinds of particles were seen in the samples: precipitates (red arrows) or vesicular-like structures (blue arrows). In the case of formulations which presented a two-phase separation at macroscopical level, Sit:OGL and Sit:DGL, both presented precipitates with a crystalline aspect at microscopic level. However, in the case of Sit:LGL sample, which was macroscopically homogeneous, only the spheric particles were observed, without precipitates in the sample.

Going deeper into the nanometric scale thanks to the cryo-TEM technique, the same trend was observed. Analyzing the general view of cryo-TEM grid of each formulation (**Figure 3.17C**, top panel) it was clearly seen that Sit:OGL and Sit:DGL samples presented aggregates, whereas the Sit:LGL system showed an homogeneous distribution over the grid. When analyzing the samples more in depth, (**Figure 3.17C**, bottom panel), in the case of Sit:OGL sample, there were only big aggregates. In contrast, when the agglomerates of the Sit:DGL formulation were examined, aggregates of NVs were perceived. However, there was not a homogeneous distribution of these NVs, all of them were agglomerated. Finally, in the Sit:LGL systems, a large amount of NVs were observed and all of them were homogeneously distributed in the grid. Such differences in the NVs distribution can explain the macroscopical appearance of the samples, where the agglomeration of Sit:DGL NVs formed unstable aggregates that sediment, whereas the Sit:LGL NVs remained in suspension as they were homogeneously distributed.

Finally, the samples were analyzed by DLS (**Table 3.8**). In the case of Sit:OGL (particle size 4041 ± 1013 nm and PdI 1.60 ± 0.23) and Sit:DGL (particle size 7462 ± 2528 nm and PdI 0.6 ± 0.2), the samples were so heterogeneous that the measures did not met the quality criteria of the measurements, meaning that the data was not reliable. On the other hand, Sit:LGL NVs (particle size 250 ± 4 nm and PdI 0.23 ± 0.06) met the quality criteria of the measurement (**Section 8.3.1.1**) and the particle size was in the nanometric range with a narrow particle size distribution. Speaking of ζ-Pot, it was curious that in both cases were the samples were sedimented (OGL and DGL formulations), the value was positive and below 30 mV, whereas in the case of LGL were the formulation was macroscopically more stable, the ζ-Pot was negative and around -30 mV.

In conclusion, both manufacturing methods, DELOS and TFH, showed the same trend: the formation of stable and homogeneous formulations of NVs with Sit and APGs was only possible with APGs of carbon chain length ≥ C12, i.e., lauryl glucoside or APGs with higher carbon chain lengths. Thus, the results obtained were not dependent on the method used to produce the NVs.

According to these results, the formulations for further studies were prepared with LGL and LGC, APGs with carbon chain lengths of ≥ C12, both pure and cosmetic grade.

3.5. Loading of α-tocopherol in the nanovesicles

After obtaining different stable and homogeneous Sit:APGs NVs, it was of our interest to evaluate their potential application as delivery system of active molecules. As a first approach, the integration of a hydrophobic active ingredient, α-tocopherol (TCP), was tested.

TCP is a lipophilic small biomolecule (**Figure 3.18**) with antioxidant properties and the most abundant form of vitamin E in human tissues, essential for human health[43]. It is widely used in cosmetics as antioxidant and skin conditioning[16] ingredient at different concentrations, normally between 1% to 5% (w/w) in the final formulation[44,45].

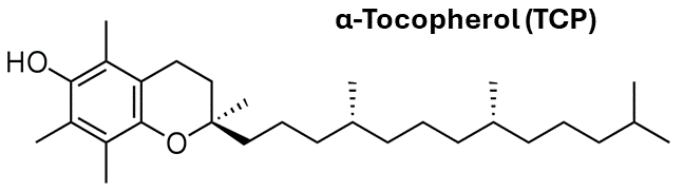


Figure 3.18. Molecular structure of α-tocopherol (TCP).

In this regard, the Sit:LGL:LGC (1:0.8:0.2) vesicular system was chosen to evaluate the integration of TCP (**Table 3.9**). TCP was dissolved in the organic phase during the DELOS process (**Figure 3.19** and **Section 8.2.1**), at a final theoretical concentration of 0.75 mg/mL, which was equivalent to a 20% (w/w) of the membrane components of the formulation.

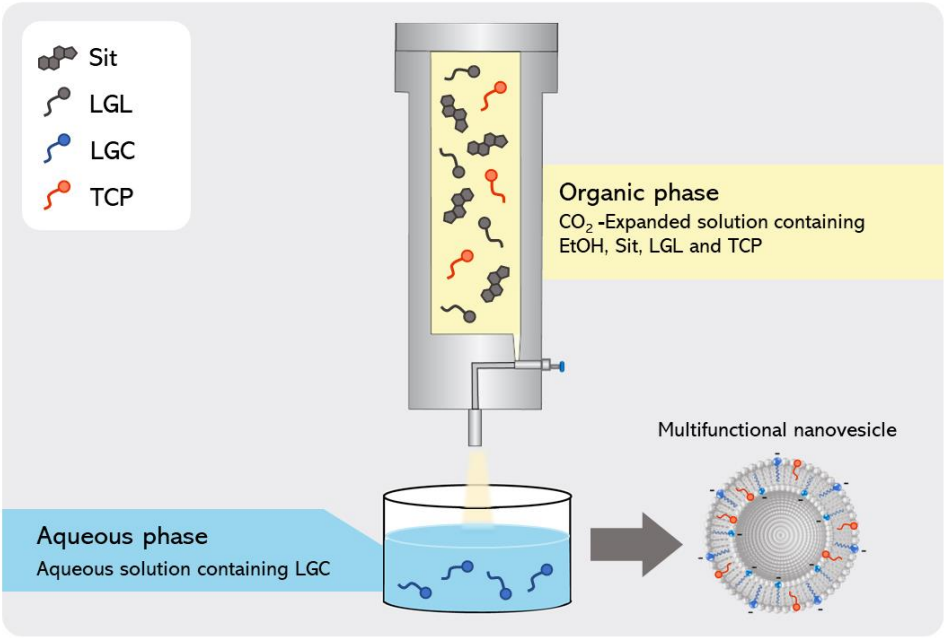


Figure 3.19. Schematic representation of DELOS methodology used for the preparation of nanovesicles composed of Sit:LGL:LG NVs (1:0.8:0.2 molar ratio) loaded with antioxidant ingredient TCP.

Table 3.9. Composition and physicochemical characterization of Sit:LGL:LGC nanovesicle formulation loaded with antioxidant ingredient TCP (n = 3).

System (molar ratio)	TCP concentration[a)]	Hydrodynamic diameter mean [nm]	Size PDI	Apparent ζ-Pot [mV]	EE [%]
Sit:LGL:LGC[b)] (1:0.8:0.2)	0.75 mg/mL 20% (w/w)	131 ± 4	0.19 ± 0.01	-41 ± 1	49 ± 12

[a)] *Theoretical concentration.*

[b)] *LGC reagent used was a mixture of APGs, intended as alkyl glucosides of C10-16 chain length, and the corresponding carboxylates; thus, the ratio 1:0.8:0.2 refers to the mixture and not the real content of LGC.*

A formulation containing TCP-loaded NVs was achieved, showing macroscopical appearance (**Figure 3.20A**) and physicochemical properties similar to the plain NVs (**Table 3.9**). In this case, it was also of interest to evaluate the entrapment efficiency (EE) of TCP into the NVs following the methodology described in **Section 8.3.5.1**. As TCP is a lipophilic molecule, it was expected to be loaded inside the bilayer of the NVs, in which there is a hydrophobic environment. An EE of 49 ± 12% was calculated from UV-vis measurements.

In terms of NVs morphology, cryo-TEM images show the same morphology than blank NVs, with the coexistence of unilamellar and multilamellar vesicles (**Figure 3.20B**). Additionally,

the presence of lipophilic emulsions on an aqueous environment was also perceived in some image frames, as opaque spherical globules. These structures were not seen in the plain vesicles' images, meaning that was probably the presence of lipophilic TCP which originated this new structuration. The emulsion droplets had the same size than nanovesicles, so it was not possible to differentiate them by DLS.

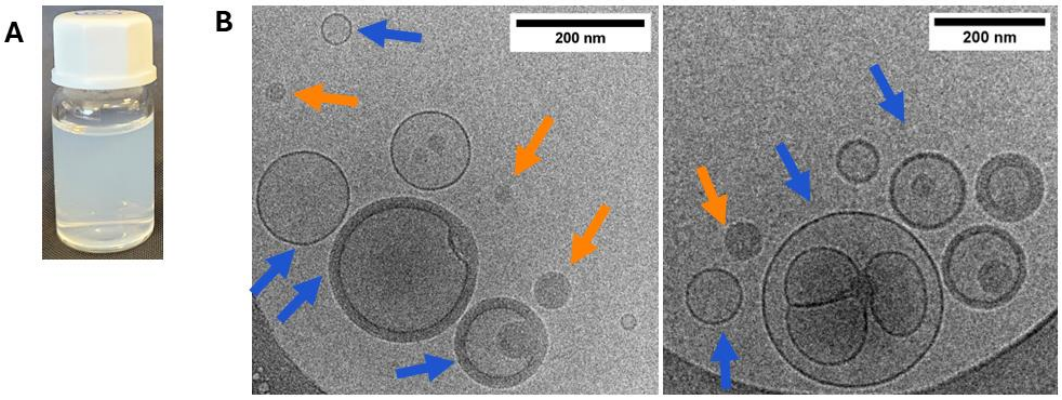


Figure 3.20. (A) Macroscopical appearance of the TCP-loaded NVs sample (Sit:LGL:LGC, molar ratio 1:0.8:0.2) 1 year after production. **(B)** Representative cryo-TEM images of the TCP-loaded NVs 10 days after production. Vesicular-like structures (blue arrows) and precipitates (orange arrows).

To go a step further, it was of our interest not only to analyze the proper integration of TCP in the Sit:LGL:LGC NVs formulation, but also to investigate if the molecule was still active after encapsulation, i.e., if it maintained the antioxidant activity. To do so, we used the 2,2-diphenyl-1-picrylhydrazyl (DPPH) assay, a simple and well stablished method to evaluate free radical scavenging ability of antioxidants (described in **Section 8.5.1**). Briefly, DPPH is a stable free radical able to be reduced in presence of antioxidants, undergoing to color changes that can be followed by absorbance measurements with a UV-vis spectrophotometer (**Figure 3.21A**)[46,47].

The activity of TCP after encapsulation in the NVs was compared with the activity of free TCP dissolved in ethanol after 7 days of production or preparation of the samples. The assay was performed in a molar ratio DPPH:TCP of 1:0.3. Considering that 1 mol of TCP reduces 2 mol of DPPH, the antioxidant capacity expected in this assay was 60%[47]. Results showed that both samples, free TCP and TCP-loaded NVs, had the above-mentioned antioxidant capacity (58 ± 13% and 63 ± 3%, respectively), showing that the encapsulation of TCP in the NVs did not affect the functionality of the molecule (**Figure 3.21B**). Furthermore, to verify that the antioxidant capacity came from TCP in the TCP-loaded NVs samples, blank NVs were also evaluated. The formulation of NVs was the same but without TCP (Sit:LGL:LGC, molar ratio

1:0.8:0.2), and the same analysis procedure was followed. As it can be seen in **Figure 3.21B**, as expected the blank NVs did not show antioxidant capacity (3 ± 1%), confirming that all the antioxidant activity observed in TCP-loaded NVs come from active TCP.

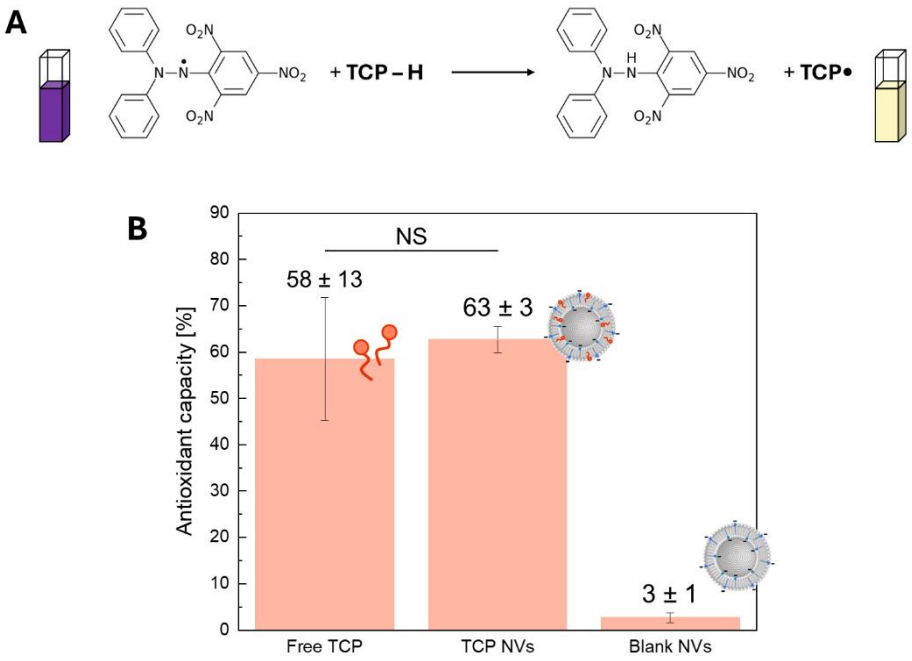


Figure 3.21. **(A)** Schematic representation of the reaction of DPPH with an antioxidant molecule such as TCP. **(B)** Antioxidant capacity of free TCP, TCP-loaded NVs (Sit:LGL:LGC, molar ratio 1:0.8:0.2), and blank NVs (Sit:LGL:LGC, molar ratio 1:0.8:0.2). Values represent the antioxidant capacity mean ± s.d of two independent experiments. Statistical analysis to compare free TCP and TCP NVs was performed by T-test. $p < 0.05$ and NS: non-significant differences.

To sum up, we achieved to stabilize a lipophilic vitamin in an aqueous formulation maintaining intact its antioxidant capacity. The formulation presented promising physicochemical properties although further optimization could be done in terms of improving EE values. Nevertheless, these first results were encouraging to test the encapsulation of other lipophilic active molecules but also other type of payloads like small hydrophilic molecules, peptides and proteins.

3.6. Impact of membrane composition on the lamellarity of the nanovesicles

Throughout all this **Chapter**, we have been reporting different new nanovesicular systems formed by Sit, LGL and LGC. During the characterization of these formulations with cryo-TEM, it was recurrent to find vesicles with different morphologies. Normally, there was the coexistence of unilamellar and multilamellar vesicles.

To gain further understanding of the impact of membrane composition in the morphology of the nanovesicles, the most promising formulations described in the previous sections were characterized by small-angle X-ray scattering (SAXS)[1].

SAXS is a useful characterization technique widespread in colloidal science to study the structure of materials on the molecular scale (see **Section 8.3.4**). It presents different features since it is non-invasive, non-destructive and can give statistical data of the bulk sample. When applied to soft materials like nanovesicles, SAXS allows the study of structural information including membrane thickness, lamellarity, ordering or contribution of some component[48,49].

For the purpose of fully characterizing the new nanovesicular systems developed, SAXS analysis was performed to study the multilamellarity and cross-section structure (**Figure 3.22A**) of four of the most promising formulations, they are listed below:

1. **Sit:LGL-m$_{C12-16}$**, molar ratio 1:1, membrane components concentration 2.86 mg/mL
2. **Sit:LGC**, molar ratio 1:1, membrane components concentration 2.86 mg/mL
3. **Sit:LGL:LGC**, molar ratio 1:0.8:0.2, membrane components concentration 3 mg/mL
4. **Sit:LGL:LGC + TCP**, molar ratio 1:0.8:0.2, membrane components concentration 3 mg/mL, TCP concentration 0.75 mg/mL

All formulations were evaluated after 4 months from the preparation to enable the stabilization of the vesicular systems. The experimental details are in **Section 8.3.4**.

The analysis of the results is presented in **Figure 3.22** and **Table 3.10**. They clearly revealed the impact of the membrane composition on the lamellar structure of the nanovesicles. **Figure 3.22B** shows the experimental SAXS patterns in symbols and the fitted model in

[1] These measurements were performed at ALBA synchrotron (Spain) and they were analyzed in collaboration with Dr. Cristián Huck-Iriart from ALBA synchrotron (Spain) and Prof. Jan Skov Pedersen from Aarhus University (Denmark).

continuous line. SAXS data suggested that the samples were somewhat heterogeneous where the peak near 0.1 Å^{-1} is related to the multilamellarity (N_{av} in **Table 3.10**) with influence from the bilayer form factor. The only exception was the sample Sit:LGC (1:1) that did not show the peak from the multilamellarity structure factor, but just a broad bump related to the bilayer cross-section structure was observed. However, for this sample, a very sharp but low-intensity peak was observed indicating the presence of crystals.

The formulation not only affected the multilamellarity, but also the electron density profile from the bilayer cross section (**Figure 3.22C**). The results from the fitting, shown in **Table 3.10**, show the relationship between the packing and the bilayer structural parameters. While Sit:LGC (1:1) profile presented a broader profile of the head groups, which may results in a more disordered structure, this sample had no evidence of multilamellar structure. However, the other samples showed a decrease in the width and an increase in the amplitude of the Gaussian function of the head groups with an increase of the average number of layers.

Table 3.10. Fit results from SAXS modelling.

Formulation	χ^2	S_{head}	σ_{head} [Å]	f_{mono}	N_{av}	D [Å]
Sit:LGL-m$_{C12-16}$ (1:1)	0.57	0.608 ± 0.005	9.77 ± 0.09	0.61 ± 0.02	1.6 ± 0.2	55.8 ± 0.1
Sit:LGC (1:1)	1.43	0.54 ± 0.01	11.1 ± 0.3	1.0	-	-
Sit:LGL:LGC (1:0.8:0.2)	0.50	0.66 ± 0.01	9.0 ± 0.2	0.49 ± 0.03	3.2 ± 0.2	47.7 ± 0.1
Sit:LGL:LGC + TCP (1:0.8:0.2)	0.49	0.65 ± 0.01	8.6 ± 0.1	0.76 ± 0.01	3.5 ± 0.3	48.0 ± 0.2

χ^2 is the reduced weighted chi-square; S_{head} is the scale of the Gaussian for the head layers; σ_{head} is the sigma of the head layer Gaussian; f_{mono} is the fraction of monolayers; N_{av} is the average number of layers; D is the repeat distance

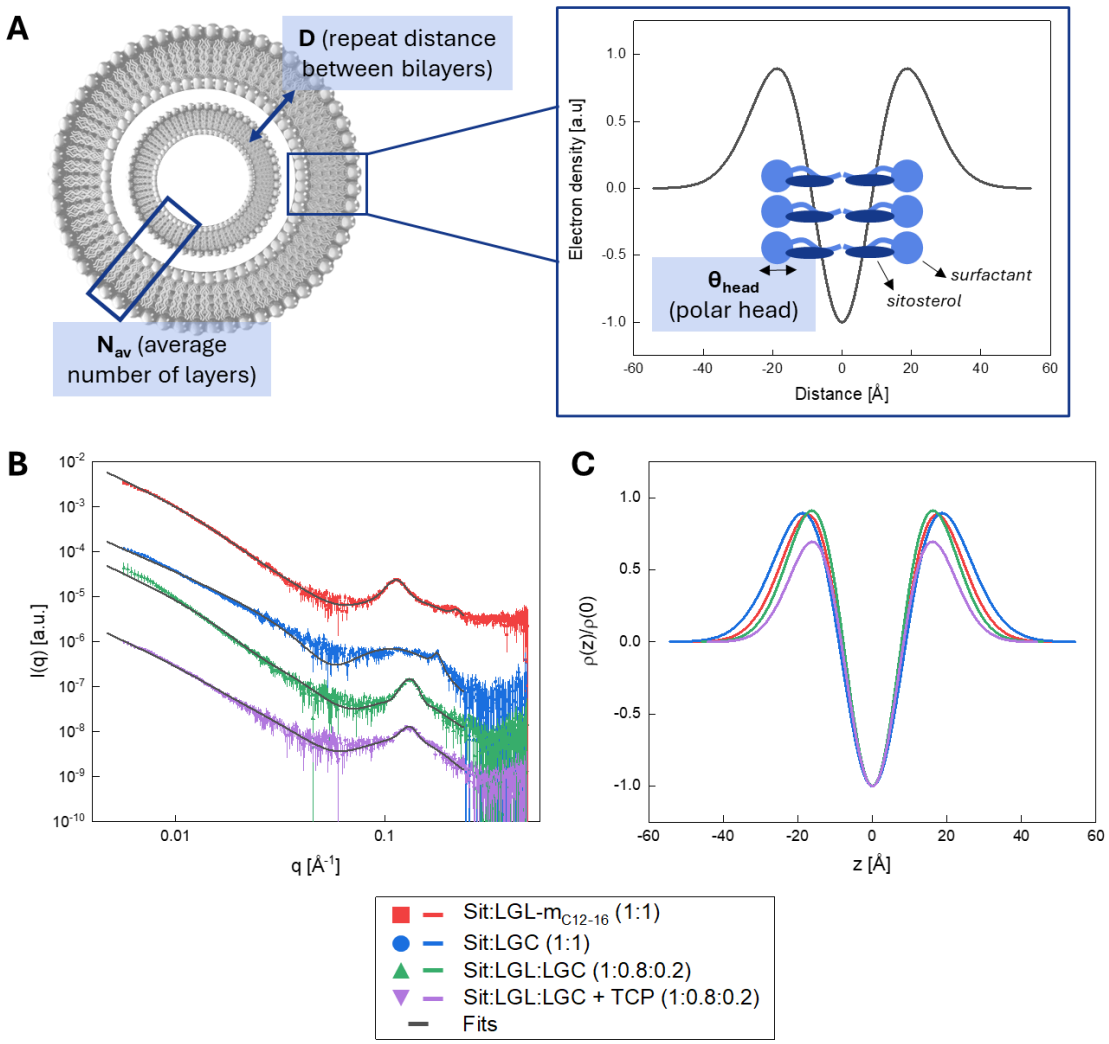


Figure 3.22. **(A)** Scheme of the nanovesicle parameters and a representative cross-section profile which could be determined after SAXS data modelling: N_{av} is the average number of layers in the nanovesicles, D is the distance between bilayers in multilamellar vesicles and θ_{head} is the size of the polar head. Adapted from Tomsen-Melero[50]. **(B)** SAXS data plotted in log-log scale, the experimental data as symbols and the model as continuous curves. **(C)** Electron density profile of the bilayer cross section obtained from the model. In blue Sit:LGL-m_{C12-16} NVs, in red Sit:LGC NVs, in green Sit:LGL:LGC NVs and in purple Sit:LGL:LGC + TCP NVs.

From the results, it was evident that the presence of LGL in the formulation lead to the formation of multilamellar vesicles (**Table 3.10**). For Sit:LGL-m_{C12-16} and Sit:LGL:LGC samples, the analysis gave an average number of layers (N_{av}) above 1 (1.6 ± 0.2 and 3.2 ± 0.2 respectively) and a fraction of monolayers (f_{mono}) of 0.61 ± 0.02 and 0.49 ± 0.03, respectively. These results were also indicating that the type of LGL used affected the lamellarity of the vesicles formed. The use of LGL-m_{C12-16} reduced both the average number of layers and the number of multilamellar vesicles because the fraction of monolayers was higher. When pure LGL was used in combination with a small percentage of LGC, the average number of layers

doubled. The distance between bilayers was also slightly different, being higher in the case of LGL-$_{mC12-16}$ (55.8 ± 0.12 Å) than for pure LGL (47.7 ± 0.13 Å). All this information was indicating that the quality and purity of LGL was affecting the final properties of the vesicles. In contrast, the sample composed of Sit:LGC (1:1) was the only formulation that mainly presented unilamellar vesicles. Clearly, the negatively charged part of the LGC molecule seemed to promote the formation of vesicles with only one membrane.

All these results were in accordance with cryo-TEM images already reported in the previous sections (**Figure 3.23**). It is important to highlight that in cryo-TEM images, usually multilamellar vesicles are observed as vesicles with thicker membranes due to the stack of different bilayers that the microscope cannot resolve and differentiate well. Considering this point, the sample composed of Sit:LGL:LGC (molar ratio 1:0.8:0.2) was the one that in the images presented the vesicles with thicker membranes. For Sit:LGL-m$_{C12-16}$ formulation (molar ratio 1:1), there were some vesicles that presented bilayers with an increased thickness, but qualitatively they seemed thinner and in a lower quantity, which was confirmed by SAXS analysis, a more robust and quantitative technique (**Table 3.10**). Finally, for Sit:LGC formulation (molar ratio 1:1) the vesicles were mainly unilamellar and with thin bilayers, indicating the absence multilamellar vesicles as also shown by SAXS measurements (**Table 3.10**).

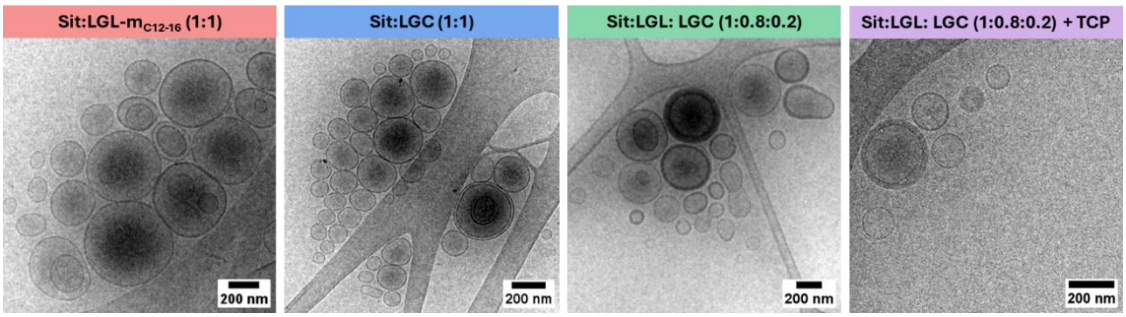


Figure 3.23. Recapitulation of cryo-TEM images of the different systems analyzed by SAXS.

Furthermore, the impact of the incorporation of TCP in the Sit:LGL:LGC NVs (molar ratio 1:0.8:0.2) was also analyzed. As demonstrated in **Table 3.10**, the presence of TCP increased the fraction of monolayers from 0.49 ± 0.03 for empty NVs to 0.76 ± 0.01 for TCP NVs, whereas the average number of layers was maintained approximately the same, 3.2 ± 0.2 and 3.5 ± 0.3, respectively. Therefore, the presence of TCP in the formulation promoted the formation of unilamellar vesicles, but when multilamellar vesicles were formed they tended to have approximately the same average number of layers and the same repeat distance between them.

Overall, SAXS analysis appeared to be a complementary technique with cryo-TEM both pointing to similar results. LGL, a neutral surfactant without charge, promoted the formation of multilamellar NVs, whereas LGC, a negative charge surfactant, tended to form unilamellar NVs. As mentioned in previous sections, the negative charge of LGC may cause electrostatic repulsion between bilayers promoting the formation of mainly unilamellar NVs. In contrast, since LGL has no charge, do not existed this electrostatic repulsion allowing the formation of multilamellar structures, although the type of LGL used has an impact on the quantity of multilamellar NVs and the average number of bilayers.

3.7. Biocompatibility and skin permeation analysis of the new nanoformulations

To complete the characterization of this new platform of NVs based on Sit and APGs, the suitability of these systems for topical applications was evaluated. To do so, as a proof of concept, two different assays were performed: an *in vitro* skin irritancy test with human epidermis models, and an *ex vivo* skin permeation assay of a fluorophore loaded in our NVs systems[2]. APG surfactants are promising candidates for enhanced skin absorption and efficient dermal delivery without exerting skin irritation[51,52], so the specific objective was to evaluate whether the NVs containing APGs behave similarly.

3.7.1. *In vitro* skin irritation assays

To assess the skin sensitivity to the new formulations, an *in vitro* skin irritation test was carried out based on the OECD (Organization for Economic Co-operation and Development) guideline 439[53]. The objective of this guideline is to stablish the basis to assess *in vitro* skin irritation of chemicals (substances or mixtures) using reconstructed human epidermis (RHE) models. These models are commercially available, and the OECD guideline indicates the validated ones to perform the assays. Briefly, the experiment consists of the exposure of

[2] These studies were performed in collaboration with the groups of Prof. Silvia Pescina (ADDRes Lab, Department of Food and Drug) and Prof. Cristina Sissa (Department of Chemistry, Life Sciences and Environmental Sustainability), both from the University of Parma (Italy), in the frame of a stay under "Micro4Nano" project.

the tested substance to the RHE model during a certain time period (depending on the RHE model used) and the evaluation of the cell viability 42 h after exposure.

The experimental conditions used are detailed in **Section 8.6.1**.

To perform the skin irritation study, the most promising and well characterized nanovesicular systems were selected: Sit:LGL-m_{C12-16} (1:1), Sit:LGC (1:1), Sit:LGL:LGC (1:0.8:0.2) and Sit:LGL:LGC + TCP (1:0.8:0.2) (molar ratio). Furthermore, the dispersant media of the NVs (water/EtOH 15% (v/v)) was also evaluated as an internal control.

The results obtained are represented in **Figure 3.24**, where negative (i.e., DPBS) and positive control (i.e., 5% of sodium dodecyl sulfate (SDS) in DPBS (w/v)) are shown along with the tested NVs samples. Results showed that under the applied experimental conditions, none of the four tested formulations or neither the dispersant media showed irritant effect, considering that cell viability was far above the 50% threshold level with respect to the negative control[53].

Therefore, the new platform of Sit:LGL:LGC nanovesicles can be classified as non-irritant and suitable for topical application.

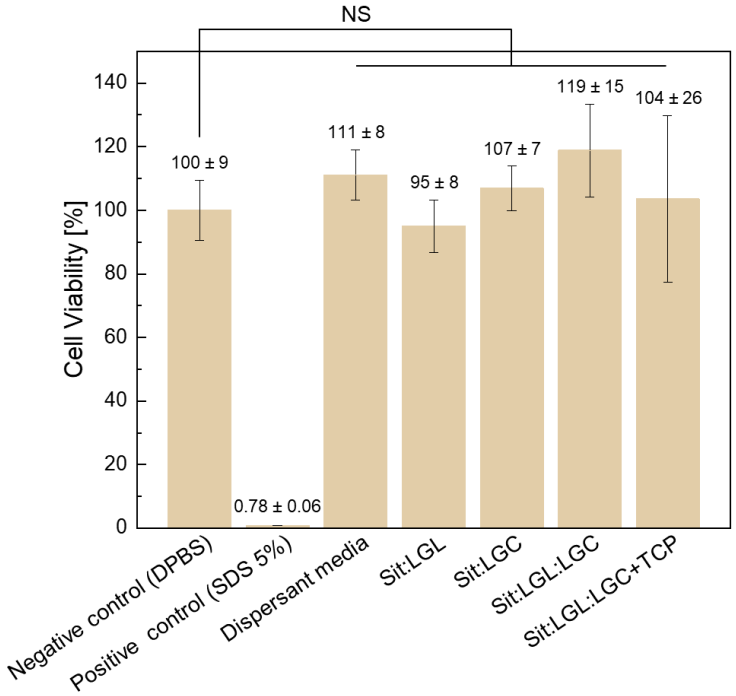


Figure 3.24. *In vitro* skin irritation assay of Sit:LGL-m_{C12-16} (1:1), Sit:LGC (1:1), Sit:LGL:LGC (1:0.8:0.2) and Sit:LGL:LGC + TCP (1:0.8:0.2) NVs and the corresponding controls (negative and positive control and dispersant media (water/EtOH 15% (v/v))) in the SkinEthic™ RHE models. Bars represent the mean of 3 independent experimental replicates ± standard deviation. All statistical analyses were conducted by one-way ANOVA followed by Tukey pairwise comparison. $p < 0.01$ and NS: non-significant differences.

3.7.2. Retention of the nanovesicles in skin explants assessed by two-photon microscopy

The permeation and retention levels in the skin of active ingredients is an important feature for topical local applications. When a payload must exert its function on the skin, as is the case for dermocosmetic products, it is crucial to cross the stratum corneum, a process that can be difficult depending on the nature of the molecule, and which can be enhanced be the presence of nanovesicles as vehicles for the payloads. However, it is also important that the ingredients do not reach the systemic circulation. Thus, for topical delivery of active ingredients it is important to have a balance enhancing permeation trough the epidermis without reaching the systemic circulation. For this, it is necessary to evaluate the skin permeation behavior of the topical ingredients.

Skin permeation of payloads contained in topical formulations can be evaluated *in vitro*, *ex vivo* or *in vivo* with different techniques[54]. When evaluating the skin permeation there are two steps: the permeation assay itself, and the analysis of this permeation. First, to evaluate the permeation there are different set ups, but diffusion techniques are the most used, in particular, the Franz-type diffusion cell (**Figure 3.25**), which was the set-up chosen for these experiments. Second, the permeation of a payload through the skin can be evaluated in a qualitative way, e.g., with microscopic techniques; or in a quantitative way, e.g., using chromatographic techniques such as high-performance liquid chromatography.

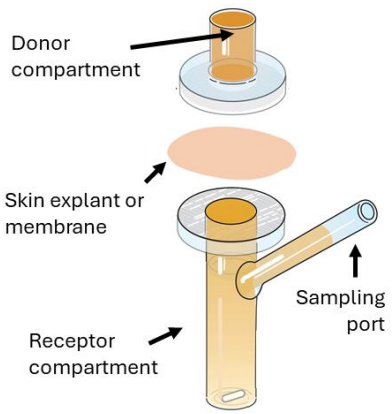


Figure 3.25. Scheme of a Franz-type diffusion cell adapted from *PermeGear, Inc*.

In collaboration with the University of Parma, in this Thesis two-photon microscopy (2PM), was used to evaluate the permeation of a fluorophore loaded in the newly developed nanovesicular systems. Specifically, 2PM is a fluorescence imaging technique mostly exploited to visualize thick biological tissues[55]. 2PM allows to collect images in depth, thanks

to the excitation with near infrared light, that penetrates deeper in biological tissues compared to UV-vis light due to the presence of transparency windows in this spectral region, and reduced scattering. 2PM relies on nonlinear interactions between matter and light (two-photon excited fluorescence (TPEF) and second harmonic generation (SHG)), that can occur only if the photon density is high, i.e., in a small volume around the focal point of the excitation beam photon densities. Thus, 3D images can be acquired by moving the focal point within the sample. 2PM has been demonstrated to provide useful information in permeation studies in skin[56], eye[57,58] and buccal mucosa[59].

To better understand the permeation of the vesicles through skin tissues and allow their visualization using imaging techniques, the fluorophore Nile red (NR) was loaded in Sit:LGL:LGC NVs (molar ratio 1:0.8:0.2). NR is a poorly water-soluble fluorescent probe (**Figure 3.26A** and **B**) with emission spectra that undergoes spectral shifts in environments of different polarity[60].

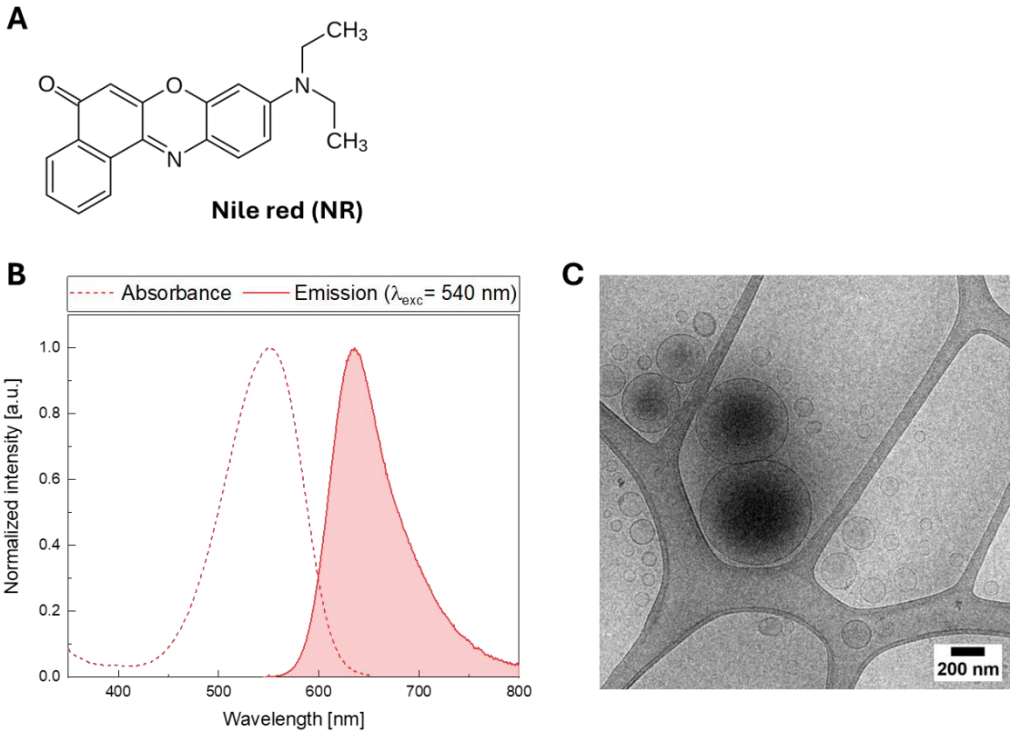


Figure 3.26. (A) Molecular structure of Nile red (NR). **(B)** Absorption and emission bands of NR in dimethyl sulfoxide (DMSO). **(C)** Representative cryo-TEM image of NR NVs (Sit:LGL:LGC, molar ratio 1:0.8:0.2).

The NR-loaded NVs were produced by DELOS methodology as explained in **Section 8.2.1**, dissolving the NR in the organic phase in ethanol. Homogeneous small vesicles were obtained (**Table 3.11** and **Figure 3.26C**) with similar physicochemical properties to blank

NVs. In addition, the NR concentration in the final was calculated by UV-vis spectroscopy (see **Section 8.3.5.2**) giving a value of 1.6 μM. The final NR concentration in NVs was enough to evaluate its skin permeation through 2PM.

Table 3.11. Composition and physicochemical characterization of NR-loaded nanovesicle formulation prepared in **Section 3.7.2**.

System (molar ratio)	Hydrodynamic diameter mean [nm]	Size PDI	Apparent ζ-Pot [mV]	NR concentration[a] [μM]
Sit:LGL:LGC[b] (1:0.8:0.2)	165 ± 1	0.20 ± 0.02	-59 ± 3	1.6

[a] *Calculated concentration by UV-vis spectroscopy.*

[b] *LGC reagent used was a mixture of APGs, intended as alkyl glucosides of C10-16 chain length, and the corresponding carboxylates; thus, the ratio 1:0.8:0.2 refers to the mixture and not the real content of LGC.*

The NR-loaded NVs formulation was applied for 3 h or 6 h on a full-thickness porcine skin specimen (see **Section 8.6.2.1**). Moreover, blank Sit:LGL:LGC NVs (molar ratio 1:0.8:0.2), the dispersant media (water/EtOH 15% (v/v)) and NR solution (1.6 μM) in water/DMSO 1% (v/v) were evaluated as controls, using the same procedure adopted for the formulation. Results are presented as 3D renderings of the skin specimens in **Figure 3.27**.

First, the use of the dispersant media (water/EtOH 15% (v/v)) affected the integrity of the stratum corneum which appeared damaged, even after only 3 h (**Figure 3.27A**). In contrast, the skin tested with blank NVs in the same dispersant media presented less alteration of the skin structure[56] (**Figure 3.27C, D** and **Figure 3.28**). This result indicated that the vesicles could protect the skin from the damage of ethanol and agreed with those obtained with the dermal irritancy assay, confirming that the new formulations of NVs are biocompatible.

When the skin was put in contact with NR in a water/DMSO 1% (v/v) solution, the emission collected came from both NR and endogenous fluorophores (autofluorescence). In **Figure 3.27E** it can be observed that, after 3 h of permeation, the fluorescence signal detected on the surface of the sample was not homogeneous: some regions presented a more intense NR emission (orange/yellow regions) while others presented a more greenish emission due to autofluorescence. On the other hand, in **Figure 3.27F** (6 h permeation), the signal acquired on the surface of the skin was a homogeneous yellow/orange emission due to both NR and endogenous fluorophores. Nevertheless, NR emission could not be detected through the whole epidermis, suggesting that its permeation was limited to the most superficial skin layers.

The application of NR NVs onto skin samples depicted a different outcome: the red/orange signal observed in **Figure 3.27G** and **Figure 3.27H** came mainly from NR that overcame the autofluorescence signal. These images demonstrate that, when loaded in NVs, NR permeated deeper through the skin to the epidermis. Furthermore, in the sample after 6 h of permeation, an enhanced diffusion front was observed.

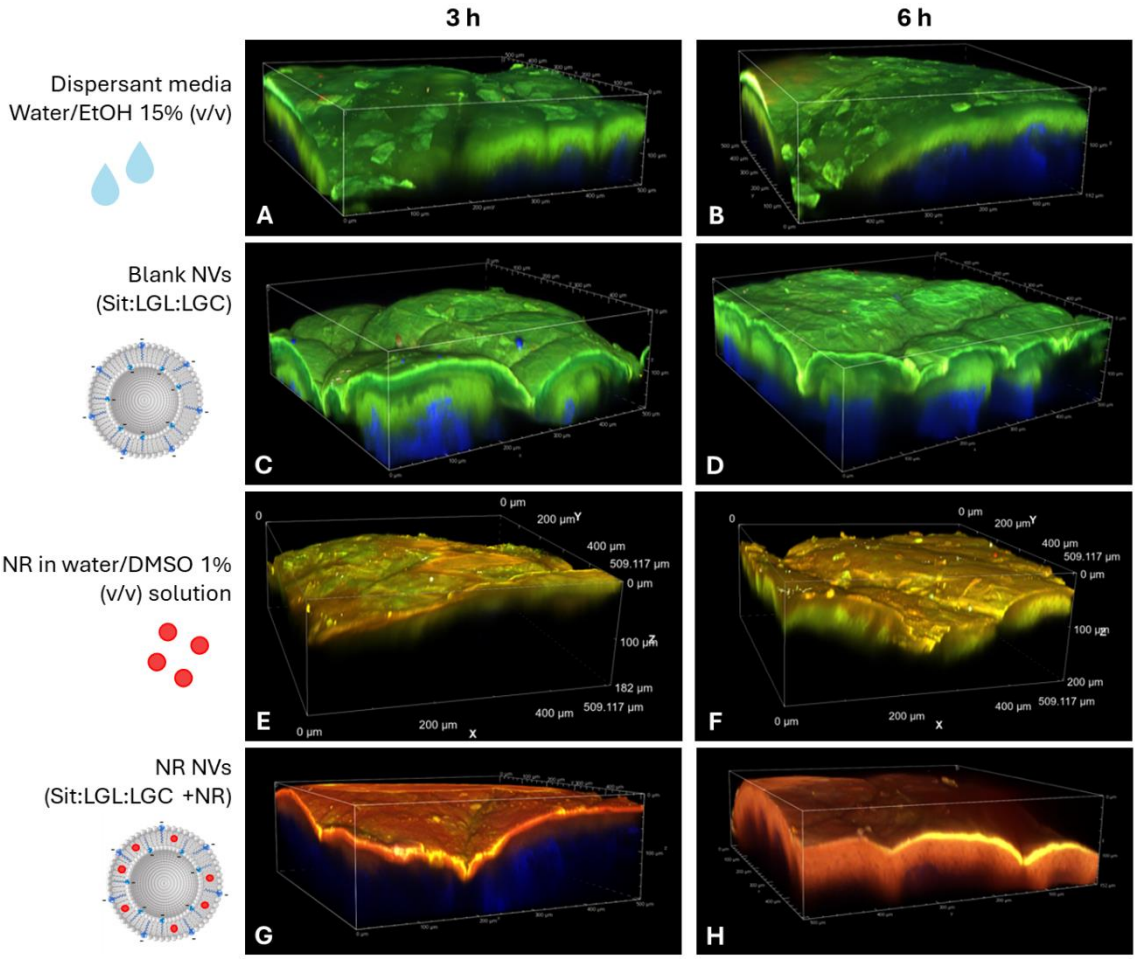


Figure 3.27. 3D renderings of the different skin samples. In panels **A** and **B** (dispersant media) and panels **C** and **D** (blank NVs) the detected fluorescence signal comes from endogenous fluorophores (autofluorescence): in green epidermis, while in blue the SHG signal due to dermis collagen. In panels **E** and **F** (NR water/DMSO 1% (v/v) solution) the detected fluorescence signal comes from both endogenous fluorophores (in green) and NR (in red). In panels **G** and **H** (NR NVs) in red NR fluorescence signal, while in blue SHG signal due to dermis collagen. All images were collected exciting the samples at 850 nm, the laser power and detector gains were adjusted for each sample to prevent detector saturation.

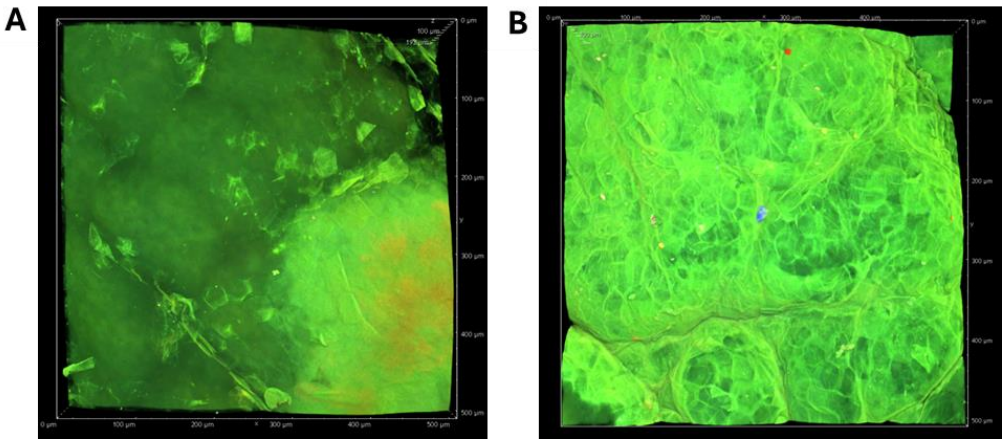


Figure 3.28. **(A)** XY view of a Z-stack acquired on skin sample treated with the dispersant media (water/EtOH 15% (v/v)). **(B)** XY view of a Z-stack acquired on skin sample treated with plain NVs (blank Sit:LGL:LGC NVs (molar ratio 1:0.8:0.2)). Images acquired exciting the samples at 850 nm.

It is worth noticing that NR signal was always localized inside epithelia cells, independently if this was loaded in NVs or free (**Figure 3.29**). Nevertheless, for NR-loaded NVs the fluorescence signal acquired was more intense, suggesting that NVs positively contribute to the permeation of emissive NR into the tissue when compared to free dye.

It is important to highlight that, at our experimental conditions, NR was not detected in the dermis, a crucial feature for dermocosmetic applications since regulation forbids cosmetic ingredients to reach the circulatory system[61]. Nevertheless, it is worth mentioning that, in **Figure 3.27G** (3 h permeation) only second harmonic generation arising from the dermis, and no NR fluorescence was detected, while in **Figure 3.27H** (6 h permeation) neither the SHG nor NR fluorescence were detected (**Figure 3.30**). This could be ascribed to the thick front of NR preventing the laser radiation to reach the inner strata of the tissue or, vice versa, the signal arising from inner strata to reach the microscope objective.

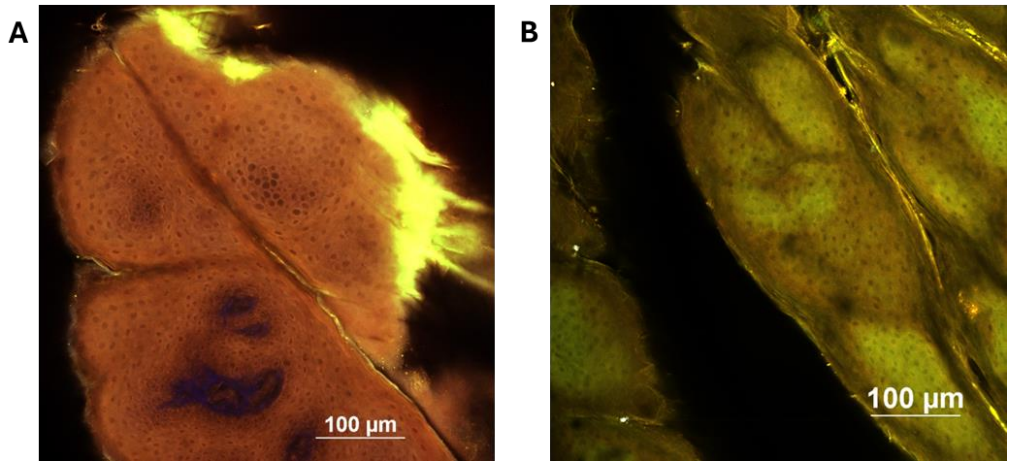


Figure 3.29. **(A)** XY view of a Z-stack acquired on skin sample treated with NR NVs for 6 h. **(B)** XY view of a Z-stack acquired on skin sample treated with NR in water/DMSO 1% solution for 6 h. Images acquired exciting the samples at 850 nm.

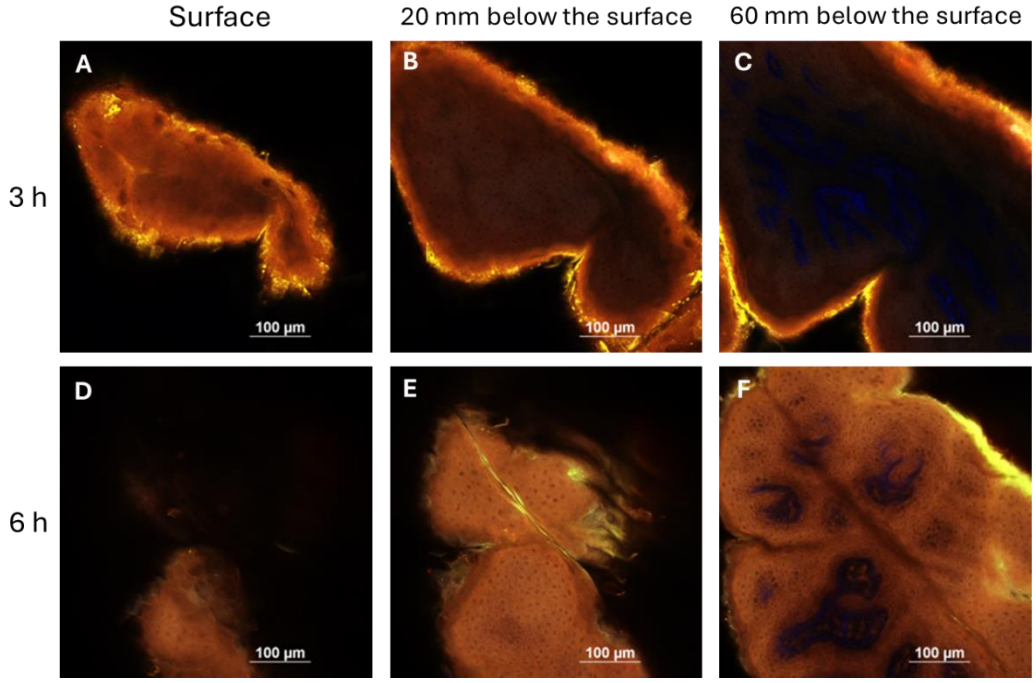


Figure 3.30. Upper panels: XY views taken at different depth of skin sample treated with NR NVs for 3 h. Panel **(A)**: surface. Panel **(B)**: 20 µm below the surface. Panel **(C)**: 60 µm below the surface. Bottom panels: XY views taken at different depth of skin sample treated with NR NVs for 6 h. Panel **(D)**: surface. Panel **(E)**: 20 µm below the surface. Panel **(F)**: 60 µm below the surface. Images acquired exciting the samples at 850 nm.

As stated above, the solvatochromic properties of NR can be exploited to gain information on its local environment. To this aim, the emission spectra acquired on the different skin samples were compared with the emission spectrum collected on a aqueous-based suspension of NR-loaded NVs. In **Figure 3.31**, the maximum of the emission of NR suspension

was different from the ones acquired on skin tissues. The spectra of NR-loaded NVs and NR in water/DMSO solution in skin fell in the same spectral region and their maxima were shifted towards higher wavelength compared to the spectrum acquired on the suspension. These two factors suggested that NVs release NR once they permeate in the skin tissue. This is a preliminary indication that NR could be released from the NVs in the skin and delivered to the cells. Further permeation studies should however confirm these results obtained by 2PM.

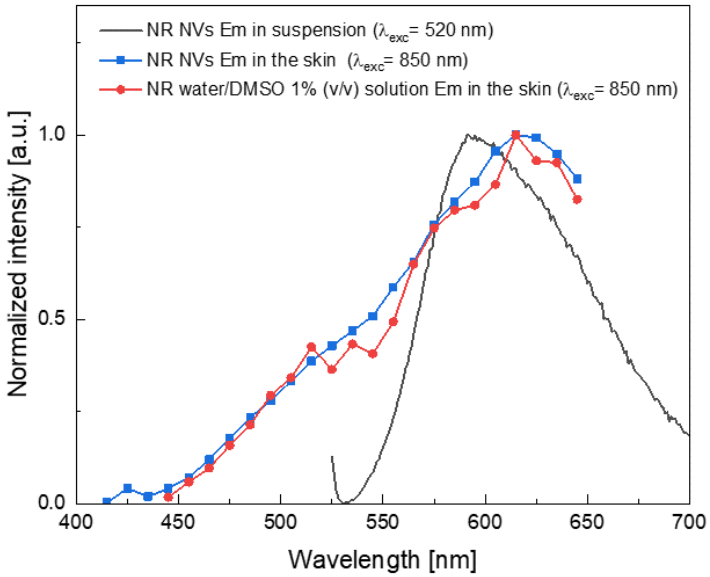


Figure 3.31. Emission spectrum acquired on the differently treated skin samples 40 μm below the surface (red, and blue lines) with the two-photon microscope exciting the sample at 850 nm and emission spectrum acquired on a solution of NR-loaded Sit/LGL/LGC NVs in suspension (black line) with a fluorimeter exciting the sample at 520 nm.

In conclusion, both studies indicated that the vesicular systems tested composed by the combination of Sit, LGL and LGC were biocompatible and non-irritant with the skin. Furthermore, it seemed that NR loaded in Sit/LGL/LGC NVs permeates more efficiently, deeper and faster, compared to NR in an aqueous solution alone. These results indicate that this new nanovesicle delivery platform could be used for topical applications of poorly-water-soluble payloads delivering them to epithelial cells.

3.8. Summary of the Chapter and future perspectives

In **Chapter 3** the development of new plant-based topical delivery systems has been reported. Phytosterol and alkyl polyglucoside surfactants have been used to produce novel stable nanovesicles by self-assembly of β-sitosterol, lauryl glucoside and lauryl glucose carboxylate, in a single step, using DELOS manufacturing method.

These vesicular systems have been characterized by DLS, ELS, cryo-TEM and SAXS, showing variation in physicochemical properties as a function of membrane components. A platform of homogeneous NVs is formed with a hydrodynamic diameter range of 150-220 nm and a negative surface charge that varies from -40 to -70 mV depending on the amount of LGC used. The lamellarity of the NVs also depended on the membrane components employed, obtaining unilamellar vesicles with Sit:LGC systems but multilamellar ones when any combination of Sit:LGL or Sit:LGL:LGC are used. Three formulations have been selected as the most promising in terms of colloidal stability and physicochemical properties: Sit:LGL-m$_{C12-16}$ (1:1), Sit:LGC (1:1) and Sit:LGL:LGC (1:0.8:0.2) (molar ratio).

The possibility of modulating the physicochemical properties of the obtained NVs is very interesting because they have a direct impact on their biological performance.

On the one hand, negatively charged vesicles have been found to enhance skin permeation in relation to neutral or positively charged vesicles[62,63], as also reported here. As the platform present a negative surface charge, it is aligned with the trends found in the bibliography to be a promising system for skin delivery.

On the other hand, it is known that the lamellarity of NVs impacts on the release profile of the loaded active molecules[64–66]. For this reason, the ability to control the lamellarity of each system by modulating the composition of NVs, could be exploited to tailor the release profile according to the characteristic of different payloads.

The formation of these Sit:LGL NVs has not been obvious. As it has been demonstrated, the purity of the APGs used and the alkyl chain length is directly related to the formation of these NVs. In this way, Sit:APGs NVs are only formed when using carbon chains above C12. In addition, the experimental conditions to produce the new NVs were not the same if using pure reagents or a mixture of APGs due to difference on their T_K. In contrast, we have also evaluated the impact of the manufacturing methodology comparing DELOS process with thin film hydration. The results showed that the vesicles were formed independently of the method used, but only with APG surfactants with ≥ C12, and showing different physical characteristics.

Furthermore, we have proved that these new platform of NVs can be used as delivery systems by using Sit:LGL:LGC NVs (1:0.8:0.2) to integrate the antioxidant compound α-tocopherol as a model of hydrophobic payload. It is interesting not just that TCP can be efficiently loaded, but also that the molecule maintained its antioxidant activity.

The tested systems also proved promising functionality in the *in vitro* assays performed, showing skin biocompatibility using human reconstructed epidermis models and exhibited in *ex vivo* skin permeation studies deeper and more efficient permeation of Nile red fluorophore compared to the molecule in aqueous suspension.

All in all, in **Chapter 3** a new delivery platform of NVs using plant-derived ingredients, presenting stable and homogeneous vesicles, biocompatible and able to deliver payloads to the epidermis, has been presented. This platform could cover an unmet need for vegan patients and consumers, being a potential attractive platform for topical delivery in pharmaceutical and healthcare industries.

These first studies opened new perspectives, such as further research in loading and delivery of biomolecules, to gain knowledge in the topical delivery of small hydrophilic molecules and proteins, which are presented in the following **Chapters**.

3.9. Bibliography

1. M. Grit, D.J.A. Crommelin. Chemical stability of liposomes: implications for their physical stability. *Chem. Phys. Lipids* **1993**, 64, 3–18.

2. A. V. Yadav, M.S. Murthy, A.S. Shete, S. Sakhare. Stability aspects of liposomes. *Indian J. Pharm. Educ. Res.* **2011**, 45, 402–413.

3. V.G.S. Sainaga Jyothi, R. Bulusu, B. Venkata, et al. Stability characterization for pharmaceutical liposome product development with focus on regulatory considerations: An update. *Int. J. Pharm.* **2022**, 624, 122022.

4. S. Taymouri, J. Varshosaz. Effect of different types of surfactants on the physical properties and stability of carvedilol nano-niosomes. *Adv. Biomed. Res.* **2016**, 5, 1–16.

5. Z. Ertekin, Z. Bayindir, N. Yuksel. Stability Studies on Piroxicam Encapsulated Niosomes. *Curr. Drug Deliv.* **2015**, 12, 192–199.

6. M. Köber, S. Illa-Tuset, L. Ferrer-Tasies, et al. Stable nanovesicles formed by intrinsically planar bilayers. *J. Colloid Interface Sci.* **2023**, 631, 202–211.

7. U.S. Department of Health and Human Services. Inactive Ingredient Search for Approved Drug Products https://www.accessdata.fda.gov/scripts/cder/iig/index.cfm?event=BasicSearch.page (accessed Mar 7, 2024).

8. Official Journal of the European Union. COMMISSION REGULATION (EU) No 866/2014 of 8 August 2014 amending Annexes III, V and VI to Regulation (EC) No 1223/2009 of the European Parliament and the Council on cosmetic products; **2014**.

9. Y. Jiao, L. na Niu, S. Ma, et al. Quaternary ammonium-based biomedical materials: State-of-the-art, toxicological aspects and antimicrobial resistance. *Prog. Polym. Sci.* **2017**, 71, 53–90.

10. M. Kamiński, K. Skonieczna-Żydecka, J.K. Nowak, E. Stachowska. Global and local diet popularity rankings, their secular trends, and seasonal variation in Google Trends data. *Nutrition* **2020**, 79–80, 110759.

11. Y.H. Choi, K.H. Lee. Ethical Consumers' Awareness of Vegan Materials: Focused on Fake Fur and Fake Leather. *Sustainability* **2021**, 13, 436.

12. Suryamani, R. Sindhu, I. Singh. Phytosterols: physiological functions and therapeutic applications. In *Bioactive Food Components Activity in Mechanistic Approach*; **2021**; pp 223–238.

13. Innovations in Food Technology: Current Perspectives and Future Goals; Mishra, P., Mishra, R. R., Adetunji, C. O., Eds.; Springer, **2020**.

14. E.J. Dufourc. Sterols and membrane dynamics. *J. Chem. Biol.* **2008**, 1, 63–77.

15. S. Saeidnia, A. Manayi, A.R. Gohari, M. Abdollahi. The Story of Beta-sitosterol- A Review. *European J. Med. Plants* **2014**, 4, 590–609.

16. European Commission. CosIng - Cosmetics - GROWTH - European Commission https://ec.europa.eu/growth/tools-databases/cosing/index.cfm?fuseaction=search.details_v2&id=74131 (accessed Apr 28, 2023).

17. M. Bin Sayeed, S. Karim, T. Sharmin, M. Morshed. Critical Analysis on Characterization, Systemic Effect, and Therapeutic Potential of Beta-Sitosterol: A Plant-Derived Orphan Phytosterol. *Medicines* **2016**, 3, 25.

18. S. Chanioti, M. Katsouli, C. Tzia. β-Sitosterol as a functional bioactive. In *A Centum of Valuable Plant Bioactives*; Academic Press, **2021**; pp 193–212.

19. M.S. Ferreira, J.M. Sousa Lobo, I.F. Almeida. Sensitive skin: Active ingredients on the spotlight. *Int. J. Cosmet. Sci.* **2022**, 44, 56–73.

20. K. Tai, M. Rappolt, X. He, et al. Effect of β-sitosterol on the curcumin-loaded liposomes: Vesicle characteristics, physicochemical stability, in vitro release and bioavailability. *Food Chem.* **2019**, 293, 92–102.

21. A.A. Jovanović, B.D. Balanč, A. Ota, et al. Comparative Effects of Cholesterol and β-Sitosterol on the Liposome Membrane Characteristics. *Eur. J. Lipid Sci. Technol.* **2018**, 120, 1800039.

22. T.A. Debele, S.L. Mekuria, H.C. Tsai. Synthesis and characterization of redox-sensitive heparin-β-sitosterol micelles: Their application as carriers for the pharmaceutical agent, doxorubicin, and investigation of their antimetastatic activities in vitro. *Mater. Sci. Eng. C* **2017**, 75, 1326–1338.

23. O. Afzal, M.H. Akhter, I. Ahmad, et al. A β–Sitosterol Encapsulated Biocompatible Alginate/Chitosan Polymer Nanocomposite for the Treatment of Breast Cancer.

Pharmaceutics **2022**, 14, 1711.

24. I. Pantelic, B. Cuckovic. Alkyl Polyglucosides: An emerging class of sugar surfactants. In *Alkyl Polyglucosides - From Natural -Origin Surfactants to Prospective Delivery Systems*; **2014**; pp 1–19.

25. D. Geetha, R. Tyagi. Alkyl Poly Glucosides (APGs) Surfactants and Their Properties: A Review. *Tenside, Surfactants, Detergents*. 2012, pp 417–427.

26. W. Von Rybinski. Natural surfactants. *Curr. Opin. Colloid Interface Sci.* **2001**, 6, 146–147.

27. M. Salim, O.K. Abou-Zied, H. Udani Kulathunga, et al. Alkyl mono- and di-glucoside sugar vesicles as potential drug delivery vehicles: detecting drug release using fluorescence. *RSC Adv.* **2015**, 5, 55536–55543.

28. C.M. Keck, A. Kovačević, R.H. Müller, et al. Formulation of solid lipid nanoparticles (SLN): The value of different alkyl polyglucoside surfactants. *Int. J. Pharm.* **2014**, 474, 33–41.

29. C. Scomoroscenco, M. Teodorescu, C.L. Nistor, et al. Preparation and In Vitro Characterization of Alkyl Polyglucoside-Based Microemulsion for Topical Administration of Curcumin. *Pharmaceutics* **2023**, 15, 1420.

30. S. Bhattacharjee. DLS and zeta potential-What they are and what they are not? *J. Control. Release* **2016**, 235, 337–351.

31. P. Gill, T.T. Moghadam, B. Ranjbar. Differential scanning calorimetry techniques: Applications in biology and nanoscience. *J. Biomol. Tech.* **2010**, 21, 167–193.

32. M. Cano-Sarabia, A. Angelova, N. Ventosa, S. Lesieur, J. Veciana. Cholesterol induced CTAB micelle-to-vesicle phase transitions. *J. Colloid Interface Sci.* **2010**, 350, 10–15.

33. H. Lu, I. Pezron, T. Gaudin, A. Drelich. Non-equilibrium micelles formed by sugar-based surfactants under their Krafft temperature. *Colloids Surfaces A Physicochem. Eng. Asp.* **2018**, 540, 167–176.

34. A. Ohta, N. Ozawa, S. Nakashima, T. Asakawa, S. Miyagishi. Krafft temperature and enthalpy of solution of N-acyl amino acid surfactants and their racemic modifications: Effect of the amino acid residue. *Colloid Polym. Sci.* **2003**, 281, 363–369.

35. R. Muzzalupo, L. Tavano, C. La Mesa. Alkyl glucopyranoside-based niosomes containing methotrexate for pharmaceutical applications: Evaluation of physico-chemical and biological properties. *Int. J. Pharm.* **2013**, 458, 224–229.

36. I. Sopyan, K. Insan Sunan, D. Gozali. A Review: A Novel of Efforts to Enhance Liposome Stability as Drug Delivery Approach. *Syst. Rev. Pharm.* **2020**, 11, 555–562.

37. D. Lombardo, P. Calandra, M.T. Caccamo, S. Magazù, M.A. Kiselev. Colloidal stability of liposomes. *AIMS Mater. Sci.* **2019**, 6, 200–213.

38. J. Tomsen-Melero, S. Passemard, N. García-Aranda, et al. Impact of chemical composition on the nanostructure and biological activity of α-galactosidase-loaded nanovesicles for Fabry disease treatment. *ACS Appl. Mater. Interfaces* **2021**, 13, 7825–7838.

39. M.S. Roberts, H.S. Cheruvu, S.E. Mangion, et al. Topical drug delivery: History, percutaneous absorption, and product development. *Adv. Drug Deliv. Rev.* **2021**, 177, 113929.

40. S.A.V. Morris, R.T. Thompson, R.W. Glenn, K.P. Ananthapadmanabhan, G.B. Kasting. Mechanisms of anionic surfactant penetration into human skin: Investigating monomer, micelle and submicellar aggregate penetration theories. *Int. J. Cosmet. Sci.* **2019**, 41, 55–66.

41. L. Ferrer-Tasies, E. Moreno-Calvo, M. Cano-Sarabia, et al. Quatsomes: Vesicles formed by self-assembly of sterols and quaternary ammonium surfactants. *Langmuir* **2013**, 29, 6519–6528.

42. M. Antonietti, S. Förster. Vesicles and Liposomes: A Self-Assembly Principle Beyond Lipids. *Adv. Mater.* **2003**, 15, 1323–1333.

43. M. Keen, I. Hassan. Vitamin E in dermatology. *Indian Dermatol. Online J.* **2016**, 7, 311.

44. C.A.S. de Oliveira Pinto, T.E.A. Martins, R.M. Martinez, et al. Vitamin E in Human Skin: Functionality and Topical Products. In *Vitamin E in Health and Disease - Interactions, Diseases and Health Aspects*; **2021**; pp 3–26.

45. M.M. Fiume, B. Heldreth, W.F. Bergfeld, et al. Safety Assessment of Tocopherols and Tocotrienols as Used in Cosmetics. *Cosmetic Ingredient Review*. 2014.

46. G. Marinova, V. Batchvarov. Evaluation of the methods for determination of free radical scavenging activity by DPPH. *Bulg. J. Agric. Sci.* **2011**, 17, 11–24.

47. S.B. Kedare, R.P. Singh. Genesis and development of DPPH method of antioxidant assay. *J. Food Sci. Technol.* **2011**, 48, 412–422.

48. T. Li, A.J. Senesi, B. Lee. Small Angle X-ray Scattering for Nanoparticle Research. *Chem. Rev.* **2016**, 116, 11128–11180.

49. E. Di Cola, I. Grillo, S. Ristori. Small angle X-ray and neutron scattering: Powerful tools for studying the structure of drug-loaded liposomes. *Pharmaceutics* **2016**, 8, 10.

50. J. Tomsen Melero. Study of New Liposomes for the Delivery of Enzymes through Biological Membranes, **2021**.

51. M. Tasic-Kostov, S. Vesic, S. Savic. Objective skin performance evaluation: How mild are APGs to the skin? In *Alkyl Polyglucosides: From Natural-Origin Surfactants to Prospective Delivery Systems*; **2014**; pp 135–161.

52. I. Pantelic, M. Lukic, R. Daniels, S. Savic. Alkyl Polyglucoside-based delivery systems: In vitro/in vivo skin absorption assessment. In *Alkyl Polyglucosides: From Natural-Origin Surfactants to Prospective Delivery Systems*; **2014**; pp 107–134.

53. OECD. Test Guideline No. 439 In Vitro Skin Irritation : Reconstructed Human Epidermis Test Method In Vitro. *OECD Guidelines for the Testing of Chemicals*. 2021.

54. M. Kumar, A. Sharma, S. Mahmood, et al. Franz diffusion cell and its implication in skin permeation studies. *J. Dispers. Sci. Technol.* **2024**, 45, 943–956.

55. F. Helmchen, W. Denk. Deep tissue two-photon microscopy. *Nat. Methods* **2005**, 2, 932–940.

56. M. Ghezzi, S. Pescina, A. Delledonne, et al. Improvement of imiquimod solubilization and skin retention via tpgs micelles: Exploiting the co-solubilizing effect of oleic acid. *Pharmaceutics* **2021**, 13, 1476.

57. M. Ghezzi, I. Ferraboschi, A. Fantini, et al. Hyaluronic acid – PVA films for the simultaneous delivery of dexamethasone and levofloxacin to ocular tissues. *Int. J. Pharm.* **2023**, 638, 122911.

58. M. Ghezzi, I. Ferraboschi, A. Delledonne, et al. Cyclosporine-loaded micelles for ocular delivery: Investigating the penetration mechanisms. *J. Control. Release* **2022**, 349, 744–755.

59. A. Fantini, L. Giulio, A. Delledonne, et al. Buccal Permeation of Polysaccharide High

Molecular Weight Compounds: Effect of Chemical Permeation Enhancers. *Pharmaceutics* **2023**, 15, 129.

60. B. Boldrini, E. Cavalli, A. Painelli, F. Terenziani. Polar dyes in solution: A joint experimental and theoretical study of absorption and emission band shapes. *J. Phys. Chem. A* **2002**, 106, 6286–6294.

61. SCCS guideline. The Scientific Committee on Consumer Safety's (SCCS) notes of guidance for the testing of cosmetics substances and their safety evaluation 8th revision http://ec.europa.eu/health/scientific_committees/consumer_safety/docs/sccs_s_006.pdf (accessed Feb 23, 2024).

62. A. Gillet, P. Compère, F. Lecomte, et al. Liposome surface charge influence on skin penetration behaviour. *Int. J. Pharm.* **2011**, 411, 223–231.

63. C. Sinico, M. Manconi, M. Peppi, et al. Liposomes as carriers for dermal delivery of tretinoin: In vitro evaluation of drug permeation and vesicle-skin interaction. *J. Control. Release* **2005**, 103, 123–136.

64. G. V Betageri, D.L. Parsons. Drug encapsulation and release from multilamellar and unilamellar liposomes. *Int. J. Pharm.* **1992**, 81, 235–241.

65. Y. Matsuura-Sawada, M. Maeki, S. Uno, K. Wada, M. Tokeshi. Controlling lamellarity and physicochemical properties of liposomes prepared using a microfluidic device. *Biomater. Sci.* **2023**, 11, 2419–2426.

66. S.L. Gosangari, K.L. Watkin. Effect of preparation techniques on the properties of curcumin liposomes: Characterization of size, release and cytotoxicity on a squamous oral carcinoma cell line. *Pharm. Dev. Technol.* **2012**, 17, 103–109.

4 Formulation of the vitamin D precursor 7-dehydrocholesterol in alkyl polyglucosides and β-sitosterol nanovesicles

4.1. Vitamin D supplementation: an increased necessity worldwide

Vitamin D is a fat-soluble vitamin that is naturally present in the human body (vitamin D_3 and vitamin D_2). For a long time, the function of vitamin D was thought to be just related with calcium metabolism and the maintenance of bone structure. Nevertheless, in the last decades it has been seen that it has also other roles in the endocrine function, immune system, cardiovascular system or even the skin[1–3].

The human body can naturally produce vitamin D_3. It is synthesized from 7-dehydrocholesterol (7-DHC), its precursor that is present in the skin, which is transformed to previtamin D after ultraviolet radiation B (UVB) of wavelength between 280-320 nm. Then previtamin D is converted to vitamin D_3 (cholecalciferol, vitD) by thermal isomerization (**Figure 4.1**)[4,5]. It is vitD which arrives to systemic circulation, and it is then distributed to all the body. Besides being produced by the organism, vitamin D can be also obtained from diet. Vitamin D_3 is present in animal derived products, whereas vitamin D_2 comes from the intake of plants and mushrooms[6]. Then, the liver and kidneys are able to transform vitD to the active hormone calcitriol[7].

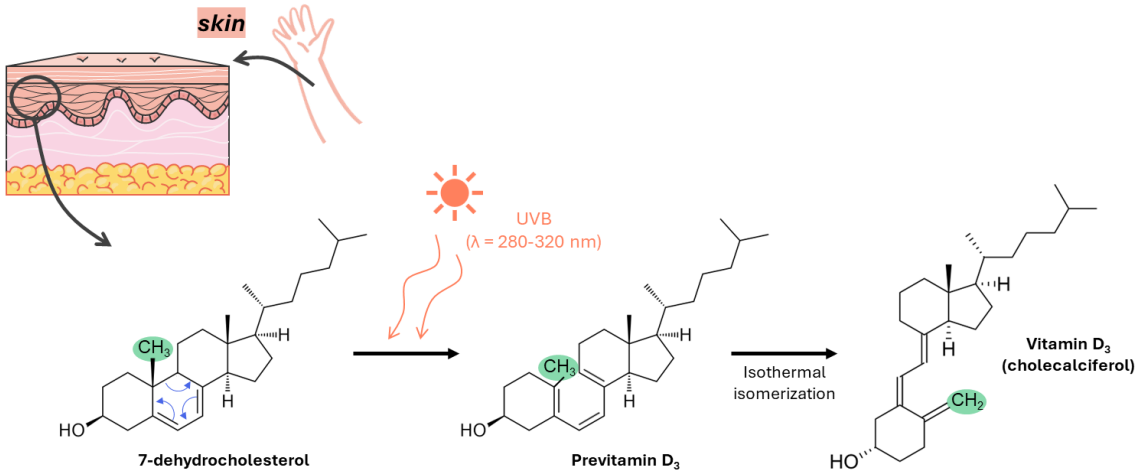


Figure 4.1. Schematic representation of 7-dehydrocholesterol (7-DHC) transformation to vitamin D_3 in the skin.

In the last years, there has been a global prevalence of vitamin D deficiency basically due to an increase of an indoor lifestyle and sun avoidance which makes our body to produce less amount of vitD, and also, diets highly based on processed food which neither contain vitamin D_3 nor D_2[8–10]. For these reasons, its use as a nutritional supplement has become very popular although there is still some controversy on the appropriate doses for general or healthy population[6,11]. Both agencies from Europe (European Food Safety Authority) and US (National Institutes of Health) recommend that the adequate dose of vitD intake per day for healthy individuals is between 10 and 20 µg (10 µg/day for infants of less than 1 year of age, 15 µg/day for individuals over one year of age and 20 µg/day for adults over seventy-one years of age)[6,12,13].

Thus, in the last years vitamin D has attracted the interest of different industrial sectors. Besides nutraceutical industry, which is the most exploited market with dietary supplements, vitD derivatives can also be administered topically for healthcare applications.

*This **Chapter** describes the development of new aqueous-based formulations containing 7-DHC loaded in Sit:LGL:LGC nanovesicles, for topical applications in healthcare and dermocosmetics products. Here it is investigated the possibility of producing 7-DHC-loaded nanovesicle formulations, and further, the loading capacity of the nanovesicles to integrate this payload is evaluated. A screening replacing Sit by 7-DHC in the nanovesicle membrane has been performed as they both have a sterol structure. The resulting formulations have been characterized in terms of physicochemical properties like size, surface charge, morphology and lamellarity, capacity of 7-DHC to be transformed to vitD by UV irradiation after encapsulation and finally in vitro skin biocompatibility using reconstructed human epidermis models* (**Figure 4.2**).

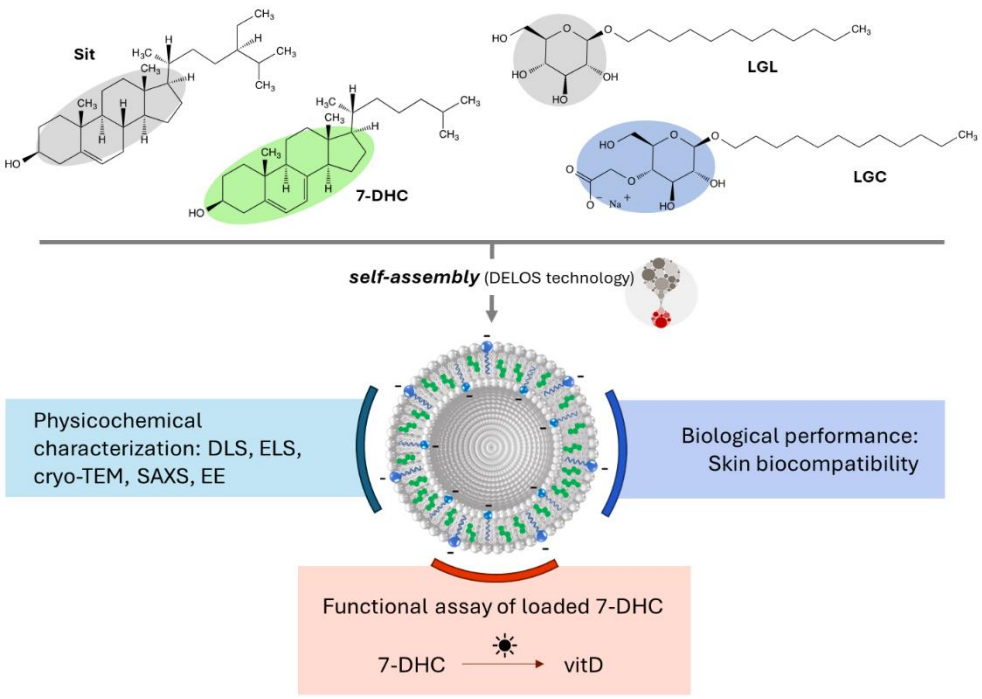


Figure 4.2. Graphical summary of the work described in **Chapter 4** to develop 7-DHC loaded plant based nanovesicles.

4.1.1. The role of vitamin D in the skin

Focusing on the skin, vitD has an active role. First, it is in the skin where it is synthesized, as previously explained in **Section 4.1** (**Figure 4.1**). Nonetheless, it has specific functions in this organ, where VitD acts as a regulator of proliferation, differentiation and apoptosis of keratinocytes, the main cells of the epidermis. It also has a role on the epidermal barrier maintenance and immunomodulatory actions among others[3,4].

In cosmetics, the use of vitamin D itself is not allowed, but the precursor 7-DHC and other plant extracts that can contain other enhancers of vitD production are permitted and used. 7-DHC has been largely used in cosmetics for other functions such as emulsion stabilizing, skin conditioning and viscosity control[14]. Nevertheless, scarce marketed products use 7-DHC as vitD precursor to administer it topically, such as that commercialized by Zelens (**Table 4.1**). Other companies like Freshly Cosmetics or Segle choose plant extracts and claim their use to optimize the production of vitamin D in the skin[15].

Table 4.1. Marketed dermocosmetic products containing precursors or enhancers of vitD production.

Product	**Manufacturer** ***(Country of origin)***	**Active ingredient**
Power D Vitamin D Concentrate Power D Fortifying and Restoring Serum	Zelens *(United Kingdom)*	7-dehydrocholesterol
Vitamin D3 precursor	Delia Cosmetics *(Poland)*	7-dehydrocholesterol
Vitamin D Skin Booster	Freshly Cosmetics *(Spain)*	Lithops Pseudotruncatella Callus Lysate
Vitamin D Activating Serum 2%	Skin generics *(Spain)*	Lithops Pseudotruncatella Callus Lysate
Vitamin D Urban SPF30	Segle *(Spain)*	Lithops Pseudotruncatella Callus Lysate
Vitamin D Serum	Bali Body *(Australia)*	Non-defined

Thus, our specific objective was to use 7-dehydrocholesterol integrated in nanovesicles to be administered topically as a dermoscosmetic ingredient or product, which is a novel approach not found in the market. Thus, after its administration and permeation across the skin, 7-DHC could naturally be transformed into vitamin D by the keratinocytes. We hypothesized that 7-DHC, a sterol-like lipophilic molecule with a similar molecular structure to cholesterol and β-sitosterol (**Figure 4.3**), could be loaded into the newly developed sugar-based nanovesicles by DELOS technology, with the final aim of obtaining aqueous based suspensions of 7-DHC NVs for topical applications able to transform it to vitD in the skin.

This strategy of integrating 7-DHC in the newly developed delivery systems, along with enabling the formulation of a lipophilic molecule in an aqueous suspension, could also enhance the permeation through the epidermis, as demonstrated previously in **Chapter 3** and consequently improve the uptake of 7-DHC by the keratinocytes. This factor is important because keratinocytes are the cells which transform 7-DHC to vitD.

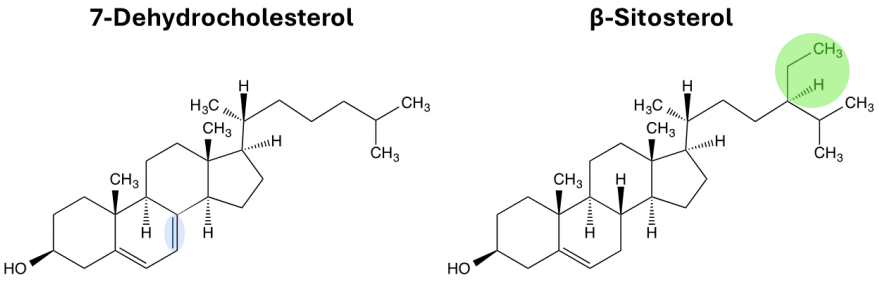


Figure 4.3. Comparison of the molecular structure of 7-dehydrocholesterol (7-DHC) and β-sitosterol.

4.2. Preparation of the 7-DHC loaded nanovesicles

With the intention of formulating 7-DHC in aqueous suspensions, nanovesicles composed by Sit and sugar-based surfactants were chosen as delivery systems. In particular, the starting system used was composed by Sit and the surfactants LGL (pure-grade reagent) and LGC, with a molar ratio 1:0.8:0.2. This nanovesicular system has been described in detail previously in **Chapter 3**.

As 7-DHC is a sterol, the possibility to use it as a structural molecule that self-assembles in a bilayer with the selected LGL and LGC surfactants, forming nanovesicles, was evaluated. If this was possible, the molecule could have a double role: bioactive and structural. To do so, an experimental screening replacing Sit by 7-DHC was carried out by changing the Sit:7-DHC molar ratio from 1:0 to 0:1 (**Figure 4.4**) and by keeping the LGL and LGC ratio constant, obtaining 5 different formulations.

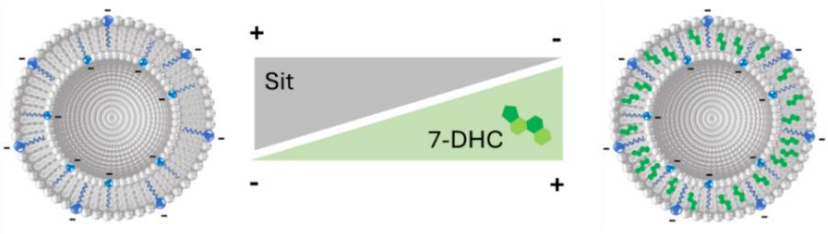


Figure 4.4. Schematic representation of NVs screening replacing Sit by 7-DHC.

All formulations were produced by DELOS methodology using the bench scale equipment (see **Section 8.2.1**). 7-DHC, as it is a lipophilic compound, was dissolved in the organic phase with ethanol (**Figure 4.5**). The five formulations had the same dispersant media (water/EtOH 15% (v/v)) and concentration of membrane components (3 mg/mL).

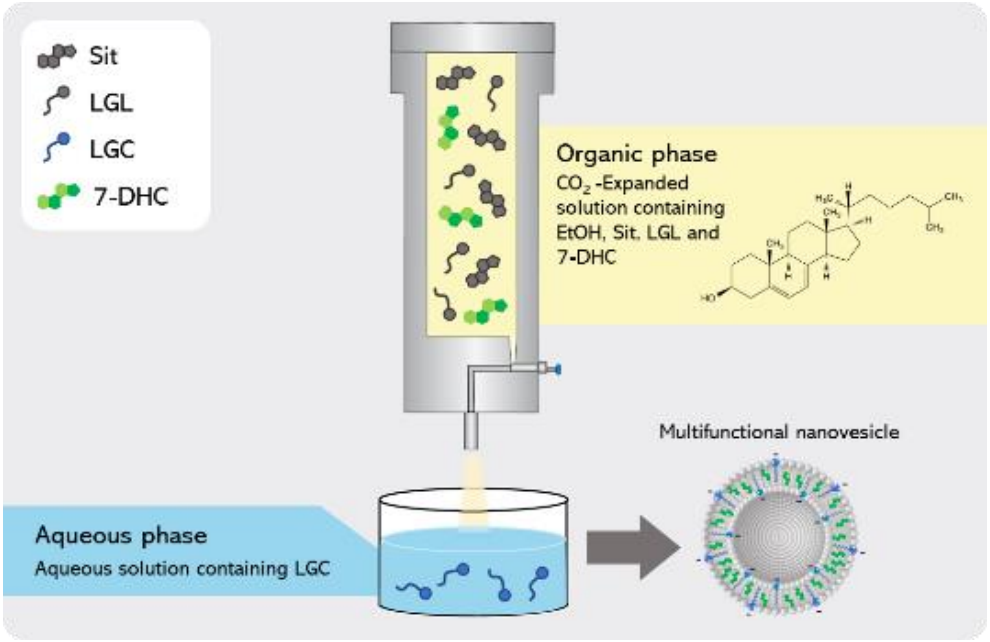


Figure 4.5. Schematic representation of DELOS methodology used for the preparation of nanovesicles composed of Sit:7-DHC:LGL:LGC described in **Chapter 4**.

The formulations obtained were characterized by DLS, ELS and cryo-TEM as described in **Sections 8.3.1** and **8.3.2**. As it can be seen in **Table 4.2** and **Figure 4.6A**, the combination of the four membrane components at different molar ratios gave rise to the formation of promising nanovesicular formulations in all cases, with a macroscopical appearance of opalescent whitish stable dispersions. The physicochemical characteristics of the colloidal systems containing 7-DHC were similar to blank nanovesicles without 7-DHC. Small and homogeneous NVs were obtained with hydrodynamic diameters ranging from 210 to 135 nm, and low size PDI values between 0.1-0.2. The results seemed to indicate that NVs with lower amounts of 7-DHC, i.e., Sit:7-DHC molar ratios of (0.8:0.2) and (0.5:0.5) had similar size and PDI values compared to blank vesicles without 7-DHC (molar ratio 1:0). In contrast, when the presence of 7-DHC was increased, particle size and PDI tended to decrease. In relation to vesicles' morphology, cryo-TEM images (**Figure 4.6B**) showed the presence of both, unilamellar and multilamellar NVs in all the samples.

Regarding stability, all systems were stable for at least 12 months in terms of particle size and PDI (**Figure 4.6C**). Furthermore, another sign of colloidal stability was their ζ-Pot values, which were around -50 mV (**Table 4.2**), above the threshold of ζ-Pot > |30 mV| which indicates the possible colloidal stability of systems in suspension.

Table 4.2. Composition and physicochemical characterization of nanovesicle formulations containing 7-DHC prepared in **Chapter 4** (n = 3).

Sit:7-DHC:LGL:LGC[a)] NVs (X:Y:0.8:0.2 molar ratio)					
Molar ratio Sit:7-DHC	**7-DHC concentration[b)] [mg/mL]**	**Hydrodynamic diameter mean [nm]**	**Size PDI**	**Apparent ζ-Pot [mV]**	**EE [%]**
1:0	0	182 ± 9	0.22 ± 0.01	-61 ± 2	NA
0.8:0.2	0.30	200 ± 20	0.23 ± 0.01	-55 ± 4	71 ± 15
0.5:0.5	0.77	211 ± 14	0.22 ± 0.02	-58 ± 4	75 ± 14
0.2:0.8	1.24	159 ± 16	0.12 ± 0.03	-53 ± 7	78 ± 12
0:1	1.56	135 ± 3	0.09 ± 0.02	-48 ± 4	91 ± 7

[a)] LGC reagent used was a mixture of APGs, intended as alkyl glucosides of C10-16 chain length, and the corresponding carboxylates; thus, the ratios X:Y:0.8:0.2 refer to the mixture and not the real content of LGC.

[b)] Theoretical concentration.

It was also important to evaluate the EE of 7-DHC in the nanovesicular systems. Since it is a sterol-like molecule with similar structure to Sit, a good integration in the bilayers of NVs, acting as a membrane structural molecule, was expected. EE was evaluated by UV-vis spectroscopy measurements (see **Section 8.3.5.3**) and the results are shown in **Table 4.2**.

In accordance with the expectations, the EE values were high in all cases, although some differences were detected. When 7-DHC was combined with Sit at any molar ratio (0.8:0.2, 0.5:0.5 and 0.2:0.8), EE values were similar (between 71 – 78%) with higher values of standard deviation. In contrast, when 7-DHC was the only sterol used, the EE increased to 91% and the standard deviation was lower.

To conclude with this **Section**, the analysis of all these results points out that 7-DHC was well integrated and stabilized in the aqueous sugar-based nanovesicular formulations in all the conditions tested, obtaining homogeneous and stable colloidal formulations.

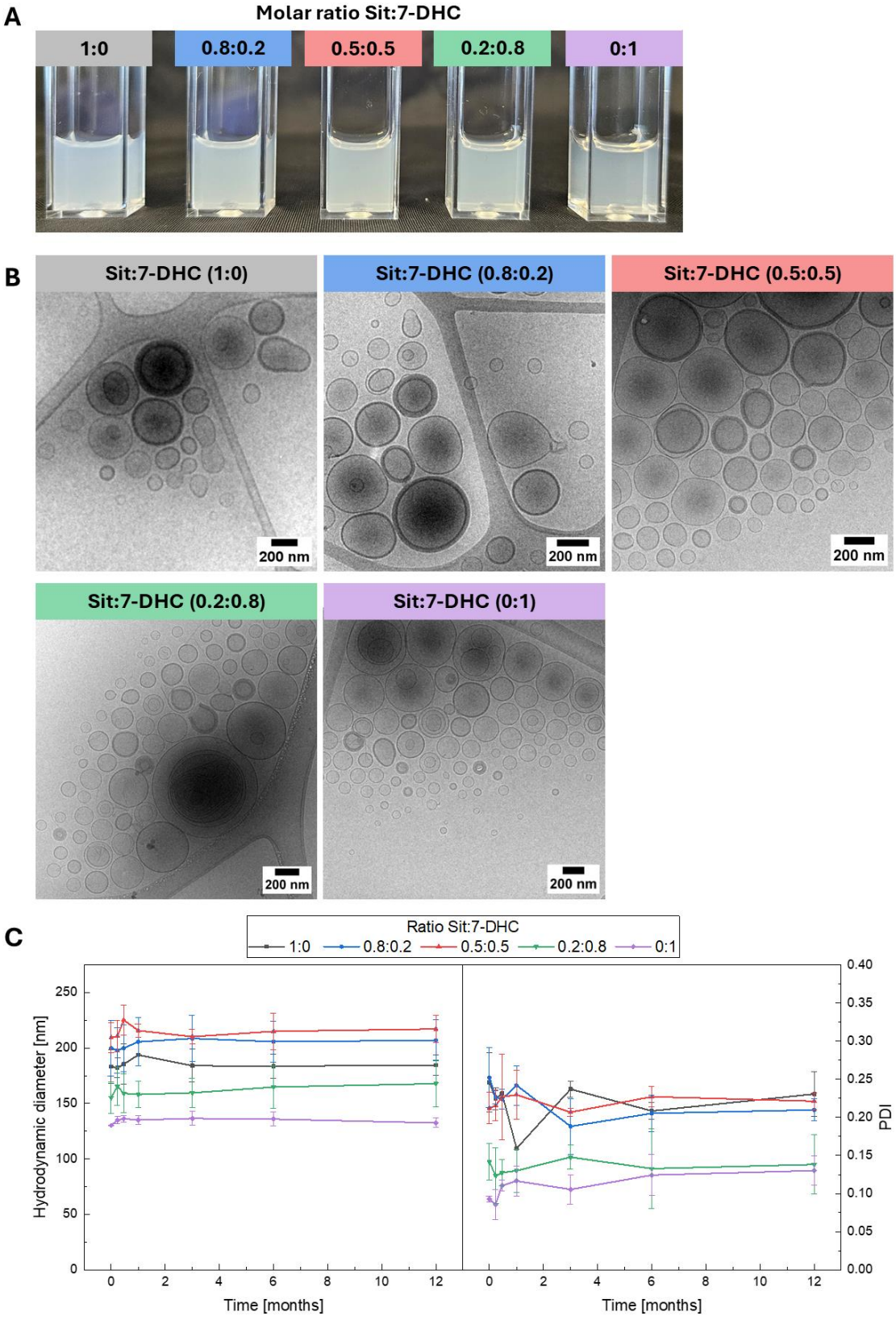


Figure 4.6. **(A)** Macroscopical appearance of the 7-DHC loaded samples 1 year after production. **(B)** Representative cryo-TEM image of the Sit:7-DHC:LGL:LGC NVs at different molar ratios Sit:7-DHC. **(C)** Stability over time in terms of particle size and size PDI (n = 3).

4.3. Impact of the Sit:7-DHC ratio on the lamellarity of the nanovesicles

The samples containing Sit, 7-DHC, LGL and LGC presented a mixture of unilamellar and multilamellar vesicles. For this reason, SAXS[3] was used to evaluate the impact of Sit:7-DHC molar ratio in the structural features of the obtained NVs. As explained in **Chapter 3 - Section 3.6**, SAXS is a useful characterization technique to obtain structural information like membrane thickness, lamellarity or membrane ordering.

A SAXS analysis was performed to study the multilamellarity and cross-section structure. The samples characterized were the following: Sit:LGL:LGC NVs (molar ratio 1:0.8:0.2), Sit:7-DHC:LGL:LGC NVs (0.5:0.5:0.8:0.2) and 7-DHC:LGL:LGC NVs (1:0.8:0.2). We selected the two formulations containing just one sterol (just Sit or 7-DHC), and the center point containing both molecules at the same molar ratio Sit:7-DHC of (0.5:0.5).

In the case of Sit:LGL:LGC NVs (1:0.8:0.2), it was the same sample already characterized in **Chapter 8** after 4 months of production. In the case of NVs containing 7-DHC, Sit:7-DHC:LGL:LGC NVs (0.5:0.5:0.8:0.2) and 7-DHC:LGL:LGC NVs (1:0.8:0.2), they were evaluated 1 year after production since their physicochemical characteristics and macroscopical aspect show them to be stable. The experimental details are in **Section 8.3.4**.

The results are presented in **Figure 4.7** and **Table 4.3**. In this case, they show again the impact of the membrane composition on the lamellar structure of the NVs. **Figure 4.7A** represent the experimental SAXS patterns in symbols and the fitted model in a continuous line. The data suggested that the NVs samples containing Sit, either Sit:LGL:LGC or Sit:7-DHC:LGL:LGC, were heterogeneous, where the peak near 1 nm^{-1} is related to the multilamellarity (N_{av} in **Table 4.3**) with influence from the bilayer form factor. In contrast, in the sample containing just 7-DHC as sterol, 7-DHC:LGL:LGC NVs, the presence of the peak related with the multilamellarity was practically nonexistent and it was mainly seen the broad bump related to the bilayer cross-section.

Differences between formulations were also perceived in the electron density profile (**Figure 4.7B**). It was very interesting to observe that the increase of 7-DHC content in the formulations implied a narrower profile, meaning a more compact bilayer structure. This

[3] These measurements were performed at ALBA synchrotron (Spain) and they were analyzed in collaboration with Dr. Cristián Huck-Iriart from ALBA synchrotron (Spain) and Prof. Jan Skov Pedersen from Aarhus University (Denmark).

could be also perceived in the σ_{head} value from **Table 4.3** which decreased with the greater presence of 7-DHC, meaning a decrease on the amplitude of the Gaussian function of the head groups. Furthermore, 7-DHC:LGL:LGC NVs also presented higher membrane density compared with the two other formulations, which could be related to the compaction factor of the bilayer.

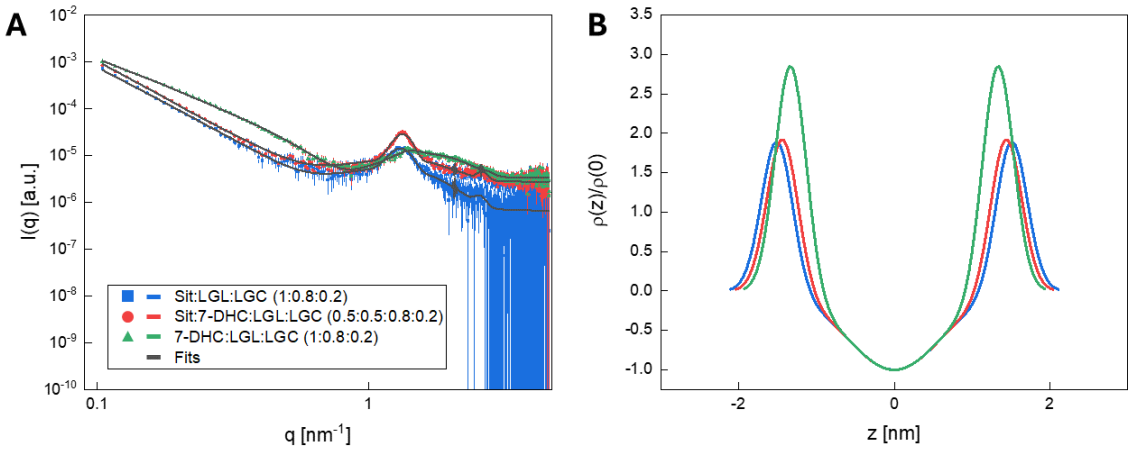


Figure 4.7. **(A)** SAXS data plotted in log-log scale, the experimental data as symbols and the model as continuous curves. **(B)** Excess electron density profile of the bilayer cross-section obtained from the model. In blue Sit:LGL:LGC NVs (molar ratio 1:0.8:0.2), in red Sit:7-DHC:LGLLGC NVs (0.5:0.5:0.8:0.2) and in green 7-DHC:LGL:LGC NVs (1:0.8:0.2).

Table 4.3. Fit results from SAXS modelling.

Formulation	χ^2	S_{head}	σ_{head} [nm]	f_{mono}	N_{av}	D [nm]
Sit:LGL:LGC (1:0.8:0.2)	0.34	0.65 ± 0.04	0.96 ± 0.03	0.64 ± 0.03	4.5 ± 0.1	4.78 ± 0.01
Sit:7-DHC:LGL:LGC (0.5:0.5:0.8:0.2)	0.54	0.66 ± 0.02	0.87 ± 0.01	0.53 ± 0.02	5.1 ± 0.1	4.72 ± 0.01
7-DHC:LGL:LGC (1:0.8:0.2)	0.55	0.9833 ± 0.004	0.75 ± 0.01	0.91 ± 0.04	4.0 ± 0.2	4.52 ± 0.04

χ^2 is the reduced weighted chi-square; S_{head} is the scale of the Gaussian for the head layers; σ_{head} is the sigma of the head layer Gaussian; f_{mono} is the fraction of monolayers; N_{av} is the average number of layers; D is the repeat distance

These results revealed that the sterol used had also an impact on the formation of multilamellar vesicles (**Table 4.3**). On one hand, formulations containing Sit were heterogeneous with a presence of multilamellar and unilamellar NVs at similar proportion, since their fraction of monolayers (f_{mono}) were around 0.6-0.5. On the other hand, NVs just containing 7-DHC as sterol presented a f_{mono} nearer to 1, meaning that most of the NVs were unilamellar. From these results, it seemed that there was not a clear difference when Sit was

used alone or in combination with 7-DHC in terms of multilamellarity. Nevertheless, when 7-DHC was used alone a clear difference was detected since most of the NVs were unilamellar.

Regarding the average number of layers (N_{av}) and the repeat distance between them (D), the values for the formulations containing Sit were similar between them in both cases, showing again no differences among Sit alone or a combination of it with 7-DHC. In the case of NVs with only 7-DHC, N_{av} and D values were also similar to the two other samples, but it is worth mentioning that the error associated to the calculation of this values was higher than with the other samples as the peak related with multilamellarity of this sample was almost imperceptible. For these reasons, N_{av} and D values related with 7-DHC:LGL:LGC NVs were less reliable.

In conclusion, the presence of 7-DHC and its quantity in the membrane of the nanovesicles has a direct impact on the structuring of the bilayers. On one side, it was seen an increase of the compactness of the bilayer with the increase of 7-DHC molar ratio. On the other side, the presence of Sit was directly related to the formation of multilamellar vesicles used with or without the combination of 7-DHC. In opposite, the use of 7-DHC alone gave rise to formulation with mainly unilamellar vesicles.

4.4. 7-DHC is successfully converted to vitamin D when structured in nanovesicles

As explained in the introduction of this **Chapter** and in **Figure 4.1**, 7-DHC is converted to vitamin D in the skin by sun irradiation. This transformation can be mimicked at laboratory scale to evaluate rate of 7-DHC conversion. This reaction has been previously studied in solution by different authors and it is well described[16,17]. The reaction in solution is not that simple as it occurs *in vivo* because other photoisomers could also be formed from the previtamin D (**Figure 4.8**). Several parameters such as irradiation time, temperature or dispersant media are important factors to be considered to achieve an optimal transformation from 7-DHC to vitD.

Therefore, once 7-DHC was successfully loaded in Sit:LGL:LGC NVs, the next step was to assess if 7-DHC could still be effectively converted to vitD while being integrated within the nanovesicle membrane.

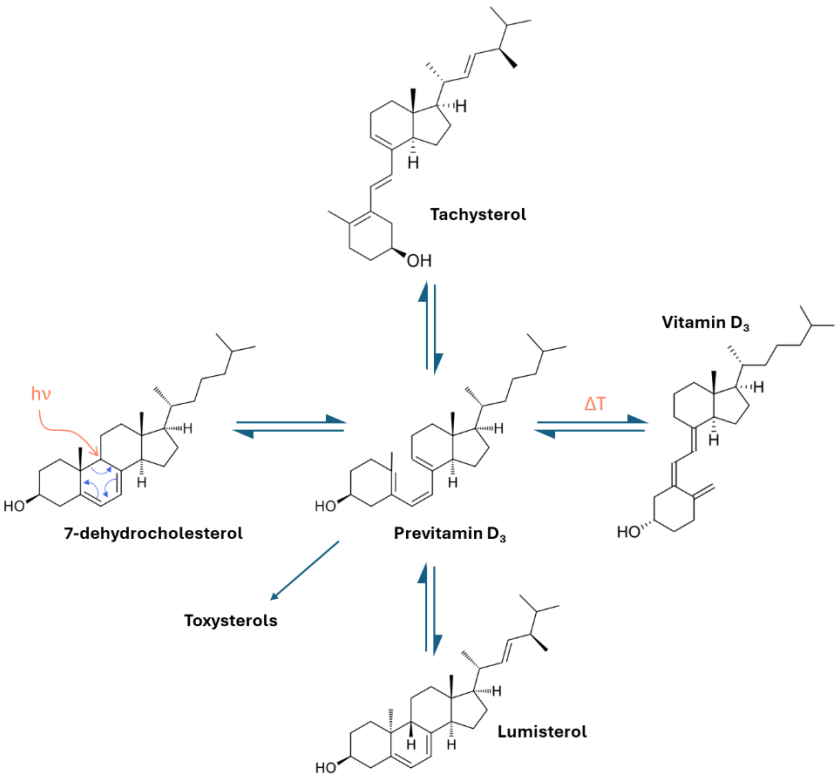


Figure 4.8. Scheme of the chemical reactions involved in vitamin D synthesis in solution and their possible subproducts.

To study the impact of 7-DHC encapsulation in vitD conversion, we performed an irradiation assay to compare how 7-DHC behaved in aqueous media when it was integrated in NVs and when it was free in the dispersant media (as described in **Section 8.5.2**). After some trials to optimize the method in the desired conditions, we finally achieved to develop a procedure where a portion of the 7-DHC was transformed to vitD. Briefly, samples of free 7-DHC and 7-DHC-loaded NVs, both in water/EtOH 15% (v/v), were irradiated using a UV-lamp of $\lambda = 302$ nm. This UV-lamp was chosen because its wavelength was within the range of irradiation wavelengths required by 7-DHC to be converted to previtamin D_3 (**Figure 4.1**). Samples were irradiated for 30 min or 1 h and then stored for 48 h to allow the conversion to the final product, vitD. Finally, the samples content was quantified by high-performance liquid chromatography (HPLC). In this case, it was not possible to evaluate them directly by UV-vis spectroscopy because 7-DHC and vitD absorb at the same range of the spectra, so it

was not possible to distinguish them in the same sample when they were together. It was for this reason that we needed a chromatographic technique to separate and quantify them.

We performed the assay with one of the developed 7-DHC loaded NVs systems. Considering that the physicochemical properties and EE of all the samples were similar, the formulation of NVs with a Sit:7-DHC molar ratio of 0.2:0.8 was selected not only because it contained all the membrane components evaluated, i.e., Sit, 7-DHC, LGL and LGC, but also because it had a high concentration of 7-DHC to better evaluate its transformation to vitD. As a control, the conversion of free 7-DHC in water/EtOH 15% (v/v) was also studied, the same dispersant media as the nanovesicles, at the same measured concentration evaluated in the NVs sample, which was 832 µg/mL.

The irradiation of these two samples, free 7-DHC and 7-DHC-loaded NVs (Sit:7-DHC molar ratio 0.2:0.8), at 30 min and 1 h, showed a partial conversion of 7-DHC to vitD (**Figure 4.9**). As seen in **Figure 4.9A**, either for free 7-DHC or loaded in NVs, a decrease on 7-DHC concentration was observed. This reduction was progressive along time and similar in both samples (after 1 h from 832 µg/mL to 389±4 µg/mL and 350±12 µg/mL respectively), indicating that the loading of 7-DHC in the vesicles did not affect its conversion to vitD. Regarding VitD content shown in **Figure 4.9B**, the increase was also gradual and the levels after 1 h were also similar between samples with free 7-DHC and loaded in NVs (15±1 µg/mL and 17±4 µg/mL). Due to these results, it could be concluded that after loading 7-DHC in nanovesicles, its capacity to be transformed to vitamin D was maintained.

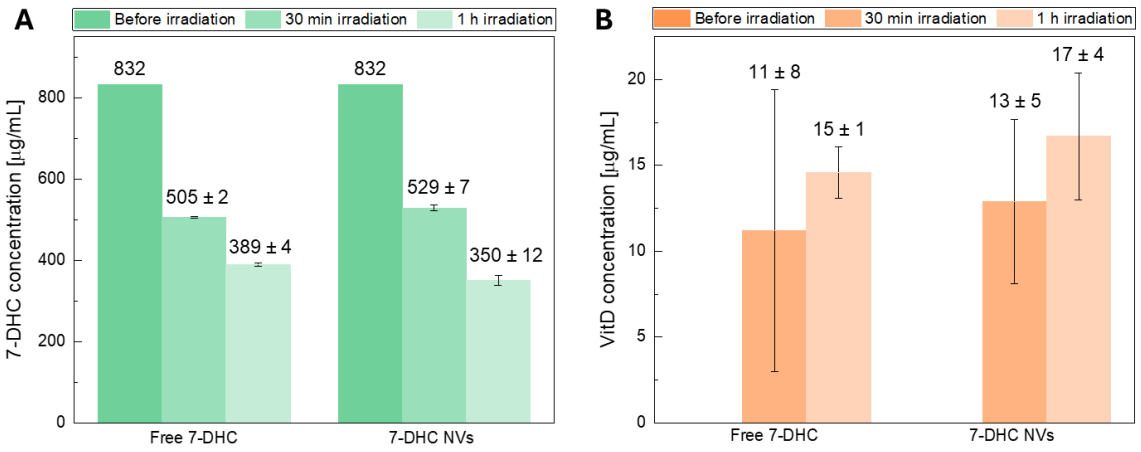


Figure 4.9. Concentration of **(A)** 7-DHC and **(B)** vitD, before and after 30 min and 1 h of irradiation at 302 nm, for samples of free 7-DHC and 7-DHC-loaded NVs (Sit:7-DHC:LGL:LGC, molar ratio 0.2:0.8:0.8:0.2), measured by HPLC. Bars represent the mean of 3 independent experimental replicates ± relative standard deviation.

Nevertheless, it is worth mentioning that the reduction of 7-DHC concentration when irradiating the samples was not proportional to vitD production. There was more reduction on 7-DHC content than increase of vitD. This could be because, as shown in **Figure 4.8**, the 7-DHC conversion reaction in suspension is not simple, and the precursor of the vitD (previtamin D) could coexist together with different isomers, such as tachysterol and lumisterol, at the same time.

In any case, this study was designed to demonstrate that the 7-DHC loaded in the NVs was still able to be converted to vitD, as when being in free form, and did not lose its functionality, as demonstrated by the results here obtained.

Furthermore, the obtained vitD contents after irradiation were in well accordance with the range of recommended dose of vitamin D intake per day, which is between 10 and 20 µg, depending on the age, for healthy individuals[12,13]. Considering these values, under these experimental conditions applying 1 mL of the formulation here reported could be enough to convert the vitamin D necessary for one day.

4.5. Biocompatibility analysis of the 7-DHC nanoformulations

Given the promising results with the nanovesicle formulations containing different amounts of 7-DHC in terms of physicochemical properties, stability and functionality, it was of interest to evaluate their biocompatibility with the skin. As these formulations were thought for topical administration, it was important to assess their skin irritation effect. With this purpose, we performed the assay based on the OECD guideline 439 using *in vitro* models of reconstructed human epidermis[18], previously used and reported in reported **Chapter 3 - Section 3.7.1** for the plain Sit/LGL/LGC systems.

The detailed experimental conditions used in this study are described in **Section 8.6.1**. Briefly, the selected samples were exposed to the RHE models for 24 h. After this time, cell viability of each model was evaluated using the MTT assay and compared to a negative irritation control based on PBS and a positive irritation control based on a solution of SDS at 5% in PBS (w/v).

We evaluated the following samples:

- Sit:LGL:LGC NVs (molar ratio 1:0.8:0.2), i.e., NVs just with Sit.
- 7-DHC:LGL:LGC NVs (molar ratio 1:0.8:0.2), i.e., NVs just containing 7-DHC.
- Sit:7-DHC:LGL:LGC NVs (molar ratio 0.2:0.8:0.8:0.2), a system containing both sterols also evaluated in the functional irradiation assay (**Section 4.4**).
- Furthermore, this last system containing Sit:7-DHC at a molar ratio 0.2:0.8, was also tested after 1 h of irradiation at λ = 302 nm to ensure that after irradiation the formulation was still non-irritant and that vitD or any other subproduct of the reaction was not harmful to the skin.
- Finally, 7-DHC free in water/EtOH 15% (v/v), the same dispersant media than the NVs, was also evaluated at a concentration of 832 µg/mL, the same used in **Section 4.4** in the irradiation study and which corresponded to the concentration of 7-DHC in the NVs containing Sit and 7-DHC at a molar ratio 0.2:0.8. This sample was also evaluated before and after 1 h of irradiation at λ = 302 nm.

The results are represented in **Figure 4.10**. The assay showed that under the applied experimental conditions, none of the six tested formulations showed irritant effect, considering that cell viability was far above the threshold level of 50% with respect to the negative control, which is the value below the samples are considered as irritant[18]. The four tested formulations of NVs showed similar cell viability values around 100%, including the irradiated formulation. The free 7-DHC group showed the same non-irritant behavior with cell viability values around 100%, as expected because it is a compound already approved for topical dermocosmetic use.

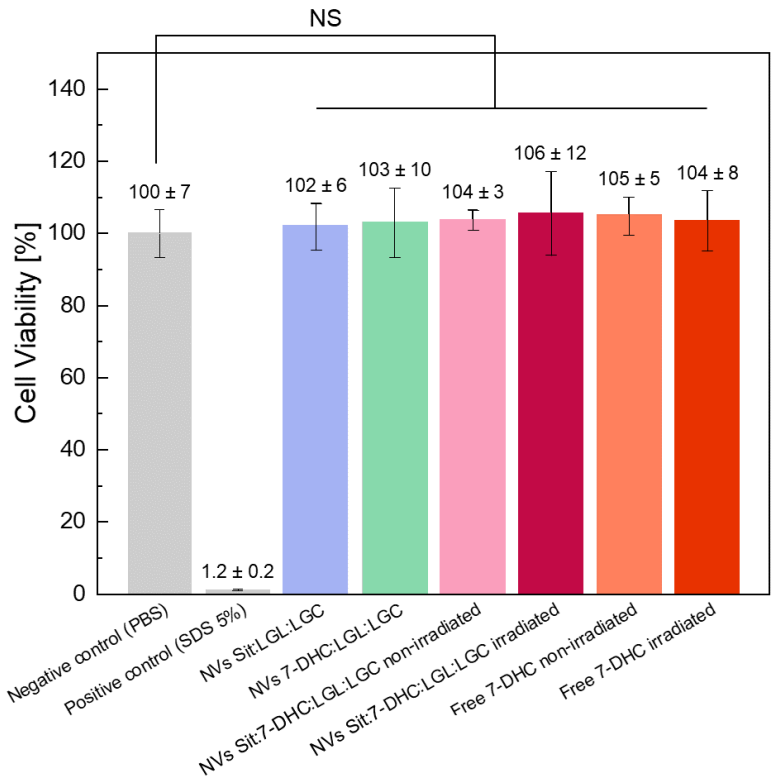


Figure 4.10. *In vitro* skin irritation assay of Sit:LGL:LGC NVs (molar ratio 1:0.8:0.2) (blue), 7-DHC:LGL:LGC NVs (1:0.8:0.2) (green), Sit:7-DHC:LGL:LGC NVs (0.2:0.8:0.8:0.2) non-irradiated (light pink) and irradiated for 1 h (dark pink), free 7-DHC non-irradiated (light orange) and irradiated for 1 h (dark orange), and the corresponding negative and positive control (grey) with the SkinEthic™ RHE models. Bars represent the mean of 3 independent experimental replicates ± standard deviation. All statistical analyses were conducted by one-way ANOVA followed by Tukey pairwise comparison. $p < 0.01$ and NS: non-significant differences.

In conclusion, all the nanoformulations containing 7-DHC were biocompatible with the skin, even the irradiated ones. For this reason, these 7-DHC nanoformulations could be suitable for topical applications taking into account further *in vitro* and *in vivo* studies would be required to complete the safety and efficacy demonstration.

4.6. Summary of the Chapter and future perspectives

Overall, the results presented in **Chapter 4** show the development of aqueous nanoformulations stabilizing the lipophilic precursor of the vitamin D,

7-dehydrocholesterol, in novel nanovesicles based on phytosterols and alkyl polyglucosides surfactants.

Taking as basis the nanovesicles described in **Chapter 3** containing Sit, pure-grade LGL and LGC at a molar ratio 1:0.8:0.2, we have conducted an experimental progressive screening replacing Sit by 7-DHC as a sterol-like molecule able to build the nanovesicle membrane together with the APGs surfactants, until achieving a complete replacement of Sit. Along the **Chapter**, it has been proved that it was possible to obtain stable NVs with 7-DHC as a building block using DELOS manufacturing method.

The different NVs formulations obtained with increasing 7-DHC content were characterized by DLS, ELS, cryo-TEM and SAXS, showing similar physicochemical characteristics. Nevertheless, the formulations containing higher amounts of 7-DHC showed smaller particle size and size PDI (size of 135 - 160 nm and PDI ∼ 0.1) compared to the NVs with higher content in Sit (size of 180 - 200 nm and PDI ∼ 0.2). Besides, increasing content of 7-DHC in the nanovesicles had an impact on their lamellar structuration, with an increased compactness of the bilayers and also an increased ratio of unilamellar vesicles. In contrast, the surface charge was similar in all nanovesicular systems regardless of the presence of 7-DHC, with apparent ζ-Pot values between -50 and -60 mV, probably due to their equal proportion of anionic surfactant LGC in the system composition.

Additionally, this work proved that 7-DHC has the ability to be transformed to vitamin D when irradiated at certain conditions although being loaded in the NVs, an essential characteristic for its active role in formulated final products. Thus, after being loaded in the NVs and integrated in the nanovesicular bilayer, a more constricted space compared to when it is in suspension, the chemical reaction to produce vitD can still take place, meaning that the loading of this payload does not suppress its activity. Nonetheless, this assay was performed in a liquid medium, and it would be important for future work to also evaluate its transformation to vitD in cells. In this sense, studies with human keratinocytes could be performed, either using *in vitro* cell cultures or reconstructed human epidermis models, administering the 7-DHC-loaded NVs and irradiating them to evaluate the capacity of keratinocytes to produce vitamin D by themselves. Furthermore, as the formulations are stable at the physicochemical level, it could be also interesting in future steps to evaluate the activity of the molecule after storage under controlled conditions for several months.

Finally, the biocompatibility of the formulations for topical administration was assessed *in vitro* using human reconstructed epidermis models. The results showed that these novel nanoformulations containing 7-DHC were not irritant.

All in all, this **Chapter 4** presents the development of stable and functional aqueous formulations of 7-DHC, a lipophilic payload, loading the molecule in the novel plant-based nanovesicles containing APGs described in the previous chapter. Homogeneous and stable formulations of Sit:7-DHC:LGL:LGC NVs were obtained. This formulation containing 7-DHC, a vitD precursor, is interesting in terms of market needs, since vitamin D supplementation is a trending topic in the last years due to the general prevalence of its deficiency worldwide and there is a clear commercial opportunity for this type of advanced functional ingredients in the dermocosmetic field.

4.7. Bibliography

1. H.F. DeLuca. Overview of general physiologic features and functions of vitamin D. *Am. J. Clin. Nutr.* **2004**, 80, 1689S-96S.
2. M.A. Zmijewski. Vitamin D and Human Health. *Int. J. Mol. Sci.* **2019**, 20, 145.
3. D.D. Bikle. Vitamin D and the skin: Physiology and pathophysiology. *Rev. Endocr. Metab. Disord.* **2012**, 13, 3–19.
4. M. Umar, K.S. Sastry, F. Al Ali, et al. Vitamin D and the Pathophysiology of Inflammatory Skin Diseases. *Skin Pharmacol. Physiol.* **2018**, 31, 74–86.
5. D.D. Bikle. Vitamin D metabolism, mechanism of action, and clinical applications. *Chem. Biol.* **2014**, 21, 319–329.
6. P. Pludowski, M.F. Holick, W.B. Grant, et al. Vitamin D supplementation guidelines. *J. Steroid Biochem. Mol. Biol.* **2018**, 175, 125–135.
7. R. Vieth. Vitamin D supplementation: cholecalciferol, calcifediol, and calcitriol. *Eur. J. Clin. Nutr.* **2020**, 74, 1493–1497.
8. A. Cui, T. Zhang, P. Xiao, et al. Global and regional prevalence of vitamin D deficiency in population-based studies from 2000 to 2022: A pooled analysis of 7.9 million participants. *Front. Nutr.* **2023**, 10, 1070808.
9. K.D. Cashman, K.G. Dowling, Z. Škrabáková, et al. Vitamin D deficiency in Europe: Pandemic? *Am. J. Clin. Nutr.* **2016**, 103, 1033–1044.
10. K. Amrein, M. Scherkl, M. Hoffmann, et al. Vitamin D deficiency 2.0: an update on the current status worldwide. *Eur. J. Clin. Nutr.* **2020**, 74, 1498–1513.
11. R. Bouillon, D. Manousaki, C. Rosen, et al. The health effects of vitamin D supplementation: evidence from human studies. *Nat. Rev. Endocrinol.* **2022**, 18, 96–110.
12. European Food Safety Authority. Vitamin D: EFSA Sets Dietary Reference Values https://www.efsa.europa.eu/en/press/news/161028 (accessed Jun 29, 2023).
13. National Institutes of Health. Vitamin D - Consumer https://ods.od.nih.gov/factsheets/VitaminD-Consumer/ (accessed Jun 29, 2023).
14. European Commission. CosIng - Cosmetics - GROWTH - European Commission

https://ec.europa.eu/growth/tools-databases/cosing/details/74521 (accessed Mar 7, 2024).

15. Vytrus Biotech. Nectaria Lithops™ https://www.vytrus.com/es/natural-active/nectaria-lithops/ (accessed Mar 26, 2024).

16. O. Dmitrenko, T. Orlova, I. Terenetskaya. Medium controlled photochemistry of Provitamin D: From solutions to liquid crystals. *J. Mol. Liq.* **2018**, 267, 428–435.

17. M. Escribà-Gelonch, T. Noël, V. Hessel. Microflow High-p,T Intensification of Vitamin D3 Synthesis Using an Ultraviolet Lamp. *Org. Process Res. Dev.* **2018**, 22, 147–155.

18. OECD. Test Guideline No. 439 In Vitro Skin Irritation : Reconstructed Human Epidermis Test Method In Vitro. *OECD Guidelines for the Testing of Chemicals*. 2021.

5 Formulation of hydrophilic payloads in alkyl polyglucosides and β-sitosterol nanovesicles

5.1. Formulation of hydrophilic payloads with vesicles

As explained in the **Introduction**, vesicles are versatile delivery systems since they can load either hydrophobic or hydrophilic molecules, or even both at the same time (**Figure 5.1**)[1]. On one hand, hydrophobic molecules can be loaded inside the bilayer where there is a lipophilic environment. On the other, hydrophilic molecules can be loaded inside the aqueous lumen of the vesicles or interacting with the outer and inner bilayer, by binding. This interaction can be electrostatic, if the payload and the bilayer have opposite charge, or by hydrophobic interactions when speaking of macromolecules like proteins which can have hydrophobic and hydrophilic domains. In these cases, the hydrophobic part of the molecule interacts with the bilayer, while the hydrophilic domain is in contact with the aqueous environment.

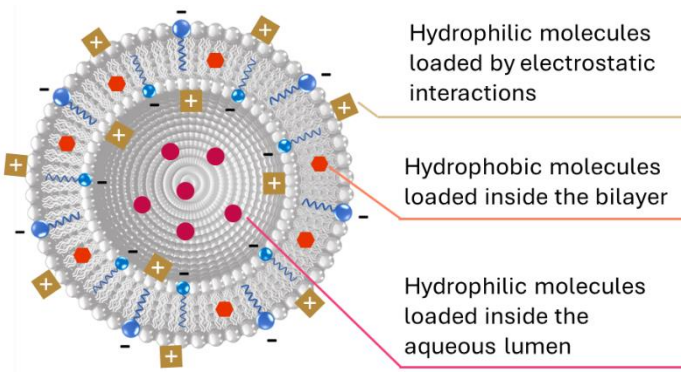


Figure 5.1. Schematic representation of the integration of payloads in vesicles depending on their nature.

In **Chapters 3** and **4** of this Thesis, hydrophobic payloads like α-tocopherol, 7-dehydrocholesterol or Nile red compounds were efficiently loaded in the sugar-based Sit/APGs nanovesicles. However, to prove the full potential of this new platform of delivery systems the integration of hydrophilic molecules should also be evaluated.

Although it can be thought that hydrophilic active molecules are not as challenging to deliver as hydrophobic molecules, since they can be easily dissolved in body fluids, they also have to face different barriers to arrive at the target place.

Hydrophilic payloads can be differentiated in two groups depending on their molecular weight, since the obstacles which they have to deal with are different: small molecules and larger biological molecules.

In the case of small hydrophilic molecules, although aqueous solubility enhances the initial mobility within the body fluids, they are susceptible to rapid elimination and low permeation across lipid barriers, leading to reduction of drug lifetime, bioavailability and low cellular absorption[2,3]. In the specific case of topical applications, the main barrier to deliver hydrophilic small molecules is the stratum corneum. As previously explained in **Section 1.4** of **Chapter 1**, this outermost layer of the skin is tightly packed with corneocytes and an extracellular matrix basically composed of lipids, which make hydrophilic compounds inadequate candidates to cross this layer due to the low solubility in this extracellular matrix although their low molecular weight (< 500 Da)[4].

Regarding larger hydrophilic biomolecules, there are different types: proteins (e.g., enzymes, monoclonal antibodies, cytokines, hormones or growth factors), vaccines, nucleic acid-based products (DNA or RNA), and gene- and cell-based therapeutics[5]. In this Thesis, the focus was set on the first group, proteins. Biologics normally show better specificity,

potency and targeting ability compared to conventional small active molecules[5]. However, protein stability, route of administration and distribution are all factors that can hinder the successful application of proteins. Since they are large molecules, normally they present difficulties to cross body barriers and cell membranes. Additionally, their half-life can be affected by the presence of proteases, protein-modifying chemicals or other clearance mechanisms. Finally, it is also worth mentioning that biologics may cause an immune response of the body against the payload[6]. Focusing on skin delivery, again the main challenge for protein delivery is to cross the stratum corneum. Proteins are macromolecules of more than 500 Da that normally have hydrophilic character, which are two limitations to cross this outermost skin barrier[5].

Due to the constraints that hydrophilic compounds present to be administered topically, their formulation with delivery systems could promote skin permeation since they could act as penetration enhancers. This ***Chapter*** *describes a first prove of concept to integrate either proteins or small hydrophilic molecules, in the novel NVs composed of Sit and alkyl polyglucosides developed in this Thesis. The payloads evaluated were the vitamins niacinamide and ascorbyl glucoside as small molecules, and the basic fibroblast growth factor as an example of large biomolecule* (**Figure 5.2**). *The selected NVs formulation to study the hydrophilic loadings was Sit and LGC at 1:1 molar ratio.*

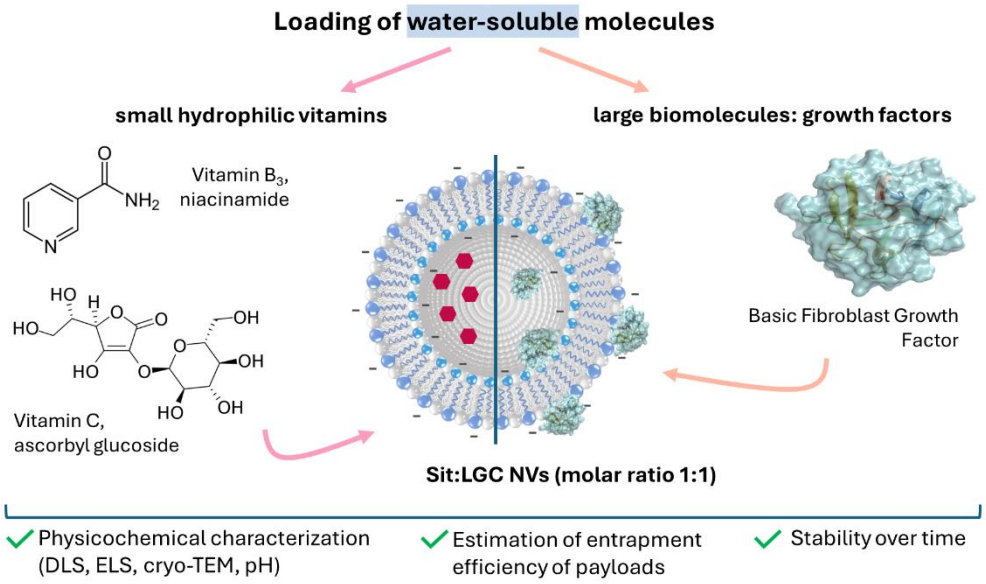


Figure 5.2. Graphical summary of the work performed to encapsulate hydrophilic molecules in the plant-based nanovesicles, described in this **Chapter 5**.

5.2. Loading the basic fibroblast growth factor in Sit:LGC nanovesicles

5.2.1. Use of growth factors in healthcare and cosmetic products

Skin aging is a natural process that depends on internal stimuli, i.e., physiological and genetic changes; and external stimuli such as ultraviolet radiation, pollution or pathogens. At the end, the consequences are basically the thinning of the epidermis, a decrease in the contact surface between the dermis and the epidermis, and the reduction of basal cell proliferation, including keratinocytes, fibroblasts and melanocytes. Thus, the production of fibrous extracellular matrix components of the dermis such as collagen, elastin or fibrillin is more limited at aging. All these changes cause disruption of the skin structure including thinning, dryness, loss of elasticity, fragility or wrinkles[7,8].

Growth factors are biologically active proteins that are secreted and affect cell growth, differentiation and/or cell division. There are different types of growth factors such as the epidermal growth factor (EGF), the keratinocyte growth factor (KGF) or the fibroblasts growth factors (FGF). These proteins can be exogenously produced by biotechnological means and have attracted the attention of the healthcare industry due to their role in skin homeostasis. It is known that growth factors play an important role in wound healing, and this knowledge has led to evaluate their function in the repair of skin structures. As the regeneration of skin cells decrease with aging, also does the production of these growth factors, and an exogenous supplementation can promote the repair of aging skin and revitalize it[8,9].

As mentioned above, aging causes the senescence of fibroblasts, which are the responsible cells of producing the extracellular dermal matrix, causing its gradual degradation which is the main contribution factor to the aging phenotypes like wrinkles and loss of elasticity[8,9]. Fibroblast growth factors are a family of proteins that increase the proliferation and activation of fibroblasts[10], which can fight against skin aging trough the repair of extracellular matrix.

Within the fibroblast growth factors family, basic fibroblast growth factor (bFGF) activates new skin cells and stimulates their proliferation, mainly fibroblasts and keratinocytes. It is suggested that bFGF may be important in the modulation of processes such as angiogenesis, wound healing and tissue repair, as well as anti-aging actions[10].

In the cosmetic market, there are already marketed products containing bFGF (**Table 5.1**), but to the best of our knowledge none of them report the use of delivery systems.

Table 5.1. Marketed cosmetic products containing bFGF and other growth factors. Adapted from Araújo *et al.*[10].

Product	**Manufacturer** ***(Country of origin)***	**Other growth factors**
TNS Recovery Complex	Skin Medica *(USA)*	Isolated
D Cosmeceutical Eye Cream	Dermaheal *(South Korea)*	aFGF, EGF, IGF, peptides
GF Adcanced Derm Cream	G.M. Collin *(Canada)*	TGF-β
Firm-X	Peter Thomas Roth *(USA)*	TGF-β
Skin Factor	Buona Vita *(Brasil)*	EGF, IGF, VEGF

aFGF, acidic FGF; EGF, epidermal growth factor; IGF, insulin growth factor; TGF-β, transforming growth factor β; VEGF, vascular endothelial growth factor

In the study presented in this **Chapter**, the bFGF was selected. The bFGF employed to perform the encapsulation experiments was a peptide of 16.4 kDa and an isoelectric point (pI) of 9.63 (INCI name: sh-Polypeptide-1). As the recommended working pH with the protein is pH = 7, and the pI = 9.63 > pH = 7, the protein was positively charged at the working pH conditions. To enhance the electrostatic binding of the positively charged protein with the nanovesicles, and with the aim of promoting and improving the loading, the system of Sit:LGC NVs, which are negatively charged, was used in this proof of concept study.

This strategy was adopted from a previous project in which epidermal growth factor was successfully loaded in nanovesicles using DELOS method for the topical treatment of complex wounds intended for pharmaceutical usage[11]. In that case, the nanovesicles were composed of cholesterol and CTAB, a cationic quaternary ammonium surfactant. As the protein EGF had a pI = 4.6, at physiological conditions (pH ≈ 7) presented negative charge, enabling the electrostatic interaction between the cationic vesicles and the protein[12]. EGF was efficiently loaded in the NVs with EE values of almost 100%, and the formulation showed promising results increasing the activity of the protein when it was loaded in NVs in comparison to free EGF. In views of the success of the EGF-loaded NVs formulation, and

considering the similarities, i.e., topical application and opposite charge between NVs and growth factor; it was tried to load the positively charged bFGF in the novel nanovesicles developed in this **Thesis** with the anionic surfactant LGC.

5.2.2. Loading of bFGF in Sit:LGC nanovesicles by DELOS process

To integrate the positively charged protein bFGF, the formulation of Sit:LGC (1:1) nanovesicles was selected. The common and well-known 10 mM PBS buffer was used to control the pH of the aqueous phase at a value of 7.4.

The concentration of protein was set at 50 µg/mL, an appropriate concentration based on previous experience with entrapment of growth factors in nanovesicles and bibliography[11,13]. Additionally, blank formulations were obtained at the same operating conditions and evaluated as control, since all the previous formulations produced up to this moment were prepared in water instead of a saline buffer.

The formulations were produced using the DELOS methodology in a bench scale equipment (see **Section 8.2.1**). The bFGF payload, as it is hydrophilic, was dissolved in the PBS 10 mM aqueous phase together with the LGC (**Figure 5.3**). The colloidal systems obtained, blank and bFGF-loaded NVs, had the same dispersant media (PBS 10 mM/EtOH 15% (v/v)) and a concentration of membrane components of 2.82 mg/mL.

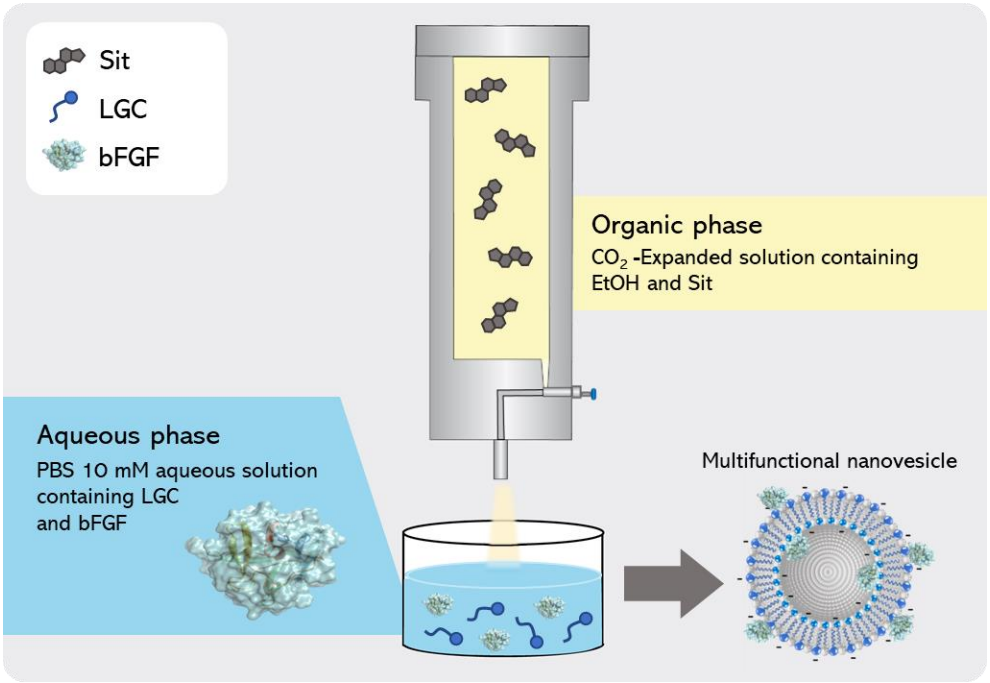


Figure 5.3. Schematic representation of the DELOS methodology used for the preparation of nanovesicles composed of Sit:LGC (1:1) and loaded with bFGF 50 µg/mL, using PBS 10 mM as aqueous phase, as described in **Section 5.2**.

In this particular case, to eliminate impurities coming from the starting materials (basically Sit and APGs mixtures) the NVs samples obtained after DELOS were first centrifugated instead of filtered, and then diafiltrated by tangential flow filtration (TFF) to eliminate the free bFGF which was not loaded in the NVs (see **Section 8.3.6.2**). Blank NVs were treated equally.

TFF is a filtration technique that allows the separation of components based on size using microfiltration membranes of different pore sizes. The portion of the starting sample containing the non-incorporated components dissolved in the dispersant media passes through the membrane, whereas the remainder is recirculated back to the feed samples reservoir containing in our case the nanovesicles with the integrated payload.

Thus, two NVs prototypes were then characterized: centrifugated samples (CENT) and centrifugated and diafiltrated samples (DIAF). The prototypes were characterized by DLS, ELS and pH measurements as described in **Sections 8.3.1** and **8.3.7**. Centrifugated samples were further characterized by cryo-TEM as explained in **Section 8.3.2**.

Table 4.2 and **Figure 5.4** show the physicochemical characterization of the blank and bFGF-loaded NVs, after centrifugation and after centrifugation and diafiltration.

First of all, it was possible to obtain Sit:LGC NVs in PBS 10 mM buffer, either with or without bFGF. As shown in **Figure 5.4A** the centrifugated samples had macroscopical appearance of opalescent whitish stable dispersions. Regarding the physicochemical properties of blank NVs obtained in 10 mM PBS, a slight increase on their particle size was observed in comparison to the size presented by the Sit:LGC NVs prepared in water (particle size around 160 nm, reported in **Chapter 3**), which can be due to 10 mM PBS as aqueous phase or the postprocessing method to eliminate impurities (centrifugation instead of filtration)

When comparing blank and bFGF-loaded systems in terms of particle size, the bFGF-loaded NVs presented significantly higher particle size values than blank NVs. In any case, the size PDI and the stability over time of both centrifugated formulations in PBS 10 mM (blank and bFGF loaded) were promising, without significant variation up to 3 months after production. In terms of ζ-Pot, again the values were negative for both systems, as expected with LGC nanovesicles, and above -30 mV, indicating that the colloidal systems were stable.

Analyzing cryo-TEM images from **Figure 5.4B**, differences between centrifugated samples loaded or not with bFGF were detected. As reported in **Chapter 3**, Sit:LGC formulations in water mainly presented unilamellar vesicles, as indicated by cryo-TEM images and SAXS measurements. In the case of blank NVs obtained in PBS 10 mM this behavior was

maintained, since the formulation presented mostly unilamellar NVs. In contrast, bFGF-loaded NVs presented an increased proportion of multilamellar and multivesicular NVs in comparison to the blank formulation, and in some cases deformed vesicles attached one to another by a small patch were observed. These changes observed in vesicles' morphology probably were due to the presence of the protein. Since proteins are large biomolecules with different hydrophobic and hydrophilic domains they could act as adhesive, interacting with different domains with more than one vesicle, deforming them[14]. Although the morphology of this protein nanoformulation was not as homogeneous as for other loaded nanovesicles, it was a promising sign that could indicate that the protein bFGF was integrated in the Sit:LGC NVs.

Table 5.2. Physicochemical characterization of blank and bFGF-loaded NVs formulations, obtained by DELOS methodology using 10 mM PBS as aqueous phase, after centrifugation (CENTR) and after centrifugation and diafiltration (DIAF) (for blank formulations, n = 1; for bFGF-loaded formulations, n = 2). The prototypes loaded with bFGF were prepared at initial protein concentration of 50 μg/mL.

Sit:LGC[a] NVs (1:1 molar ratio)					
Prototype	**Hydrodynamic diameter mean [nm]**	**Size PDI**	**Apparent ζ-Pot [mV]**	**pH**	**EE [%]**
Blank – CENTR	296 ± 2	0.28 ± 0.03	-54.0 ± 0.3	6.19	NA
Blank – DIAF	354 ± 8	0.38 ± 0.01	-	7.16	
bFGF - CENTR	359 ± 2	0.33 ± 0.03	-55 ± 4	6.82 ± 0.01	64 ± 9
bFGF – DIAF	900 ± 700	0.5 ± 0.3	-	7.4 ± 0.2	

In the case of blank formulations where n = 1, the error in DLS and ELS values correspond to the standard deviation of the triplicate measurements performed for each sample.

[a] LGC reagent used was a mixture of APGs, intended as alkyl glucosides of C10-16 chain length, and the corresponding carboxylates; thus, the ratio 1:1 refers to the mixture and not the real content of LGC.

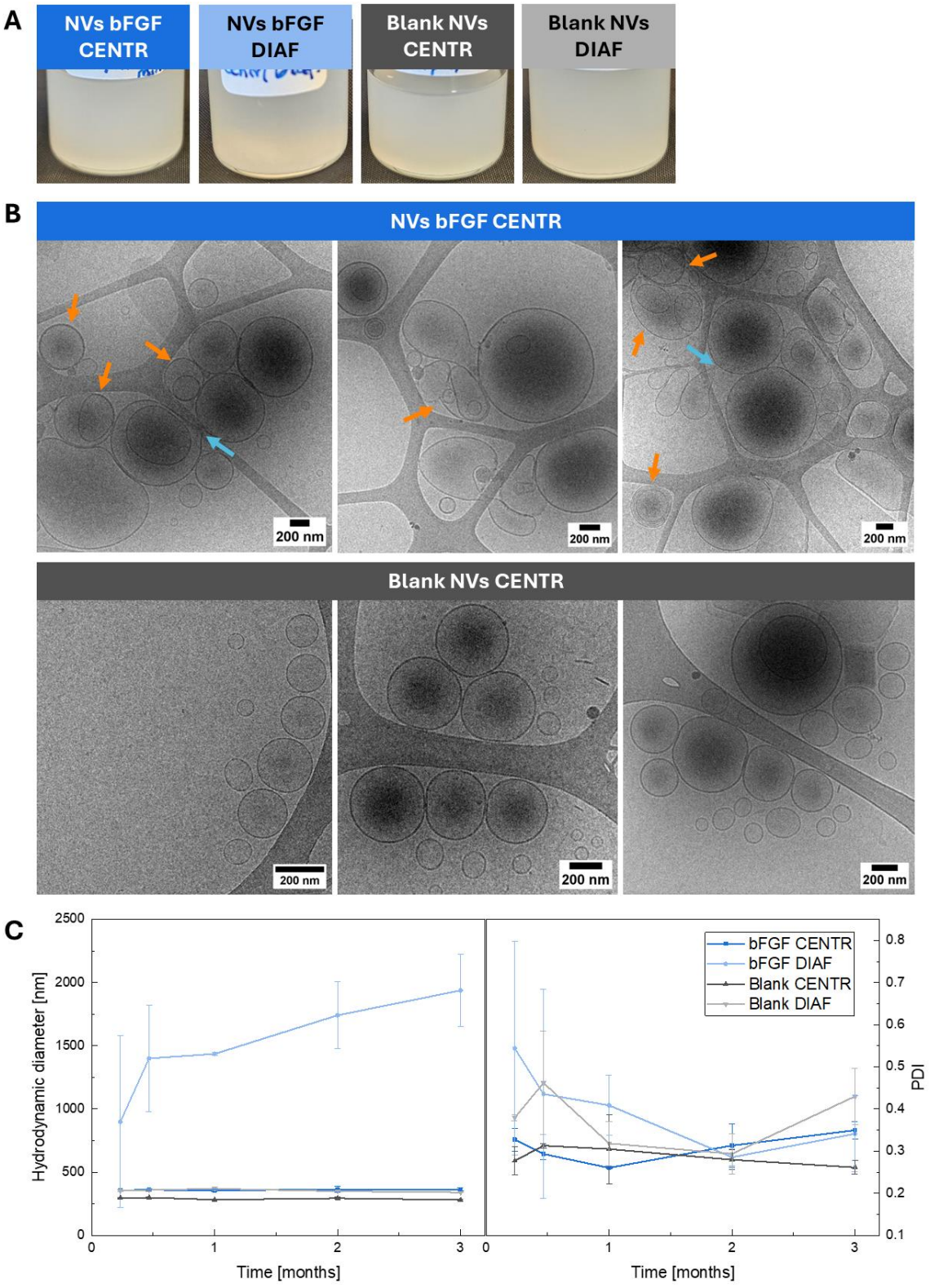


Figure 5.4. **(A)** Macroscopical appearance of blank and bFGF-loaded Sit:LGC (1:1) NVs 1 month after production by DELOS method, and post-processed with centrifugation (CENTR) or centrifugated and diafiltrated (DIAF). **(B)** Representative cryo-TEM images of bFGF-loaded and blank NVs. Multilamellar vesicles and multivesicular vesicles (orange arrows) and deformed nanovesicles (blue arrows) can be distinguished. **(C)** Stability over time in terms of particle size and size PDI (for blank formulations, n = 1; for bFGF formulations, n = 2).

Table 4.2 and Figure 5.4 also show the physicochemical characterization of the diafiltrated NVs, blank and loaded with bFGF. Although diafiltration process was carried out with the aim of separating the free bFGF from the bFGF-loaded NVs, and calculate its EE (see **Section 8.3.6.2**), the diafiltrated formulations were also characterized to evaluate the impact of this process operation on the properties of the NVs. Through the diafiltration process, there was a buffer exchange to remove the free bFGF present in the NVs formulation and other small non-integrated compounds such as free surfactant, and replace it by fresh PBS 10 mM/EtOH 15% (v/v) buffer. Therefore, no changes in the physicochemical characteristics were expected after diafiltration, since there were not significant changes in buffer composition. In the case of blank formulations, the NVs behave as expected: macroscopical appearance before and after diafiltration remained the same (Figure 5.4A), and particle size and PDI did not show significant differences (average particle size for centrifugated formulations was 296 nm and for the diafiltrated ones 354 nm).

However, there was a significant change in the NVs characteristics after diafiltration of bFGF-loaded samples. In the case of macroscopical appearance, a sediment appeared at the bottom of the vial. The particle size increased from 359 nm to 899 nm with a high value of standard deviation. Furthermore, as Figure 5.4C shows, the samples were not stable and the particle size continuously increased with time.

The most probable reason for this behavior was the elimination of a compound through diafiltration process, which stabilized the NVs when it was present, but which elimination by diafiltration destabilized the system. Probably, free surfactant could be stabilizing the NVs by interacting with their surface, but since the cosmetic-grade reagents used contain other unknown impurities, this hypothesis could not be confirmed. Further experiments should be done in the future to better understand these results and the difference observed in particle size and stability when post-processing blank and bFGF-loaded formulations, performing more replicates of both systems to obtain more robust tendencies. In this regard, development of HPLC methods to understand changes in the composition of the systems could be useful.

Regarding EE calculation, as explained in **Section 8.3.6.2**, fluorescence spectroscopy measurements were performed comparing the emission intensity of the centrifugated samples with that of centrifugated and diafiltrated samples (Figure 5.5). First, it was evaluated the fluorescence emission spectra of free bFGF to study its behavior, as well as CENTR and DIAF blank NVs in 10 mM PBS (Figure 5.5A). These exploratory assays showed that the protein bFGF and blank NVs had a fluorescence emission peak at the same range of

the spectra. Furthermore, CENTR and DIAF blank NVs presented different spectra in terms of shape and intensity. CENTR blank NVs presented two emission peaks (λ ≈ 325 nm and 375 nm), whereas DIAF samples presented just one peak (λ ≈ 325 nm) and of lower intensity. As it has been discussed previously in this **Section**, fluorescence spectroscopy also pointed to the hypothesis that during diafiltration process part of the components of the samples were removed, and these components could emit fluorescence under the applied conditions. Thus, due to the impact of NVs components on the emission of bFGF, as a first approximation in this **Thesis** it was decided to calculate the EE of bFGF-loaded NVs by comparing the emission intensity of CENTR samples (containing free and loaded in NVs bFGF) with DIAF ones (containing just bFGF loaded in NVs) (**Figure 5.5B**). The emission spectra of the bFGF-loaded samples were corrected using the emission spectra of blank CENTR or DIAF NVs. Using this approach, it was not possible to obtain the quantitative concentration of bFGF in each sample, but an approximated value of EE.

The EE value obtained for bFGF-loaded NVs was 64% ± 9 (**Table 4.2**), which for a first prove of concept was a promising value. Additionally, it has to be considered that post-processing by centrifugation and diafiltration can have an impact on this parameter. Thus, further assays have to be done in the future to gain knowledge about the impact of post-processing operations on the concentration and activity of the loaded protein.

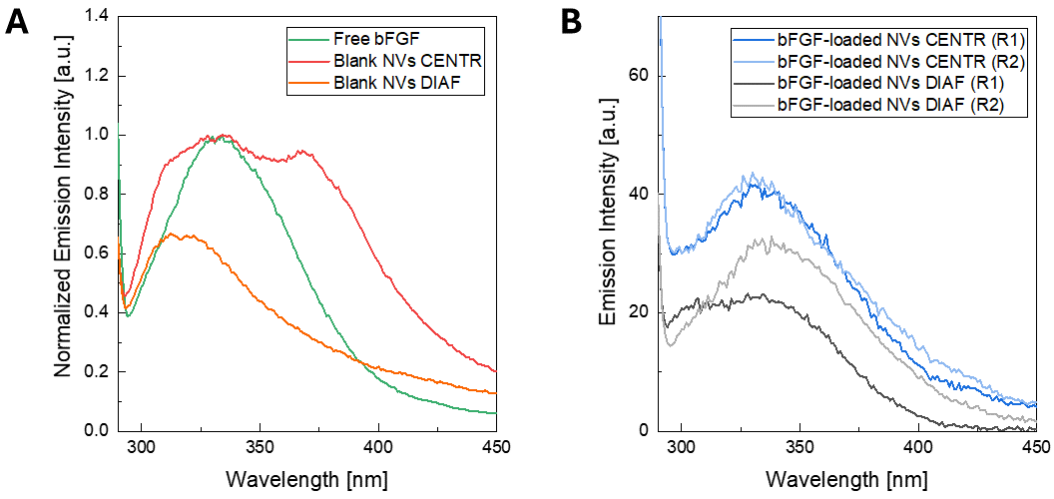


Figure 5.5. (A) Normalized fluorescence emission spectra of free bFGF (in green), blank Sit:LGC NVs (1:1) centrifugated (CENTR) (in red) and centrifugated and diafiltrated (DIAF) (in orange). DIAF blank NVs were normalized in relation to CENTR blank NVs. **(B)** Fluorescence emission spectra of bFGF-loaded Sit:LGC NVs. In blue the two replicates (R) of the formulation centrifugated (CENTR) and in grey the two replicates centrifugated and diafiltrated (DIAF). All the spectra were corrected using blank formulations treated by the same processes.

5.2.3. Summary of the Section and future perspectives on the nanoformulation of growth factors

Growth factors are of interest for healthcare and cosmetic industries. In this study a preliminary formulation of the growth factor bFGF with potential topical use was achieved by loading the protein in plant-based Sit:LGC nanovesicles. However, further work has to be done to optimize the NVs formulation with bFGF and efficacy studies to evaluate the activity of the protein after laoding. Besides, also other growth factor candidates, such as epidermal GF, insulin GF, transforming GF β or vascular endothelial GF, which can be relevant for the market[10] would be interesting to explore in the future to build an ingredient pipeline. Loading of growth factors can be also combined with other types of payloads such as small hydrophobic active molecules searching for synergic effects of different ingredients.

Overall, from this section, it was concluded that the first prove of concept to integrate large biomolecules like growth factors using the novel plant-based nanovesicles was promising. In particular, NVs formulations composed of Sit and the anionic surfactant LGC were produced satisfactorily in PBS 10 mM obtaining stable formulations with optimal physicochemical properties in terms of particle size, size PDI and ζ-Pot. These nanovesicles could efficiently load the growth factor bFGF when working at a protein concentration of 50 µg/ml, since the bFGF was positively charged at the working pH = 7, thus promoting a possible electrostatic interaction between the payload and the negatively charged nanovesicle membrane. However, it is known for previous experience that electrostatic interactions are not the only ones which can promote the interaction between the vesicles and the proteins. In the case of loading other growth factors which at pH = 7 are not positively charged, interactions such as hydrogen bonding or π-stacking with the aromatic amino acids could occur.

Nonetheless, further investigation could be planned to explore potential applications. First, additional studies to evaluate the stability of bFGF NVs formulations variating the post-processing parameters, to gain knowledge into which factors could stabilize or, on the contrary, destabilize the nanoformulations. Then, it would be also necessary to develop an analytical method to quantify the concentration of protein in the formulations. From the presented results, the preliminary method presented here to calculate EE and based on fluorescence emission, enabled to obtain an EE percentage but not to calculate the bFGF concentration on each sample. For this, it would be helpful to have an analytical method in place based on fluorescence analysis or other techniques to be able to calculate concentration values for the different formulations produced.

Besides growth factors, there are other types of proteins, like enzymes, that are also interesting for the healthcare and cosmetic market. For example, superoxide dismutase (SOD) enzyme which can prevent free radicals damage, or different types of plant-based proteases used for skin exfoliation, are common active ingredients used for cosmetic applications[9]. Their nanoformulation using the Sit/APGs NVs can enhance their skin permeation and increase their stability over time. Given the promising results with this first trial other proteins could be also evaluated in the future.

5.3. Loading of vitamins C and B_3 in Sit:LGC nanovesicles

5.3.1. Use of hydrophilic vitamins in healthcare and cosmetic products

There are several small molecules that are typically used in healthcare and cosmetic products, principally for skincare, because of their benefits to the human skin. Some examples are vitamins, carotenoids, or polyphenols. Although some of them are lipophilic, like vitamins A and E or carotenoids, others are hydrophilic molecules such as vitamin C (ascorbic acid), and vitamin B_3 (niacin)[15].

5.3.1.1. Vitamin C as active ingredient

L-Ascorbic acid is the biologically active form of vitamin C and the most abundant antioxidant in the skin (**Figure 5.6A**). Humans are not able to produce vitamin C by our own since we do not have the enzyme to produce the molecule, thus it must be obtained from diet or from other sources such as healthcare products. Vitamin C is widely used in skincare formulations due to its benefits for the skin: antioxidant function treating oxidative damage generated after UV radiation exposure and environmental pollution; cofactor in collagen synthesis having an antiaging effect; and reduction of melanogenesis and skin hyperpigmentation due to the inhibition of tyrosinase enzyme[16,17].

In spite of all this promising functions, ascorbic acid is a weak, highly unstable water-soluble organic acid which can be easily degraded or oxidized by light, presence of oxygen, high temperatures and pH or metal ions[16,18]. Furthermore, due to its hydrophilic character and the fact that it is a charged molecule at skin pH, it presents a poor penetration through the skin[15,17,18].

Due to these challenges, several strategies have been followed to stabilize ascorbic acid, and one of them is the modification of ascorbic acid to produce more stable and easier to formulate derivatives. Different options have been explored[16,19], from lipophilic derivatives

(e.g., ascorbyl 6-palmitate or tetra-isopalmitoyl ascorbic acid) to hydrophilic molecules such as saline derivatives (e.g., ascorbyl 2-phosphate formulated with sodium or magnesium).

Another hydrophilic derivate is ascorbyl 2-glucoside (ascorbyl glucoside, AG) (**Figure 5.6B**). It has been found that this molecule has higher stability against degradation at high temperatures, pH and metal ions since the glucose molecule is bound to ascorbic acid in the carbon-2 hydroxyl, which is directly related with the pharmacological activity and responsible for the degradation process[19]. Besides, when applied to the skin is easily metabolized and converted to the active form, ascorbic acid, and glucose[18,19]. Nevertheless, as it is a hydrophilic molecule it has difficulties to permeate trough the stratum corneum and it is for this reason that it is interesting to formulate it through delivery systems that can enhance its permeability.

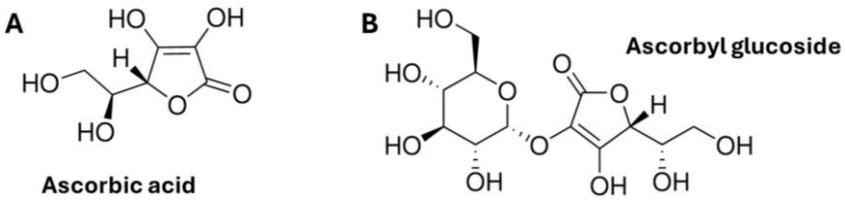


Figure 5.6. Molecular structure of **(A)** ascorbic acid and **(B)** ascorbyl glucoside (AG).

The skincare market is a leading segment of the cosmetic industry, with products that enhance skin health, including vitamin C products[16]. Some examples are listed in **Table 5.3**, with a large variety of products which show the high potential of vitamin C market, including vitamin C derivatives loaded in liposomes.

Table 5.3. Marketed cosmetic products containing vitamin C or derivatives.

Product	Manufacturer *(Country of origin)*	Active ingredient
Skin Renewing Vitamin C Serum	CeraVe *(USA)*	L-Ascorbic acid
C E Ferulic	SkinCeuticals *(USA)*	L-Ascorbic acid
Banana Bright Vitamin C Serum	OleHenriksen *(USA)*	3-O-Ethyl ascorbic acid
Pure Vitamin C10 Serum	La Roche-Posay *(France)*	L-Ascorbic acid
C-VIT Liposomal Serum	Sesderma *(Spain)*	Liposomal 3-O-Ethyl ascorbic acid
Tónico regenerante purificante	Atashi *(Spain)*	Liposomal tetra-isopalmitoyl ascorbic acid

5.3.1.2. Vitamin B_3 as active ingredient

Niacinamide (NCA) (**Figure 5.7B**) is the amide and active form of the hydrophilic vitamin B_3 (niacin) (**Figure 5.7A**). Niacinamide is a component of the coenzymes involved in hydrogen transfer, nicotinamide adenine dinucleotide (NAD) and nicotinamide adenine dinucleotide phosphate (NADP)[20]. Both molecules, niacinamide and niacin, have the same activity, although niacinamide is softer and secure to the skin since niacin can cause flushing[21]. It is for this reason that niacinamide is the molecule which is used for skincare treatments.

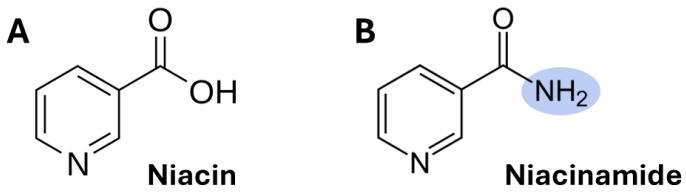


Figure 5.7. Molecular structure of **(A)** niacin and **(B)** niacinamide (NCA).

When applied to the skin, niacinamide can provide several benefits. It has anti-aging effect since it is related with the synthesis of proteins of the dermal extracellular matrix. Furthermore, stimulates ceramide synthesis, one of the main components of stratum corneum, improving the skin barrier function. In some products it is also search the anti-inflammatory effects of niacinamide, reducing skin redness, blemishes and acne[20,22].

However, the molecular mechanisms that cause these changes are still under research. It is still unclear if its efficacy is directly related to niacinamide itself or indirectly promoted as a precursor of other active metabolites[21].

As reported in **Table 5.4**, there are different marketed products containing niacinamide for different applications, from serums for skincare to masks or facial cleansers, and at different concentrations[20]. Nonetheless, niacinamide can be challenging to deliver to the skin due to its high aqueous solubility, which hinders its permeation through the lipophilic stratum corneum. Again, like in the case of vitamin C, it is the reason why loading of niacinamide in delivery systems such as vesicles is an interesting approximation.

Table 5.4. Marketed cosmetic products containing niacinamide (vitamin B_3). Adapted from Ong *et al*.[20].

Product	**Manufacturer** ***(Country of origin)***
Micellar cleansing water with niacinamide & ceramides for all skin types	CeraVe *(USA)*
Ultra Pure 5.0% Niacinamide Oil-Minimising High-Potency Serum	Kiehl's *(USA)*
Pure niacinamide 10 serum	La Roche-Posay *(France)*
Clear & Defend+ 4% Niacinamide + Panthenol	Neutrogena *(USA)*
Niacinamide 24 + Vitamin E Eye Cream	Olay *(USA)*
2% Niacinamide + Kale Detox Ampoule Sheet Mask	Garnier *(France)*

5.3.2. Loading of ascorbyl glucoside and niacinamide in Sit:LGC nanovesicles by DELOS process

The aim of this study was to fulfill a proof of concept to evaluate the formulation of both vitamins, AG and NCA, in Sit:LGC NVs, loading them and providing an added value to the payloads through the NVs. The concentration of payload used in both cases was 1.25 mg/mL, that corresponded to a 20% (w/w) in relation to the nanovesicle membrane components.

The NVs formulations were produced by DELOS methodology using the bench scale equipment (see **Section 8.2.1**). AG and NCA, as they are hydrophilic molecules, were

dissolved in the aqueous phase (water) with LGC (**Figure 5.8**). Both formulations were produced using the same dispersant media (water/EtOH 15% (v/v)) and a concentration of membrane components of 5 mg/mL.

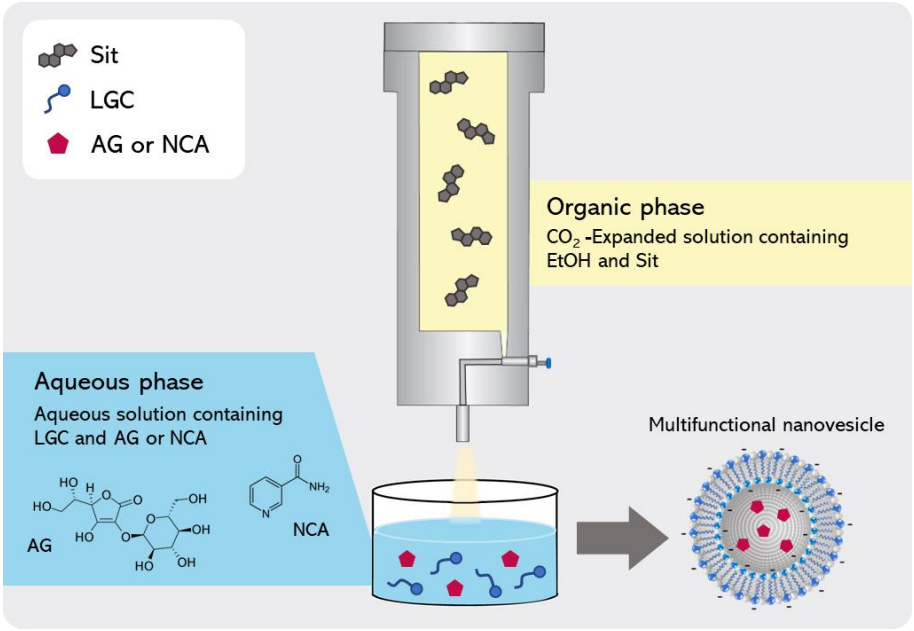


Figure 5.8. Schematic representation of the DELOS methodology used for the preparation of nanovesicles composed of Sit:LGC (1:1) loaded with ascorbyl glucoside (AG) or niacinamide (NCA) at 1.25 mg/mL, as described in **Section 5.3.**

The two formulations were characterized by DLS, ELS and cryo-TEM as explained in **Sections 8.3.1** and **8.3.2**.

Table 5.5 and **Figure 5.9** represent the physicochemical results obtained for each formulation, AG and NCA-loaded systems. In both cases homogeneous opalescent and whitish formulations were obtained.

In terms of physicochemical properties, the dispersions presented acceptable parameters, with a particle size around 180 nm in both cases and a PDI below 0.3, meaning that the population of vesicles was homogeneous. Regarding the ζ-Pot, as expected in both cases the obtained value was negative, since the surfactant used, LGC, is negatively charged. Still, a slight difference was observed in the case of AG-loaded NVs, which had a lower value of ζ-Pot (-40 mV) in comparison with blank NVs (-70 mV as reported in **Chapter 3**), or even NCA-loaded NVs (-55 mV) which had an intermediate value between blank and AG-loaded nanovesicular systems. This decrease on ζ-Pot could suggest an interaction between the

payload and the surface of the NVs, affecting the measured surface charge of the NVs. However, this possible interaction was not highly correlated with the EE values obtained.

The EE was estimated by UV-vis spectrophotometry as explained in **Section 8.3.5.4**. In this specific case, the EE values were calculated indirectly, i.e., by measuring the concentration of the free non-integrated compound, and comparing it with the initial theoretical value. For AG-loaded NVs formulations, which presented the highest decrease on ζ-Pot, the EE was relatively low (EE = 7.7%). For NCA-loaded nanovesicles, the EE was slightly higher, around 20%. Nonetheless, it was obvious that in comparison with previous payloads such as the lipophilic small molecules TCP and 7-DHC, or the protein bFGF, these hydrophilic small molecules were not as efficiently loaded as the other tested cargos.

Table 5.5. Physicochemical characterization of nanovesicle formulations loaded with the hydrophilic small molecules AG and NCA, typical cosmetic ingredients (n = 1).

Sit:LGC[a)] NVs (1:1 molar ratio)				
Payload	**Hydrodynamic diameter mean [nm]**	**Size PDI**	**Apparent ζ-Pot [mV]**	**EE [%]**
AG	178 ± 6	0.19 ± 0.03	-40 ± 4	7.7
NCA	188 ± 2	0.25 ± 0.04	-55 ± 3	19.6

The error in DLS and ELS values correspond to the standard deviation of the triplicate measurements performed for each sample.

a) LGC reagent used was a mixture of APGs, intended as alkyl glucosides of C10-16 chain length, and the corresponding carboxylates; thus, the ratio 1:1 refers to the mixture and not the real content of LGC.

With respect to the morphology of the NVs obtained, both AG and NCA-loaded NVs presented mainly unilamellar vesicles with no significant changes in the overall morphology of the nanovesicular formulation compared to the blank systems (**Figure 5.9B)**.

Finally, the vitamin-loaded nanoformulations were stable for up to 12 months in terms of particle size and size PDI, presenting similar colloidal stability values than those of blank NVs. This could indicate that the presence of the vitamin payloads did not affect the stability of NVs.

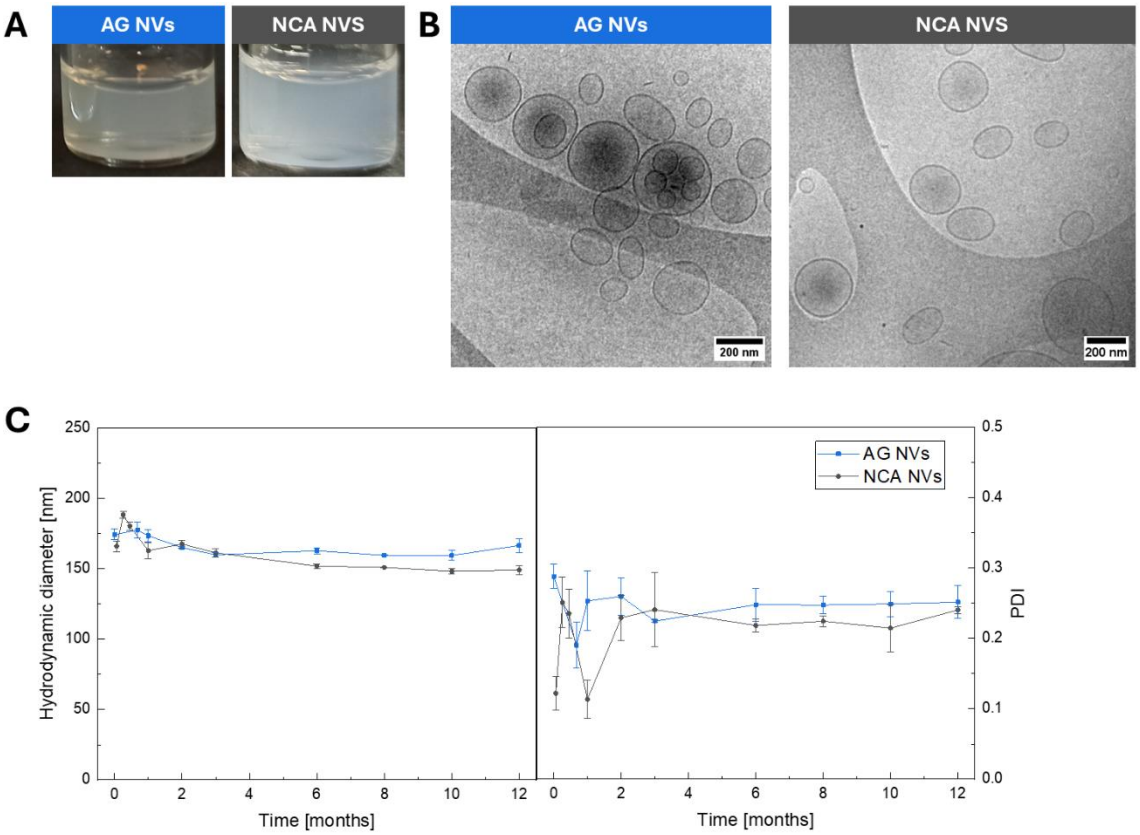


Figure 5.9. **(A)** Macroscopical appearance of AG and NCA-loaded NVs (Sit:LGC, molar ratio 1:1) one week after production. **(B)** Representative cryo-TEM image of AG NVs and NCA NVs. **(C)** Stability over time in terms of particle size and size PDI (n = 1).

5.3.3. Summary of the Section and future perspectives on the nanoformulation of hydrophilic small molecules

This first proof of concept performed to load two different hydrophilic small molecules, the vitamin C derivative ascorbyl glucoside, and vitamin B_3, niacinamide, in the plant-based delivery platform, showed the capacity to obtain stable and homogeneous nanovesicular systems in terms of physicochemical properties. Despite this, in terms of entrapment efficiency the results, obtaining values below 20%, could be improved and were lower than for the other types of payloads tested in the previous studies, and with EE between 50 – 90%.

These results, however, are in accordance with bibliography. It is well known that hydrophilic payloads usually are encapsulated with lower efficiency values as a consequence of the large volume of dispersant aqueous media in comparison to the volume of the vesicle aqueous lumen[23]. When the payloads can interact with the nanovesicular membranes, for example by electrostatic interaction like in the case of bFGF, these EE values

can be higher. For these reasons, there are different strategies to increase EE of small hydrophilic molecules, such as passive methods changing membrane composition or surface charge, and active methods to load the molecules through transmembrane transportation inside the aqueous lumen.

As future perspectives, it is important to highlight that the results here presented were a preliminary proof of concept, meaning that further replicates to deeply understand the behavior of these formulations are needed. The strategies above mentioned to increase EE could be explored to investigate if certain parameters of the formulations and/or the manufacturing process could impact the EE of these small hydrophilic molecules in the nanovesicular system.

Even the low entrapment efficiency, it is also interesting to note that the formulations obtained were stable in the presence of this type of molecules such as AG and NCA, which can be easily formulated in aqueous media. The formulation of hydrophilic vitamins with vesicles can enable its codelivery with lipophilic molecules loaded inside the bilayers in aqueous formulations whereas the hydrophilic molecules can be dissolved in the aqueous phase. For example, it is reported the benefits and complementarity of vitamin E (tocopherol) and vitamin C codelivery[16,17], a lipophilic vitamin which as reported in **Chapter 3,** could be loaded in the novel Sit/LGL/LGC NVs, and a hydrophilic molecule. They can be difficult to deliver in the same formulation because of their opposite solubility. This new delivery platform could be useful for the codelivery of different molecules of interest for the healthcare industry that are difficult to formulate on the same product due to their difference natures.

5.4. Bibliography

1. E. Elizondo, E. Moreno, I. Cabrera, et al. Liposomes and other vesicular systems: Structural characteristics, methods of preparation, and use in nanomedicine. In *Progress in Molecular Biology and Translational Science*; **2011**; Vol. 104, pp 1–52.
2. D. Hawthorne, A. Pannala, S. Sandeman, A. Lloyd. Sustained and targeted delivery of hydrophilic drug compounds: A review of existing and novel technologies from bench to bedside. *J. Drug Deliv. Sci. Technol.* **2022**, 78, 103936.
3. S. Arpicco, L. Battaglia, P. Brusa, et al. Recent studies on the delivery of hydrophilic drugs in nanoparticulate systems. *J. Drug Deliv. Sci. Technol.* **2016**, 32, 298–312.
4. S.N. Murthy. Approaches for Delivery of Drugs Topically. *AAPS PharmSciTech* **2020**, 21, 1–2.
5. A. Zeb, I. Rana, H.-I. Choi, et al. Potential and Applications of Nanocarriers for Efficient Delivery of Biopharmaceuticals. *Pharmaceutics* **2020**, 12, 1184.
6. B. Leader, Q.J. Baca, D.E. Golan. Protein therapeutics: a summary and pharmacological classification. *Nat. Rev. Drug Discov.* **2008**, 7, 21–39.
7. S.H. Shin, Y.H. Lee, N.K. Rho, K.Y. Park. Skin aging from mechanisms to interventions: focusing on dermal aging. *Front. Physiol.* **2023**, 14, 1195272.
8. G. Büyükköroğlu, B. Şenel, G. Sevim. Biotechnology in cosmetics. In *Biotechnology in Healthcare, Volume 2*; **2022**; pp 273–287.
9. C. Gomes, A.C. Silva, A.C. Marques, J.S. Lobo, M.H. Amaral. Biotechnology applied to cosmetics and aesthetic medicines. *Cosmetics* **2020**, 7, 1–14.
10. R. de Araújo, M. Lôbo, K. Trindade, D.F. Silva, N. Pereira. Fibroblast Growth Factors: A Controlling Mechanism of Skin Aging. *Skin Pharmacol. Physiol.* **2019**, 32, 275–282.
11. L. Ferrer-Tasies, H. Santana, I. Cabrera-Puig, et al. Recombinant Human Epidermal Growth Factor/Quatsome Nanoconjugates: A Robust Topical Delivery System for Complex Wound Healing. *Adv. Ther.* **2021**, 4, 2000260.
12. L. Ballell i Hosa. Translation of DELOS nanovesicle formulations into new pharmaceutical candidates, Universitat Autònoma de Barcelona, **2022**.
13. O. Eskens, S. Amin. Challenges and effective routes for formulating and delivery of epidermal growth factors in skin care. *Int. J. Cosmet. Sci.* **2021**, 43, 123–130.

14. M. Wytrwal, J. Bednar, M. Nowakowska, P. Wydro, M. Kepczynski. Interactions of serum with polyelectrolyte-stabilized liposomes: Cryo-TEM studies. *Colloids Surfaces B Biointerfaces* **2014**, 120, 152–159.

15. M.C. Kouassi, M. Grisel, E. Gore. Multifunctional active ingredient-based delivery systems for skincare formulations: A review. *Colloids Surfaces B Biointerfaces* **2022**, 217, 112676.

16. C.D. Enescu, L.M. Bedford, G. Potts, F. Fahs. A review of topical vitamin C derivatives and their efficacy. *J. Cosmet. Dermatol.* **2022**, 21, 2349–2359.

17. F. Al-Niaimi, N.Y. Zhen Chiang. Topical Vitamin C and the Skin: Mechanisms of Action and Clinical Applications. *J. Clin. Aesthet. Dermatol.* **2017**, 10, 14–17.

18. S. Ravetti, C. Clemente, S. Brignone, et al. Ascorbic Acid in Skin Health. *Cosmetics* **2019**, 6, 58.

19. A.C. Caritá, B. Fonseca-Santos, J.D. Shultz, et al. Vitamin C: One compound, several uses. Advances for delivery, efficiency and stability. *Nanomedicine Nanotechnology, Biol. Med.* **2020**, 24, 102117.

20. R.R. Ong, C.F. Goh. Niacinamide: a review on dermal delivery strategies and clinical evidence. *Drug Deliv. Transl. Res.* **2024**.

21. Y.C. Boo. Mechanistic Basis and Clinical Evidence for the Applications of Nicotinamide (Niacinamide) to Control Skin Aging and Pigmentation. *Antioxidants* **2021**, 10, 1315.

22. W. Gehring. Nicotinic acid/niacinamide and the skin. *J. Cosmet. Dermatol.* **2004**, 3, 88–93.

23. J. Oliveira Eloy, M. Claro De Souza, R. Petrilli, et al. Liposomes as carriers of hydrophilic small molecule drugs: Strategies to enhance encapsulation and delivery. *Colloids Surfaces B Biointerfaces* **2014**, 123, 345–363.

Tuning of alkyl polyglucosides and β-sitosterol nanovesicles for pharmaceutical applications

6

6.1. New horizons for alkyl polyglucosides and β-sitosterol nanovesicles: pharmaceutical applications

In the previous **Chapters**, the development of a novel delivery platform composed of β-sitosterol and alkyl polyglucosides has been focused on their potential application in personal care and cosmetic formulations for topical administration. Nonetheless, after proving the capacity of the plant-based vesicles to load different types of active molecules, generating novel dermocosmetic ingredients, it was also interesting to evaluate their versatility to be employed for pharmaceutical use, taking into account other possible administration routes and delivery of active pharmaceutical ingredients. Thus, to increase the applicability of the Sit/APG nanovesicles we explored the tailoring of the colloidal platform to pharmaceutical applications.

For this purpose, the first thing to consider was the use of pharma compatible membrane components, therefore pure-grade reagents were selected as membrane components. Then, the aim was to stabilize the nanovesicles composed of Sit and pure-grade LGL. As reported in **Chapter 3**, the use of pure-grade LGL with Sit yielded heterogeneous and unstable

vesicular systems with the need to heat the aqueous phase to 60 °C during production process. Thus, additives that are approved for pharmaceutical use but not for cosmetic applications were explored. Specifically, two cholesterol derivatives with different properties were employed (**Figure 6.1**). First, cholesterol-(polyethylene glycol-600) (Chol-PEG_{600}), a PEG moiety of 600 Da covalently bound to a cholesterol molecule, where PEG moiety is expected to provide steric hindrance and increase colloidal stability. On the second place, DC-cholesterol (DC-chol) was also evaluated. DC-cholesterol is an ionizable cationic cholesterol derivative which was selected to provide positive charge to the nanovesicle bilayer, increasing colloidal stability by charge repulsion.

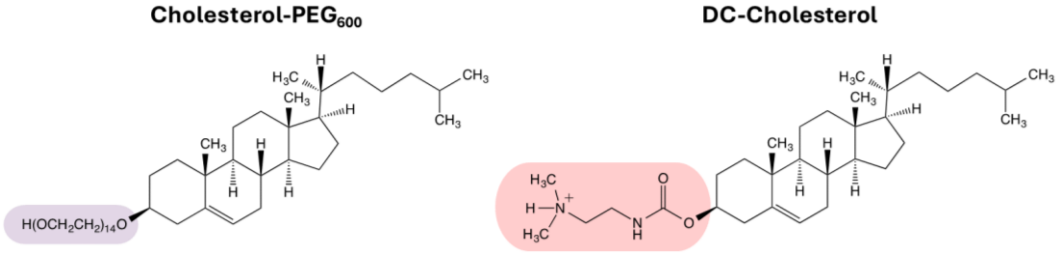


Figure 6.1. Molecular structure of cholesterol-PEG_{600} and DC-cholesterol.

*This **Chapter** is focused on the development of Sit/LGL vesicular systems using sterol-based additives accepted for pharmaceutical applications (**Figure 3.1**). In particular, cholesterol-PEG_{600} and DC-cholesterol were selected to combine with Sit and LGL (pure-grade) membrane components and to provide novel properties to the surface of the nanovesicles, such as steric hindrance for colloidal stabilization and pH-sensitive systems with cationic surface charge, not studied yet with these delivery systems, and with the final aim of obtaining a versatile delivery platform.*

The different vesicular systems obtained were deeply characterized in terms of size, stability and morphology. Furthermore, the loading capacity of Sit/LGL/DC-chol vesicles was tested with three different types of active molecules: cannabidiol, a hydrophobic small molecule to treat seizures; methotrexate, an anticancer hydrophilic small molecule; and the human growth hormone, a protein used for growth disorder treatments.

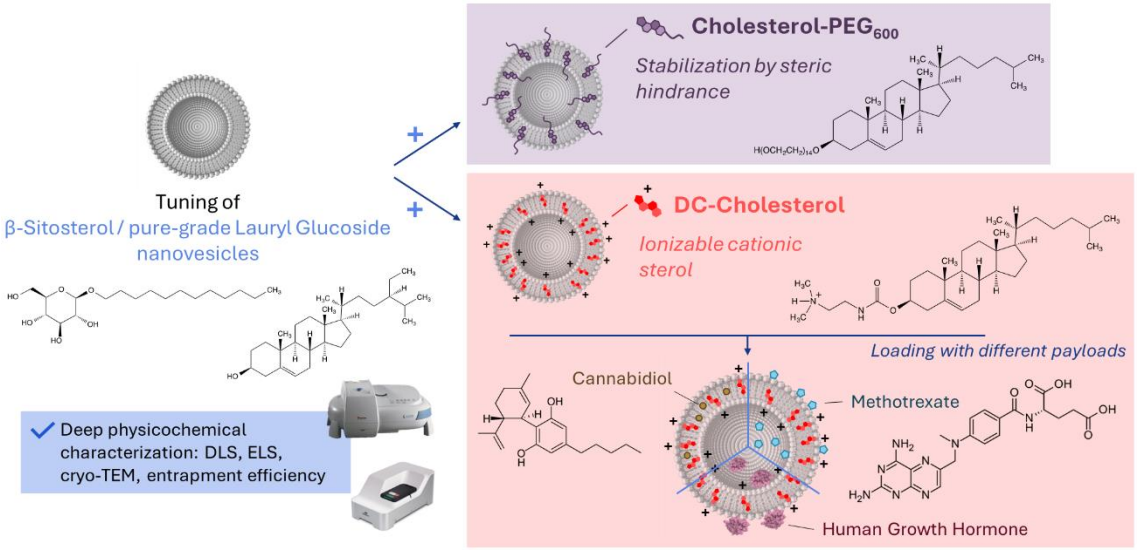


Figure 6.2. Graphical summary of the work presented in **Chapter 6** to develop novel Sit/APG nanovesicle formulations including cholesterol-PEG_{600} (chol-PEG_{600}) or DC-cholesterol (DC-chol) as membrane components for pharmaceutical applications.

6.2. Synthesis of Sit/LGL nanovesicles stabilized with cholesterol-PEG_{600}

6.2.1. Cholesterol-PEG_{600} as building block

Polyethylene glycol (PEG) is a non-ionic polymer extensively used in chemical, food and medical applications. Its molecular structure consists on repetitions of ethylene oxide units ($HO\text{-}[CH_2\text{-}CH_2\text{-}O]_n\text{-}H$) where *n* determines the molecular weight of the PEG molecule used (**Figure 6.3**)[1,2].

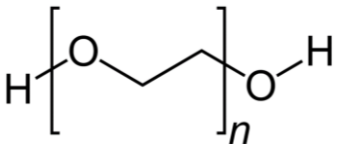


Figure 6.3. Molecular structure of polyethylene glycol (PEG).

PEG possesses different properties that have made it the most widely used polymer in the drug delivery field. It is soluble in aqueous and organic media (e.g., ethanol, acetonitrile or dichloromethane)[3], biocompatible, biodegradable, non-toxic and, until very recently, it was also thought to be non-immunogenic[1]. PEG was classified as a GRAS ingredient by the FDA in 1973[4], and it has been widely used as excipient in already approved nanomedicines such as the well-known chemotherapy medication Doxil®, the first FDA-approved drug based on

liposomes[1,5]. However, after COVID-19 pandemic, it was suspected that the PEGylated lipids used in mRNA COVID-19 vaccines, as stabilizer reducing the aggregation of the lipid nanoparticles entrapping the nucleic acids and the non-specific uptake by immune cells[6], could be causing allergies due to a hypersensitivity to this molecule[4,7]. For this reason, nowadays alternative polymers to substitute PEG in different food, cosmetic and pharmaceutical formulations are being investigated[8].

Besides these evidences, PEG is still the *gold standard* of stealth polymers due to the multiple properties that confer to nanoparticles. PEG can enhance drug encapsulation and its release behavior, avoids non-specific adsorption of plasma proteins and delays the clearance by the mononuclear phagocyte system, both increasing the circulation lifetime of nanoparticles in blood and improving the efficacy of nanoformulations[3,9]. Additionally, due to its structure with chemically active hydroxyl groups at both ends, it is easy to conjugate with functional groups that enhance active targeting and cellular internalization through the incorporation of targeting moieties [9].

Yet, the most interesting property of PEG in relation to this Thesis project, was its ability to increase colloidal stability of nanoparticles. The presence of PEG on the surface of nanoparticles increases the colloidal stability through steric repulsion between PEG molecules of different particles[9,10]. Due to the low stability of the NVs obtained with Sit and pure-grade LGL, reported in **Chapter 3**, it was interesting to evaluate the effect of a PEG-derivative to stabilize this nanovesicular formulation. Previously, in **Chapter 3,** anionic surfactants were used to increase the stability of Sit:LGL nanovesicles. Here, in this **Section,** the effect of steric repulsion to improve colloidal stability is evaluated.

There are different strategies to PEGylate nanoparticles. For example, PEG can be added by physical adsorption by electrostatic or hydrophobic interactions with the surface of the particle[11,12], or by chemical conjugation forming a covalent bond with an exposed reactive group on the surface of the nanoparticle[13,14]. In this study, the addition of PEG to the nanovesicles was done by a third pathway: self-assembly of a PEG conjugate with a hydrophobic moiety, specifically cholesterol (although there are other hydrophobic polymers or lipids that could be also employed instead).

In particular, a cholesterol molecule covalently bound to a PEG molecule of 600 Da, i.e., cholesterol-PEG_{600} (**Figure 6.1**), was used to investigate the possibility of stabilizing the Sit/ pure-LGL nanovesicles. This strategy has been already used in Nanomol group for the formulation of liposomes[15] and *quatsomes*[16]. It is known that PEG's molecular weight and its density are key factors that will directly affect the physicochemical properties and stability

of the nanovesicles and its biological performance[9]. For these reasons, previous results obtained in Nanomol's group were taken as reference.

Regarding PEG's molecular weight, molecules from 200 to 1000 Da have been previously evaluated, seeing that these different PEG lengths could affect the physicochemical properties of the vesicles obtained, like lamellarity when using high molecular weight PEG (1000 Da)[16], or their biological performance when using the lowest molecular weight PEG (200 Da)[15].

On regards of PEG density, i.e., the percentage of cholesterol-PEG in relation to the total membrane components of the vesicular systems, previously amounts from 3 mol % to 21 mol % have been used. The highest proportion of 21% has been demonstrated to negatively affect the stability of nanovesicles and, consequently, it was discarded. The most outstanding percentages previously stablished were between 3 and 7%[15,16].

Therefore, to stabilize the Sit:LGL nanovesicles by adding a cholesterol-PEG to the formulation, an intermediate PEG molecular weight of 600 Da and a 3 mol % density were selected. This 3 mol % density was equivalent to 7.4 % (w/w) in relation to the total membrane components.

From this point on in this **Chapter**, LGL will refer to pure-grade LGL.

6.2.2. Synthesis and stabilization of Sit:LGL nanovesicles using chol-PEG$_{600}$

For the purpose of evaluating the self-assembly of Sit:LGL nanovesicles with 7.4 % (w/w) of chol-PEG$_{600}$, the formulation was produced by the DELOS single-step procedure using the bench scale equipment, as described in **Section 8.2.1**.

With the objective to maintain the molar ratio of sterol to surfactant molecules to a 1:1 proportion, the molar ratio between Sit:LGL:Chol-PEG$_{600}$ components was set at 0.94:1:0.06 (see **Table 8.4** of **Section 8.2.1**). To produce the nanovesicles by DELOS methodology, all membrane components Sit, LGL and Chol-PEG$_{600}$ were dissolved in the organic phase (**Figure 6.4**). Finally, to eliminate impurities coming from the starting materials, in this case mainly from Sit, since the pure LGL surfactant was used, the samples were filtered through 0.45 µm PES membrane syringe filters.

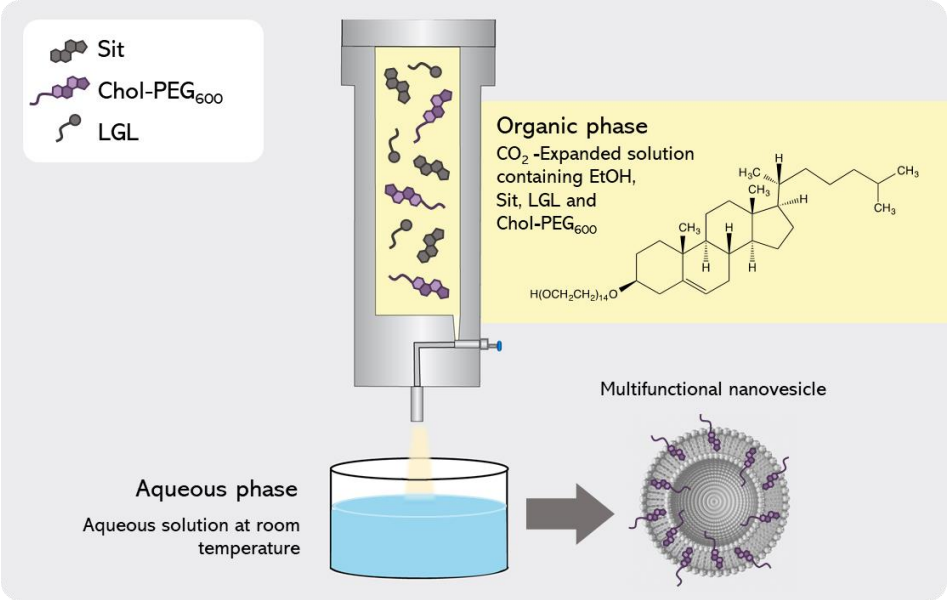


Figure 6.4. Schematic representation of the DELOS methodology used for the preparation of nanovesicles composed of Sit, LGL and Chol-PEG_{600} (molar ratio 0.94:1:0.06) in **Section 6.2.2**.

First of all, it is worth to remind the reader that previously, for the formation of Sit and LGL nanovesicles using the pure-grade surfactant it was necessary to heat the aqueous phase up to 60 °C during DELOS procedure (see **Section 3.2.2** and **Chapter 3**), due to the T_K of LGL.

In this case, when adding cholesterol-PEG_{600} to the Sit:LGL nanoformulation, nanovesicles were successfully obtained at room temperature. Thus, as in the case of stabilization of Sit:LGL NVs using anionic surfactants as additives (also reported in **Chapter 3**), the addition of cholesterol-PEG_{600} to the nanoformulation avoided the heating of the aqueous phase during DELOS process. This factor allowed the possibility to work with thermolabile compounds, i.e., molecules sensitive to high temperatures like proteins.

The nanoformulation obtained presented a homogeneous macroscopical appearance with a whitish color (**Figure 6.5A**). It was characterized by DLS to study the mean hydrodynamic diameter and size PDI, by ELS to evaluate the apparent ζ-Pot, and by cryo-TEM to obtain an individual inspection of the morphology of each sample at the nanoscale (see **Sections 8.3.1** and **8.3.2**).

Table 6.1 reports the DLS and ELS results obtained for the Sit:LGL:Chol-PEG_{600} NVs. The values obtained for the hydrodynamic diameter and size PDI were comparable to those obtained with Sit:LGL NVs stabilized with negatively-charged surfactants (particle size between 160-190 nm and a size PDI around 0.2). In contrast, ζ-Pot values were rather different. In the case of the NVs stabilized with anionic molecules, as expected, ζ-Pot values

were negative, between -40 and -50 mV. However, in the case of Sit:LGL:Chol-PEG_{600} NVs, as PEG is a non-ionic polymer surrounding the surface of the vesicle, the apparent ζ-Pot turned to a neutral value around 2 mV. In this case, the stability of the colloidal system was given by the steric hindrance of the PEG instead of the electrostatic repulsion of the NVs. Thus, for these NVs a neutral ζ-Pot was not indicating colloidal instability.

Table 6.1. Composition and physicochemical characterization of Sit:LGL:Chol-PEG_{600} nanovesicle formulations prepared in **Section 6.2.2** (n = 3).

Membrane components	Molar ratio	Hydrodynamic diameter mean [nm]	Size PDI	Apparent ζ-Pot [mV]	Stability [months]
Sit:LGL:Chol-PEG_{600}	0.94:1:0.06	131 ± 5	0.18 ± 0.05	2 ± 6	6

In relation to vesicular morphology, representative cryo-TEM images are shown in **Figure 6.5B**. Mainly spherical multilamellar nanovesicles were observed in the images, although it was difficult to determine by cryo-TEM in a quantitative way if there were more multilamellar structures present than with other membrane additives used.

Finally, concerning the stability, it is reported in **Figure 6.5C**. As it is shown in the graphics, the stability was of less than 6 months, which was lower than for the NVs stabilized with anionic surfactants (> 12 months). It is worthy to highlight that after 2 months, there was a slight increase on both, particle size and PDI, that was maintained until the 6 months timepoint (highlighted in yellow in the graph). However, after 6 months a progressive increase on both parameters (highlighted in red in the graph) was observed indicating that the formulation was not stable after these 6 months.

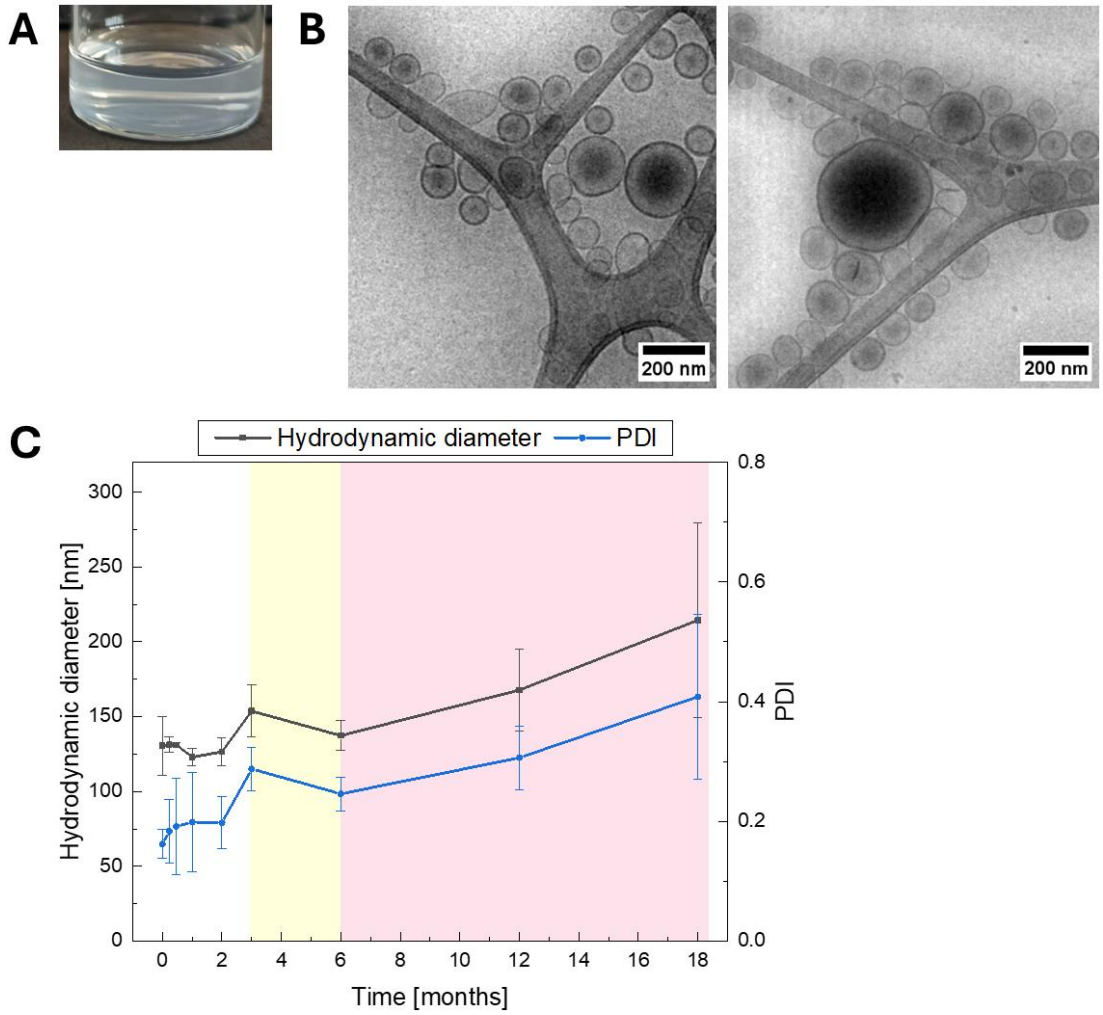


Figure 6.5. **(A)** Macroscopical appearance of Sit:LGL:Chol-PEG$_{600}$ NVs (molar ratio 0.94:1:0.06) one week after production. **(B)** Representative cryo-TEM image of Sit:LGL:Chol-PEG$_{600}$ NVs after 10 days of production. **(C)** Stability over time in terms of particle size and size PDI (n = 3).

6.2.3. Summary of the Section and future perspectives

This **Section 6.2** presented the possibility of formulating stable nanovesicles composed of Sit, pure LGL and chol-PEG$_{600}$ (molar ratio 0.94:1:0.06) by the single-step DELOS methodology at room temperature. Homogenous nanovesicles of 130 nm and a PDI of 0.2 were obtained with a stability around 6 months, which is an important improvement with regards of Sit:LGL NVs (1:1) that were stable for less than 1 month. The morphology of the nanovesicles obtained, spherical vesicles which could be uni or multilamellar and were studied by cryo-TEM, was similar to the samples of Sit:LGL NVs stabilized previously with anionic surfactants and reported in **Chapter 3**.

After this first evaluation, it was clear that cholesterol-PEG_{600} could be incorporated by self-assembly in Sit:LGL nanovesicles, although there is further work to be done. For example, other PEG lengths and densities could be evaluated because, as reported in previous works, they could have an impact on both, physicochemical properties and also biological performance.

6.3. Synthesis of pH-sensitive Sit/LGL nanovesicles with DC-cholesterol

6.3.1. DC-Cholesterol as building block

The research in the last years has proved that cationic nanoparticles are internalized inside cells more efficiently, an important feature for drug delivery. Although the exact mechanism is not yet described and could be different depending on the type of nanoparticle, it is thought that the positive charges at the surface of the nanoparticles are a key factor in this improvement of cell internalization. These positive charges would enhance the adsorption on the cell membrane that is in most of the cases negatively charged, by endocytosis-like mechanisms[17,18].

The advantage that seems to confer the positive charge for the internalization of nanoparticles has been highly exploited during the last years for the specific intracellular delivery of nucleic acids, either for gene therapy or RNA therapeutics such as mRNA vaccines[19,20]. Besides, this strategy has been also used for the delivery of proteins[21,22] or antigens[23,24].

In the field of vesicular systems, cationic lipids are used to confer positive charge to the vesicles' surface. Cationic lipids are composed of a positively charged headgroup, e.g., tertiary or quaternary ammonium groups or polyamines, and a hydrophobic domain, e.g., alkyl chains or a cholesterol molecule[17,20]. Several phospholipid derivatives have been synthesized and commercialized, like DOTAP (1,2-dioleoyl-3-trimethylammonium propane) or DOEPC (1,2-dioleoyl-sn-glycero-3-ethylphosphocholine). In the case of cholesterol derivatives, DC-cholesterol is one of the most used ionizable cationic sterols.

DC-Cholesterol (3β-[N-(N′,N′-dimethylaminoethane)-carbamoyl] cholesterol) (DC-chol) is a pH-sensitive derivative of cholesterol with a tertiary amine (**Figure 6.1**). Its pH-dependent behavior is interesting for intracellular delivery when loading active molecules by electrostatic interaction, like in the case of nucleic acids. At neutral pH and below, the lipid

is positively charged (pKa ≈ 7.8[25]), and the cationic nanovesicles containing it can interact with the cell membranes, being internalized by the endocytic pathway. Afterwards, the cationic vesicles in the acidic pH environment of the endosomes can interact with the anionic membrane of endosome, boosting the release of the payload[26].

This ionizable sterol has already been used to formulate different types of vesicles, such as liposomes for nucleic acids delivery combining phospholipids with DC-chol[26,27], but also with other types of non-liposomal vesicles, for example to obtain pH-sensitive *quatsomes* composed of DC-chol and quaternary ammonium surfactants with DELOS technology for miRNA therapeutics[28].

In this study, DC-chol was evaluated as membrane component to stabilize the nanovesicles of Sit:LGL by electrostatic repulsion, in order to confer a net positive charge to the colloidal system. As described in the following sections, the plant-based neutral sterol (Sit) was progressively replaced by the cationic sterol DC-chol to obtain a variety of stable nanovesicles. Finally, different payloads were tested to evaluate the loading capacity of these novel formulations of Sit:LGL:DC-Chol: two small molecules, cannabidiol as hydrophobic molecule and methotrexate as hydrophilic drug, and a larger biomolecule which was the protein human growth hormone.

6.3.2. Synthesis and stabilization of Sit:LGL nanovesicles by adding 3% of the cationic lipid DC-chol

As a first approach, following the same strategy than in **Chapter 3** with the stabilization of Sit:LGL NVs with anionic surfactants, a 3% (w/w) of DC-chol was added to the formulation. The addition of this amount of DC-chol set the following molar ratio between the nanovesicle membrane components (Sit:LGL:DC-chol) = (1:1:0.05).

These Sit:LGL:DC-chol NVs (1:1:0.05) were produced by the DELOS single-step procedure using the bench scale equipment (see **Section 8.2.1**). In this case, all the membrane components, Sit, LGL and DC-chol were dissolved in the organic phase (**Figure 6.6**). Finally, to eliminate impurities coming from the starting materials, in this case mainly from Sit, the samples were filtered with 0.45 µm pore size PES membrane syringe filters. Then, the samples obtained were characterized by DLS, ELS and cryo-TEM (see **Sections 8.3.1** and **8.3.2**).

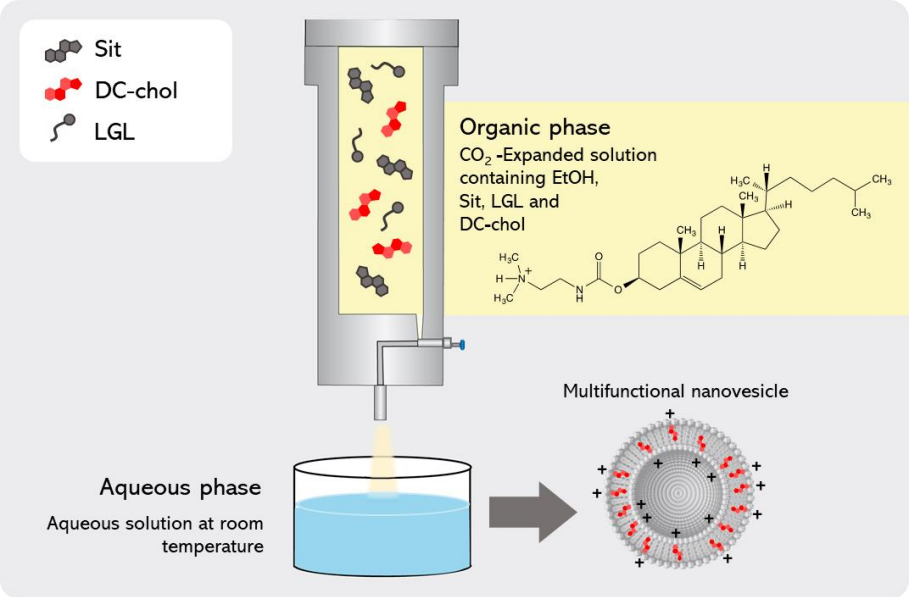


Figure 6.6. Schematic representation of the DELOS methodology used for the preparation of pH-sensitive nanovesicles composed of Sit, LGL and DC-chol at different molar ratios in **Section 6.3.**

The incorporation of just a 3% (w/w) of DC-chol to the Sit:LGL system allowed to obtain a stable and homogeneous formulation at room temperature, without the need of high temperatures during vesicle formation (**Figure 6.7A**). As reported in **Table 3.4**, the nanovesicles obtained had a size around 100 nm and a size PDI of 0.16. The ζ-Pot value, proving the incorporation of the cationic lipid, turned positive (around 64 mV), in comparison to all the other formulations obtained in this Thesis. Finally, as expected, pH of the dispersion was below the pKa of DC-chol, meaning that the molecule was protonated.

Table 6.2. Composition and physicochemical characterization of the nanovesicle formulation obtained when adding DC-Chol to stabilize Sit:LGL nanovesicles, prepared in **Section 6.3.2** (n = 3).

Sit:LGL:DC-chol		Hydrodynamic diameter mean [nm]	Size PDI	Apparent ζ-Pot [mV]	pH	Stability [months]
Molar ratio	Concentration[a] [mg/mL]					
1:1:0.05	2.76	100 ± 11	0.16 ± 0.05	64 ± 3	7.2 ± 0.3	12

[a] *Theoretical concentration.*

Regarding the morphology of the vesicles, studied by cryo-TEM (**Figure 6.7B**), the presence of unilamellar and multilamellar NVs was seen, as in previous samples of Sit:LGL systems with other additives. Some of the vesicles were found to have oval form instead of spherical,

most of them unilamellar vesicles, which could be due to the integration of DC-chol to the nanovesicular membrane.

The resulting positively charged NVs showed a high stability of up to 12 months (**Figure 6.7C**) as expected due to the addition of a cationic molecule to the bilayer. In comparison to the other cholesterol derivative used, chol-PEG_{600}, which had a stability of 6 months, DC-chol addition increased the stability of the nanovesicles.

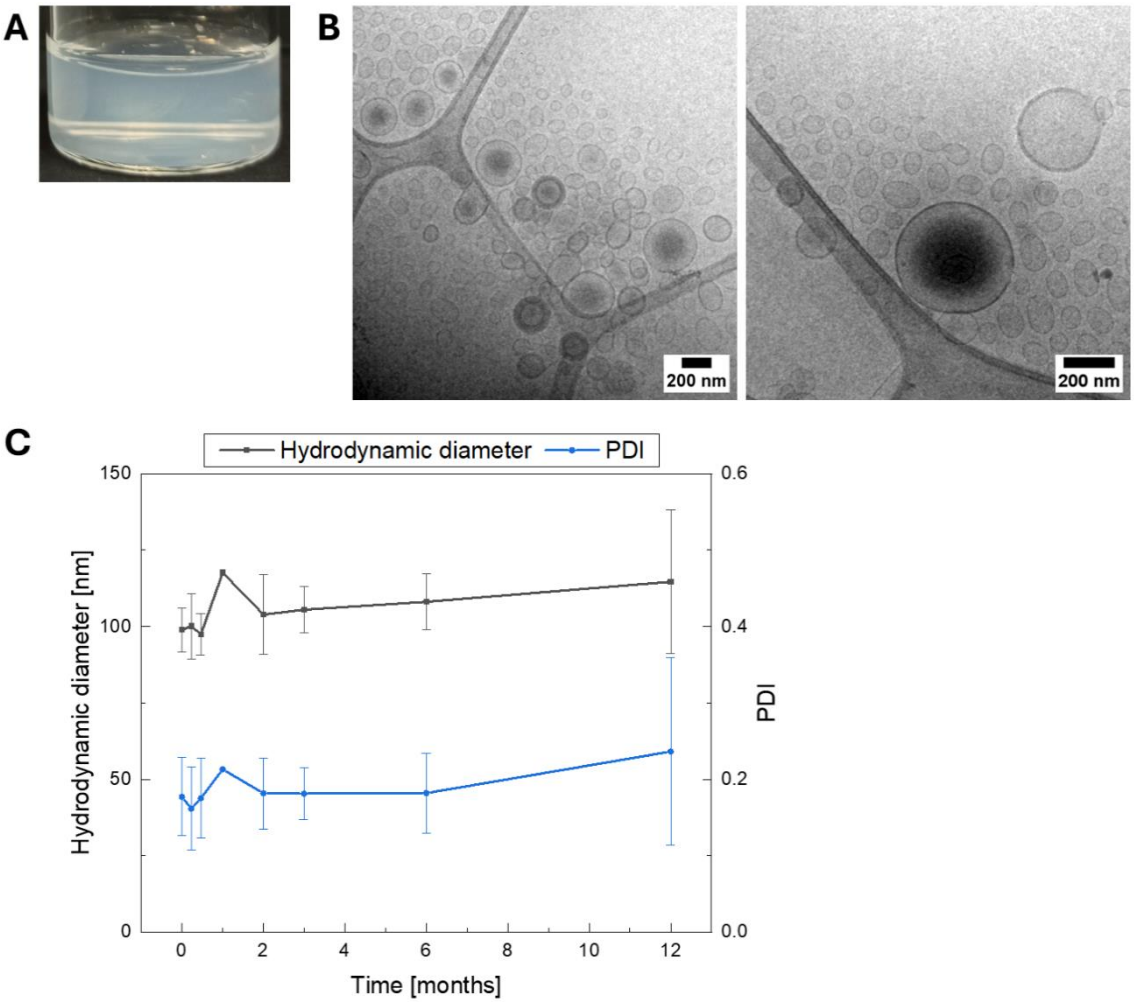


Figure 6.7. **(A)** Macroscopical appearance of the Sit:LGL:DC-chol NVs (molar ratio 1:1:0.5) one week after production. **(B)** Representative cryo-TEM image of Sit:LGL:DC-chol NVs after 10 days of production. **(C)** Stability over time in terms of particle size and size PDI (n = 3).

These results show the versatility of the new sugar-based NVs platform to form either positively or negatively charged vesicular systems by adding a cationic sterol (DC-chol) or an anionic surfactant (LGC, reported in the previous chapters) respectively. This versatility in the desired surface charge could help to load a large variety of active modalities, besides

allowing to explore the tuning of their interactions with biological tissues, thus expanding the potential applications resulting from this delivery platform.

6.3.3. Screening and replacement of the neutral lipid Sit by the ionizable lipid DC-chol

The versatility of the cationic version of the NVs was further explored by screening nanovesicle formation with different amounts of the ionizable sterol until the complete replacement of Sit by DC-chol. The same strategy explained in **Section 3.3.2** of **Chapter 3** was followed, where the non-ionic LGL was progressively replaced by the anionic surfactant LGC. A serial replacement modifying the molar ratio Sit:DC-chol was performed, testing different intermediate values until the molar ratio Sit:DC-chol (0:1) was tested.

The different nanoformulations were produced by DELOS process (**Figure 6.6**), filtered and characterized as in **Section 6.3.2**.

Table 6.3. Composition and physicochemical characterization after 2 months of production of nanovesicle formulations prepared in **Section 6.3.3** (n = 3), replacing progressively the Sit with the cationic Dc-Chol. All the formulations were prepared at a membrane component's theoretical concentration of 2.76 mg/mL.

Molar ratio (Sit:LGL:DC-chol)	Hydrodynamic diameter mean [nm]	Size PDI	Apparent ζ-Pot [mV]	pH	Stability [months]
0.8:1:0.2	97 ± 5	0.11 ± 0.02	72 ± 15	7.4 ± 0.2	> 12
0.5:1:0.5	73 ± 8	0.11 ± 0.03	88 ± 13	7.4 ± 0.2	> 12
0.2:1:0.8	64 ± 10	0.13 ± 0.02	72 ± 18	7.5 ± 0.1	> 12
0:1:1	72 ± 14	0.18 ± 0.03	88 ± 13	7.5 ± 0.1	> 12

As demonstrated in **Table 3.5** and **Figure 6.8B**, a complete replacement of Sit by DC-chol was achieved, obtaining 4 stable and homogeneous nanovesicle formulations.

Macroscopically, some differences between formulations were obsereved (**Figure 6.8B**). The increasing proportion of DC-chol turned the samples more translucent, being the sample with higher amount of DC-Chol, fully replacing the Sit, the most translucent and less whitish.

It is important to highlight that, in comparison with the other systems evaluated in this Thesis, the nanovesicular systems containing DC-chol seemed to need a longer stabilization time, i.e., the time needed to reach a stable value of particle size and size PDI. For all other systems evaluated, after 7 days of production the physicochemical properties were

generally stable. In contrast, with DC-chol NVs, there was a different tendency observed, the particle size tended to increase until the two months timepoint (**Figure 6.8E**). From that point on, the particle size remained stable up to 12 months. In relation to size, it can be also highlighted that all formulations with DC-chol presented lower particle size values in comparison to the different formulations evaluated in this Thesis, all near or below 100 nm. In the case of size PDI, as expected the behavior was the opposite, it decreased with time until reaching the 2 months when it was stabilized. The decrease and stabilization of PDI indicated also that the system stabilized over time. These tendencies were more noticeable with higher proportions of DC-chol, being the sample with higher amount of DC-chol the one with an increased change in particle size and PDI over the first 2 months. For this reason, the representative values presented in **Table 3.5** were the ones measured at the 2 months after production.

By comparing the results with the different molar ratios tested, the greatest decrease in the hydrodynamic diameter was observed between Sit:DC-chol molar ratios of 0.8:0.2 and 0.5:0.5, then increasing the amount of DC-chol did not affect the particle size (**Figure 6.1D**). In terms of size PDI and ζ-Pot, no significant changes were observed between the systems containing increasing amounts of DC-chol.

In relation to pH values, as expected, they were also below the pKa of DC-chol, meaning that in all cases the molecule was protonated.

In relation to vesicles' morphology, the NVs prepared with full replacement of Sit by DC-chol (Sit:DC-chol = 0:1) were evaluated by cryo-TEM (**Figure 6.8C**). In this case, a homogeneous population of small unilamellar vesicles was observed. Similarly to the NVs of Sit:LGC containing just a negatively-charged surfactant, which also were mainly unilamellar as demonstrated in **Chapter 3** by cryo-TEM and SAXS, the NVs containing just the ionizable cationic lipid DC-chol were also mainly unilamellar vesicles. This fact reflects the role of charged molecules on the structuration of the nanovesicles and their lamellarity.

To conclude, stable and homogeneous cationic nanovesicles, based on pure LGL surfactant, containing increasing proportions of the ionizable lipid DC-Chol, were achieved. Furthermore, the use of DC-chol in any of the molar ratios tested increased the stability of Sit:LGL NVs from less than 1 month, as reported in **Chapter 3**, to more than 12.

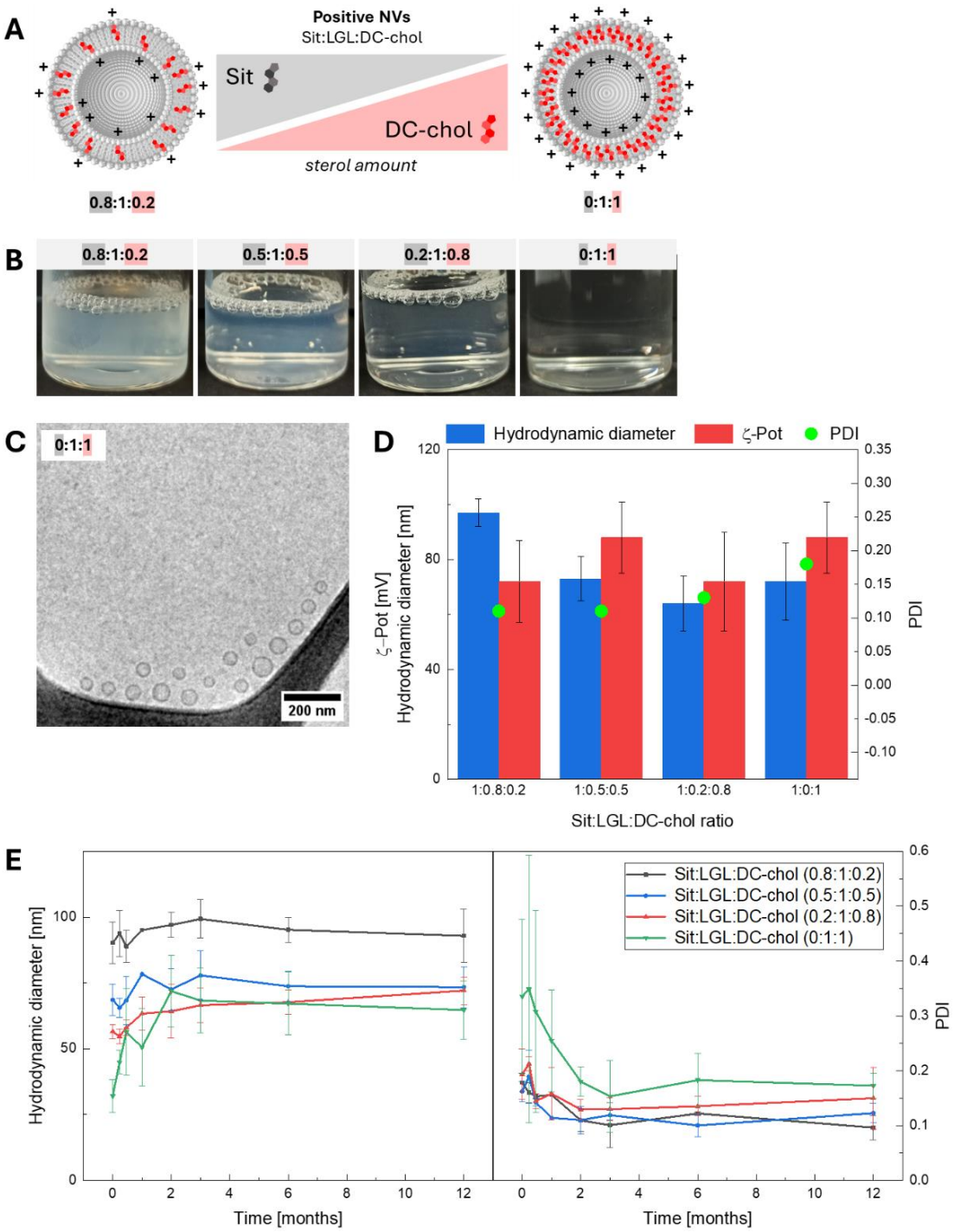


Figure 6.8. **(A)** Schematic representation of nanovesicles and the screening performed replacing Sit by DC-chol in Sit/LGL/DC-chol nanovesicles. **(B)** Macroscopical appearance of Sit/LGL/DC-chol NVs (Sit:DC-chol molar ratio 0.8:0.2 to 0:1) 1 week after production. **(C)** Representative cryo-TEM image of Sit:LGL:DC-chol NVs (molar ratio 0:1:1). **(D)** Physicochemical characterization of positively charged Sit:LGL:DC-chol NVs in terms of hydrodynamic diameter, size PDI and apparent ζ-Pot of three independent replicates. **(E)** Stability over time in terms of particle size and size PDI (n = 3).

6.4. Loading of payloads in the cationic Sit:LGL:DC-chol nanovesicles by DELOS process

With the objective of evaluating the versatility of these Sit:LGL:DC-chol nanovesicle formulations for medical applications, it was of special interest to evaluate the integration of active payloads with different physicochemical properties. For these, two different small molecules were selected: cannabidiol (CBD) as a lipophilic drug that could be potentially loaded inside the vesicular bilayer; and methotrexate (MTX), a well-known chemotherapy agent which is hydrophilic and ionizable, to load it through a possible electrostatic interaction with the cationic bilayer. As a third active ingredient, a larger biomolecule was selected, the human growth hormone (HGH), which is a protein that acts as a growth factor and at the working pH (pH= 7.4) is negatively charged.

In all cases, the vesicular system selected to integrate the active molecules was the same, i.e., nanovesicles composed of Sit:LGL:DC-chol (molar ratio 0.8:1:0.2) at a concentration of 2.82 mg/mL. The formulations were produced by DELOS process as schematized in **Figure 6.9**. CBD, as it is lipophilic, was dissolved in the organic phase, while MTX and HGH were dissolved in the aqueous phase because of their hydrophilic nature.

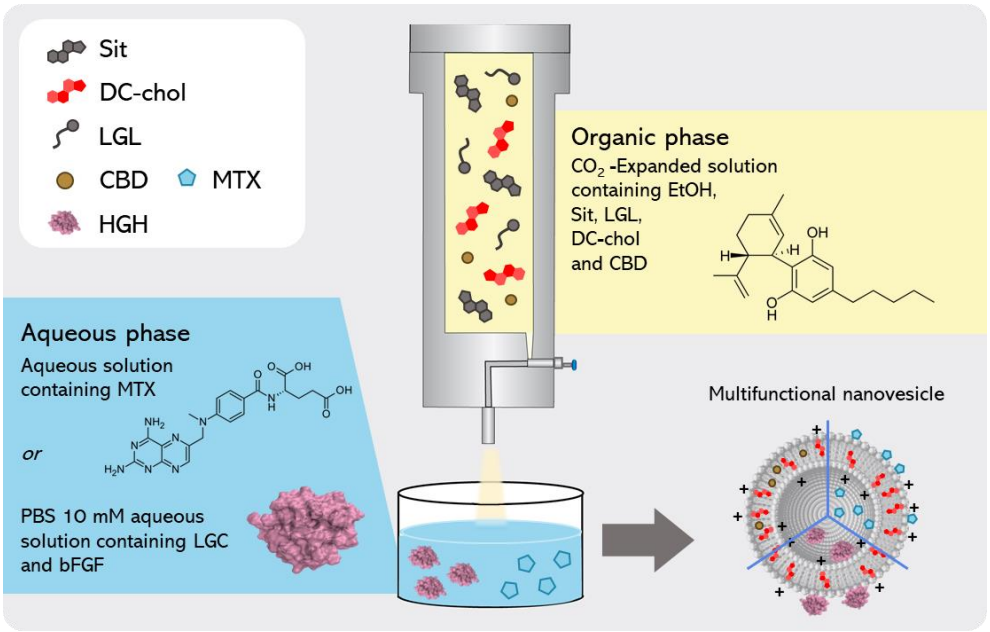


Figure 6.9. Schematic representation of the DELOS methodology used for the preparation of cationic nanovesicles composed of Sit, LGL and DC-chol (0.8:1:0.2) with different payloads: CBD 0.7 mg/mL, MTX 0.26 mg/mL (both prepared in water as aqueous phase), and HGH 16 µg/mL (using PBS 10 mM as aqueous phase), as described in **Section 6.4.**

6.4.1. Loading of cannabidiol in the nanovesicles

CBD (**Figure 6.10**) is one of two main cannabinoids of *Cannabis sativa*, together with delta-9-tetrahydrocannabionol (Δ^9-THC). Unlike Δ^9-THC, CBD does not possess psychoactivity and does not affect the motor function, memory or the body temperature[29]. It is for these reasons that the World Health Organization (WHO) considers that CBD has a good safety profile and it is generally well tolerated[30].

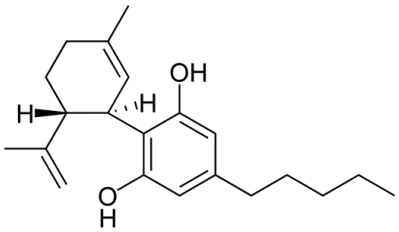


Figure 6.10. Molecular structure of cannabidiol (CBD).

Humans have an endocannabinoid system, with the cannabinoid receptor type 1 (CB1) and the cannabinoid receptor type 2 (CB2). On one hand, CB1 receptors are located mainly in the central nervous system cells, but they are also present in lower amounts in cardiac, lung, small intestine, kidney and liver tissues and immune cells. On the other hand, CB2 receptors are mainly on immunce cells, the gastrointestinal tract and in lower amounts in the central nervous system[31]. It has been reported that CBD has lower binding affinity to CB1 and 2 with respect to other cannabinoids such as Δ^9-THC, and that it can act outside the endocannabinoid system[32]. Despite this fact, related with the tissues with high presence of cannabinoid receptors, different pharmacological effects have been reported for CBD to treat several pathologies: inflammatory and neurodegenerative diseases, epilepsy, autoimmune disorders or cancer[29,31].

Due to all these potential benefits of CBD, there has been an increasing interest for CBD-products that different industries have exploited during the last years, from cosmetics to over-the-counter supplements and prescription drugs[33]. In 2024, the global CBD market size value is of 9.14 billion USD[34]. However, even all this interest on CBD, it is worth noting that only one CBD-based drug is approved by the FDA and EMA which is Epidiolex® to treat seizures[32]. One of the causes of this lack of products containing CBD could be the low motivation of pharmaceutical companies to invest on drugs which could not be patent protected[32].

There are different forms to administer CBD (mainly smokable or oral products)[32] but there is an intrinsic difficulty on its formulation that relies on the lipophilicity of the molecule. The loading in a nanovesicular system would enable the formulation of CBD in aqueous formulations, which is not usual in the marketed products.

For these reasons and also for the potential interest that CBD has shown in the last years, it was selected as a lipophilic payload model to integrate it into the Sit:LGL:DC-chol NVs. The encapsulation of CBD into the NVs would give to the product an added value, obtaining fat-less water-based formulations that could potentially enhance the performance and bioavailability of CBD to the target organ or cells.

To encapsulate CBD, as explained at the beginning of this **Section**, the Sit:LGL:DC-chol (0.8:1:0.2) systems was selected and the nanovesicles were prepared by DELOS process (**Figure 6.9**). The final CBD theoretical concentration was 0.7 mg/mL, which was equivalent to 20% (w/w) of the membrane components. Afterwards, the formulation was characterized by DLS, ELS and cryo-TEM (see **Sections 8.3.1** and **8.3.2**). Additionally, the EE was calculated by UV-vis spectroscopy as explained in **Section 8.3.5.5**.

As demonstrated in **Figure 6.11A** and **Table 3.9**, a homogeneous formulation of CBD NVs was obtained. In terms of physicochemical properties, the system presented similar characteristics to blank NVs (results reported in **Section 6.3.3**), with a particle size below the 100 nm and a low PDI value indicating a narrow population in terms of size. In relation to the EE of CBD in the nanovesicles, the results were positive with a value of 90% of EE for this first proof of concept, meaning that the CBD molecules were well integrated in the bilayer of the NVs. However, just one replicate was done to do the proof of concept, and more replicates have to be done in the future to confirm these results.

Table 6.4. Composition and physicochemical characterization of the CBD-loaded nanovesicle formulation (n = 1).

System (molar ratio)	CBD concentration[a)]	Hydrodynamic diameter mean [nm]	Size PDI	Apparent ζ-Pot [mV]	EE [%]
Sit:LGL:DC-chol (0.8:1:0.2)	0.7 mg/mL 20% (w/w)	88 ± 5	0.16 ± 0.04	69 ± 5	89.7

[a)] *Theoretical concentration.*

When the morphology of these CBD-loaded NVs was analyzed by cryo-TEM (**Figure 6.11B**), the coexistence of NVs and nanoemulsions (black spheres) was seen. The NVs seen were

mainly unilamellar and some of them had elongated form. Similar elongated NVs were already observed in blank Sit:LGL:DC-chol NVs (1:1:0.05) (**Section 6.3.2**), which could mean that DC-chol was causing the elongation of the NVs. On the other hand, the presence of emulsions was not previously seen in blank NVs samples, probably appearing due to the presence of CBD, which is highly lipophilic, and could be partially stabilized in emulsions instead of inside the nanovesicular bilayer. The formation of these nanoemulsions could be further evaluated in the future.

Finally, when analyzing the colloidal stability of the formulation by DLS (**Figure 6.11C**), it was seen that the formulation was stable for the first 3 months, but after that timepoint a continuous increase in particle size was observed. In the case of PDI, it seemed to be more stable with time, however, the standard deviation increased along time.

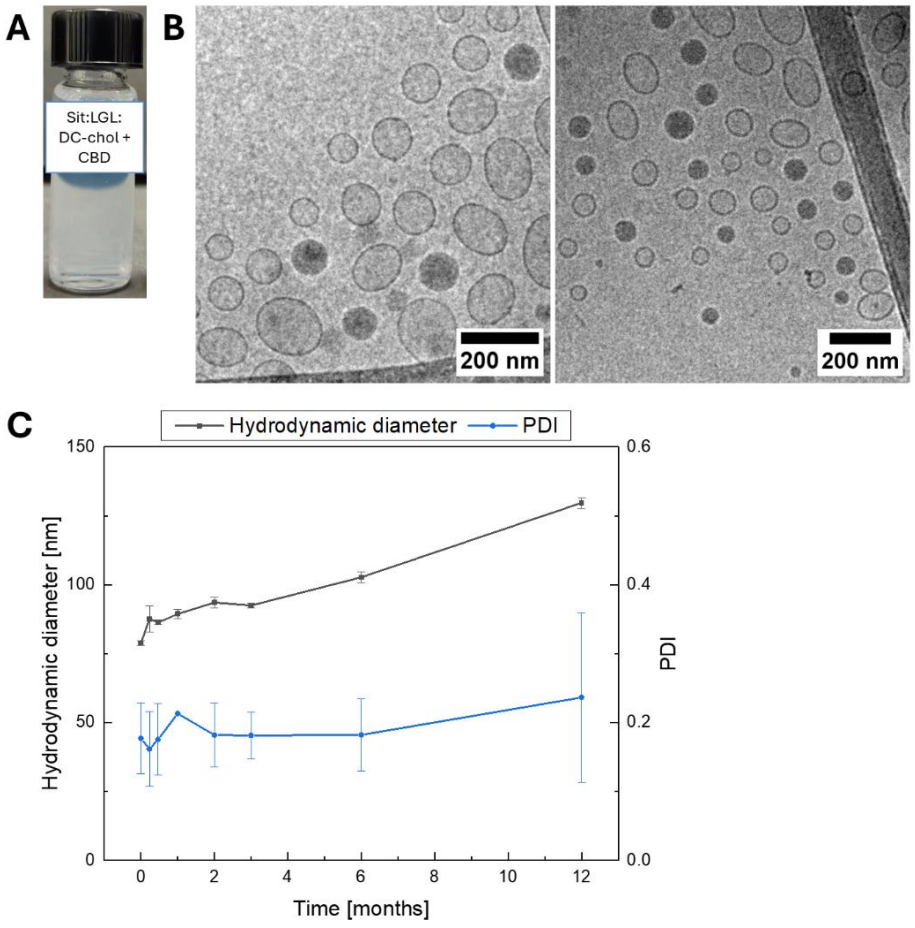


Figure 6.11. **(A)** Macroscopical appearance of Sit:LGL:DC-chol NVs (0.8:1:0.2) loaded with CBD 1 week after production. **(B)** Representative cryo-TEM images of CBD NVs (Sit:LGL:DC-chol, molar ratio 0.8:1:0.2). **(C)** Stability over time in terms of particle size and size PDI (n = 1).

To conclude with this proof of concept, it can be said that lipophilic payloads such as CBD could be efficiently loaded in the Sit:LGL:DC-chol NVs. A homogeneous water-based dispersion was achieved, containing a mixture of small unilamellar vesicles with a nano emulsion, and presenting a high EE (90%). Further replicates should be performed to reproduce these results, and further improvements could be done in the future to better understand the formation of emulsions and to improve the stability over the 3 months.

6.4.2. Loading of methotrexate in the nanovesicles

Interestingly, glycoside-based carriers could represent a strategy for targeted drug delivery to many types of tumor cells since they over-express glucose transporters (GLUT)[35]. Considering this premise and the fact of using LGL as membrane component, we thought on the possibility to load as a proof of concept a chemotherapy drug for its targeted delivery. As a model molecule we selected methotrexate.

MTX was designed during '40s decade as a folic acid antagonist to treat leukemia. Nowadays, besides its use as a chemotherapeutic agent it is also prescribed for the treatment of autoimmune diseases like rheumatoid arthritis or the topical disorder of psoriasis[36].

When used to treat cancer, MTX is used in high doses, while when it is administered for the treatment of rheumatoid arthritis the doses are lower[36]. However, when it is delivered at higher doses, MTX present severe side effects such as liver, kidney or hematological toxicity[37,38], and decreased bioavailability[39]. Thus, it is of interest loading MTX in delivery systems to decrease the side effects and increase the bioavailability of the drug.

The formulation of MTX with Sit:LGL:DC-chol NVs was also interesting because of the ionizable properties of this payload. MTX is an ionizable hydrophilic small molecule. Depending on the pH, it presents different states of protonation (**Figure 6.12**)[40]. Above pH = 2.68, the molecule presents a negative-charged group, which is relevant to this work since it could electrostatically interact with the DC-chol (ionizable cationic lipid) present in the membrane bilayer, this favouring the loading in the nanovesicle and promoting a higher EE of these hydrophilic small molecule.

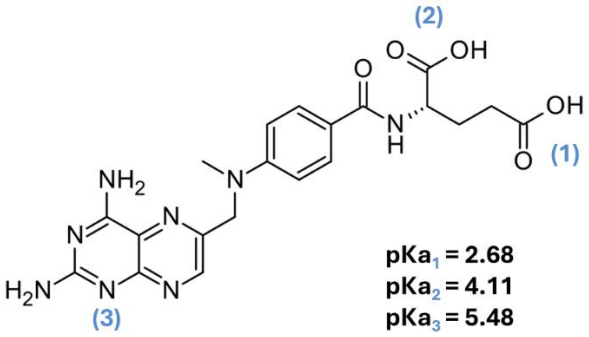


Figure 6.12. Molecular structure of methotrexate (MTX) and its pKa values. Adapted from Alva-Ensastegui *et al.*[40].

Following this basis, a formulation of Sit:LGL:DC-chol NVs (0.8:1:0.2) with MTX at a concentration of 0.26 mg/mL was produced by DELOS methodology (**Figure 6.9**). The concentration of MTX was adapted from other studies from bibliography[39,41]. The dispersion obtained was characterized by DLS and ELS (**Section 8.3.1**) and the EE was calculated by UV-vis spectroscopy as explained in **Section 8.3.5.6**.

A homogenous and stable formulation with a yellowish color, coming from the MTX, was obtained (**Figure 6.13A**). The physicochemical properties were analyzed, and it was seen that in terms of hydrodynamic diameter and size PDI the values were similar to blank NVs (reported in **Section 6.3.3**). However, regarding ζ-Pot, the value of surface charge decreased in comparison to the blank NVs from 70 mV to 40 mV. This change could be related with the integration of MTX interacting with the outer membrane of the NVs. As DC-chol is a cationic lipid at the working pH, blank NVs presented a high positive ζ-Pot. When MTX was added to the formulation, this value related with the surface charge of the nanoparticle decreased, meaning that the surface of the vesicles was less positive. For this reason, it could indicate that the MTX, which was negatively charged, was interacting with the surface of the NVs.

This hypothesis was supported by the high value of EE = 87% obtained. In comparison to other small hydrophilic molecules evaluated as payloads in **Chapter 5** (**Section 5.3**), where the EE was below 20%, here the EE was significantly increased. This enhancement of the loading of a hydrophilic small molecule could be related with the possible interaction between the payload and the vesicle, which promotes the efficient loading.

In relation to the dispersion's pH, it was seen a decrease in relation to blank NVs (pH ≈ 7.4), which could be related with the presence of MTX,

Table 6.5. Composition and physicochemical characterization of MTX-loaded Sit:LGL:DC-chol (0.8:1:0.2 nanovesicle formulations (n = 1).

MTX concentration[a)]	Hydrodynamic diameter mean [nm]	Size PDI	Apparent ζ-Pot [mV]	pH	EE [%]
0.26 mg/mL	116 ± 7	0.12 ± 0.03	41 ± 6	6.1	87.0

[a)] *Theoretical concentration.*

Finally, in relation to colloidal stability, the nanovesicles of Sit:LGL:DC-chol loaded with MTX were highly stable and showed no alteration of particle size and PDI values over a 1 year period (**Figure 6.13B**), a similar behavior to blank Sit:LGL:DC-chol samples.

All in all, it can be concluded that as a first proof of concept the hydrophilic small molecule MTX could be successfully formulated in Sit:LGL:DC-chol NVs with promising characteristics. The formulation turned out to be homogeneous and stable over 1 year with a high value of EE, showing the importance of the electrostatic interaction between the payload and the nanoparticle for an improved integration.

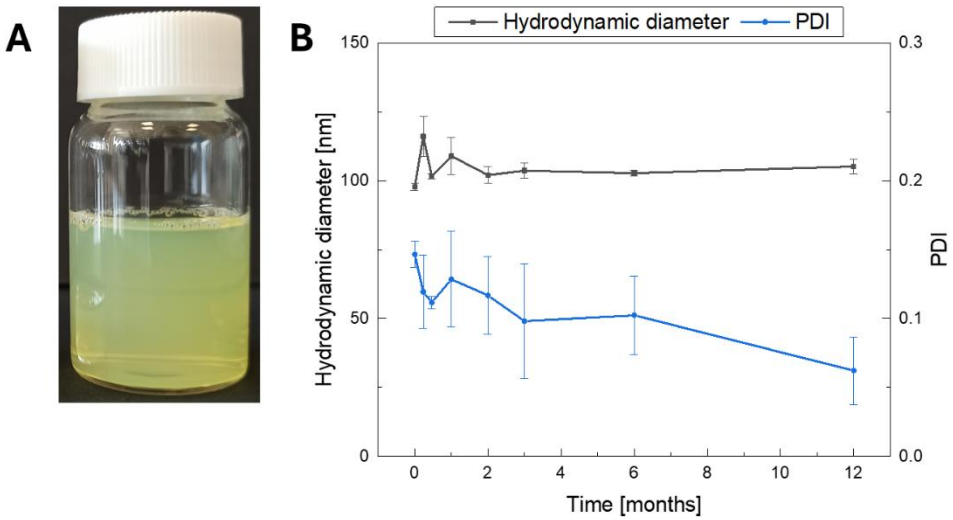


Figure 6.13. **(A)** Macroscopical appearance of Sit:LGL:DC-chol NVs (molar ratio 0.8:1:0.2) with MTX 1 week after production. **(B)** Stability over time in terms of particle size and size PDI (n = 1).

6.4.3. Loading of human growth hormone in the nanovesicles

To fulfill this proof of concept by loading different types of molecules in the Sit:LGL:DC-chol formulations, a larger biomolecule was also tested: the protein human growth hormone.

HGH was selected as a model protein because it is a peptide with an isoelectric point of 5.0[42,43], meaning that when working at pH = 7.4 the protein will be negatively charged. In this way, if the NVs have a positive surface charge, they can electrostatically interact with the net negative charge of the protein, boosting its loading in the Sit:LGL:DC-chol NVs.

From the therapeutic point of view, recombinant HGH has been used to treat growth hormone deficiency as well as other growth disorders. The objective of the treatments are usually the normalization of the height during childhood, the achievement of a normal pubertal growth in addition to a normalization of the body composition and metabolism[44]. However, these treatments are normally associated with periodical injections that can cause poor adherence to HGH therapies[45]. In this way, the loading of HGH in NVs could enhance the bioavailability of the protein decreasing the doses of the treatment.

The HGH used was a peptide of 22 kDa that is found in a solution of phosphate buffer 20 mM at pH = 7.0. As the other formulations described in this **Chapter**, the protein was formulated in Sit:LGL:DC-chol NVs (molar ratio 0.8:1:0.2) using DELOS process (**Figure 6.9**). However, to prepare these nanovesicles loaded with HGH, instead of water as aqueous phase 10 mM PBS buffer at pH = 7.4 was used. The objective was to have a better control on pH, maintaining it above the pI of the protein which was 5.0 to have the protein negatively charged. The final concentration of the protein was 16 µg/mL.

As Sit:LGL:DC-chol NVs (molar ratio 0.8:1:0.2) were not produced before in PBS 10 mM, a blank formulation as control was also prepared to ensure its compatibility with the selected buffer.

After production, as with all the other formulations of this Thesis, the samples were filtered using syringe filters of PES and 0.45 µm. The prototypes then were diafiltrated by tangential flow filtration to eliminate the free HGH, i.e., the protein which was not loaded in the NVs, as explained in further detail in **Section 8.3.6.3**. Both prototypes, the filtered (FILT) and diafiltrated (DIAF) were characterized. The blank samples were treated equally.

Both prototypes (FILT and DIAF) were characterized by DLS, ELS and pH measurements, as described in **Sections 8.3.1** and **8.3.7**. The filtered samples were further characterized by cryo-TEM, as explained in **Section 8.3.2**.

Table 6.6. Physicochemical characterization of blank and HGH-loaded Sit:LGL:DC-chol nanovesicle formulations (n = 1), prepared with DELOS methodology using 10 mM PBS buffer at pH = 7.4 as aqueous phase.

Sit:LGL:DC-chol NVs (0.8:1:0.2 molar ratio)					
Prototype	**Hydrodynamic diameter mean [nm]**	**Size PDI**	**Apparent ζ-Pot [mV]**	**pH**	**EE [%]**
Blank - FILT	82 ± 4	0.06 ± 0.03	55 ± 3	6.11	NA
Blank – DIAF	94 ± 2	0.19 ± 0.03	39 ± 1	7.32	
HGH - FILT	84 ± 2	0.08 ± 0.01	57 ± 3	6.11	20
HGH – DIAF	104 ± 1	0.20 ± 0.02	35 ± 2	7.11	

Table 4.2 and **Figure 6.14** represent the results obtained for the blank and HGH-loaded NVs, and for each formulation, the filtered and the diafiltrated one. Together, the presented results confirm the possibility to formulate stable and homogeneous Sit:LGL:DC-chol NVs loaded with HGH in PBS 10 mM and 15% of EtOH (v/v).

To start with the macroscopical characterization, as **Figure 6.14A** shows, all samples had the same appearance, not only between the FILT and DIAF samples but also between the blank and HGH formulations. They were opalescent whitish colloidal formulations.

Regarding physicochemical properties (**Table 4.2**), blank and HGH-loaded NVs were almost equally in terms of hydrodynamic diameter, size PDI and ζ-Pot. This indicated that the addition of HGH did not affect the self-assembly of the NVs. Additionally, the characteristics were also similar to blank NVs produced in water instead of PBS 10 mM as aqueous phase (**Table 3.5**). However, some differences were detected between FILT and DIAF samples, especially for ζ-Pot, which was reduced after diafiltration. Probably, this was due to the purification of the sample through TFF, which besides the removal of free HGH, could also cause the clearance of positively charged molecules, i.e., the cationic lipid DC-chol. As it was the only cationic component of the formulation, DC-chol was the most probable molecule which could cause the decrease on ζ-Pot. Nonetheless, it does not mean that it was the only component potentially removed with TFF, but further analysis with a quantitative technique such as HPLC would be needed to evaluate the final membrane composition after the diafiltration process.

The pH values were also different between FILT and DIAF samples, being higher in the case of DIAF samples. These differences were probably due to the presence of CO_2 dissolved in form of carbonic acid in the NVs dispersion due to DELOS depressurization (the bubbling of

CO_2 saturates the medium with carbonic acid until the carbonic-CO_2 (gas) equilibrium), which acidify the nanovesicles dispersant media. After diafiltration, because of the purification of the sample, the carbonic acid is removed, increasing the pH of the sample. However, during filtration, the concentration of dissolved carbonic acid is only decreased by the evacuation of CO_2 (gas) during the flow processing, and shifting the chemical equilibrium of carbonic-CO_2 (gas). Thus, due to the presence of this remaining dissolved CO_2, FILT samples presented a more acidic pH than DIAF samples. Additionally, in comparison to blank DC-chol NVs (**Section 6.3**), which presented higher pH values, the measurements were done 2 months after production, allowing the CO_2 (gas) to eventually evaporate. However, the measurements for FILT samples presented here were performed just after 7 days of production and, thus, giving less time to CO_2 (gas) present in the samples to evaporate.

Table 4.2 also shows the value of EE obtained, which was a 20%. It is notable that it was not as optimal as in previous systems, such as Sit:LGC NVs with bFGF (**Chapter 5**), but it could be further optimized in the future. In this sense, some parameters that could be modified to improve the loading of HGH are the concentrations of membrane components and the protein or the buffer employed to manufacture the NVs. For this optimization, a Design of Experiments could be performed.

Figure 6.14B shows representative cryo-TEM images of filtered blank and HGH-loaded NVs. In the case of blank NVs, prepared here in PBS 10 mM, there were depicted small and homogeneous unilamellar vesicles, with a certain tendency to find elongated NVs. The sample was similar to the blank one obtained in water with Sit:LGL:DC-chol NVs (1:1:0.5), described in **Section 6.3.2**. The sample of HGH-loaded NVs also presented homogeneous small unilamellar vesicles. Yet, the morphology of the vesicles seemed to be more spherical. In some spots of this sample, additionally, there were detected some vesicles that were attached to others (highlighted with blue arrows). In the point where they were interacting, a small patch could be seen which could correspond to protein that was acting as adhesive for different NVs. This same behavior was also noticed with Sit:LGC NVs loaded with bFGF (**Section 5.2.2**).

Finally, the stability of the formulations was followed up to three months after production in terms of particle size and PDI (**Figure 6.14C**). As it can be observed, all formulations were stable during this period.

Overall, as a proof of concept it was possible to formulate the HGH protein with Sit:LGL:DC-chol NVs, obtaining stable and homogeneous samples. Nonetheless, for this

particular system further optimization could be done to enhance some parameters such as improving the EE.

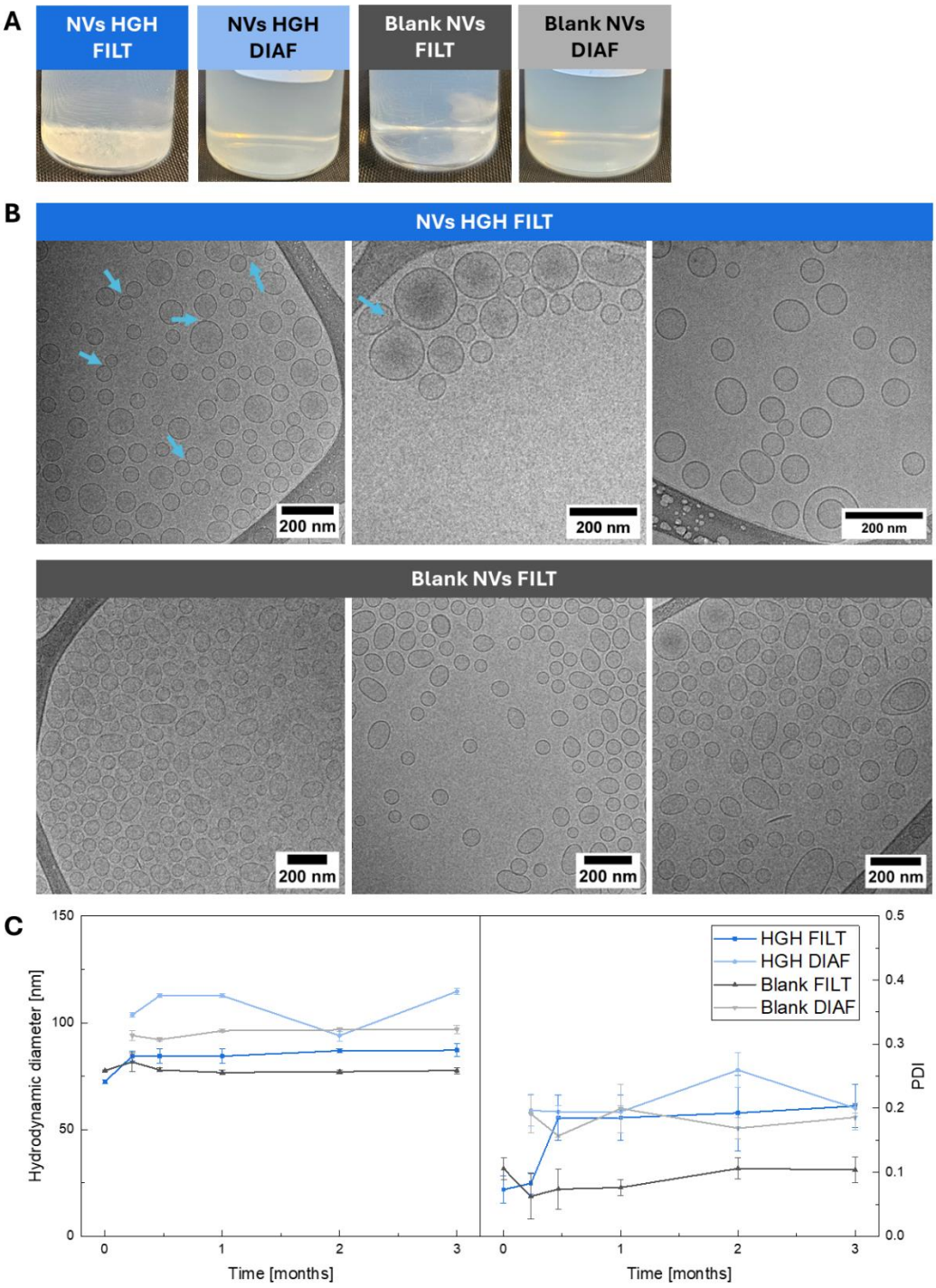


Figure 6.14. **(A)** Macroscopical appearance of the blank and HGH-loaded NVs (Sit:LGL:DC-chol molar ratio 0.8:1:0.2) 1 month after production, filtrated and diafiltrated samples. **(B)** Representative cryo-TEM image of filtrated NVs loading HGH and blank NVs. Vesicles attached to others (blue arrows) can be distinguished. **(C)** Stability over time in terms of particle size and size PDI (n = 1).

6.4.4. Summary of the Section

As a brief summary of **Sections 6.3** and **6.4** comprising the production of Sit:LGL:DC-chol NVs by DELOS process, we have shown the possibility to integrate the ionizable cationic lipid DC-chol at different proportions to Sit and pure LGL NVs.

Different proportions of DC-chol have been tested, from its presence as additive in small amounts (a molar ratio of Sit:LGL:DC-chol of 1:1:0.05) to the complete replacement of Sit by DC-chol thus obtaining NVs of DC-chol:LGL (molar ratio 1:1). The particle size of the NVs varied from 100 to 70 nm depending on the amount of DC-chol present in the formulation, being the particle size lower as the presence of DC-chol increased. In terms of PDI, in all cases were below 0.2 indicating the presence of monodisperse populations of NVs. The ζ-Pot were positive values in agreement with the incorporation of a cationic lipid into the bilayer. The formulations were stable up to 12 months in all cases.

After confirming the obtention of stable formulations incorporating DC-chol as membrane component, the loading of different active molecules with different properties was evaluated: CBD, as a model of lipophilic small molecule; MTX as a hydrophilic small molecule; and HGH as a model of larger biomolecule. With all the prototypes stable formulations were obtained with similar physicochemical properties to blank NVs, meaning that the loading of these molecules did not affect abruptly to the self-assembly of the vesicles and confirming the high versatility of the sugar-based delivery platform.

6.5. Future perspectives

In this Thesis great progress has been done for the preparation of novel plant-based delivery systems for personal care and cosmetic applications, with the integration of different payloads and the biological evaluation of the nanovesicles. In this last **Chapter**, the aim was to build the first foundations for the introduction of these delivery systems based on Sit and sugar-based surfactants for pharmaceutical applications.

Some requirements had to be considered, such as the types and purity of the components used, as well as the expansion of possible delivery routes, not just the topical administration, to perform a tuning of the vesicles developed. In this sense, preliminary approaches have been presented here with the integration of pharmaceutical accepted excipients such as cholesterol derivatives, which gave to the novel NVs new properties. In this way, besides chol-PEG_{600} and DC-chol, other sterols- derivatives could be used to tune the formulations

designing each system on demand for each particular therapy and delivery route. Furthermore, additional work with DC-cholesterol nanovesicles could be done, evaluating their behavior at different pH to study the ionization state of DC-chol under different conditions. Moreover, other ionizable lipids could be also tested, as well as the integration and delivery of nucleic acids. Delivery of mRNA could follow as an interesting line of research to explore since it has been reported that β-sitosterol enhances the transfection of mRNA[46,47].

6.6. Bibliography

1. S. Zalba, T.L.M. ten Hagen, C. Burgui, M.J. Garrido. Stealth nanoparticles in oncology: Facing the PEG dilemma. *J. Control. Release* **2022**, 351, 22–36.

2. A.A. D'souza, R. Shegokar. Polyethylene glycol (PEG): a versatile polymer for pharmaceutical applications. *Expert Opin. Drug Deliv.* **2016**, 13, 1257–1275.

3. D. Shi, D. Beasock, A. Fessler, et al. To PEGylate or not to PEGylate: Immunological properties of nanomedicine's most popular component, polyethylene glycol and its alternatives. *Adv. Drug Deliv. Rev.* **2022**, 180, 114079.

4. Y.W. Kong, E.C. Dreaden. PEG: Will It Come Back to You? Polyethelyne Glycol Immunogenicity, COVID Vaccines, and the Case for New PEG Derivatives and Alternatives. *Front. Bioeng. Biotechnol.* **2022**, 10, 879988.

5. Y. Barenholz. Doxil ®-The first FDA-approved nano-drug: Lessons learned. *J. Control. Release* **2012**, 160, 117–134.

6. E. Fang, X. Liu, M. Li, et al. Advances in COVID-19 mRNA vaccine development. *Signal Transduct. Target. Ther.* **2022**, 7, 94.

7. M. Ibrahim, E. Ramadan, N.E. Elsadek, et al. Polyethylene glycol (PEG): The nature, immunogenicity, and role in the hypersensitivity of PEGylated products. *J. Control. Release* **2022**, 351, 215–230.

8. T. Thanh, H. Thi, E.H. Pilkington, D.H. Nguyen, J.S. Lee. The Importance of Poly (ethylene glycol) Alternatives for Overcoming PEG Immunogenicity in Drug. *Polymers (Basel).* **2020**, 12, 298.

9. L. Shi, J. Zhang, M. Zhao, et al. Effects of polyethylene glycol on the surface of nanoparticles for targeted drug delivery. *Nanoscale* **2021**, 13, 10748–10764.

10. J. V. Jokerst, T. Lobovkina, R.N. Zare, S.S. Gambhir. Nanoparticle PEGylation for imaging and therapy. *Nanomedicine*. Nanomedicine (Lond) June 2011, pp 715–728.

11. Y. Liu, T. Lang, Z. Zheng, et al. In Vivo Environment-Adaptive Nanocomplex with Tumor Cell–Specific Cytotoxicity Enhances T Cells Infiltration and Improves Cancer Therapy. *Small* **2019**, 15, 1902822.

12. Z. Shen, D.T. Loe, A. Fisher, et al. Polymer stiffness governs template mediated self-assembly of liposome-like nanoparticles: Simulation, theory and experiment.

Nanoscale **2019**, 11, 20179–20193.

13. B. Yin, L.W. Cola Ho, S. Liu, et al. Sub-10 nm substrate roughness promotes the cellular uptake of nanoparticles by upregulating endocytosis-related genes. *Nano Lett.* **2021**, 21, 1839–1847.

14. Q. He, J. Zhang, J. Shi, et al. The effect of PEGylation of mesoporous silica nanoparticles on nonspecific binding of serum proteins and cellular responses. *Biomaterials* **2010**, 31, 1085–1092.

15. J. Tomsen Melero. Study of New Liposomes for the Delivery of Enzymes through Biological Membranes, **2021**.

16. G. Vargas Nadal. Novel Quatsome nanovesicles, prepared using CO2, for the development of advanced nanomedicines, Universitat de Barcelona, **2020**.

17. C. Lonez, M. Vandenbranden, J.M. Ruysschaert. Cationic lipids activate intracellular signaling pathways. *Adv. Drug Deliv. Rev.* **2012**, 64, 1749–1758.

18. R.R. Arvizo, O.R. Miranda, M.A. Thompson, et al. Effect of nanoparticle surface charge at the plasma membrane and beyond. *Nano Lett.* **2010**, 10, 2543–2548.

19. R. Tenchov, R. Bird, A.E. Curtze, Q. Zhou. Lipid Nanoparticles from Liposomes to mRNA Vaccine Delivery, a Landscape of Research Diversity and Advancement. *ACS Nano*. American Chemical Society November 23, 2021, pp 16982–17015.

20. L. Wasungu, D. Hoekstra. Cationic lipids, lipoplexes and intracellular delivery of genes. *J. Control. Release* **2006**, 116, 255–264.

21. K. Yamaguchi, M. Inoue, N. Goshima. Efficient protein transduction method using cationic peptides and lipids. *J. Biomed. Biotechnol.* **2011**, 2011.

22. D. Dalkara, C. Chandrashekhar, G. Zuber. Intracellular protein delivery with a dimerizable amphiphile for improved complex stability and prolonged protein release in the cytoplasm of adherent cell lines. *J. Control. Release* **2006**, 116, 353–359.

23. C.R. Alving, Z. Beck, G.R. Matyas, M. Rao. Liposomal adjuvants for human vaccines. *Expert Opin. Drug Deliv.* **2016**, 13, 807–816.

24. F. Khademi, R.A. Taheri, A.A. Momtazi-Borojeni, et al. Potential of cationic liposomes as adjuvants/delivery systems for tuberculosis subunit vaccines. In *Reviews of Physiology, Biochemistry and Pharmacology*; Springer Verlag, **2018**; Vol. 175, pp 47–

70.

25. D. Pozzi, C. Marchini, F. Cardarelli, et al. Mechanistic evaluation of the transfection barriers involved in lipid-mediated gene delivery: Interplay between nanostructure and composition. *Biochim. Biophys. Acta - Biomembr.* **2014**, 1838, 957–967.

26. S. Rayamajhi, J. Marchitto, T.D.T. Nguyen, et al. pH-responsive cationic liposome for endosomal escape mediated drug delivery. *Colloids Surfaces B Biointerfaces* **2020**, 188, 110804.

27. T. Michel, D. Luft, M.K. Abraham, et al. Cationic Nanoliposomes Meet mRNA: Efficient Delivery of Modified mRNA Using Hemocompatible and Stable Vectors for Therapeutic Applications. *Mol. Ther. Nucleic Acids* **2017**, 8, 459–468.

28. A. Boloix, N. Feiner-Gracia, M. Köber, et al. Engineering pH-Sensitive Stable Nanovesicles for Delivery of MicroRNA Therapeutics. *Small* **2021**, 18, 2101959.

29. S. Pisanti, A.M. Malfitano, E. Ciaglia, et al. Cannabidiol: State of the art and new challenges for therapeutic applications. *Pharmacol. Ther.* **2017**, 175, 133–150.

30. World Health Organization (WHO). Cannabidiol (CBD). Critical Review Report. Expert Committee on Drug Dependence.; **2018**.

31. S.C. Britch, S. Babalonis, S.L. Walsh. Cannabidiol: pharmacology and therapeutic targets. *Psychopharmacology (Berl).* **2021**, 238, 9–28.

32. C.A. Legare, W.M. Raup-Konsavage, K.E. Vrana. Therapeutic Potential of Cannabis, Cannabidiol, and Cannabinoid-Based Pharmaceuticals. *Pharmacology* **2022**, 107, 131–149.

33. K.M. Nelson, J. Bisson, G. Singh, et al. The Essential Medicinal Chemistry of Cannabidiol (CBD). *J. Med. Chem.* **2020**, 63, 12137–12155.

34. Cannabidiol Market Size, Share & Trends Analysis Report, 2030 https://www.grandviewresearch.com/industry-analysis/cannabidiol-cbd-market (accessed Jun 9, 2024).

35. P.B. Ancey, C. Contat, E. Meylan. Glucose transporters in cancer – from tumor cells to the tumor microenvironment. *FEBS J.* **2018**, 285, 2926–2943.

36. V. Maksimovic, Z. Pavlovic-Popovic, S. Vukmirovic, et al. Molecular mechanism of action and pharmacokinetic properties of methotrexate. *Mol. Biol. Rep.* **2020**, 47,

4699–4708.

37. K.M. Hamed, I.M. Dighriri, A.F. Baomar, et al. Overview of Methotrexate Toxicity: A Comprehensive Literature Review. *Cureus* **2022**, 14, e29518.

38. H. Aghaei, A.R. Solaimany Nazar, J. Varshosaz. Double flow focusing microfluidic-assisted based preparation of methotrexate–loaded liposomal nanoparticles: Encapsulation efficacy, drug release and stability. *Colloids Surfaces A Physicochem. Eng. Asp.* **2021**, 614, 126166.

39. G.M. Demirbolat, E. Aktas, G.P. Coskun, O. Erdogan, O. Cevik. New Approach to Formulate Methotrexate-Loaded Niosomes: In Vitro Characterization and Cellular Effectiveness. *J. Pharm. Innov.* **2022**, 17, 622–637.

40. J.C. Alva-Ensastegui, E. Morales-Avila, A.P. de la Luz, M.J. Bernad-Bernad. Determination of pKa values and deprotonation order of methotrexate using a combined experimental-theoretical study and binding constants of the methotrexate-Laponite complex at different pH values. *J. Photochem. Photobiol. A Chem.* **2024**, 449, 115406.

41. R. Muzzalupo, L. Tavano, C. La Mesa. Alkyl glucopyranoside-based niosomes containing methotrexate for pharmaceutical applications: Evaluation of physico-chemical and biological properties. *Int. J. Pharm.* **2013**, 458 (1), 224–229.

42. R.M. Meyer, S. Aleshkevich, L. Berger, et al. Characterization of the aggregation propensity of charge variants of recombinant human growth hormone. *Int. J. Pharm.* **2022**, 621, 121760.

43. P. Gellerfors, G. Eketorp, K. Fhölenhag, et al. Characterisation of a secreted form of recombinant derived human growth hormone, expressed in Escherichia coli cells. *J. Pharm. Biomed. Anal.* **1989**, 7, 173–183.

44. M.B. Ranke, J.M. Wit. Growth hormone-past, present and future. *Nat. Rev. Endocrinol.* **2018**, 14 (5), 285–300.

45. S. Mohseni, Z. Heydari, M. Qorbani, M. Radfar. Adherence to growth hormone therapy in children and its potential barriers. *J. Pediatr. Endocrinol. Metab.* **2018**, 31, 13–20.

46. S. Patel, N. Ashwanikumar, E. Robinson, et al. Naturally-occurring cholesterol analogues in lipid nanoparticles induce polymorphic shape and enhance intracellular delivery of mRNA. *Nat. Commun.* **2020**, 11, 1–13.

47. S. Douka, L.E. Brandenburg, C. Casadidio, et al. Lipid nanoparticle-mediated messenger RNA delivery for ex vivo engineering of natural killer cells. *J. Control. Release* **2023**, 361, 455–469.

7 General Conclusions

The main result of this Industrial PhD Thesis is a novel platform of nanovesicles for topical applications based on plant-based ingredients, which has been patent protected. Below are detailed the principal conclusions:

1. Phytosterol and alkyl polyglucoside surfactants were successfully employed to produce for the first time novel stable nanovesicles by self-assembly of β-sitosterol (Sit), lauryl glucoside (LGL) and lauryl glucose carboxylate (LGC), using the single step DELOS manufacturing method. A platform of homogeneous nanovesicles was obtained with a hydrodynamic diameter range of 150-220 nm and a negative surface charge that varied from -40 to -70 mV depending on the amount of anionic surfactant used. The lamellarity of the nanovesicular systems also depended on the membrane components employed, obtaining unilamellar vesicles with Sit/LGC systems but multilamellar ones when any combination of Sit/LGL or Sit/LGL/LGC were used.

2. The formation of the Sit/LGL nanovesicles was not obvious. The purity of the alkyl polyglucoside surfactants used and the surfactant alkyl chain length were directly related to the formation of these nanovesicles. In this way, stable Sit/alkyl polyglucoside

surfactants nanovesicles were only formed when using carbon chains above C12. These results were independent of the methodology employed to prepare the colloidal systems, since both DELOS and thin film hydration methods showed the same tendency, although different vesicle sizes are achieved.

3. In order to evaluate the potential role and versatility of the new nanovesicular platform as dermocosmetic delivery system, different types of active payloads (hydrophilic and hydrophobic small chemical molecules, and proteins) were evaluated:

    I. The nanovesicles composed by Sit:LGL:LGC (molar ratio 1:0.8:0.2) were used to integrate the antioxidant ingredient α-tocopherol and 7-dehydrocholesterol, a precursor of Vitamin D, as models of hydrophobic molecules. Not only both ingredients were efficiently loaded, but also the molecules maintained their activity. In the first case, α-tocopherol could act as an antioxidant after loading, and in the second, 7-dehydrocholesterol was able to be transformed to vitamin D after irradiation of the loaded nanovesicles.

    II. The Sit:LGC nanovesicles were selected to integrate two models of small hydrophilic payloads: niacinamide and ascorbyl glucoside. Although the integration of both molecules was not as efficient as with hydrophobic ingredients, the formulations presented similar physicochemical properties in comparison with blank nanovesicles and showed to be stable for more than a year.

    III. Finally, nanovesicles composed by Sit:LGC were able to load the protein basic fibroblast growth factor, which is a larger hydrophilic biomolecule. In this case the aqueous phase was PBS 10 mM pH 7.4, which demonstrated to not affect the self-assembly of the nanovesicles. The protein was effectively loaded maintaining the physicochemical properties of the nanovesicles as a stable dispersion.

4. The nanovesicles composed by Sit and alkyl polyglucosides were also characterized in terms of biological performance *in vitro* and *ex vivo*. The tested systems proved *in vitro* skin biocompatibility using human reconstructed epidermis models. Furthermore, *ex vivo* skin permeation studies done using two-photon microscopy demonstrated that the fluorophore nile red loaded in nanovesicles exhibited deeper and more efficient permeation compared to the free fluorophore in aqueous suspension.

5. Besides cosmetic applications, it was possible to tune the nanovesicular formulations for future pharmaceutical applications using components approved for drug products as nanovesicle membrane components. Two cholesterol derivatives, cholesterol-PEG_{600} and DC-cholesterol were efficiently incorporated to the self-assembled nanovesicles together with Sit and pure LGL, giving new surface properties to the vesicles. Homogeneous and stable nanovesicles were obtained with both molecules. Cholesterol PEG_{600} provided steric hindrance and increased colloidal stability, whereas DC-cholesterol as an ionizable cationic cholesterol derivative offered positive charge to the nanovesicle bilayer, increasing colloidal stability by charge repulsion and allowing to load negatively charged payloads.

6. Finally, Sit/LGL/DC-cholesterol nanovesicles proved to be promising delivery systems loading different types of molecules of pharmaceutical interest: cannabidiol as hydrophobic small molecule, the anticancer methotrexate as hydrophilic small molecule, and human growth hormone as a larger biomolecule.

In summary, all these results point to the successful development of an attractive, versatile and tunable platform for the topical delivery of active molecules in cosmetic, healthcare and pharmaceutical industries, presenting for the first time stable and homogeneous vesicles composed by plant-derived, biocompatible and biodegradable ingredients.

Experimental section 8

8.1. Materials

Components used in the preparation of nanovesicles

Phytopin DERMexpert, a mixture of pine phytosterols containing 79.7% of β-sitosterol, was obtained from Pharmactive (Alcobendas, Spain). Plantacare® 1200 UP (LGL-m_{C12-16}), Plantacare® 2000 UP (DGL-m_{C8-16}), Plantacare® 810 UP (DGL-m_{C8-10}) and Plantapon® LGC Sorb (LGC) were kindly provided by BASF (Ludwigshafen, Germany). BergaSoft LG 50 (LGL-m_{C10-16}) was kindly given by Berg+Schmidt (Libertyville, IL, USA). Dodecyl beta-D-glucopyranoside (LGL) and decyl beta-D-glucopyranoside (DGL) were obtained from Carbosynth Ltd. (Compton, UK). Sodium laurate (SL) was provided by TCI Europe N.V (Zwijndrecht, Belgium). Sodium lauroyl sarcosinate (SLS) and n-octyl-beta-D-glucopyranoside (OGL) were purchased from Thermo Fisher Scientific (Waltham, MA, USA).

3β-[N-(N′,N′-Dimethylaminoethane)-carbamoyl] cholesterol hydrochloride (DC-Chol) and cholesterol-polyethylene glycol-600 (Chol-PEG_{600}) were purchased from Merck.

All surfactants were pure (>95%) except for those marked as mixtures of different chain lengths ($m_{Cn-(n+X)}$) that were cosmetic grade reagents.

Ethanol HPLC grade was purchased from Scharlab (Barcelona, Spain). Carbon dioxide and nitrogen were supplied by Carburos Metálicos S.A. (Barcelona, Spain). The water used was pre-treated with a MilliQ® Advantage A10 water purification system (Millipore Ibérica, Madrid, Spain).

Active molecules

Dl-alpha-Tocopherol (TCP) and niacinamide (NCA) were kindly donated by DSM (Heerlen, Netherlands). Nile red (NR), 7-dehydrocholesterol (7-DHC), cholecalciferol (VitD), 2-O-a-D-glucopyranosyl-L-ascorbic acid (ascorbyl glucoside, AG) and methotrexate (MTX) were purchased from Merck (Darmstadt, Germany). Basic fibroblast growth factor (bFGF) was supplied by PnP Biopharm (Seoul, Republic of Korea). Cannabidiol (CBD) was purchased from CBD Cure (Barcelona, Spain). Recombinant Human Growth Hormone (HGH) was from Prospec (Ness-Ziona, Israel).

Buffers

Phosphate buffered saline (PBS) and Dulbecco's Phosphate Buffered Saline (DPBS) were from Merk (Darmstadt, Germany).

Others

To evaluate antioxidant capacity of TCP, 2,2-diphenyl-1-picrylhydrazyl (DPPH) was purchased from Merck (Darmstadt, Germany).

For cell viability assays, 3-(4,5-dimethylthiazol-2-yl)-2,5-diphenyltetrazolium bromide (MTT) was acquired from Merck (Darmstadt, Germany).

HPLC analysis was performed using Ultra HPLC supergradient, ACS methanol > 99.9% purchased from PanReac AppliChem (Barcelona, Spain). Optima® LC/MS Grade 2-Propanol > 99.9% was obtained from Thermo Fisher Scientific (Waltham, MA, USA). Formic acid >98% was acquired from Merck (Darmstadt, Germany). The water used was pre-treated with a MilliQ® Advantage A10 water purification system (Millipore Ibérica, Madrid, Spain).

8.2. Preparation of nanovesicles

8.2.1. Preparation of nanovesicles by DELOS methodology

8.2.1.1. Equipment and procedure for preparation at lab-scale

DELOS nanovesicles were prepared using DELOS methodology, based on compressed CO_2 and developed by Nanomol group (ICMAB-CSIC) and commercially exploited by Nanomol Technologies SL. Depending on the desired batch size, two different configurations were used: the bench scale equipment (7.5 mL high-pressure vessel, batch size 25 – 75 mL) or the intermediate scale equipment (25 or 50 mL high-pressure vessel, batch size 150 – 900 mL).

Configuration of bench scale equipment (7.5 mL high-pressure vessel)

The bench scale equipment used to prepare nanovesicles using DELOS methodology is schematized in **Figure 8.1**. Briefly, the configuration consists of a 7.5 mL high pressure vessel (R), for which the temperature is maintained using an external fluid heating jacket. CO_2 is pumped into the reactor through a thermostatic syringe pump (model 260D, ISCO Inc., Lincoln, NE, USA) (P) to introduce CO_2 inside the vessel until reaching working pressure. Further, the expanded liquid solution contained in the vessel is depressurized into an aqueous phase placed in a collector (C) at atmospheric pressure, while at the same time, nitrogen (N_2) is introduced directly from a pressurized reservoir to the vessel.

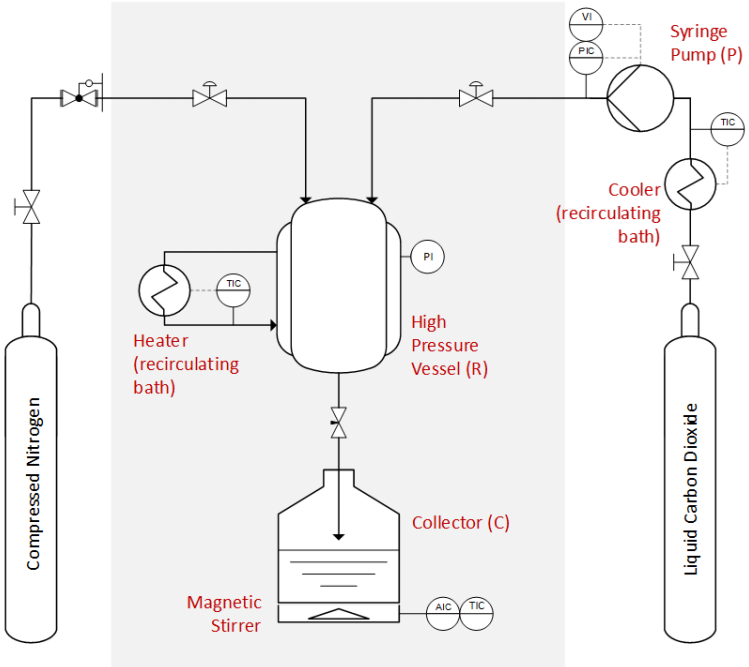


Figure 8.1. Process diagram of the bench scale equipment (7.5 mL high-pressure vessel) used for the preparation of nanovesicles by DELOS methodology.

Configuration of intermediate scale equipment (25/50 mL high-pressure vessel)

The intermediate scale equipment used for the preparation of nanovesicles using DELOS methodology is schematized in **Figure 8.2**. Briefly, the configuration consists of a 25 mL or 50 mL high pressure vessel (R) (independent and interchangeable), for which the temperature is maintained using an external fluid heating jacket. Temperature and pressure are controlled by a temperature controller (TI) and a pressure indicator controller (PI). CO_2 is pumped into the reactor through a thermostatic syringe pump (model 260D, ISCO Inc., Lincoln, NE, USA) (P) to introduce CO_2 inside the vessel until reaching working pressure. A variable speed stirrer (VF) inside R, ensures the homogeneity of the mixture in the volumetrically expanded phase. Further, the expanded liquid solution contained in the vessel is depressurized into an aqueous phase placed in a collector (C) at atmospheric pressure, while at the same time, nitrogen (N_2) is introduced directly from a pressurized reservoir to the vessel.

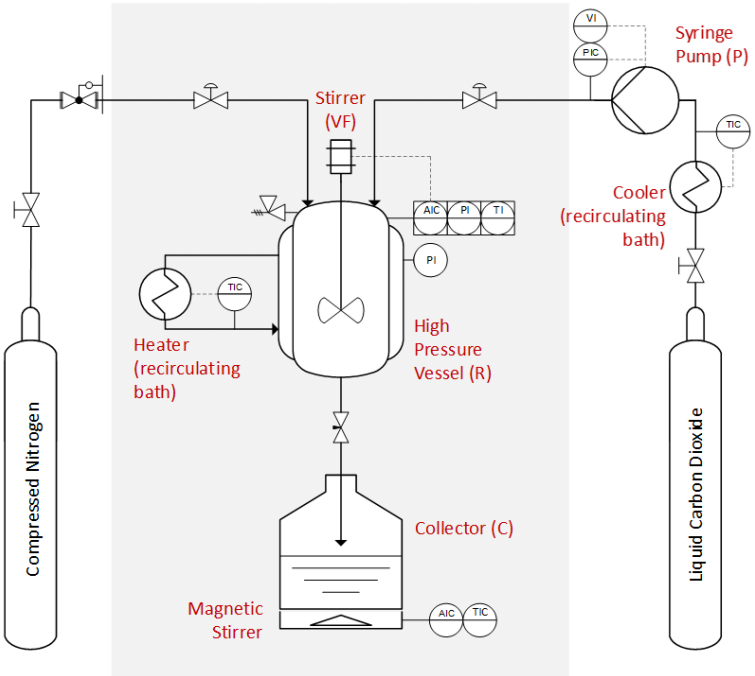


Figure 8.2. Process diagram of the intermediate scale equipment (25/50 mL high-pressure vessel) used for the preparation of nanovesicles by DELOS methodology.

8.2.1.2. Experimental procedure in the bench and intermediate scale equipment

Nanovesicles were prepared using the DELOS manufacturing methodology according to the following procedure:

a. Preparation of the organic solution containing the membrane components solubilized in ethanol (β-sitosterol, pure lauryl glucoside, decyl glucoside and octyl glucoside, sodium lauroyl sarcosinate, sodium laurate, cholesterol-PEG_{600}, DC-cholesterol) and lipophilic actives (α-tocopherol, Nile red, 7-dehydrocholesterol, cannabidiol) at 40 °C. Loading of the organic phase at atmospheric pressure into the vessel which was previously heated to the working temperature (T_W = 40 °C).
b. Addition of liquid compressed CO_2 and formation of a CO_2-expanded solution with all the membrane components dissolved, at a CO_2 molar fraction of X_{CO2} = 0.3 or 0.5, T_W = 40 °C and working pressure, P_W = 8.5-10 MPa.
c. Depressurization of the CO_2-expanded solution from P_W to atmospheric pressure into an aqueous solution (if not specified, purified water through a Milli-Q® Advantage A10 water purification system) containing the water-soluble surfactants (mixture of alkyl glucosides) and the hydrophilic active molecules (basic fibroblast growth factor, niacinamide, ascorbyl glucoside, methotrexate, human growth hormone). A flow of nitrogen (N_2) at a working pressure of P_W = 10-13.5 MPa is used to plunge the CO_2-expanded solution from the reactor, maintaining a constant pressure inside the vessel during depressurization.

All the produced samples were filtered with 0.45 μm pore size polyethersulfone (PES) membrane syringe filters to eliminate impurities coming from the starting materials (mainly from β-sitosterol and APGs mixtures).

The only exception were the Sit:LGC systems (molar ratio 1:1) loading the protein basic fibroblast growth factor and their corresponding blanks, which were centrifugated at 4500 rpm during 30 min at 4 °C to eliminate impurities coming from the starting materials.

With this procedure, homogeneous, opalescent colloidal dispersions of NVs in water with 15% of ethanol (v/v) were obtained.

All nanovesicle samples were stored at 5 ± 3 ºC.

8.2.1.3. Composition of nanovesicles prepared by DELOS methodology

The detailed composition and processing parameters of the samples prepared in the different **Chapters** are described in the following tables: **Table 8.1**, **Table 8.2**, **Table 8.3**, **Table 8.4** and **Table 8.5**.

Table 8.1. Composition of nanovesicles prepared by DELOS methodology in **Chapter 3.**

Composition	Components molar ratio	NVs concentration[a] [mg/mL]	CO_2 molar fraction	NVs dispersant media
Sit:LGL-m_{C12-16}	1:0.75	4.67	0.3	Water/EtOH 15% (v/v)
Sit:LGL-m_{C12-16}	1:1	2.86 / 5.3	0.5 / 0.3	Water/EtOH 15% (v/v)
Sit:LGL-m_{C12-16}	1:1.25	5.99	0.3	Water/EtOH 15% (v/v)
Sit:LGL-m_{C10-16}	1:1.5	5.99	0.3	Water/EtOH 15% (v/v)
Sit:LGL-m_{C10-16}	1:2	7.11	0.3	Water/EtOH 15% (v/v)
Sit:LGL	1:1	2.76	0.5	Water/EtOH 15% (v/v)
Sit:LGL:LGC[b]	1:1:0.05	2.76	0.5	Water/EtOH 15% (v/v)
Sit:LGL:SLS	1:1:0.08	2.76	0.5	Water/EtOH 15% (v/v)
Sit:LGL:SL	1:1:0.1	2.76	0.5	Water/EtOH 15% (v/v)
Sit:LGL:LGC[b]	1:0.8:0.2	3	0.5	Water/EtOH 15% (v/v)
Sit:LGL:LGC[b]	1:0.5:0.5	3	0.5	Water/EtOH 15% (v/v)
Sit:LGL:LGC[b]	1:0.2:0.8	3	0.5	Water/EtOH 15% (v/v)
Sit:LGC[b]	1:1	2.86	0.5	Water/EtOH 15% (v/v)
Sit:OGL	1:1	3.4	0.5	Water/EtOH 15% (v/v)
Sit:DGL	1:1	2.76	0.5	Water/EtOH 15% (v/v)
Sit:DGL:LGC[b]	1:1:0.05	2.65	0.5	Water/EtOH 15% (v/v)
Sit:DGL:SLS	1:1:0.05	2.65	0.5	Water/EtOH 15% (v/v)
Sit:DGL-m_{C8-C10}	1:1	4.7	0.3	Water/EtOH 15% (v/v)
Sit:DGL-m_{C8-C16}	1:1	5.15	0.3	Water/EtOH 15% (v/v)
Sit:LGL:LGC[b]:TCP	1:0.8:0.2:0.4	3	0.5	Water/EtOH 15% (v/v)
Sit:LGL:LGC[b]:NR	1:0.8:0.2:0.01	3	0.5	Water/EtOH 15% (v/v)

[a] *Theoretical concentration.*

[b] *LGC reagent used was a mixture of LGL, intended as alkyl glucosides of C10-16 chain length, and the corresponding carboxylates; thus, the ratios refer to the mixture and not the real content of LGC.*

Table 8.2. Composition of nanovesicles prepared by DELOS methodology in **Chapter 4.**

Composition	Components molar ratio	NVs concentration[a] [mg/mL]	CO_2 molar fraction	NVs dispersant media
Sit:7-DHC:LGL:LGC[b]	1:0:0.8:0.2	3	0.5	Water/EtOH 15% (v/v)
	0.8:0.2:0.8:0.2	3	0.5	Water/EtOH 15% (v/v)
	0.5:0.5:0.8:0.2	3	0.5	Water/EtOH 15% (v/v)
	0.2:0.8:0.8:0.2	3	0.5	Water/EtOH 15% (v/v)
	1:1:0.8:0.2	3	0.5	Water/EtOH 15% (v/v)

[a] *Theoretical concentration.*

[b] *LGC reagent used was a mixture of LGL, intended as alkyl glucosides of C10-16 chain length, and the corresponding carboxylates; thus, the ratios x:y:0.8:0.2 refer to the mixture and not the real content of LGC.*

Table 8.3. Composition of nanovesicles prepared by DELOS methodology in **Chapter 5.**

Sit:LGC[a] nanovesicles		Payload information		CO_2 molar fraction	NVs dispersant media
Molar ratio	Concentration[b] [mg/mL]	Payload	Concentration[b]		
1:1	2.82	bFGF	50 µg/mL	0.5	PBS 10mM/EtOH 15% (v/v)
1:1	2.82	-	-	0.5	PBS 10mM/EtOH 15% (v/v)
1:1	5	NCA	1.25 mg/mL	0.3	Water/EtOH 15% (v/v)
1:1	5	AG	1.25 mg/mL	0.3	Water/EtOH 15% (v/v)

[a] *LGC reagent used was a mixture of LGL, intended as alkyl glucosides of C10-16 chain length, and the corresponding carboxylates; thus, the ratio 1:1 refers to the mixture and not the real content of LGC.*

[b] *Theoretical concentration.*

Table 8.4. Composition of blank nanovesicles prepared by DELOS methodology in **Chapter 6.**

Composition	Components molar ratio	NVs concentration[a)] [mg/mL]	CO_2 molar fraction	NVs dispersant media
Sit:LGL:Chol-PEG_{600}	0.94:1:0.06	2.76	0.5	Water/EtOH 15% (v/v)
Sit:LGL:DC-chol	1:1:0.05	2.76	0.5	Water/EtOH 15% (v/v)
Sit:LGL:DC-chol	0.8:1:0.2	2.76	0.5	Water/EtOH 15% (v/v)
Sit:LGL:DC-chol	0.5:1:0.5	2.76	0.5	Water/EtOH 15% (v/v)
Sit:LGL:DC-chol	0.2:1:0.8	2.76	0.5	Water/EtOH 15% (v/v)
Sit:LGL:DC-chol	0:1:1	2.76	0.5	Water/EtOH 15% (v/v)

[a)] *Theoretical concentration.*

Table 8.5. Composition of active-loaded nanovesicles prepared by DELOS methodology in **Chapter 6.**

Sit:LGL:DC-chol nanovesicles		Payload information		CO_2 molar fraction	NVs dispersant media
Molar ratio	Concentration[a)] [mg/mL]	Payload	Concentration[a)]		
0.8:1:0.2	2.82	CBD	0.75 mg/mL	0.5	Water/EtOH 15% (v/v)
0.8:1:0.2	2.82	MTX	0.26 mg/mL	0.5	Water/EtOH 15% (v/v)
0.8:1:0.2	2.82	HGH	20 µg/mL	0.3	PBS 10mM/EtOH 15% (v/v)
0.8:1:0.2	2.82	-	-	0.3	PBS 10mM/EtOH 15% (v/v)

[a)] *Theoretical concentration.*

8.2.2. Preparation of nanovesicles by thin film hydration

The preparation of nanovesicles by thin film hydration (TFH) methodology was performed according to previous reported literature (Muzzalupo *et al.*[1]).

The appropriate quantities of the membrane components (Sit, LGL, DGL and OGL) were dissolved in in chloroform. Next, the solvent was slowly evaporated using a rotatory evaporator to create a thin film of the membrane components. Once formed the film, it was hydrated with 10 mL of an aqueous solution at 60 °C with magnetic agitation for 30 minutes. Finally, after one day of production, the sample was sonicated at 60 °C for 30 minutes to obtain smaller vesicles (**Figure 8.3**).

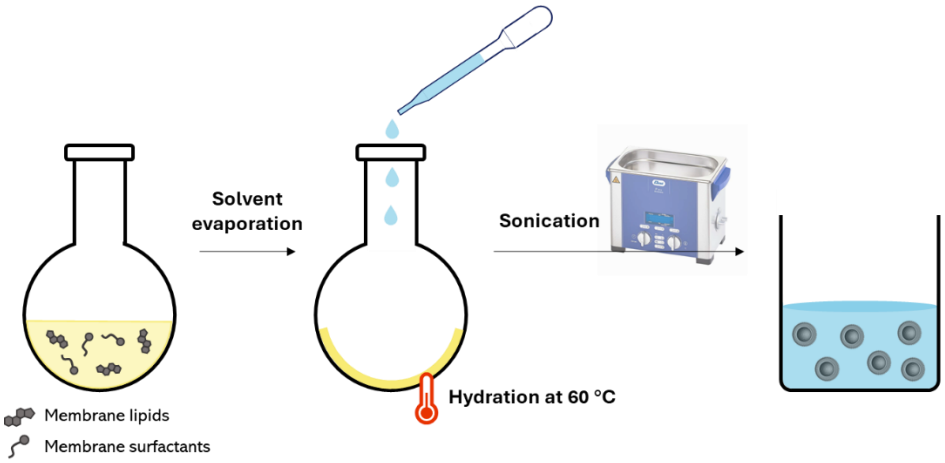


Figure 8.3. Schematic representation of nanovesicle preparation by thin film hydration method.

The detailed composition of the samples prepared by TFH in **Chapter 3** are in **Table 8.6**.

Table 8.6. Composition of nanovesicles prepared by thin film hydration method.

Composition	Sit:Surfactant (molar ratio)	Membrane Components [mg/mL]	Dispersant media
Sit:LGL	1:1	3.68	Water
Sit:DGL	1:1	3.79	Water
Sit:OGL	1:1	4.07	Water

8.3. Physicochemical characterization of nanovesicles

8.3.1. Dynamic light scattering and electrophoretic light scattering

These measurements were performed at Nanomol Technologies SL facilities or in the NANBIOSIS Soft Materials Service linked to Biomaterial Processing and Nanostructuring Unit (U6) at ICMAB-CSIC.

In all **Chapters**, the mean hydrodynamic diameter, polydispersity index (PDI), and apparent ζ-potential (ζ-Pot) were measured using a dynamic light scattering (DLS) and electrophoretic light scattering (ELS) analyzer combined with non-invasive backscatter technology (NIBS) (Zetasizer Ultra, Malvern Panalytical, UK). The instrument was equipped with a He-Ne laser (λ = 633 nm). The detector was set at 173° for particle size distribution measurements, and 13° for ζ-potential measurements.

Samples (1 mL) were placed in a disposable polystyrene cuvette (for DLS measurements) or in a disposable folded capillary cell (for ζ-potential measurements, applied voltage 40 mV) and were analyzed without any modification or dilution.

The reported values consist of three consecutive measurements at 25 °C on the same sample. Data was recorded using the Zetasizer Software (Malvern Panalytical, UK).

Size data was based on intensity size-distribution and corresponds to 3 replicates of z-average ± standard deviation between the three replicates. The use of scattered intensity is the most recommendable data when using DLS, since it comes from the original data provided by the analyzer, without further processing or involved assumptions for calculating particle size.

The reported ζ-potential values correspond to the apparent ζ potential calculated with the Helmholtz-Smoluchowski approximation and corresponds to ζ-potential average ± standard deviation between the three consecutive measurements.

The reported DLS and ELS values were normally collected 7 days after production, except for those samples which are explicitly reported at different times.

8.3.1.1. Quality parameters of DLS measurements

The quality of the data obtained from DLS measurements is directly related to the reliability of the results obtained. There are different parameters associated with the quality of the measurements: intersection of the correlation curve on the y-axis of the correlogram, mean count rate, attenuator and cuvette position, in range value and cumulants fit error[2].

8.3.2. Morphological characterization by cryogenic transmission electron microscopy

Morphology of the nanoformulations was studied by cryogenic transmission electron microscopy (cryo-TEM). This technique allows the direct analysis of colloidal systems, such as nanovesicles, in the vitrified, frozen-hydrated state, so their structure is fairly well preserved and very close to their native state. In this sense, information about size, shape, number of bilayers and bilayers distribution was gathered through cryo-TEM analysis, also allowing the study of their uniformity (heterogeneity) and coexistence of structures.

A JEOL JEM-2011 transmission electron microscope (JEOL Ltd., Tokyo, Japan) at Servei de Microscòpia of the UAB was used to obtain the images, operating at 200 kV. To prepare the vitrified samples, 4 µL were directly placed on a copper grid coated with a lacey carbon film. Then, the excess of the sample was removed by blotting with filter paper obtaining a thin

film of 20 – 400 nm. Just after film preparation, the grid was plunged into liquid ethane held at a temperature just above its freezing point (–179.15 °C), using a Leica EM GP automatic plunge freezer (Leica, Wetzlar, Germany). Afterwards, the vitrified sample was then transferred to the microscope for analysis. In order to avoid sample perturbation and the formation of ice crystals, the samples were kept cold (–196.15 °C) during the transfer and viewing procedures using a cryo-transfer holder (Gatan 626, Gatan, Pleasanton, CA, USA). Images were recorded on a Gatan RIO 16 camera using Digital Micrograph 3.50.3584.0 (Gatan Inc., Pleasanton, CA, USA).

8.3.3. Optical microscopy

Optical microscopy was used to control the homogeneity of the prepared nanovesicular formulations and the presence of precipitates if any at the micrometric scale.

To evaluate them, a drop of the sample was placed between two glass slides. Then, the microscopic examination was carried out using a Morphologi G3 (Malvern Panalytical, UK) at different magnifications to get a proper general observation of the sample (5x, 10x, 20x and 50x).

8.3.4. Study of the lamellarity by small-angle X-ray scattering

Structural and morphological features of different nanovesicular systems were measured using small-angle X-ray scattering (SAXS). This technique is used in colloidal science since it is non-invasive, non-destructive and can provide unique structural information measuring the average properties of the bulk samples with statistical information of the particle ensemble. This kind of morphological information can be otherwise obviated by using microscopic techniques such as cryo-TEM of confocal microscopy, in which just a part of the sample is characterized.

The theoretical working principle behind this technique is based on the interaction of radiation with inhomogeneities in matter that can cause small deviations of the radiation from its incident direction. This phenomenon is called small-angle scattering and can take place for a wide variety of radiation, such as X-rays (SAXS). This static light scattering technique is sensitive to electron density contrast, so that the larger the difference in electron density, the larger the scattering contribution. Thus, SAXS measures the time-average intensity of the scattered X-rays as a function of the scattering angle. Consequently, the measured intensity curve bears information on the radius of gyration, mean size, size distribution or shape among other parameters[3] (**Figure 8.4**).

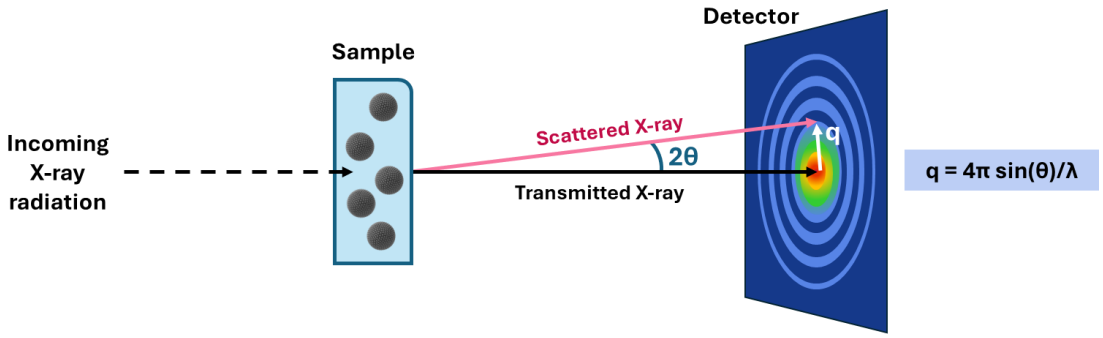


Figure 8.4. Representative scheme of SAXS measurement. The modulus of the scattering vector is defined as q, the scattering angles as 2θ, and the X-ray wavelength as λ.

In all cases, SAXS data were obtained on the NCD-SWEET beamline at the ALBA Synchrotron (Catalonia, Spain). SAXS curves were recorded by a 2D photon counting pixel X-ray detector, Pilatus 1M (DECTRIS, Switzerland). The sample to detector distance was set at 3600 mm and 15 keV of incidence X-ray energy was used resulting in a range for the modulus of the momentum transfer, q, from 0.067 to 4.8 nm^{-1}. The scattering intensity, $I(q)$, was recorded as a function of q, following **Equation 8.1**, where 2θ is the scattering angle and λ the X-ray beam wavelength. The liquid samples without dilution were placed in sample holders with Kapton® windows. The measurements were done at 22 °C.

Equation 8.1

$$q = 4\pi \sin(\theta) / \lambda$$

The data was analyzed in collaboration with Dr. Cristián Huck-Iriart from ALBA synchrotron (Spain) and Prof. Jan Skov Pedersen from Aarhus University (Denmark), which developed the methods to analyze it.

8.3.4.1. Study of the lamellarity of nanovesicles from Chapter 3

Data were fitted using Gaussian based electron density profile[4,5] with two Gaussians representing the head groups and one Gaussian representing the hydrocarbon core to represent the bilayer cross section of the constituted by the amphiphilic molecules of the vesicles. After some initial attempts to fit the data, which showed correlations between the parameters describing the profile, it was decided to fix some of the parameters at physically reasonable value. Considering the molecules geometry and size, the parameter Z, describing half the distance between the centers of the two Gaussians that model the headgroup shell, was set to 10 Å. The sigma value was kept as a fit parameter. Furthermore, the sigma value of the Gaussian that models the central hydrocarbon layer was also set to 10 Å. Thus, the

variation in the cross-section were obtained from the sigma value for the headgroup Gaussians and the amplitude of these relative to the one of the central Gaussian which was kept fixed at -1. The overall radius of the vesicles was fixed at 1500 Å as the size is larger than what is resolved in the experiment. The polydispersity of radius was set to 25%. Furthermore, for the samples with multilamellarity, a para-crystal structure factor was used with polydispersity in the number of layers, taken as a Gaussian[6,7]. For this structure factor, the sigma was kept fixed at 2, and only the average number of layers were fitted. The disorder parameter for the repeat distance was fixed at 0.01.

8.3.4.2. Study of the lamellarity of nanovesicles from Chapter 4

In **Chapter 4**, the method used to analyze the data was similar than in the previous one, with slight modifications.

Data were fitted using Gaussian based electron density profile[4,5] with two Gaussians representing the head groups and one Gaussian representing the hydrocarbon core to represent the cross-section of the bilayer constituted by the amphiphilic molecules of the vesicles. After some initial attempts to fit the data, which showed correlations between the parameters describing the profile, it was decided to fix some of the parameters at physically reasonable value. Considering the molecules geometry and size, the parameter Z, describing half the distance between the centers of the two Gaussians that model the headgroup shell as $sqrt(2log(2))(\sigma_{head}+\sigma_{core})$ with a fixed full with at half maximum of the lipophilic core to 14 Å the sigma of the head value was kept as a fit parameter. Furthermore, the sigma value of the Gaussian that models the central hydrocarbon layer was also set to 10 Å. Thus, the variation in the cross-section were obtained from the sigma value for the headgroup Gaussians and the amplitude of these relative to the one of the central Gaussian which was kept fixed at -1. The overall radius of the vesicles was fixed at 1000 Å as the size is larger than what is resolved in the experiment. The polydispersity of radius was set to 25%. Furthermore, for the samples with multilamellarity, a para-crystal structure factor was used with polydispersity in the number of layers, taken as a Gaussian[6,7]. For this structure factor, the sigma was kept fixed at 10%, and only the average number of layers were fitted. The disorder parameter for the repeat distance was fixed at 0.01.

8.3.5. UV-vis spectroscopy

8.3.5.1. Determination of α-tocopherol concentration and entrapment efficiency

Quantification of TCP concentration and entrapment efficiency (EE) were determined by UV-vis absorbance using an UV-vis spectrophotometer (Thermo Scientific™ Evolution™ 201/220 UV-Visible Spectrophotometers, Thermo Scientific, Spain).

In order to measure TCP in the nanoformulations, NV membrane was dissociated to release the active by diluting the sample in ethanol at 80% (v/v) until obtaining a value of absorption below 1 and within the calibration curve. Then, samples were placed in a micro (400 µL) quartz SUPRASIL® high precision cell (Hellma Analytics, Müllheim, Germany), with a 10 mm light path length. Finally, the absorbance spectrum was recorded using the Thermo INSIGHT software (Thermo Scientific), using 0.5 nm of data interval, 400 nm/min of scan speed. Baseline correction was applied measuring and resting the absorbance of the media of the sample alone.

A calibration standard curve was prepared by diluting TCP in ethanol at different known concentrations and measuring these standard samples by UV-vis spectroscopy. The absorbance was read at λ = 291 nm, the peak maximum point of the absorbance spectrum. A standard curve with a $R^2 > 0.99$ was used. The concentration of each sample was determined using the standard curve and the absorbance measured at λ = 291 nm, correcting the final absorbance value with the absorbance of blank NVs at λ = 291 nm.

To evaluate the EE of TCP, the concentration of the active was quantified before and after filtering process (syringe filter, 0.45 µm pore size, PES membrane) and both values were used to calculate the EE using **Equation 8.2**.

Equation 8.2

$$\text{EE } (\%) = \frac{[\text{TCP}]_{\text{filtered sample}}}{[\text{TCP}]_{\text{non-filtered sample}}} * 100$$

We previously confirmed that free TCP in the dispersant media (water/EtOH 15% (v/v)) was retained in the syringe filter, since TCP is a lipophilic molecule, and it is not soluble in aqueous media. To prove it, we prepared a control solution of TCP in water with 15% of ethanol (v/v) and filter it with the same syringe filters (PES,0.45 µm pore size). Concentration was quantified by UV-vis absorbance, and it was calculated the efficiency of filtration.

The total concentration of TCP in this control sample was 0.589 ± 0.004 mg/mL (n = 3), and after filtration (three independent filtrations were done, n = 3) the concentration of TCP was 0.040 ± 0.004 mg/mL. Through these results it was calculated that only a 6.7 % of TCP can be dissolved in the dispersant media of the NVs or formed enough small precipitates to pass through the filter. Thus, an EE higher than 6.7% indicates the loading of TCP inside the NVs.

8.3.5.2. Determination of Nile red concentration in the samples

Nile red (NR) concentration in NVs was determined by absorption measurements acquired with a PerkinElmer Lambda650 spectrophotometer (PerkinElmer, Milano, Italy).

The NVs were disrupted by diluting the sample with ethanol at 1:6 volume ratio. The samples were placed in a quartz SUPRASIL® high precision cell (Hellma Analytics, Müllheim, Germany), with a 1 cm light path length. Then, the absorbance spectrum was recorded using the UV WINLAB™ software (PerkinElmer), using 1 nm of data interval, 400 nm/min of scan speed.

The concentration of NR was determined using the Lambert-Beer law (**Equation 8.3**) where c is the concentration [M], ε is the molar extinction coefficient [$M^{-1}cm^{-1}$], and l is the light path length [cm], using $\varepsilon_{550nm,\,EtOH}$ = 36477 $M^{-1}cm^{-1}$.

Equation 8.3

$$Abs = c \times \varepsilon \times l$$

The ε was previously experimentally calculated using a calibration curve of NR dissolved in EtOH. The slope of the calibration curve corresponded to the ε, knowing that the optical path of the cuvette was 1 cm.

8.3.5.3. Determination of 7-dehydrocholesterol concentration and entrapment efficiency

Quantification of 7-DHC concentration and EE were determined by UV-vis absorbance using an UV-vis spectrophotometer (Thermo Scientific™ Evolution™ 201/220 UV-Visible Spectrophotometers, Thermo Scientific, Spain).

In order to measure 7-DHC in the nanoformulations, NV membrane was disrupted to release the active by diluting the sample in ethanol at 95% (v/v) until a value of absorption below 1 and within the calibration curve range was obtained. Then, samples were placed in a micro (400 µL) quartz SUPRASIL® high precision cell (Hellma Analytics, Müllheim, Germany), with a 10 mm light path length. Finally, the absorbance spectrum was recorded using the Thermo

INSIGHT software (Thermo Scientific), using 0.5 nm of data interval and 400 nm/min of scan speed. Baseline correction was applied measuring and resting the absorbance of the media of the sample alone.

The concentration of 7-DHC in the nanovesicular formulations was quantified by using a calibration standard curve. It was prepared by diluting 7-DHC in ethanol at different known concentrations and measuring the absorbance at λ = 281 nm, the peak maximum point of the absorbance spectrum. A standard curve with a $R^2 > 0.99$ was used. The concentration of each sample was determined using the standard curve and the absorbance measured at λ = 281 nm, correcting the final absorbance value with the absorbance of blank NVs at λ = 281 nm.

To evaluate the EE of 7-DHC, the concentration of the active was quantified before and after filtering process (syringe filter, 0.45 µm pore size, PES membrane) and both values were used to calculate the EE using **Equation 8.4**.

Equation 8.4.

$$EE\ (\%) = \frac{[7DHC]_{\text{filtered sample}}}{[7DHC]_{\text{non-filtered sample}}} * 100$$

7-DHC is a lipophilic molecule, and it is not soluble in aqueous media, so previously we confirmed that free 7-DHC in the dispersant media was retained in the syringe filter. To evaluate it, we prepared a solution of 7-DHC in water with 15% of ethanol (v/v) at the maximum theoretical concentration used to produce the NVs which was 1.56 mg/mL. Then the sample was filtered with the same syringe filters used for the NVs samples. The 7-DHC concentration of non-filtered and filtered samples was then evaluated by UV-vis absorbance, and it was calculated the efficiency of filtration.

The total concentration of 7-DHC calculated with UV-vis spectroscopy in the sample was 1.35 ± 0.04 mg/mL (n = 3), and after filtration (three independent filtrations were done, n = 3) the concentration of 7-DHC was 0.92 ± 0.09 mg/mL. Through these results it was calculated that 68.5 % of 7-DHC pass through the filter after suspension in water/EtOH 15% (v/v). As this value was higher than expected given the nature of the molecule, we evaluated more in depth the cause of this behavior.

The non-filtered and filtered samples of 7-DHC were characterized at micro and nanoscopic level by optical microscopy, DLS and cryo-TEM (**Figure 8.5**). At microscopic level, neither in non-filtered or filtered samples precipitates or aggregates were observed, as seen in optical microscopic images of **Figure 8.5A**. This was in accordance with the fact that after 0.45 µm

cut off filtration, more than 50% of the 7-DHC was still present in the sample. Afterwards, at nanoscopic level, both samples were analyzed by DLS (**Figure 8.5B**) and a peak at 100 nm was detected, which was below the filters' cut off. This peak could be related with some kind of structuration of 7-DHC in rounded amorphous aggregates, as seen in cryo-TEM images (**Figure 8.5C**).

After these results, it can be assumed that 7-DHC is integrated in NVs when EE > 68.5% and there is absence of aggregates when observed by cryoTEM.

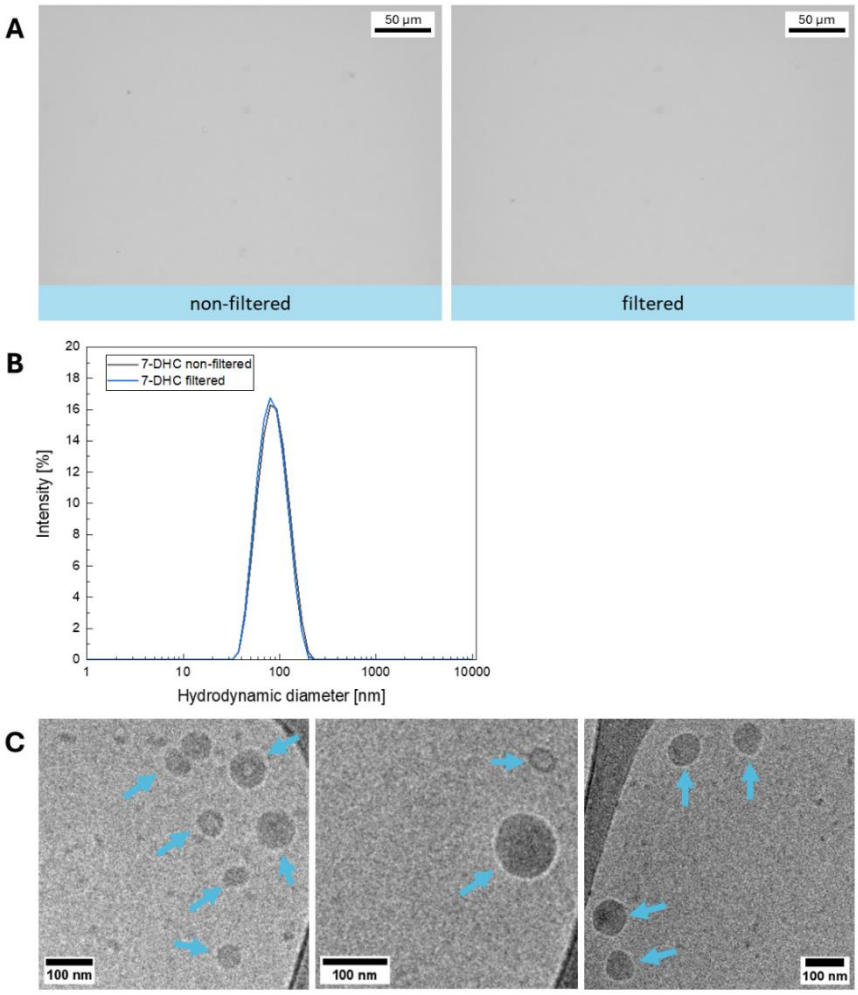


Figure 8.5. Characterization of non-filtered and filtered control samples of 7-DHC in water/EtOH 15% (v/v). **(A)** Optical microscopy images taken at 20x. **(B)** Particle size distribution of non-filtered and filtered 7-DHC samples. **(C)** Representative cryo-TEM images of the filtered samples presenting rounded amorphous structures formed by 7-DHC (blue arrows).

8.3.5.4. Determination of ascorbyl glucoside and niacinamide entrapment efficiency

The EE of AG and NCA in the nanovesicles was measured by UV-vis spectroscopy using a V-780 Double Beam UV-Visible/NIR Spectrophotometer (Jasco, Madrid, Spain), belonging to the NANBIOSIS Soft Materials Service linked to the Biomaterial Processing and Nanostructuring Unit (U6) at ICMAB-CSIC.

In this case, to calculate the EE of both payloads in NVs, the concentration of non-loaded molecule, i.e., the free active, was measured to compare it with the theoretical total concentration added to the formulation.

To calculate the concentration of each molecule, a calibration standard curve was prepared by diluting AG or NCA in water/EtOH 15% (v/v) at different known concentrations. Subsequently, absorbance spectra were recorded using the UV-vis spectrophotometer. The absorbance was read at λ = 259 nm for AG and at λ = 261 nm for NCA, the peak maximum point of the absorbance spectrum. A standard curve with a $R^2 > 0.99$ was used to calculate the concentration of the desired samples.

To calculate the EE the free payload was separated from the one loaded in NVs by ultracentrifugation. The objective was to split the integrated payloads in the NVs in the pellet and the free active molecules in the supernatant. A Sorvall Discovery M150 SE equipment and S150-AT rotor (Thermo Scientific, Waltham, MA, USA) was employed. To proceed with the separation, 1 mL of each sample was loaded in the centrifuge tubes. Then, they were placed in an 8-hole rotor, and ultracentrifugated at a constant force of 600,000 g at 4 °C for 6 h.

Afterwards, the supernatant was collected to calculate the concentration of the non-loaded active molecule. The supernatant from samples was diluted in water/EtOH 15% (v/v) until a value of absorption below 1 and inside the calibration curve was obtained. Then, they were placed in a micro (500 µL) quartz SUPRASIL® high precision cell (Hellma Analytics, Müllheim, Germany), with a 1 cm light path length. Finally, the absorbance spectra were recorded with the Spectra Manager™ software (Jasco), using 0.5 nm of data interval and 400 nm/min of scan speed. Baseline correction was applied measuring and resting the absorbance of the media of the sample alone. The concentration of the supernatants was determined using the standard curve and the absorbance measured at λ = 259 nm for AG and at λ = 261 nm for NCA.

The EE of AG and NCA was calculated using **Equation 8.5**, where the loaded payload concentration was calculated by subtracting the free payload concentration of the

supernatant to the theoretical total concentration, and divided by the same theoretical total active concentration to obtain the EE value.

Equation 8.5

$$\text{EE } (\%) = \frac{[\text{payload}]_{\text{total theoretical}} - [\text{payload}]_{\text{supernatant}}}{[\text{payload}]_{\text{total theoretical}}} * 100$$

8.3.5.5. Determination of cannabidiol concentration and entrapment efficiency

CBD concentration and EE of CBD of the NVs formulations were determined by UV-vis absorbance using a V-780 Double Beam UV-Visible/NIR Spectrophotometer (Jasco, Madrid, Spain), belonging to NANBIOSIS Soft Materials Service linked to Biomaterial Processing and Nanostructuring Unit (U6) at ICMAB-CSIC.

In the same sense of TCP and 7-DHC, to quantify CBD first the NV membrane was disrupted to release the payload by diluting the sample in 80% (v/v) until a value of absorption below 1 and within the calibration curve was achieved. Just after, the samples were placed in a micro (500 µL) quartz SUPRASIL® high precision cell (Hellma Analytics, Müllheim, Germany), with a 1 cm light path length. Finally, the absorbance spectra were recorded with the Spectra Manager™ software (Jasco), using 0.5 nm of data interval and 400 nm/min of scan speed. Baseline correction was applied measuring and resting the absorbance of the media of the sample alone.

In order to quantify CBD in the nanovesicular formulations, it was done using a calibration standard curve. It was prepared by diluting CBD in ethanol at different known concentrations and measuring these standard samples by UV-vis spectroscopy. The absorbance was read at λ = 276 nm, the peak maximum point of the absorbance spectrum. A standard curve with a $R^2 > 0.99$ was used. The concentration of each sample was determined using the standard curve and the absorbance measured at λ = 276 nm, correcting the final absorbance value with the absorbance of blank NVs at λ = 276 nm.

Finally, to calculate the EE of CBD, the concentration of the active was quantified before and after filtering process (syringe filter, 0.45 µm pore size, PES membrane) and both values were used to calculate the EE using **Equation 8.6**.

Equation 8.6

$$\text{EE } (\%) = \frac{[\text{CBD}]_{\text{filtered sample}}}{[\text{CBD}]_{\text{non-filtered sample}}} * 100$$

Like in the case of other lipophilic payloads analyzed during this Thesis, as CBD is not soluble in aqueous media, we previously confirmed that free CBD in the dispersant media (water/EtOH 15% (v/v)) was retained in the syringe filter. To prove it, it was prepared a solution of CBD in water/EtOH 15% (v/v) and it was filtered with the same syringe filters of PES and pore size of 0.45 µm. The concentration of CBD was quantified by UV-vis absorbance in the non-filtered and filtered samples and the efficiency of filtration was then calculated.

The total concentration of CBD in the sample was 0.776 ± 0.005 mg/mL (n = 3), and after filtration (three independent filtrations were done, n = 3) the concentration of CBD was 0.056 ± 0.002 mg/mL. Through these results it was calculated that only a 7.2% of CBD can be dissolved in the dispersant media of the NVs or formed enough small precipitates to pass through the filter. Thus, EE values higher than 7.2% indicate the loading of CBD inside the NVs.

8.3.5.6. Determination of methotrexate entrapment efficiency

To evaluate the MTX concentration and EE it was done by UV-vis absorbance using an UV-vis spectrophotometer (Thermo Scientific™ Evolution™ 201/220 UV-Visible Spectrophotometers, Thermo Scientific, Spain).

First, the release all the MTX from the formulation, NV membrane was disrupted by diluting the samples in ethanol 96% (v/v) until a value of absorption below 1 and inside the calibration curve was obtained. To measure the samples, they were placed in a micro (400 µL) quartz SUPRASIL® high precision cell (Hellma Analytics, Müllheim, Germany), with a 10 mm light path length. Then, the absorbance spectrum was recorded using the Thermo INSIGHT software (Thermo Scientific), using 0.5 nm of data interval, 400 nm/min of scan speed. Baseline correction was applied measuring and resting the absorbance of the media of the sample alone.

In order to calculate the concentration of MTX in each sample it was used a calibration standard curve. For its preparation, MTX was dissolved in ethanol and diluted at different known concentrations which were measured by UV-vis spectroscopy. The absorbance was read at λ = 300 nm, the peak maximum point of the absorbance spectrum. A standard curve with a $R^2 > 0.99$ was used. Then, the concentration of each NVs sample was determined using the standard curve and the absorbance measured at λ = 300 nm, correcting the final absorbance value with the absorbance of blank NVs at λ = 300 nm.

As in all the previous cases, to calculate the EE of MTX it was necessary to remove first the non-integrated payload. In this case, MTX is a hydrophilic small molecule, so the loaded MTX was separated from the free MTX using tangential flow filtration (TFF) as it is explained below. When free MTX was removed from loaded MTX NVs, EE was calculated using **Equation 8.7**, where $Abs_{300\ nm}$ is the absorbance intensity at λ = 300 nm, the starting sample is the sample containing free and MTX loaded in NVs, and TFF sample is the one containing only encapsulated MTX.

Equation 8.7

$$EE\ (\%) = \frac{Abs_{300\ nm}\ (TFF\ sample)}{Abs_{300\ nm}\ (starting\ sample)} * 100$$

Tangential flow filtration technique

Tangential flow filtration is a filtration technique that allows to differentiate components based on size using microfiltration membranes of different pore sizes. In the case of TFF, the feed stream containing the starting sample passes parallel to the membrane face. One portion of this starting sample passes through the membrane (permeate, containing the non-incorporated components dissolved in the dispersant media) whereas the remainder is recirculated back to the feed samples reservoir (retentate, containing in our case the nanovesicles with the integrated payload) (**Figure 8.6**).

TFF allows working at three different operation modes: diafiltration (purification removing components with size below pore size and replacing the permeate lose volume by the same amount of volume of the reservoir buffer which is usually the same than the starting sample), buffer exchange (same concept than diafiltration but changing the original dispersant media for a different one) and concentration (the volume lose with the permeate is not replaced so the original sample is concentrated at the same time that components with size below pore size are eliminated of the sample).

In this particular case, the objective was the purification of the samples to remove the non-incorporated components, specifically free MTX. Thus, diafiltration mode was used and the volume lose in the permeate was replaced by the same dispersant media of the vesicular systems, water with a 15% of ethanol (v/v). In this way, the only difference between the starting sample and the TFF sample was the presence of free MTX and other possible non-integrated membrane components.

To diafiltrate the samples it was used an equipment KrosFlo® Research Iii TFF System (Repligen, Waltham, MA, USA) schematized in **Figure 8.6**. To separate the non-integrated MTX from the NVs samples, a hollow fiber column of 300 kDa cut-off and modified PES was used (reference C02-E300-05-N, Repligen, Waltham, MA, USA). To completely remove all the free MTX, 6 cycles of diafiltration were performed, i.e., 6 times the volume of the starting sample pass to the permeate. The buffer reservoir to replace the lose volume was filled with the same dispersant media than the formulations: water with 15% of ethanol (v/v). After the 6 cycles of diafiltration the process was stopped and the TFF sample was obtained.

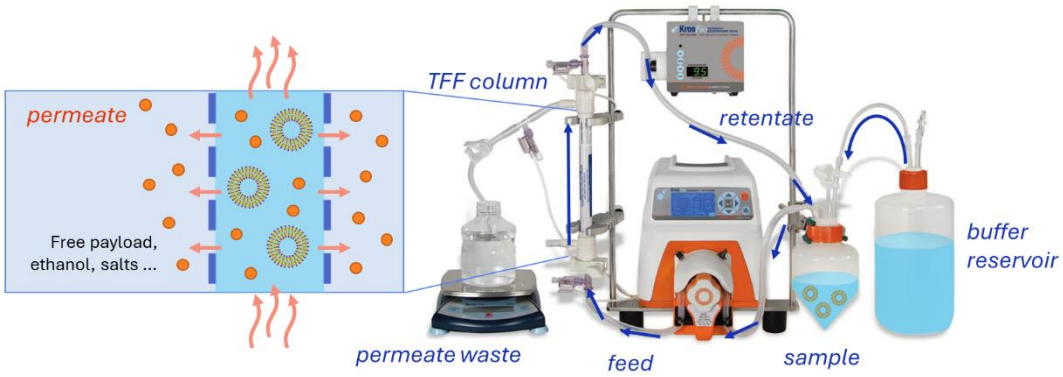


Figure 8.6. Schematic set up of KrosFlo Research Iii TFF system used for diafiltration purification step. Adapted from operating instructions of manufacturer[8].

8.3.6. Fluorescence spectroscopy

8.3.6.1. Nile red fluorescence spectroscopic characterization

Emission spectra of NR NVs and a NR solution in water were registered with an Edinburgh FLS-1000 fluorometer (Edinburgh Instruments, Livingston, UK). The samples were directly measured without further processing in a quartz SUPRASIL® high precision cell (Hellma Analytics, Müllheim, Germany) with 1 cm pathlength. Fluorescence emission spectra was collected exciting at 520 nm and the emission was collected at 525–750 nm.

8.3.6.2. Determination of basic fibroblast growth factor entrapment efficiency

The EE of bFGF in nanovesicles was measured by fluorescence emission using a Cary Eclipse fluorescence spectrophotometer (Varian Inc., Palo Alto, CA, USA). The intrinsic fluorescence emission spectra of bFGF were recorded in the range of 285 to 500 nm after excitation at 278 nm. A slit of 10 nm was applied for both, excitation, and emission. To perform the measurements, it was used a micro (45 µL) quartz SUPRASIL® high precision cell (Hellma Analytics, Müllheim, Germany) of 3 mm optical path length.

Bulk bFGF and bFGF-loaded nanovesicles were analyzed using the same method. To disrupt the vesicular membrane and release all the protein, samples were always diluted with an 80% (v/v) of ethanol. bFGF fluorescence emission depends on its structure and the exposure of the aromatic amino acids which have intrinsic fluorescence[9]. For this reason, 24 h of incubation after dilution in ethanol were required to have the bFGF completely denaturalized and thus, obtain reproducible fluorescence measurements. After this incubation period, the fluorescence spectra were recorded. The baseline was corrected using dispersant media solution for free bFGF and blank nanovesicles dispersions for bFGF-loaded nanovesicles.

To evaluate the EE of bFGF in NVs, first it was necessary to remove the free not integrated bFGF from the formulation. To do this separation, it was used TFF (see **Section 8.3.5.6**). In this particular case, the objective was the purification of the samples to remove specifically free bFGF using diafiltration mode. To diafiltrate the samples it was used an equipment KrosFlo® Research Iii TFF System (Repligen, Waltham, MA, USA) schematized in **Figure 8.6**. To separate the non-integrated bFGF from the NVs samples, a hollow fiber column of 300 kDa cut-off and modified PES was used (reference C02-E300-05-N, Repligen, Waltham, MA, USA). To completely remove all the free bFGF, 6 cycles of diafiltration were performed, i.e., 6 times the volume of the starting sample pass to the permeate. The buffer reservoir to replace the lose volume was filled with the same dispersant media than the formulations: PBS 10 mM with 15% of ethanol (v/v). After the 6 cycles of diafiltration the process was stopped and the TFF sample was obtained. The separation was done one week after batch production.

Then, EE was calculated using **Equation 8.8**, where $FI_{332\,nm}$ is the fluorescence emission intensity at 332 nm, the starting sample is the sample containing free and NVs-integrated bFGF, and TFF sample is the one containing only encapsulated bFGF. Two replicates per sample were performed.

Equation 8.8

$$EE\ (\%) = \frac{FI_{332\,nm}\ (TFF\ sample)}{FI_{332\,nm}\ (starting\ sample)} * 100$$

8.3.6.3. Determination of human growth hormone entrapment efficiency

For the determination of the HGH EE in nanovesicles it was used the protein intrinsic fluorescence emission with a Cary Eclipse fluorescence spectrophotometer (Varian Inc., Palo Alto, CA, USA). The emission was recorded in the range of 285 to 500 nm after excitation at

278 nm. A slit of 10 nm was applied for both, excitation, and emission. Samples were placed in a micro (45 µL) quartz SUPRASIL® high precision cell (Hellma Analytics, Müllheim, Germany) of 3 mm optical path length.

Bulk HGH and HGH NVs were diluted with an 80% (v/v) of ethanol to disrupt the NVs membrane and release all the protein. As in the same case than bFGF NVs (see **Section 8.3.6.3**), samples were left in EtOH for 24 h before analysis to achieve a complete denaturalization and stable fluorescence signal. Just after, the fluorescence spectra of the samples were recorded. The baseline was corrected using dispersant media solution for free HGH and blank nanovesicles dispersions for HGH nanovesicles.

For the determination of HGH EE, free HGH not integrated in the NVs was removed from the nanovesicular formulation by TFF using diafiltration mode (as explained previously in **Section 8.3.5.6**). It was used an equipment KrosFlo® Research Iii TFF System (Repligen, Waltham, MA, USA) schematized in **Figure 8.6**. A hollow fiber column of 300 kDa cut-off and modified PES was used (reference C02-E300-05-N, Repligen, Waltham, MA, USA). To completely remove all the free HGH, 6 cycles of diafiltration were performed, i.e., 6 times the volume of the starting sample pass to the permeate. The buffer reservoir to replace the lose volume was filled with the same dispersant media than the formulations: PBS 10 mM with 15% of ethanol (v/v). After the process, the equipment was stopped and the TFF sample was obtained with the NVs only containing integrated HGH. The separation was done one week after batch production.

Finally, EE was calculated using **Equation 8.8**, where $FI_{334\ nm}$ is the fluorescence emission intensity at 334 nm, the starting sample is the sample containing free and NVs-integrated HGH, and TFF sample is the one containing only encapsulated HGH. Two replicates per sample were performed.

Equation 8.9

$$EE\ (\%) = \frac{FI_{334\ nm}\ (TFF\ sample)}{FI_{334\ nm}\ (starting\ sample)} * 100$$

8.3.7. Measurements of pH

The pH for nanovesicular formulations, was determined using a pH meter pH 50+ DHS (XS Instruments, Carpi, Italy). Samples were left for 30 minutes at room temperature before measurements. The electrode was cleaned between measurements using distilled water. Sample manual agitation was carried out just before performing the measurements to ensure a proper homogenization of the sample.

8.4. Krafft temperature determination by differential scanning calorimetry

Krafft temperature (T_K) is the minimum temperature in which the surfactants can form micelles, and it can be experimentally evaluated by differential scanning calorimetry (DSC) technique.

DSC measurements were performed using a microDSC III (Setaram, Switzerland) at the *Servei d'Anàlisi Tèrmica i Calorimetria* of the *Institut de Química Avançada de Catalunya* (IQAC).

Two different surfactants were evaluated, pure LGL and LGL-m_{C12-16}, following the same methodology described previously by Lu *et al.*[10]. Briefly, solutions of both surfactants were prepared at 0.29 M (concentration above LGL CMC (critical micellar concentration), which has been reported around 0.18 mM[10]) in water/EtOH 15% (v/v), the same dispersant media as NVs, at 60 °C. Afterwards, samples were stored for 7 days at 5 ± 3 °C to let them achieve an equilibrium state. Finally, the day of the analysis around 400 mg of sample was measured in the microDSC equipment following the same sequence: 1 h at 4 °C to equilibrate the sample and a heating scan from 4 °C to 65 °C at a rate of 0.5 °C/min. The T_K was determined as the onset point of the endothermic peak obtained for each surfactant[10,11].

8.5. Functional assays of the integrated biomolecules

8.5.1. Evaluation of antioxidant capacity of α-tocopherol by DPPH assay

2,2-Diphenyl-1-picrylhydrazyl (DPPH) is a stable free radical molecule (**Figure 8.7**). The DPPH method is a stablished and simple method to measure free radical scavenging ability of antioxidants[12]. During the reaction, the odd electron of nitrogen atom in DPPH is reduced by receiving a hydrogen atom from antioxidants. DPPH in ethanol solution has a deep violet color, but when mixing DPPH solution with a substance that can donate a hydrogen atom, it gives rise to the reduced form which loss its color. All this reaction can be easily followed by absorption measurements since DPPH shows a strong absorption band at 517 nm, which disappears as the electron pairs off[13].

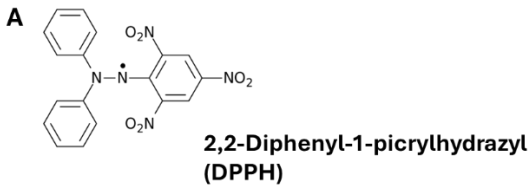


Figure 8.7. Molecular structure of 2,2-diphenyl-1-picrylhydrazyl (DPPH).

The DPPH assay to measure antioxidant capacity of TCP in our formulations was carried out in ethanol, always maintaining a molar ratio between DPPH:TCP of 1:0.3. In order to have a final volume of 3 mL, DPPH was diluted in ethanol to have a final concentration of 63.4 µM, and free TCP or TCP NVs were diluted to have a final concentration of 19 µM of TCP. Each solution was then mixed and kept at room temperature for 30 minutes in the dark. The absorbance of the solution was measured at 517 nm using a Thermo Scientific™ Evolution™ 201/220 UV-Visible Spectrophotometers (Thermo Scientific, Spain) and a micro (400 µL) quartz SUPRASIL® high precision cell (Hellma Analytics, Müllheim, Germany). The percentage of DPPH antioxidant capacity was calculated using the **Equation 8.10**[12], where $Abs_{control}$ is the absorbance at 517 nm of DPPH in ethanol and Abs_{sample} is the absorbance at 517 nm of the sample prepared as described (free TCP or TCP NVs).

Equation 8.10

$$\text{Antioxidant capacity } (\%) = \frac{Abs_{control} - Abs_{sample}}{Abs_{control}} * 100$$

Blank NVs without TCP (but maintaining the same membrane components and concentration) were also analyzed as control, to verify that the NVs itself did not possess antioxidant capacity. The volume used was the same that for TCP NVs to have the same concentration of membrane components in the final analyzed sample.

The samples were analyzed 7 days after production (for TCP NVs) or preparation (for free TCP dissolved in ethanol).

8.5.2. Study of 7-dehydrocholesterol conversion to cholecalciferol

In this dissertation it has been evaluated the capacity of 7-DHC integrated in the NVs to be transformed to VitD in aqueous suspension. The objective was to compare the ratio of conversion of 7-DHC loaded in NVs and free 7-DHC, both dispersed in the same dispersant aqueous media (water with a 15% of ethanol (v/v)).

8.5.2.1. Irradiation study

NVs composed by Sit:7-DHC:LGL:LGC at a molar ratio 0.2:0.8:0.8:0.2 were prepared by DELOS methodology described in **Section 8.2.1**. Furthermore, a suspension of 7-DHC (832 µg/mL) in water/EtOH 15% (v/v) was prepared. The concentration of free 7-DHC was adjusted to be the same than in the filtered nanovesicular formulation. Then, 1 mL of each suspension was placed in a well of a 12 well-plate by triplicate (n = 3). The samples were irradiated using a UV lamp (λ = 302 nm) during 30 min and 1 h. Finally, they were incubated at room temperature for 48 h in the absence of light before being quantified.

8.5.2.2. Determination of 7-dehydrocholesterol and cholecalciferol concentration by HPLC analysis

After 48 h, the concentration of 7-DHC and cholecalciferol of all the prepared samples were quantified specifically by an Acquity Arc ultra-high-performance liquid chromatography (UHPLC) (Waters) coupled to a PDA 2998 detector. The concentration values obtained by HPLC after irradiation were compared with the initial concentration before irradiation measured by UV-Vis spectroscopy as explained in **Section 8.3.5.3**.

7-DHC and VitD calibration curves were elaborated by separately preparing 5 different standards from 8 µg/mL to 134 µg/mL in the case of 7-DHC, and from 1 µg/mL to 21 µg/mL for vitD dissolved in methanol. The samples were analyzed by dissolving them in methanol by a 1:5 dilution factor. All standards and samples were filtered into an HPLC vial with a 0.20 µm hydrophobic polytetrafluoroethyl filter. A volume of 10 µL of each sample was injected into HPLC system. The Empower 3 (Waters, Milford, MA, USA) software was used for instrument control and data analysis.

An Atlantis Premier BEH C18 AX 2.5 um 4.6x150 mm (Waters, Milford, MA, USA) was used to separate the sample components, and their detection was carried out at 282 nm for 7-DHC and 264 nm for VitD. The column temperature was set to 40 °C. Two solvents, A: water and B: 'methanol–isopropyl alcohol-formic acid' (94.9 : 5 : 0.1, v : v : v), were used in an isocratic elution mode with 10% of mobile phase A and 90% of mobile phase B, at a flow rate of 2 mL/min. The run time for each analysis was of 23 minutes.

Quantification was performed by integration of the peak area of the corresponding analyte and interpolation of the peak area in 7-DHC or VitD standard curves. Results are represented by the mean of 3 independent experimental replicates ± relative standard deviation (RSD). The RSD was calculated using **Equation 8.11**.

Equation 8.11

$$\text{RSD} = \frac{\text{Standard deviation}}{\text{Mean value}} * 100$$

8.6. *In vitro* assays

8.6.1. Skin irritation test using *in vitro* reconstructed human epidermis

To evaluate acute skin irritation of the NVs systems, a skin irritation test was performed based on OECD guideline 439[14].

The *in vitro* reconstructed human epidermis (RHE) model SkinEthic™ RHE (EpiSkin, Lyon, France) was used. The method consisted in the application of the NVs formulations without dilution (20 µL) for 24 hours followed by cell viability determination by MTT assay. DPBS (**Chapter 3**) or PBS (**Chapter 4**) and a solution of 5% SDS (w/v) in DPBS or PBS were tested as negative and positive control, respectively, while water/EtOH 15% (v/v) was assessed as control of the dispersant media of the NVs formulations. All the samples were previously sterilized using syringe PES filters of 0.22 µm of pore size.

After 24 h of exposure of the epidermis model to NVs, each well was repeatedly rinsed with DPBS or PBS and carefully blotted with cotton swabs. Then, a 1.0 mg/mL solution of MTT in the cell media was applied to each well and left for 3 hours in the incubator (37 °C, 5% CO_2). The formazan crystals resulting from cell metabolism were dissolved with isopropanol and 100 µL of each of the resulting solutions were transferred to a 96-well plate.

In **Chapter 3**, absorbance of samples at 570 nm was measured by a Spark™ 10M plate reader (Tecan, Mannedorf, Switzerland) and used to express viability as a percentage with respect to absorbance of negative control.

In **Chapter 4**, absorbance of samples at 570 nm was measured by Infinite® M Nano+ plate reador (Tecan, Mannedorf, Switzerland) and used to express viability as a percentage with respect to absorbance of negative control.

According to this predictive model, a product is considered skin irritant when the cell viability is ≤ 50% with respect to negative control[14].

In our case the conditions slightly differed from the ones set by OECD. To work as in a "worse case" scenario, the formulations exposed to the RHE models were left for 24 h, instead of the 42 min suggested by the OECD 439. The reason was that depending on the type of

dermocosmetic product the formulations will remain for more than 42 min in contact with the skin, so we wanted to evaluate the irritation if the formulation was exposed for longer times to the skin.

8.6.2. Retention of the nanovesicles in skin explants assessed by two-photon microscopy

8.6.2.1. Skin permeation experiments

Skin permeation experiments were conducted with a well-known set up which are Franz diffusion cells.

Skin experiments were carried out using porcine tissues. Skin samples were isolated through a scalpel from the cartilage and correspond to the outer part of pig ears (both 10–11 months age male and female from Large White and Landrace, ranging in weight from 145 to 190 kg). Skin samples were frozen at -20 °C and used within 3 months.

It is important to mention that for dermocosmetic applications, it is not allowed the testing of formulations with animals[15]. Thus, for cosmetic applications these experiments should be done with human skin explants. However, these assays can be useful for pharmaceutical applications.

Thawed skin was mounted on glass Franz-type diffusion cells (DISA, Milano, Italy; 0.6 cm^2 surface area) with the stratum corneum facing the donor compartment. Donor compartment was filled with 200 µL of blank NVs systems Sit:LGL:LGC (molar ratio 1:0.8:0.2) and Sit:LGL:LGC + NR (molar ratio 1:0.8:0.2) without dilution and as a control the dispersant media water/EtOH 15% (v/v) and NR in water/DMSO 1% (v/v) solution (1.6 µM). The receiving compartment was filled with saline solution (0.9% NaCl w/v)) previously degassed and kept at 37 °C under magnetic stirring. After 3 h or 6 h the donor was carefully removed, the surface washed three times with saline solution and gently cleansed with filter paper. Then the cell was dismantled and the area of the skin sample in contact with formulation punched (area 0.6 cm^2) and visualized via the two-photon microscopy.

8.6.2.2. Two-photon microscopy

Two-photon microscopy is based on two-photon absorption phenomena (**Figure 8.8**). Normally, fluorescence emission is produced by absorption of a single photon with a wavelength within the absorption band of the excited fluorophore. Nevertheless, with the appropriate laser exciting the sample, it is possible to excite a fluorophore absorbing

simultaneously two photons with half of the wavelength. This process is strongly dependent on the light intensity of the laser used and only occurs at the focal point of the laser beam[16]. The two-photon excitation allows a deep penetration into biological tissues, low photodamage and low scattering, and this is the reason why is really interesting to evaluate biological samples such as the skin.

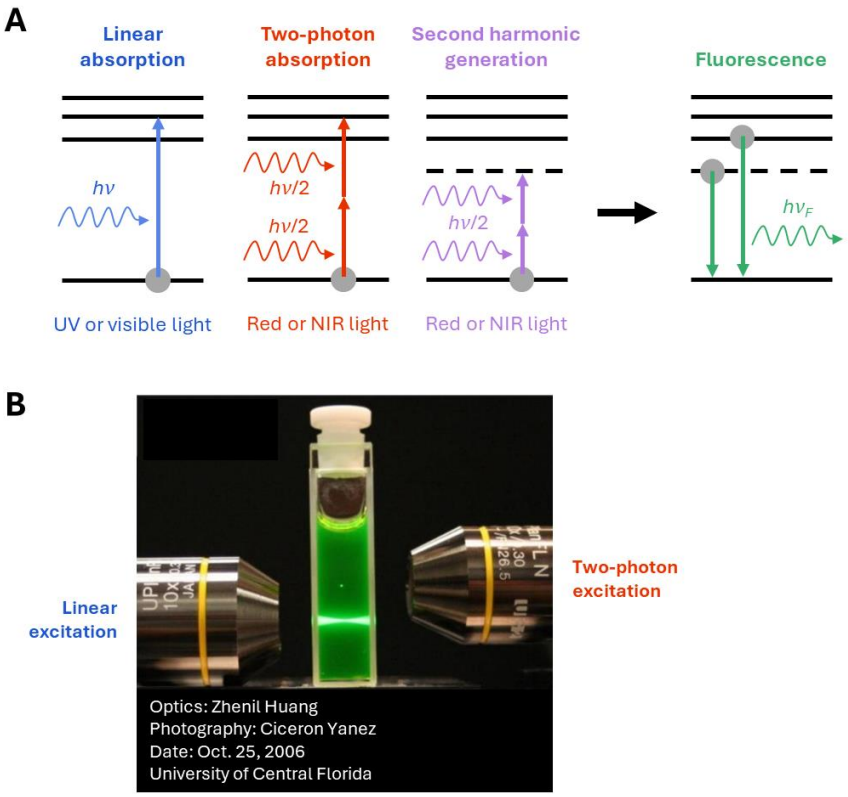


Figure 8.8. **(A)** Schematic representation of linear and two-photon absorption induced fluorescence. **(B)** Image of fluorescein molecule excited with a linear or two-photon excitation laser. Difference on the spatial confinement of signal generation with linear and two-photon excitation.

For this study, skin samples were analyzed following the same procedure described by Ghezzi *et al*[17]. Briefly, a Two-Photon Microscope Nikon A1R MP+ Upright equipped with a femtosecond pulsed laser Coherent Chameleon Discovery (~ 100 fs pulse duration with 80 MHz repetition rate, tunable excitation range 660–1320 nm) was employed for the acquisition of images (Nikon Instruments, Amstelveen, The Netherlands). It is equipped with a 25× water dipping objective with numerical aperture 1.1 and 2-mm working distance for focusing the excitation beam and collecting the two-photon excited fluorescence (TPEF) and the second harmonic generation (SHG) signals. TPEF/SHG signals were directed by a dichroic mirror to a series of three non-descanned detectors (high sensitivity GaAsP

photomultiplier tubes) allowing fast image acquisition. The three detectors are preceded by optical filters allowing the simultaneous acquisition of three separated channels: blue channel (415–485 nm), green channel (506–593 nm) and red channel (604–679 nm). Imaging overlay of the three channels and processing was performed by the operation software of the microscope. Additionally, a fourth GaAsP photomultiplier detector, connected to the microscope through an optical fiber and preceded by a dispersive element, was used to record the spectral profile of the TPEF/SHG signal (wavelength range 430 to 650 nm with a bandpass of 10 nm).

Two-photon microscopy images were collected just after removing the tissue from the Franz diffusion cell. The samples were placed in a dedicated plexiglass holder and saline solution was used to dip the objective and to avoid dehydration. Images were acquired with a typical field of view of 500 µm × 500 µm.

8.7. Statistical analysis

The statistical analyses were performed using OriginLab Software (OriginLab Corporation, Northampton, MA, USA).

8.7.1. Statistical analysis for the DPPH assay

Difference between groups in the antioxidant assay was assessed by one-way ANOVA followed by Tukey pairwise comparison using OriginLab Software (OriginLab Corporation, Northampton, MA, USA). Values of $p < 0.05$ for antioxidant assay were considered statistically significant.

8.7.2. Statistical analysis for the skin irritation assay

Difference between groups in the skin irritation assays was assessed by one-way ANOVA followed by Tukey pairwise comparison. Values of $p < 0.01$ for irritation assay were considered statistically significant.

8.8. Bibliography

1. R. Muzzalupo, L. Tavano, C. La Mesa. Alkyl glucopyranoside-based niosomes containing methotrexate for pharmaceutical applications: Evaluation of physico-chemical and biological properties. *Int. J. Pharm.* **2013**, 458, 224–229.
2. Malvern Instruments. Size quality report for the Zetasizer Nano.
3. T. Li, A.J. Senesi, B. Lee. Small Angle X-ray Scattering for Nanoparticle Research. *Chem. Rev.* **2016**, 116, 11128–11180.
4. J. Tomsen-Melero, S. Passemard, N. García-Aranda, et al. Impact of chemical composition on the nanostructure and biological activity of α-galactosidase-loaded nanovesicles for Fabry disease treatment. *ACS Appl. Mater. Interfaces* **2021**, 13, 7825–7838.
5. G. Pabst, M. Rappolt, H. Amenitsch, P. Laggner. Structural information from multilamellar liposomes at full hydration: Full q-range fitting with high quality X-ray data. *Phys. Rev. E* **2000**, 62, 4000–4009.
6. R. Hosemann, S.N. Bagchi. Direct Analysis of Diffraction by Matter, North-Holl.; Company, N.-H. P., Ed.; **1962**.
7. A. Guinier. X-ray diffraction in crystals, imperfect crystals, and amorphous bodies; W. H. Freeman and Company, Ed.; W. H. Freeman and Company, **1963**.
8. KrosFlo Research IIi TFF System: Product Information and Operating Instructions. Spectrum Labs.
9. I.B. Bekard, D.E. Dunstan. Tyrosine autofluorescence as a measure of bovine insulin fibrillation. *Biophys. J.* **2009**, 97, 2521–2531.
10. H. Lu, I. Pezron, T. Gaudin, A. Drelich. Non-equilibrium micelles formed by sugar-based surfactants under their Krafft temperature. *Colloids Surfaces A Physicochem. Eng. Asp.* **2018**, 540, 167–176.
11. A. Ohta, N. Ozawa, S. Nakashima, T. Asakawa, S. Miyagishi. Krafft temperature and enthalpy of solution of N-acyl amino acid surfactants and their racemic modifications: Effect of the amino acid residue. *Colloid Polym. Sci.* **2003**, 281, 363–369.
12. G. Marinova, V. Batchvarov. Evaluation of the methods for determination of free

radical scavenging activity by DPPH. *Bulg. J. Agric. Sci.* **2011**, 17, 11–24.

13. S.B. Kedare, R.P. Singh. Genesis and development of DPPH method of antioxidant assay. *J. Food Sci. Technol.* **2011**, 48, 412–422.

14. OECD. Test Guideline No. 439 In Vitro Skin Irritation : Reconstructed Human Epidermis Test Method In Vitro. *OECD Guidelines for the Testing of Chemicals*. 2021.

15. EU. REGULATION (EC) No 1223/2009 OF THE EUROPEAN PARLIAMENT AND OF THE COUNCIL of 30 November 2009 on cosmetic products; **2019**.

16. J.R. Lakowicz. Principles of fluorescence spectroscopy, Third Edit.; Springer, **2006**.

17. M. Ghezzi, S. Pescina, A. Delledonne, et al. Improvement of imiquimod solubilization and skin retention via tpgs micelles: Exploiting the co-solubilizing effect of oleic acid. *Pharmaceutics* **2021**, 13, 1476.

Annex I – Scientific Contributions

Patents and Papers submitted:

- Córdoba, M. Alcaina-Hernando, S. Sala, N. Ventosa and I. Malvacio. "Vesicles based on glucose-derived surfactants and phytosterols", (WO/2024/028283). *WO Patent Application filed in 03 of August of 2022*.
- M. Alcaina-Hernando, I. Malvacio, I. Ferraboschi, C. Huck-Iriart, A. Bianchera, S. Sala, J. S. Pedersen, L. Ferrer-Tasies, S. Pescina, C. Sissa, N. Ventosa and A. Córdoba. "A new plant-based drug delivery platform based on alkyl polyglucosides and β-sitosterol nanovesicles for topical delivery", *submitted*.

Papers in preparation:

- Formulation of the vitamin D precursor 7-dehydrocholesterol in alkyl polyglucosides and β sitosterol nanovesicles as advanced ingredient for water-based dermocosmetic applications